The Design, Synthesis, and Chemistry of Stable Verdazyl Radicals and Their Precursors

by

Joseph Bryan Gilroy
B.Sc., University of Victoria, 2003

A Thesis Submitted in Partial Fulfillment
of the Requirements for the Degree of

DOCTOR OF PHILOSOPHY

in the Department of Chemistry

Supervisory Committee

The Design, Synthesis, and Chemistry of Stable Verdazyl Radicals and Their Precursors

by

Joseph Bryan Gilroy
B.Sc., University of Victoria, 2003

Supervisory Committee

Dr. Robin G. Hicks, (Department of Chemistry)
Supervisor

Dr. Reginald H. Mitchell, (Department of Chemistry)
Departmental Member

Dr. J. Scott McIndoe, (Department of Chemistry)
Departmental Member

Dr. Juan Ausio, (Department of Biochemistry and Microbiology)
Outside Member

Dr. Daniel B. Leznoff, (Department of Chemistry, Simon Fraser University)
External Examiner

Abstract

Significant advances in the design, synthesis, and chemistry of verdazyl radicals have been made, including (i) the systematic study of the electrochemistry of verdazyl radicals, (ii) the development of formazans as ancillary ligands *en route* to inorganic verdazyl radicals, and (iii) magnetostructural studies of verdazyl diradicals and copper (II) verdazyl complexes.

The electrochemical properties of a family of verdazyl radicals were explored. Type I and type II verdazyl radicals were reversibly oxidized and reduced, and the potentials of such processes observed to be sensitive to substituent effects. The incorporation of electron-withdrawing substituents made verdazyl radicals harder to oxidize and easier to reduce, while the presence of electron-donating groups had the opposite effect. Type II verdazyls were harder to oxidize and less delocalized (based on relative cell potentials) than type I analogues. The difficulty in oxidation of type II verdazyls relates to the electron-withdrawing nature of the carbonyl functionality, while the decreased delocalization relates to twisting of the N-substituents. Twisting of the N-substituents was confirmed through the use of X-ray crystal structures, and DFT calculations were used to illustrate the decrease in delocalization of the unpaired electron associated with the twisting.

The similarities of formazans to β-diketiminate ligands prompted the study of their coordination chemistry. Boratatetrazines, the first main group complexes of formazans illustrated their ability to mimick β-diketiminate ligands. Reduction of boratatetrazines with cobaltocene afforded highly reactive borataverdazyl radical anions

isolobal to parent organic systems. The radicals were readily oxidized back to the boratatetrazine precursors limiting their characterization to the solid-state.

Synthetic pathways to 3-substituted formazans allowed for the incorporation of bulky N-substituents, a feature of β-diketiminates that has influenced their utility as catalysts. 3-Cyanoformazans were shown to exist as either the *open* or *closed* structure in solution and the solid-state, while 3-nitroformazans exist exclusively as the *closed* strcutre due to the presence of the relatively large nitro-substituent. A number of transition metal complexes of 3-substituted formazans were synthesized, and their X-ray crystal structures used to establish a correlation between steric bulk at the ligand and complex structure. When *ortho*-substituents are incorporated the N-aryl substituents twist relative to the formazan backbone, while relatively smaller N-aryl substituents remain relatively planar. Palladium hexafluoroacetylacetonate complexes of formazans were anticipated to have utility as precursors to palladaverdazyls due to their electron poor nature. However, although the complexes did allow for the structure property relationship of metal-formazan complexes to be further developed, palladaverdazyls were not realized. Comparison with boratatetrazines suggests the nature of the Pd-N bond may play a role in the instability of palladaverdazyls.

The synthesis and characterization of verdazyl-based spin dimers was reported. The incorporation of *iso*-propyl N-substituents allowed for the first truly stable verdazyl diradicals to be isolated. Electrochemical, electronic, and magnetic properties of diradicals bridged by *para*- and *meta*-benzene were explored. Diradicals bridged by *para*-benzene were antiferromagnetically coupled while *meta*-benzene bridged diradicals were ferromagnetically coupled. Magnetostructural studies of copper (II) complexes of

verdazyls were complicated by the coordinative flexibility of copper (II) ions and the presence of Jahn-Tellar distorted ligand fields. However, a correlation between structure and properties was established: axially bound verdazyl radicals were weakly ferromagnetically coupled to copper (II) ions, and equatorially bound verdazyl radicals were strongly antiferromagnetically coupled to copper (II).

Supervisory Committee

Dr. Robin G. Hicks, (Department of Chemistry)
Supervisor
Dr. Reginald H. Mitchell, (Department of Chemistry)
Departmental Member
Dr. J. Scott McIndoe, (Department of Chemistry)
Departmental Member
Dr. Juan Ausio, (Department of Biochemistry and Microbiology)
Outside Member
Dr. Daniel B. Leznoff, (Department of Chemistry, Simon Fraser University)
External Examiner

Table of Contents

List of Figures

List of Schemes

List of Tables

List of Numbered Compounds

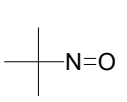

1.1

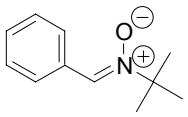

1.2

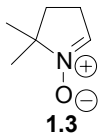

1.3

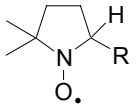

1.4

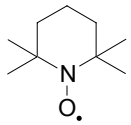

1.5

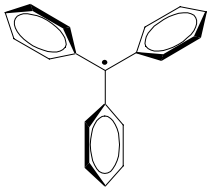

1.6

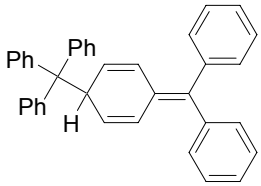

1.7

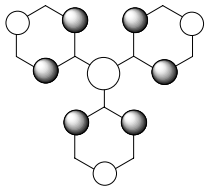

1.8

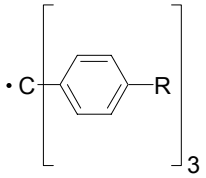

1.9

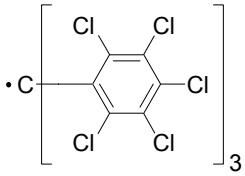

1.10

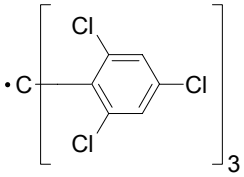

1.11

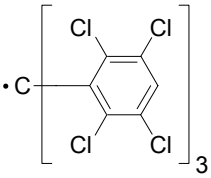

1.12

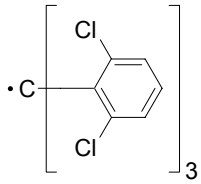

1.13

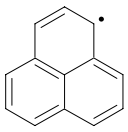

1.14

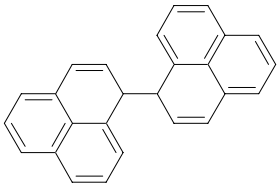

1.15

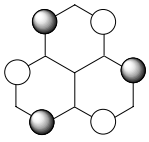

1.16

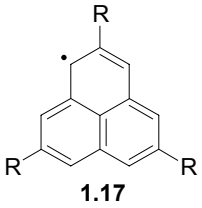

1.17

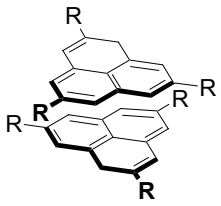

(1.17)$_2$

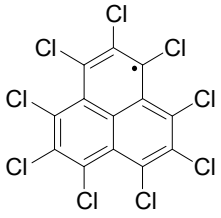

1.18

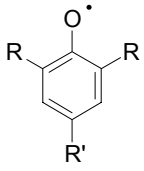

1.19

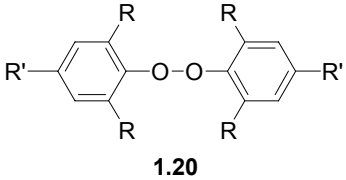

1.20

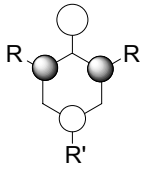

1.21

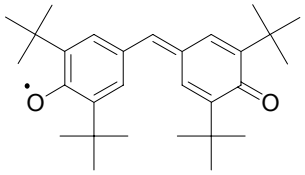

1.22

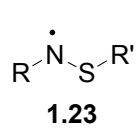

1.23

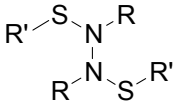

1.24

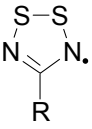

1.25

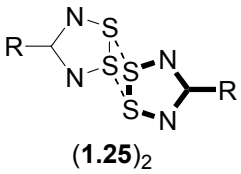

$(\mathbf{1.25})_2$

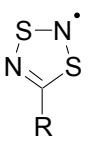

1.26

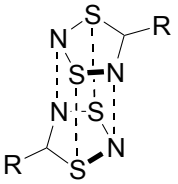

$(\mathbf{1.26})_2$

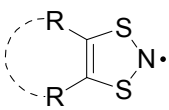

1.27

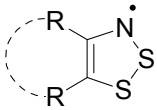

1.28

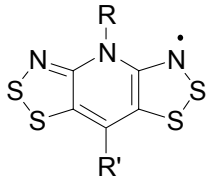

1.29

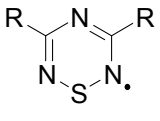

1.30

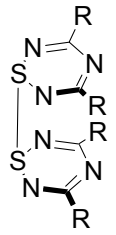

$(\mathbf{1.30})_2$

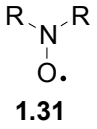

1.31

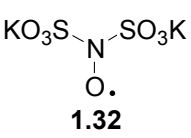

1.32

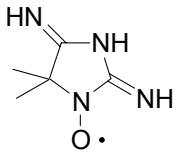

1.33

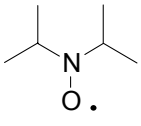

1.34

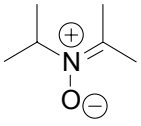

1.35

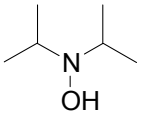

1.36

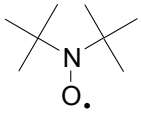

1.37

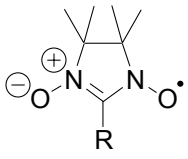

1.38

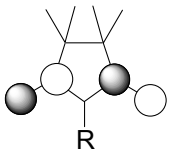

1.39

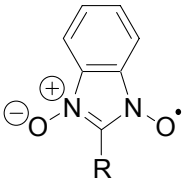

1.40

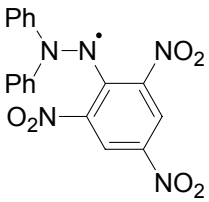

1.41

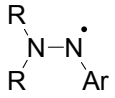

1.42

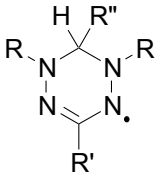

1.43

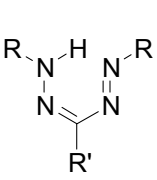

1.44

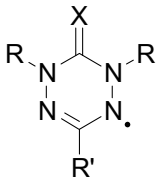

X = O,S

1.45
Type II

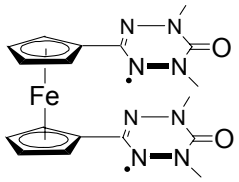

1.46

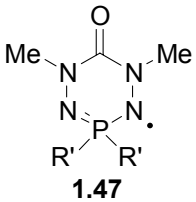

1.47

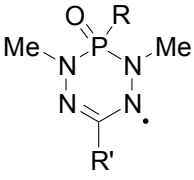

1.48

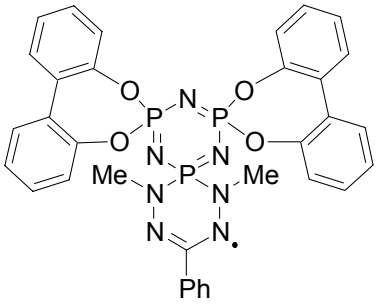

1.49

a R = H, R' = H
b R = OMe, R' = Me
c R = Me, R' = Me
d R = H, R' = Me
e R = Cl, R' = Me
f R = CN, R' = Me
g R = NO_2, R' = Me
h R = CF_3, R' = Me
i R = Me, R' = OMe
j R = Me, R' = H
k R = Me, R' = Cl
l R = Me, R' = CN
m R = Me, R' = NO_2
n R = Me, R' = CF_3

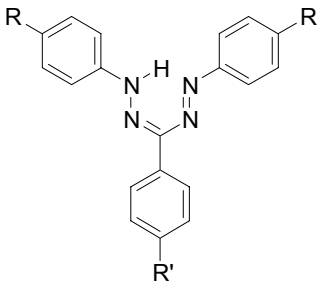

2.1a-n

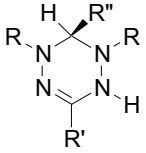

2.2

a R = H, R' = H
b R = OMe, R' = Me
c R = Me, R' = Me
d R = H, R' = Me
e R = Cl, R' = Me
i R = Me, R' = OMe
j R = Me, R' = H
k R = Me, R' = Cl

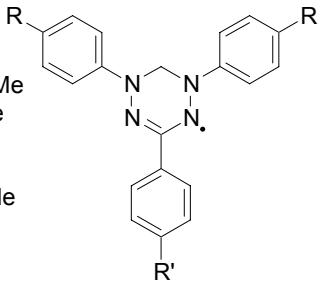

2.3a-e, i-k

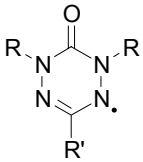

2.4a-h

a R = phenyl, R' = phenyl
b R = iPr, R' = phenyl
c R = iPr, R' = pyridyl
d R = iPr, R' = 2-imidazolyl
e R = iPr, R' = 2'-methylimidazol-5'-yl
f R = Me, R' = phenyl
g R = Me, R' = pyridyl
h R = Me, R' = 2'-methylimidazol-5'-yl

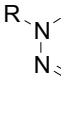

2.5

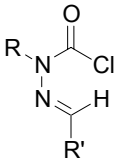

2.6

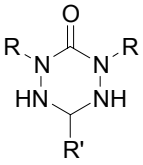

2.7

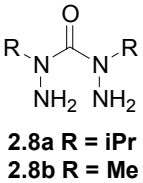

2.8a R = iPr
2.8b R = Me

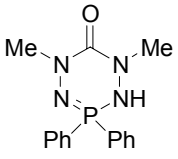

2.9

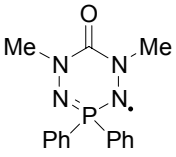

2.10

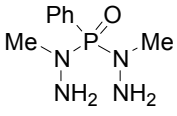

2.11

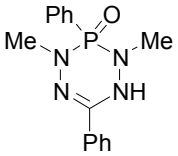

2.12

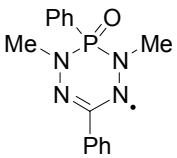

2.13

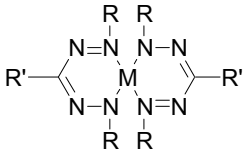

2.14a M = Pd
2.14b M = Ni

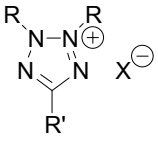

2.15

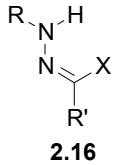

2.16

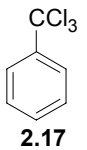

2.17

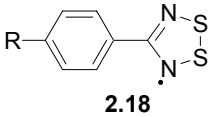

2.18

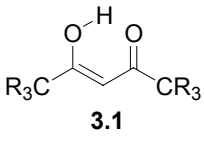

3.1

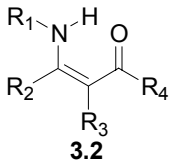

3.2

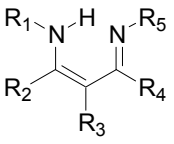

3.3

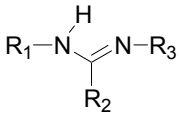

3.4

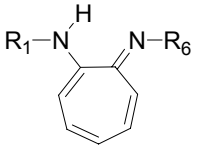

3.5

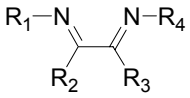

3.6

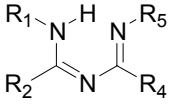

3.7

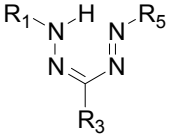

3.8

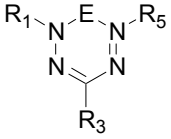

3.9

3.10

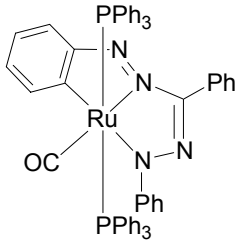

3.11

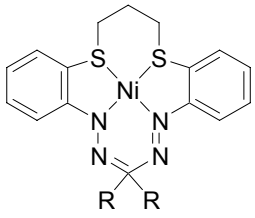

3.12

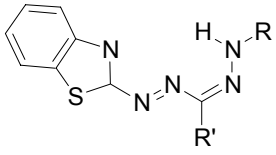

3.13

3.14a M = Cu
3.14b M = Ni
3.14c M = Co

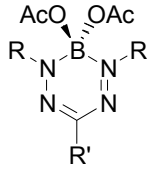

3.15d, j

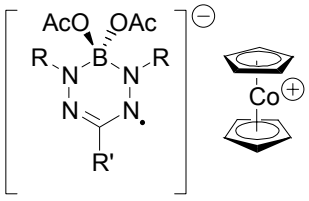

3.16d, j

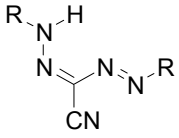

3.17a-d

a R = phenyl
b R = p-tolyl
c R = 2,6-dimethylphenyl
d R = mesityl

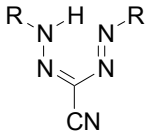

3.17e R = 2-hydroxyphenyl
3.17f R = 2-methoxyphenyl

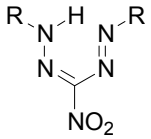

3.18a-f

a R = phenyl
b R = p-tolyl
c R = 2,6-dimethylphenyl
d R = mesityl
e R = 2,6-di-*iso*-propylphenyl
f R = 3,5-di-*tert*-butylphenyl

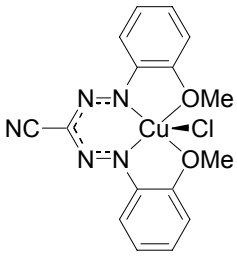

3.19

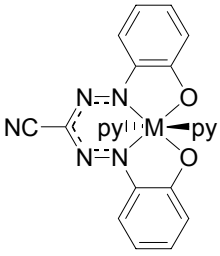

3.20a M = Fe
3.20b M = Co

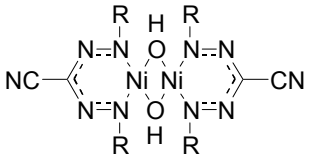

R = 2,6-dimethylphenyl
3.21

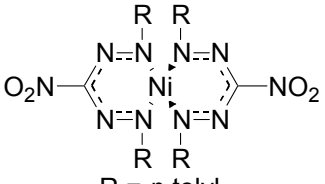

R = *p*-tolyl

3.22

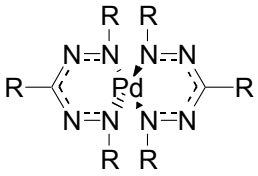

R = *p*-tolyl

3.23

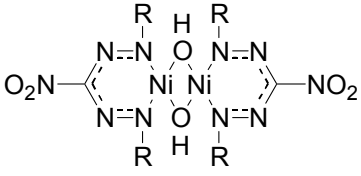

R = mesityl

3.24

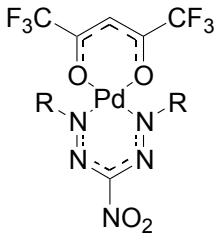

3.25b R = *p*-tolyl
3.25d R = mesityl
3.25e R = 2,6-diisopropylphenyl

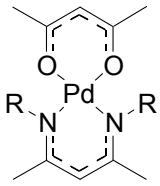

3.26

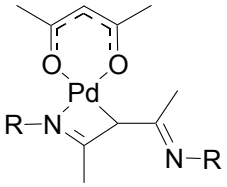

3.26'

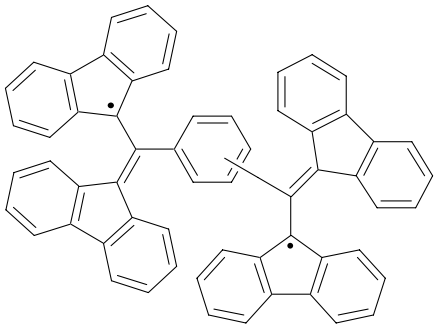

4.1

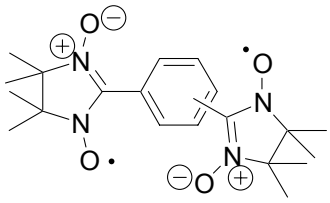

4.2

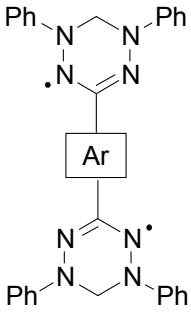

4.3a Ar = 1,4-C_6H_4
4.3b Ar = 1,4-C_6H_4

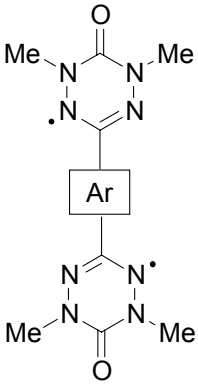

4.4a Ar = 1,4-C_6H_4
4.4b Ar = 1,3-C_6H_4
4.4c Ar = 2,5-C_4H_2S

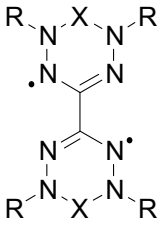

4.5a R = Ph, X = CH_2
4.5b R = Me, X = CO
4.5c R = Me, X = CS

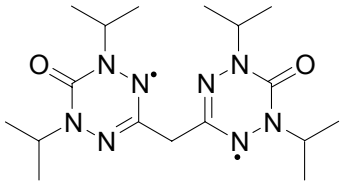

4.6

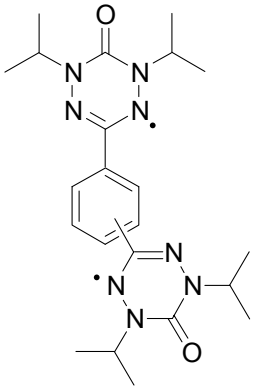

4.7a 1,4-bisverdazyl
4.7b 1,3-bisverdazyl

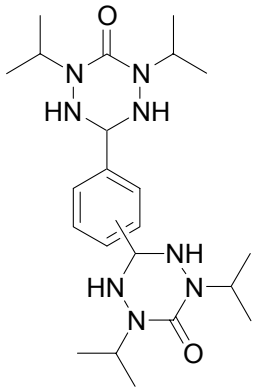

4.8a 1,4-bistetrazane
4.8b 1,3-bistetrazane

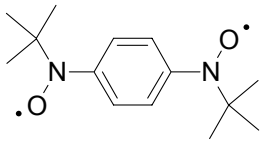

4.9

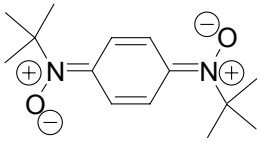

4.9'

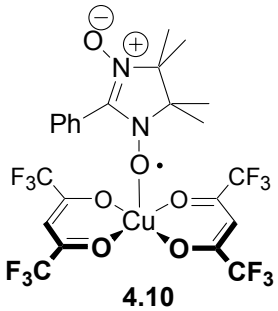

4.10

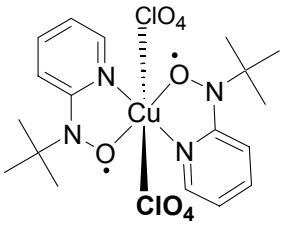

4.11

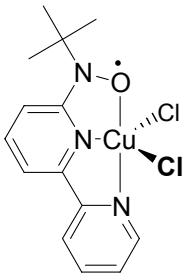

4.12

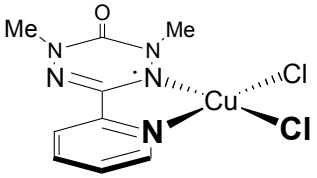

4.13

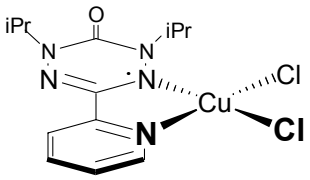

4.14

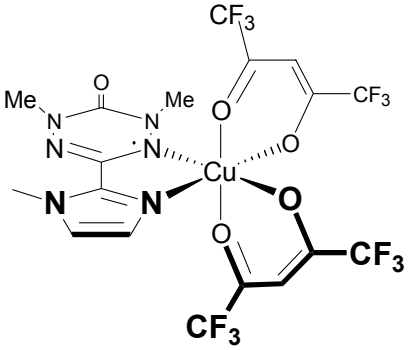

4.15

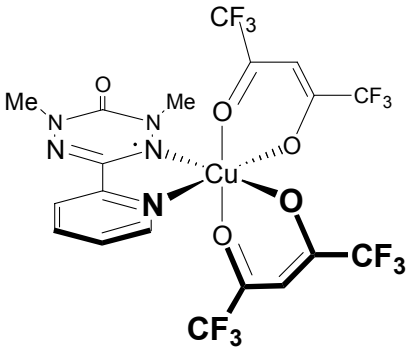

4.16

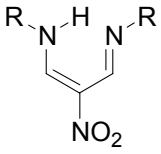

5.1

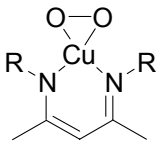

5.2

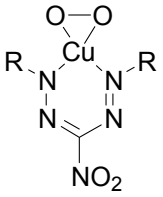

5.3

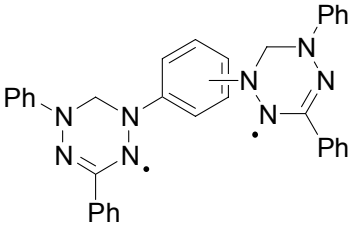

5.4a,b

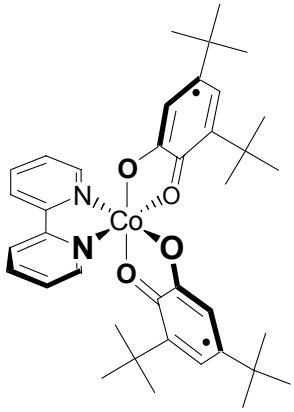

$Co^{II}(bipy)(SQ)_2$

5.5

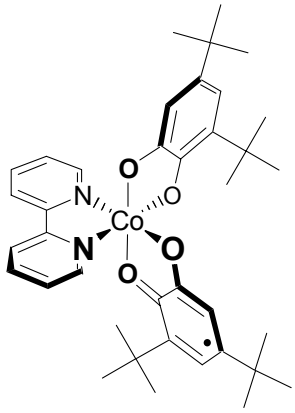

$Co^{III}(bipy)(Cat)(SQ)$

5.6

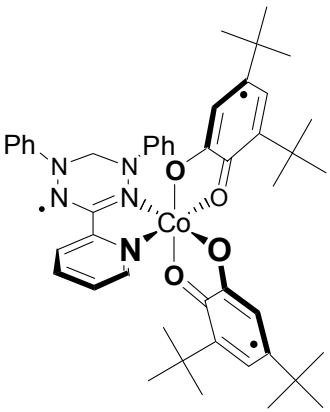

$Co^{II}(vd)(SQ)_2$

5.7

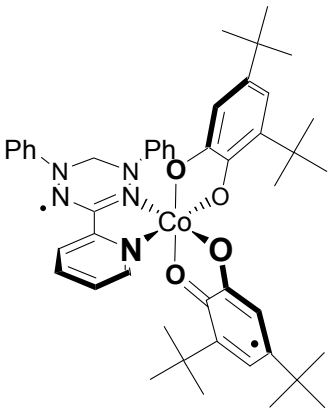

$Co^{III}(vd)(Cat)(SQ)$

5.8

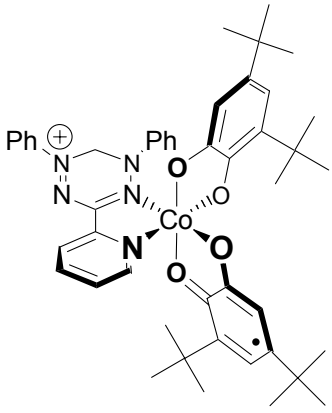

$Co^{II}(vd^{+})(Cat)(SQ)$

5.9

List of Abbreviations

a	hyperfine coupling constant
A	amperes
Å	angstroms
AcOH	acetic acid
Ac_2O	acetic anhydride
Ar	aromatic group
bipy	2,2'-bipyridine
Bu	butyl
C	Curie constant or normalization parameter
calc	calculated
Cat	catecholate ligand
°C	degrees Celsius
cm	centimeter
cm^{-1}	wavenumber
CV	cylic voltammogram
d	doublet
DFT	density functional theory
DTA	dithiazolyl
DTDA	dithiadiazolyl
DMF	dimethylformamide
DMSO	dimethylsulfoxide

DPPH	2,2-diphenyl-1-picrylhyradzyl
e-	electron
E	element or potential
E_{cell}	cell potential
$E_{ox}°$	oxidation potential
$E_{red}°$	reduction potential
EA	electron affinity
EI	electron impact
emu	electromagnetic units
ENDOR	electron-nuclear double resonance
EPR	electron paramagnetic resonance
EPRI	electron paramagnetic resonance imaging
Et	ethyl
Fc	ferrocene
Fc^+	ferrocenium
g	g-factor
g	gram
G	Gauss
h	hours
H	magnetic field or spin hamiltonian
hfac	1,1,1,5,5,5-hexafluoroacetylacetonato
HOMO	highest occupied molecular orbital
Hz	hertz

I	intensity
IP	ionization potential
iPr	*iso*-propyl
IR	infrared
J	coupling constant (NMR) or magnetic exchange parameter
k	Boltzmann constant ($1.3806580 \times 10^{2}3\ J \cdot K^{-1}$)
K	kelvin
L	liters
LMCT	ligand-to-metal charge transfer
LSIMS	liquid secondary ionization mass spectrometry
LUMO	lowest unoccupied molecular orbital
m	multiplet
m_s	magnetic spin quantum number
Me	methyl
MeOH	methanol
Me_8Fc	octamethylferrocene
Me_8Fc^+	octamethylferrocenium
min	minute(s)
MHz	megahertz
mL	milliliters
MLCT	metal-to-ligand charge transfer
Mp	melting point
MO	molecular orbital(s)

mol	mole
mmol	millimoles
MRI	magnetic resonance imaging
MS	mass spectrometry
mV	millivolt
mV/s	millivolts per second
m/z	mass per charge ratio
N	Avagadro's number (6.0221367×10^{23} mol^{-1})
n-BuLi	*n*-butyl lithium
nm	nanometres
NMR	nuclear magnetic resonance
NMRI	nuclear magnetic resonance imaging
NOE	nuclear overhauser enhancement
OAc	acetate
obs	observed
OMe	methoxy
OSWV	Osteryoung square wave voltammetry
p	para
Ph	phenyl
ppm	parts per million
PVC	polyvinylchloride
py	pyridine
q	quartet

R	generic functional group
R	agreement factor
RT	room temperature
s	seconds, singlet, or strong
S	spin quantum number
sep	septet
SOMO	singly occupied molecular orbital
SQ	semiquinone ligand
t	triplet
T	temperature
*t*Bu	*tert*-butyl
TEMPO	tetramethylpiperdine N-oxide
THF	tetrahydrofuran
UB3LYP	unrestricted Becke 3-parameter Lee Yang Parr
UV-vis	ultraviolet – visible
V	volt
vd	verdazyl radical
X^-	generic anion
ZFS	zero field splitting
χ	magnetic susceptibility
ε	extinction coefficient
λ_{max}	wavelength of maximum electronic absorption
θ	Weiss constant

ρ	purity factor
μA	microamperes
υ	frequency

Acknowledgments

I would first like to thank Robin for everything he has done for me over the past five years as a supervisor, mentor, and friend. I leave his group with a versatile skill set, and I am truly grateful for the active role he played in both my personal and professional development during this time. I would also like to thank Natia for her tutelage. In the midst of running her own group, she always had time to help me with the endless complications involved in studying magnetism. I would not have survived five years of research without the help of other Hicks group members past and present: Bryan, Dan, Dave, Eric, Kabir, Kevin, Peter, M'hamed, Raj, Sharon, Simon, Steve, and Tyler. A special thanks to Kevin for routinely 'destroying' me on the golf course. I would also like to thank many other graduate students in the department for the roles they played in my time at UVic: Brynn, Christine, Danielle, Eric, Horace, Mark, Matt, and Sarah.

I did not approach grad school with the intention of making teaching a part of my long term goals. Thank you Dave, Kelli, and Jane for opening my eyes to teaching, and providing me with the tools necessary to make teaching an integral part of my career. Special thanks to Dave for helping me develop my own teaching style, and for sharing his passion for teaching.

I owe much of my success to the Faculty and support staff at UVic: Ph.D. committee, Scott McIndoe and Reg Mitchell; chem. office, Sandra, Carol, and Shelley; science stores, Rob, Glenda, Derek, and Bev.; mass spec. lab, Dave McGillavry; NMR lab, Chris Greenwood, instrument shop, Bob Dean and Terry Wiley. I would like to thank the following collaborators for their expertise and ability to deal with my constant

harassment: Crystallographers, Bob McDonald, Michael Ferguson (U of A), and Bryan Patrick (UBC); DFT calculations, Mark Zsombor (UVic); EPR, Pierre Kennepohl (UBC), magnetic measurements, Laurie Thompson (Memorial); electrospray mass spectroscopy, Scott McIndoe (UVic).

Finally, I would like to thank my friends and family. It is difficult to survive nine years of University without a lot of help. Thank you Mom, Dad, Grandma, Grandpa, Josh, Krystal, Spencer, Jona, Jeremiah, Jessica, Bobbie, and my long-time roommates Jag and Marianne.

Chapter 1 Introduction and background

1.1 Stable radicals

Nearly all molecules based on the p-block conform to conventional bond valency arguments: they obey the octet rule, contain an expected number of bonds and lone pairs, and as a result are diamagnetic. Radicals have fewer bonds than predicted, resulting in one (or more) unpaired electron(s). In many cases the nature of the unpaired electron leads to highly reactive, short lived species due to the low activation barrier associated with, e.g., dimerization, hydrogen abstraction, disproportionation, oxidation, or reduction.

However, many examples of stable, isolable radicals exist allowing for chemistry associated with the unpaired electron to be studied. Since the report of the first stable organic radical in 1900,[1] many families of *stable* or *persistent* radicals have been reported. There is no general consensus on the classification of radicals as stable or persistent. A stable radical is defined here as one that can be isolated and handled as a pure compound, while radicals that are sufficiently long lived to be observed using conventional spectroscopic techniques are persistent. This practical definition was put forth by Ingold, and has been widely adopted across the field of stable radical chemistry.[2]

1.2 Applications and uses of stable radicals

Radicals are often studied for their 'novelty', leading to widespread investigation of their fundamental bonding, structure, and properties. Other studies are application driven, i.e., radicals are used with specific properties and function in mind. Most applications associated with stable radicals exploit the combination of open-shell

configuration and chemical stability. The applications discussed here are representative of the uses of stable radicals, and are meant only to highlight the utility of stable radicals

1.2.1 EPR applications

Electron paramagnetic resonance (EPR) spectroscopy has long been used to gain structural, dynamic, and reactivity information in systems containing stable radicals. EPR spectroscopy is the paramagnetic analogue of nuclear magnetic resonance (NMR) spectroscopy. The detection limit of EPR spectroscopy is much lower than NMR spectroscopy, allowing for observation of paramagnetic species at concentrations as low as 10^{-9} M.[3]

Radicals are exploited as reporter molecules in techniques such as spin trapping, spin labeling, and EPR imaging. Spin trapping involves a reaction of a diamagnetic molecule (radical trap) with a highly reactive radical to generate a new persistent or stable radical.[4-7] Common spin traps include 2-methyl-2-nitrosopropane **1.1**,[8, 9] phenyl-*tert*-butyl nitrone **1.2**,[10] and 5,5-dimethyl-2-pyrroline-N-oxide **1.3**.[11, 12]

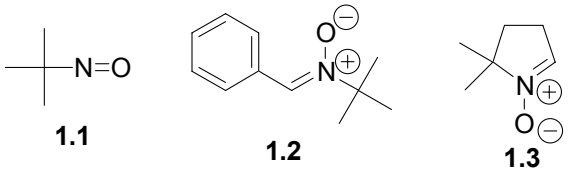

1.1 **1.2** **1.3**

An example of spin trapping by 5,5-dimethyl-2-pyrroline-N-oxide **1.3** is shown in Scheme 1.1, illustrating the production of a new radical species **1.4**. It should be noted that spin trapping provides little or no structural information about the trapped species as it is not observed directly, but does provide indirect evidence of the existence of the trapped species.

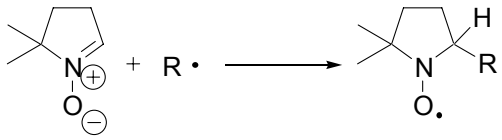

1.3 **1.4**

Scheme 1.1. Radical trapping using 5,5-dimethyl-2-pyrroline-N-oxide **1.3**.

Spin labeling is a technique used to study biological systems.[13] A stable radical is integrated into a biological system allowing for EPR spectra to be obtained, yielding information about the environment around the label (the radical), dynamic processes, and hydrophobicity/hydrophicicity.[14] Unfortunately the number of radicals that can be used as spin labels is severely limited by their compatibility with biological systems. Few radicals are soluble in aqueous media, and stable over broad pH and temperature ranges.

EPR imaging (EPRI) has emerged in the last two decades as a technique that can provide a wealth of information on systems where a stable radical has been introduced.[15-17] The technique allows for detection of paramagnetic species within a sample in three dimensions. Although the field is relatively new, it has been suggested that EPRI may act as an alternative and perhaps complementary technique to nuclear magnetic resonance imaging (NMRI or MRI) in the future.[18-20]

1.2.2 Magnetic and conducting materials

As electronic devices continue to decrease in size, there is increasing demand for new materials exhibiting improved properties compared to existing benchmarks, i.e., materials that are lighter, smaller, and easier to manipulate. At the heart of this issue are materials exhibiting magnetic and conducting properties due to their utility in virtually all electronic devices common to our lives.

Conventional magnetic materials are comprised of metals or alloys and oxides of cobalt, nickel, and iron. These materials are hampered by difficulty surrounding their manufacture as high temperature metallurgic routes are often required for their production. The materials produced do not offer significant opportunity to tune shape, size, and density, properties essential to decreasing the size of modern devices. Molecule-based magnets are attractive alternatives to conventional magnets as they have potential to allow for many of the properties described previously to be realized.

There are three basic approaches to molecule-based magnetism based on stable radicals. The first, radical crystals, relies on close intermolecular contacts between radicals in the solid-state. There are many examples of radical crystals that are ferromagnetic at cryogenic temperatures,[21-23] but there are no examples of such materials that display ferromagnetic properties near room temperature. A second approach to radical-based molecular magnets involves incorporation of stable radicals into polymers. Polymers with radicals tethered to the polymer backbone,[24-27] and those incorporating stable radicals into the polymer backbone have been reported.[28-30] Rajca has shown the latter strategy to result in polymers with large magnetic moments, confirming ferromagnetic coupling between radical subunits.[29] Perhaps the most promising approach to molecular magnetism is the metal-radical approach, which has yielded coordination networks of paramagnetic metal ions and stable radicals with magnetic properties at room temperature.[31-34] Advances in molecular magnetism based on the metal radical approach have brought radical-based magnetic materials into the limelight,[31, 32] improving the outlook on the possibility of such materials replacing conventional magnets in the future.

Haddon first envisioned neutral radical conductors in 1975 when he proposed neutral radicals as efficient charge carriers.[35] The neutral radicals required must be easily converted to related ions in order to propagate charge. As a result, ionization potential (IP), the energy associated with the loss of an electron from a stable radical species (R• → R^+ + *e*-), and electron affinity (EA), the energy associated with gaining an electron (R• + *e*- → R^-) are crucial factors in the design of neutral-radical conductors. In systems where the IP-EA are favorable, charged states are easily accessible, allowing for neutral radical conductors to be realized.[36-40]

1.2.3 Chemical reactivity

The development of a number of classes of stable radicals has allowed for the study of chemical reactivity associated with unpaired electrons to be observed under controlled conditions. Short lived, highly reactive radicals do not lend themselves to similar studies. Many reaction pathways open to reactive radicals have little or no kinetic barrier, and are thermodynamically favorable, making them very difficult to control.

Organic chemists have used stable radicals as (co)catalysts for the oxidation of alcohols to carbonyl compounds,[41-43] while other radicals have been used as antioxidants where the generation of a stable radical effectively shuts down decomposition pathways related to highly reactive radical species.[44-47] The coordination chemistry of stable radicals has captivated inorganic chemists for more than 30 years, resulting in metal complexes with interesting magnetic properties.[48-53] These properties are derived from the interaction between unpaired electrons at the metal center and the stable radical. In most cases the stable radical moiety is derivatized in order to create a chelating pocket, allowing for rapid coordination to metal centers.

Polymer chemists have benefited from the development of stable radical chemistry, often incorporating stable-radical-mediators into living radical polymerization processes.[54-56] Conventional living radical polymerization relies on reactive radicals attacking monomers to form chains of monomer (polymers) as in the polymerization of styrene. In general, the reactive radicals are susceptible to side reactions such as hydrogen abstraction and radical coupling, leading to branching and premature chain termination.

Stable-radical-mediated living radical polymerization has been used to afford high molecular weight polymers with narrow polydispersities.[57-59] The stable radical mediator does not initiate polymer growth, it reacts with the carbon centered radical, preventing its decomposition. For example, 2,2,6,6-tetramethyl-1-piperidinyloxyl (TEMPO) **1.5**, combines with a reactive polystyrene radical to form a dormant intermediate, i.e., hydrogen abstraction and radical coupling are prevented. The bond formed by the coupling of radical units is thermally labile, thus high reaction temperatures cause bond homolysis allowing for chain propagation to continue in a controlled environment (Scheme 1.2).

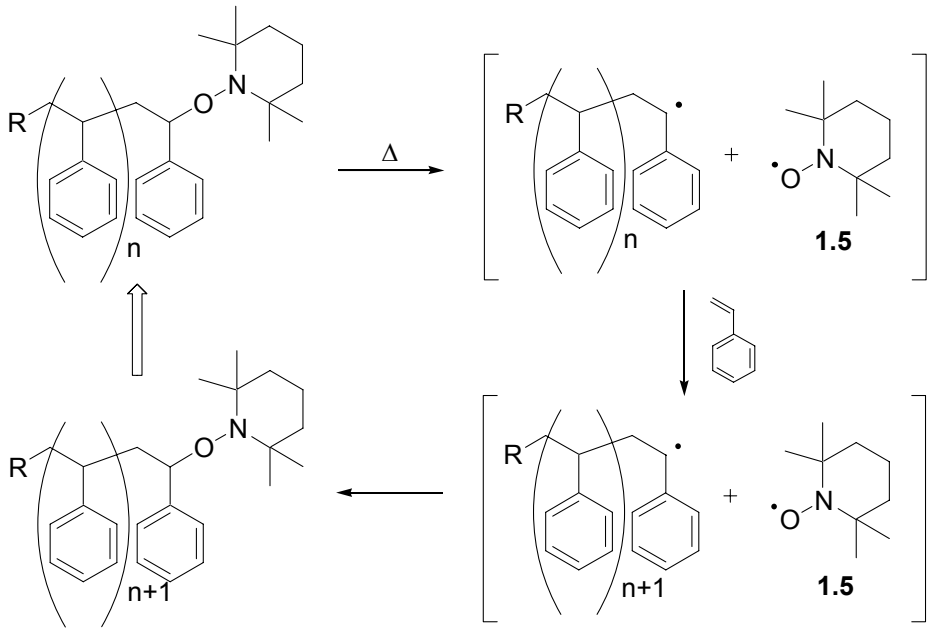

Scheme 1.2. Stable-radical-mediated living radical polymerization.

1.3 A survey of stable/persistent radicals

Stable radicals based on heavy main group elements are well known.[60] In most cases their stability is derived from the incorporation of bulky substituents in order to prevent radical decomposition. Stable radicals based on C, N, O, and S are often stable in the absence of steric bulk as a result of their unique electronic structures.[61] The following survey of stable radicals is meant to highlight some of the more common classes of stable radicals.

1.3.1 Triphenylmethyl radicals

Triphenylmethyl (trityl) radical **1.6** was accidentally made during the attempted reduction of triphenylchloromethane in the presence of zinc metal.[1] This radical is best described as persistent: in dilute, deoxygenated solutions it is in equilibrium with dimeric species **1.7** linked by a σ-bond between the central carbon of one radical and the *para*-phenyl carbon on another (not hexaphenyl ethane).

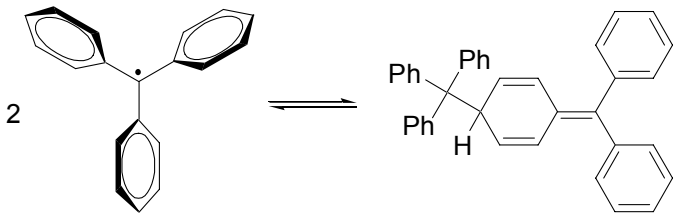

1.6 **1.7**

The existence of such a dimer is evidence that the unpaired electron does not reside on the central carbon exclusively, but is delocalized to the *ortho*- and *para*-phenyl positions (**1.6a-c**). The π-SOMO **1.8** reflects this delocalization, and is consistent with EPR studies that show larger hyperfine coupling for *ortho*- and *para*-hydrogens than for *meta*-hydrogens.[62-64]

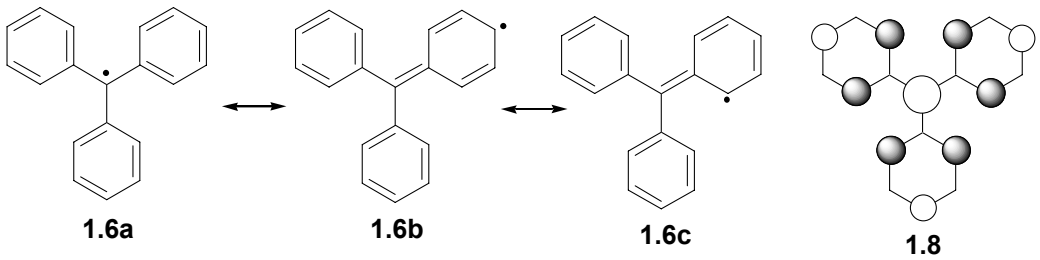

1.6a **1.6b** **1.6c** **1.8**

Efforts towards increasing the stability of trityl radicals have focused on blocking the *para*-phenyl positions involved in dimerization. Derivatives incorporating *para*-substituents **1.9** are monomeric in solution, although are still very sensitive to oxygen.[65, 66] The perchlorinated derivative, **1.10**, is not only monomeric in solution, but is not susceptible to oxidation. In fact, **1.10** is essentially chemically inert, except when subjected to extremely harsh reaction conditions.[67]

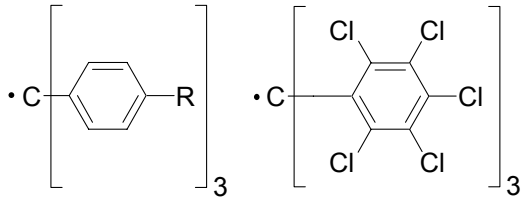

1.9 **1.10**

Many other polychlorinated trityl radicals have been reported, e.g., **1.11** and **1.12**, and display outstanding stability.[68] More recently, it has been shown that trityl radicals with chlorine atoms only at the *ortho*-positions **1.13** are also exceptionally stable.[69-71]

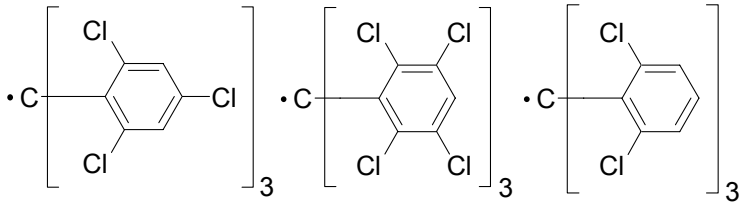

1.11 **1.12** **1.13**

1.3.2 Phenalenyl radicals

The first example of a phenalenyl radical was reported in the 1950s. Phenalenyl **1.14** was realized upon oxidation of phenalene.[72, 73] Radical **1.14** exists in equilibrium with σ-dimer **1.15**, bound through the α-carbons of two radicals.

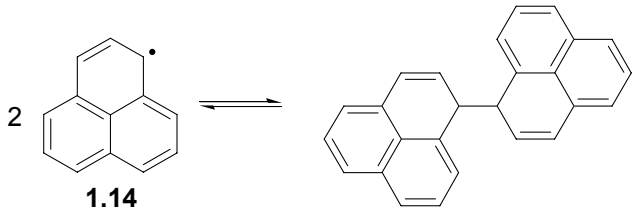

1.14 **1.15**

The unpaired electron is resonance delocalized (e.g., **1.14a-c**) over the six α-carbons in phenalenyl radicals, with very little spin density found on the central and *β*-carbons (see π-SOMO **1.16**).

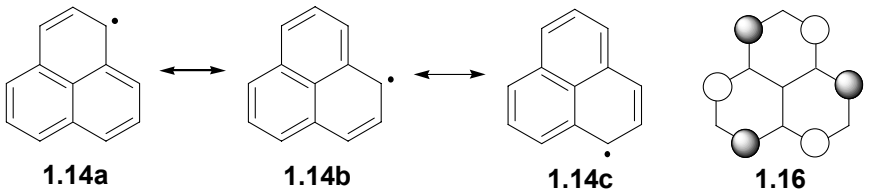

1.14a **1.14b** **1.14c** **1.16**

Introducing substituents at the β-carbon (**1.17**) renders phenalenyl radicals inert to σ-dimerization, however such radicals have been shown to form π-dimers $(\mathbf{1.17})_2$.[74-78] π-

Dimers are face-to-face associated radicals that result from bonding interactions between π-SOMO orbitals (Figure 1.1). The resulting dimers contain contacts between monomers shorter than associated van der Waals Radii, but longer than analogous σ-bonds. The perchlorinated derivative, **1.18**, is monomeric in both solution and solid-state.[79]

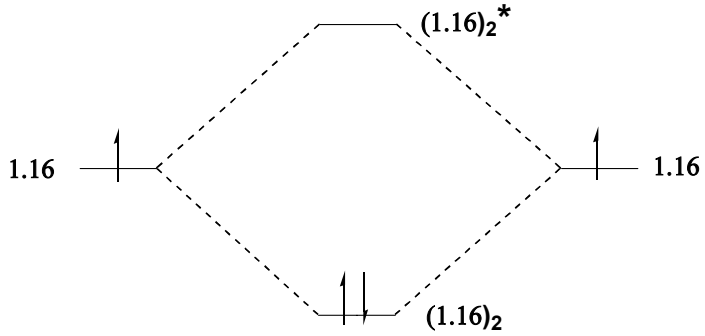

Figure 1.1. Orbital representation for π-Dimerization.

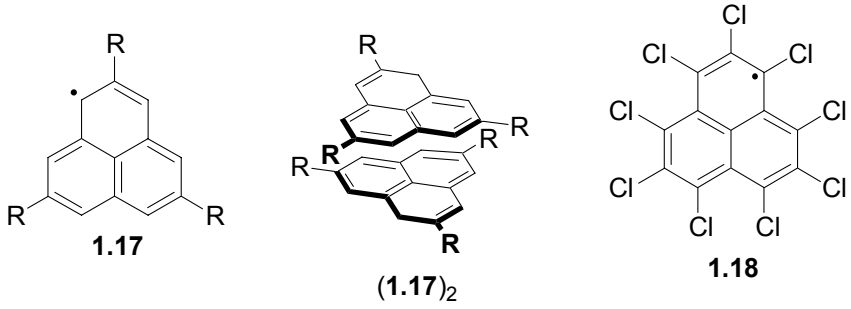

1.3.3 Phenoxyl radicals

Phenoxyl radicals **1.19** have been studied extensively.[80] It is widely recognized that *ortho*- and *para*-substituents must be present in order to prevent radical decomposition. Peroxide dimers **1.20** of phenoxyl radicals are not commonly observed, as a result of (i) lone pair repulsion between oxygen atoms, (ii) the presence of bulky *ortho*-substituents, and (iii) delocalization of the radical onto the phenyl ring.

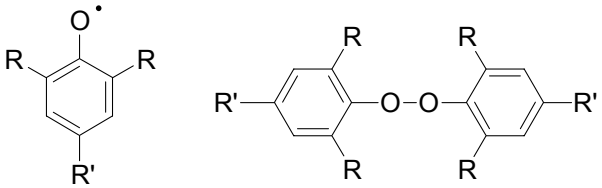

1.19 **1.20**

The unpaired electron is delocalized through resonance, such that the oxygen atom contains only marginally more spin density than the *ortho*- and *para*-carbons (**1.19a-c**) as shown in the π-SOMO **1.21**.

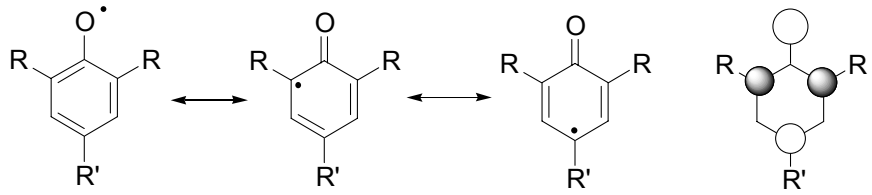

1.19a **1.19b** **1.19c** **1.21**

Among phenoxyl radicals, the galvinoxyl radical **1.22a**[81] has received much interest due to its unusual magnetic properties and exceptional stability.[82] Like conventional phenoxyl radicals, the galvinoxyl radical has been confirmed by computational methods to delocalize onto the *para*-phenyl positions of the phenoxyl ring through resonance (**1.22b**), implying that the radical has at least some allyl character.[83]

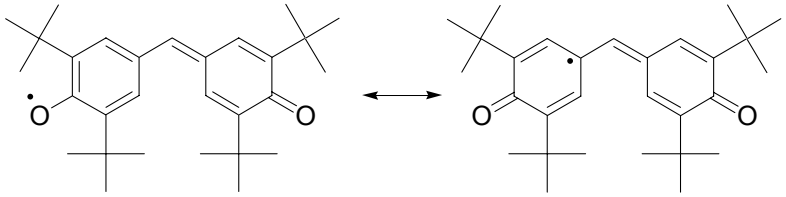

1.22a **1.22b**

1.3.4 Thioaminyl radicals

Miura has studied thioaminyl radicals **1.23** extensively.[84-93] Thioaminyl radicals are generally persistent, reversibly forming hydrazine-like dimers **1.24** in solution.[93] Incorporation of bulky N-substituents (e.g., triphenylmethyl,[85, 86] 2,4,6-trisubstituted

phenyl[90-93]) prevents dimerization, and allows for isolation of thioaminyl radicals stable towards moisture and oxygen.

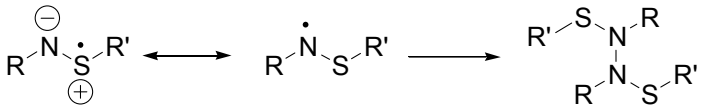

1.23 **1.24**

1.3.5 Dithiadiazolyl radicals

Among the first major classes of heterocyclic thiazyl radicals discovered were the 1,2,3,5-dithiadiazolyl (DTDA) radicals **1.25**. Considered as resonance delocalized thioaminyls, 1,2,3,5-DTDA radicals are stable indefinitely in deoxygenated solutions, and the solid-state (but see below). Furthermore, their thermal stability has been demonstrated through their purification by high vacuum, high temperature sublimation.

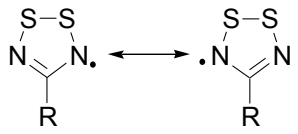

1.25

π-Dimers of 1,2,3,5-DTDA radicals exist in equilibrium with 1,2,3,5-DTDA monomers in solution. The mode of dimerization appears to be substituent dependent (Figure 1.2a,[94-99] Figure 1.2b,[100-102] Figure 1.2c,[96] and Figure 1.2d[103]). The closest intermolecular contacts within such dimers are between sulfur atoms at distances between 3.0-3.1 Å. These distances are between the van der Waals radii (~3.6 Å) and conventional S-S bonds (~2.1 Å). The only monomeric 1,2,3,5-DTDA radicals bear fluorinated phenyl substituents.[104-108]

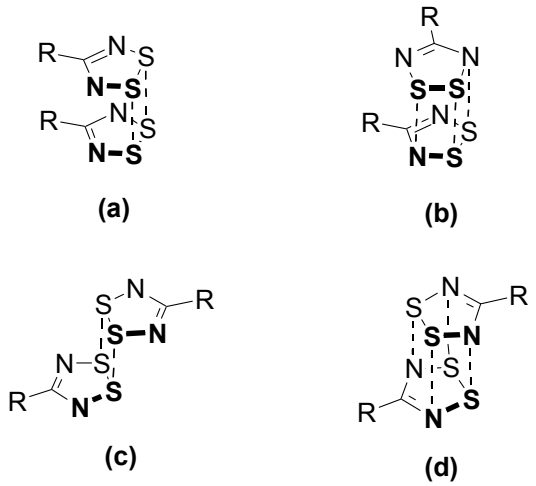

Figure 1.2. π-Dimerization modes of 1,2,3,5-Dithiadiazolyl radicals.

1,3,2,4-DTDA radicals **1.26** are isomers of 1,2,3,5-DTDA radicals. They display decreased thermodynamic stability compared to 1,2,3,5-DTDA radicals as evidenced by their conversion to the 1,2,3,5-isomer in solution and the solid-state.[109-112] The conversion has been shown to occur via a bimolecular rearrangement pathway, implicating π-dimers $(\mathbf{1.26})_2$ and $(\mathbf{1.25})_2$ as intermediates *en route* to monomers **1.26** and **1.25** (Scheme 1.3).

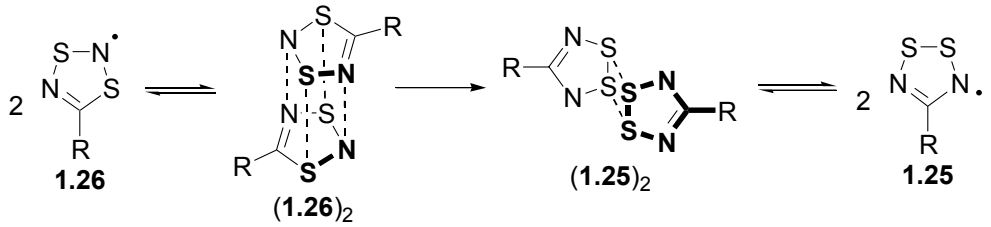

Scheme 1.3. Rearrangement of 1,3,2,4-dithiadiazolyls to 1,2,3,5-dithiadizolyls.

1.3.6 Dithiazolyl radicals

There are two kinds of dithiazolyl (DTA) radicals based on the C_2NS_2 framework. 1,3,2-DTA radicals **1.27** are stable in solution and the solid-state leading to extensive studies of their solid-state structures[113-116] and solution EPR spectra.[117-121] Most 1,2,3-

DTA radicals **1.28** are only persistent in solution and can not be isolated. However in the past decade Oakley has developed several stable derivatives shown to exist as a variety of solid-state structures involving π-stacking modes similar to those shown in Figure 1.2.[122-126] An exceptionally stable family of resonance delocalized 1,2,3-DTA radicals known as dithiazolodithiazolyl radicals **1.29**, have also been developed by Oakley. With the exception of one example,[127] dithiazolodithiazolyl radicals are monomeric in solution and solid-state.[127-130]

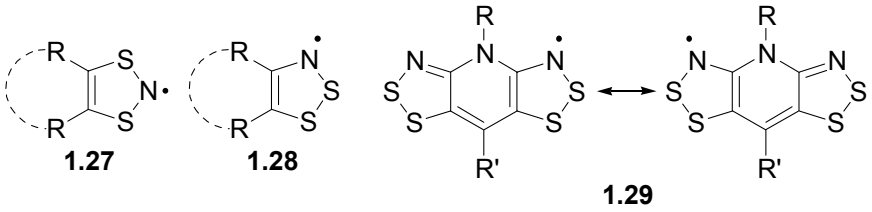

1.3.7 Thiatriazinyl radicals

1,2,4,6-thiatriazinyl radicals **1.30** form cofacial dimers in the solid-state $(\mathbf{1.30})_2$.[131-133] However, solid-state structures reveal appreciable σ-bond character between sulfur atoms (S-S ~2.66 Å). The short S-S bond distance relative to all other contacts in the cofacial dimers, as well as bowing of the thiatriazinyl rings relative to one another does not allow for $(\mathbf{1.30})_2$ to be classified as a true π-dimer.

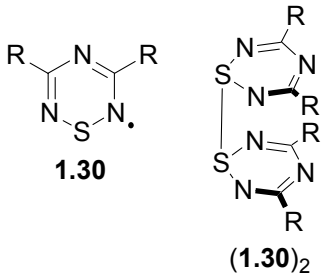

1.3.8 Nitroxide and nitronyl-nitroxide radicals

By far the most common class of stable radicals are the nitroxides **1.31.**[134-136] Fremy's salt **1.32**,[137] an inorganic nitroxide, was the first discovered. The first organic derivative **1.33** followed shortly after the discovery of trityl radicals.[138]

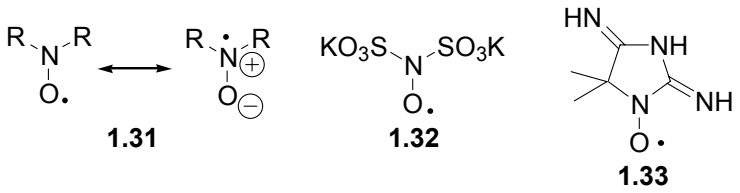

1.31 **1.32** **1.33**

Nitroxides have substantial spin density on both nitrogen and oxygen. σ-Dimers of nitroxides are unknown, demonstrating their inherent stability. The peroxide bond is very weak as a result of lone pair repulsion associated with the N-O-O-N heteroatom chain. The overall stability of nitroxides depends on the N-substituents and the tendency of the radical to decompose via disproportionation. Nitroxide radicals with alkyl substituents containing α-hydrogen atoms, e.g., **1.34**, may decompose to nitrones **1.35** by transferring H• to another nitroxide radical giving hydroxylamine **1.36** as the second byproduct.

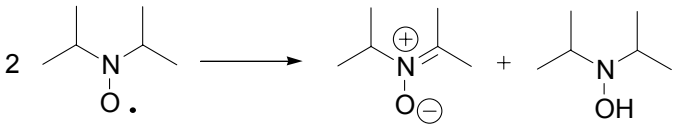

1.34 **1.35** **1.36**

Nitroxide radicals bearing N-substituents that do not contain α-hydrogen atoms are stable with respect to oxygen, water, and dimerization and can be stored indefinitely. As a result, several derivatives are commercially available, e.g., *tert*-butyl nitroxide **1.37** and TEMPO **1.5.**

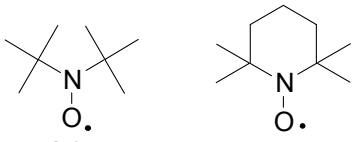

1.37 **1.5**

Nitronyl nitroxides **1.38** are considered as resonance delocalized nitroxide radicals. In the time since their discovery,[139] they have been shown to exhibit many of the stability characteristics common to nitroxide radicals, and their electronic structures have been studied extensively.[48] The unpaired electron resides mainly on the oxygen and nitrogen atoms and very little spin density is found on the R-substituent due to the presence of a nodal plane in the π-SOMO **1.39**. However, studies of benzannelated analogues **1.40** have indicated at least partial delocalization of the unpaired electron onto the annelated ring.[140, 141]

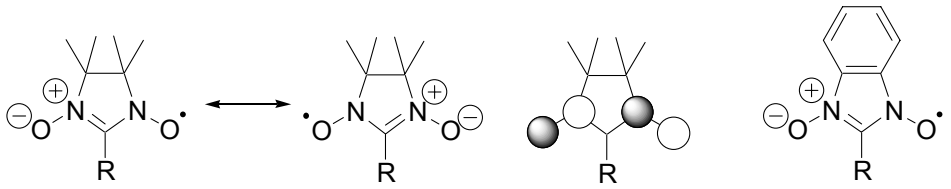

1.38 **1.39** **1.40**

1.3.9 Hydrazyl radicals

N,N'-Diphenyl-N'-picrylhydrazyl (DPPH) **1.41,** an indefinitely stable radical, has been used as an EPR reference compound for decades.[134] Other hydrazyl radicals **1.42** are only persistent in solution. The stability of DPPH relative to other hydrazyl radicals is enhanced by the presence of electron-withdrawing groups on the divalent nitrogen, which serve to enhance charge separated resonance contributions.

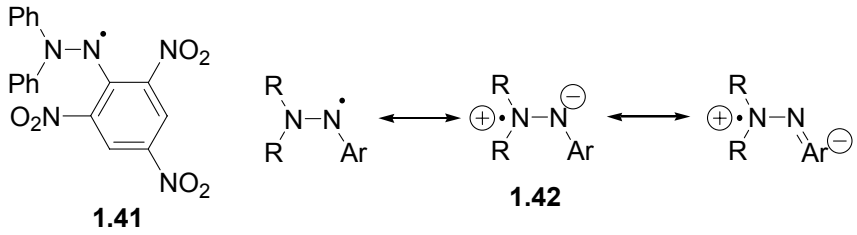

1.41 **1.42**

1.3.10 Verdazyl radicals

Verdazyl radicals are the only class of radicals with stability rivaling that of the nitroxides. The first examples of type I verdazyls **1.43**[142] were discovered during the attempted alkylation of formazans **1.44**, while the first type II verdazyls **1.45** were synthesized in the 1980s.[143, 144]

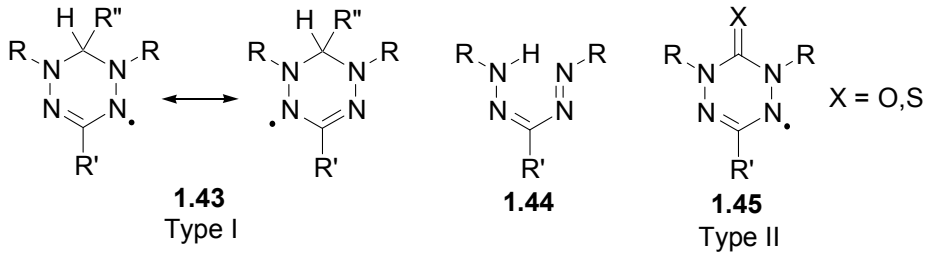

1.43 Type I **1.44** **1.45** Type II

Verdazyl radicals are, in essence, resonance stabilized hydrazyl radicals that can be isolated, stored, and handled without decomposition. They do not associate, or dimerize. However, a ferrocene bridged verdazyl diradical **1.46** has recently been reported to exist as an intramolecular π-dimer in the solid-state.[145] The π-dimer does not exist in solution, suggesting that the solid-state structure may be due in part to intermolecular packing effects.

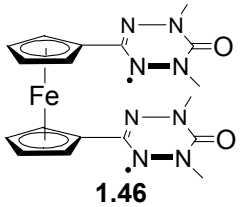

1.46

The N-substituents on type I verdazyls are limited to aromatics (R = Ar),[142] while type II verdazyls bearing alkyl and aryl (R = Me,[143, 144, 146-148] iPr,[149] Ph[150]) N-substituents have been reported. Recently, it has been shown that verdazyls with N-*iso*propyl substituents are more stable than their N-methyl counterparts.[149] EPR spectra[151-156] and magnetic properties[157-161] of early examples have been studied extensively, while recent efforts have focused on their use as ligands for transition metals,[162] and building blocks for molecule-based magnetic materials.[53]

Efforts towards incorporation of inorganic elements into the verdazyl backbone have resulted in the synthesis of phosphaverdazyls **1.47**,[163, 164] **1.48**,[163, 164] and **1.49**.[165] Phosphaverdazyls have similar electronic structure compared to parent organic systems. However, the few derivatives which have been studied to date are only persistent in solution and the solid-state, decaying to diamagnetic compounds over extended periods of time.

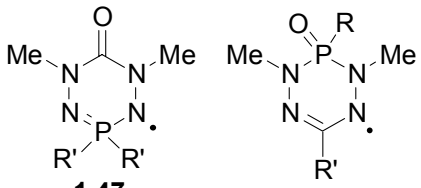

1.47

1.48

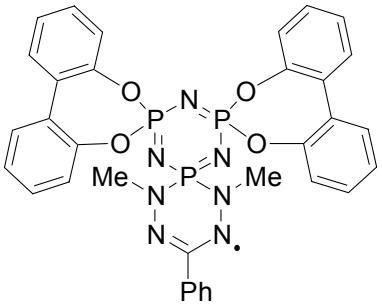

1.49

1.4 Thesis objectives

Although there are thousands of research papers highlighting their syntheses and properties, relatively few reports of research aimed specifically at the design of new, stable radicals exist. In fact, most families of stable radicals were discovered by accident.

Research in the Hicks group has previously focused on the magnetochemistry of verdazyl-based systems,[146, 148, 162, 166-170] or the design and synthesis of new verdazyl radicals.[145, 147, 163-165] The goal of this thesis was to design and explore different aspects of verdazyl radical chemistry towards development of a structure-property relationship in a variety of verdazyl-based systems.

Chapter 2 describes the synthesis and characterization of a number of type I and type II verdazyl radicals. The electrochemical properties of such verdazyls were explored in detail, emphasizing substituent effects as well as the differences between type I and type II verdazyls.[171]

Chapter 3 describes the synthesis, characterization, and properties of the first main group complexes of formazans *en route* to borataverdazyl radical anions.[172] A number of 3-cyano- and 3-nitroformazans were synthesized as second generation formazan ligands and their properties explored.[173] The coordination chemistry of 3-substituted formazans was also explored, establishing a correlation between steric bulk at the N-substituents and the structure of resulting transition metal complexes.[174] The ability of formazans to mimic β-diketimates as ligands was illustrated. The properties of metal formazan complexes were also studied in detail to assess their utility as precursors to metallaverdazyls.[175]

Chapter 4 describes communication between unpaired electrons in which one (or both) spins are verdazyl radicals. The properties of verdazyl diradicals were explored in detail, focusing on the effects of radical communication through *meta*- and *para*-benzene linkers on spectral and magnetic properties.[176] Verdazyl radicals were also coordinated

to copper (II) salts and the magnetostructural properties of the resulting complexes explored.[177]

Chapter 2 Synthesis and redox properties of verdazyl radicals

2.1 Electrochemical properties of stable radicals

As outlined in Chapter 1, stable radicals are used in many applications associated with their unpaired electron(s). Many of the applications relate directly to the presence of an unpaired electron, but others take advantage of the redox chemistry of stable radicals. The redox properties of stable radicals are studied using a variety of electrochemical techniques, and relate directly to their use in electron-transfer chemistry,[178-180] their efficacy as building blocks for single-component molecular conductors,[130, 181, 182] and their use in organic-based batteries.[183-189]

The electrochemical properties of open shell molecules must be considered differently than closed shell molecules. In closed shell molecules, oxidation involves loss of an electron from the highest occupied molecular orbital (HOMO), while reduction involve addition of an electron to the lowest unoccupied molecular orbital (LUMO). In open shell molecules, oxidation and reduction involve loss or gain of an electron from the singly occupied molecular orbital (SOMO) as depicted in Figure 2.1.

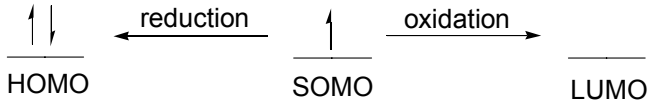

Figure 2.1. Oxidation and reduction of a neutral radical.

There have been many reports on the electrochemical properties of organic radicals.[190-200] However, few systematic studies have been reported with the exception of a limited series of nitroxide radicals;[201] the limited number of derivatives available for this study may relate to difficulties in derivitizing the nitroxide moiety. In contrast,

verdazyl radicals are relatively easily derivatized, allowing for the systematic study of substituent effects and changes in structure on electrochemical properties presented here.

2.2 Existing syntheses of verdazyl radicals

The first verdazyl radical was reported in 1964 by Kuhn and Trischmann.[202] Their serendipitous discovery occurred during the attempted alkylation of 1,3,5-triarylformazans **2.1**. The *leuco*-verdazyls **2.2** generated were spontaneously air-oxidized affording corresponding 1,3,5-triarylverdazyl (type I) radicals **2.3** (Scheme 2.1). Since then, a number of modifications to this synthesis have been reported, generally varying the base as well as the source of bridging carbon.[203, 204]

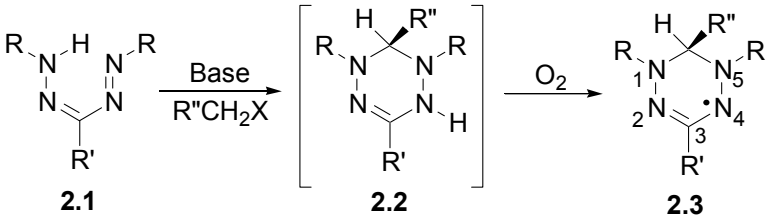

Scheme 2.1. Synthesis of 1,3,5-triarylverdazyls.

The synthesis and properties of 1,3,5-triaryl-6-oxoverdazyls (type II) **2.4** have also been reported.[150] Their synthesis is based on the reaction of diarylhydrazones **2.5** with phosgene to afford diarylcarbamoyl chlorides **2.6**, which can be subsequently reacted with arylhydrazines to yield 1,3,5-triaryl-1,2,4,5-tetrazane-6-oxides (tetrazanes) **2.7**. The tetrazanes are then oxidized to verdazyl radicals using PbO_2 (Scheme 2.2).

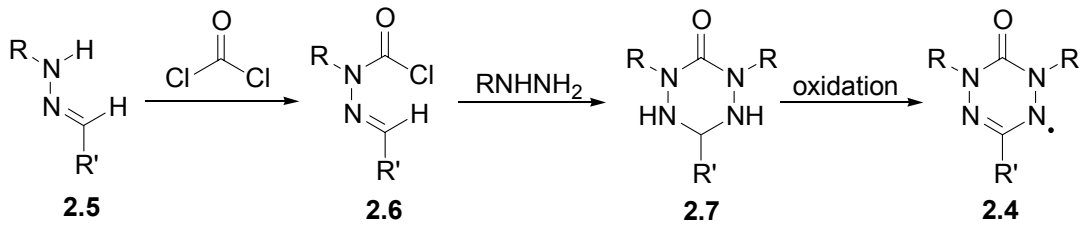

Scheme 2.2. Synthesis of 1,3,5,-triaryl-6-oxoverdazyls.

The chemistry of 1,5-dialkyl-6-oxoverdazyls (type II) has been studied extensively.[143, 144, 149] These verdazyls are prepared by reaction of carbonic acid bis(1-alkylhydrazide)s **2.8** with aldehydes to afford the corresponding tetrazanes **2.7** which can be oxidized to afford corresponding verdazyl radicals by a variety of oxidizing agents, e.g., $NaIO_4$, *para*-benzoquinone, PbO_2, or $K_3[FeCN_6]$(Scheme 2.3).

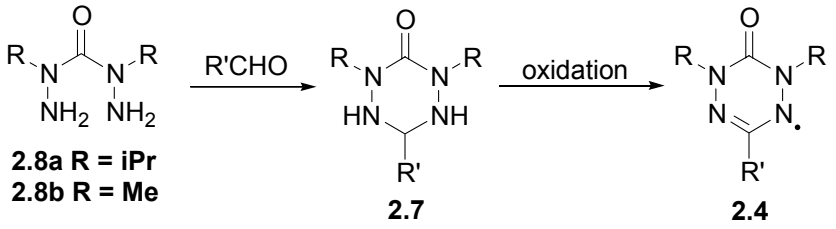

Scheme 2.3. Synthesis of 1,5-dialkyl-6-oxoverdazyls.

Similar methodologies have been employed in the synthesis of phosphaverdazyls. Reaction of carbonic acid bis(1-methylhydrazide**)** **2.8b** with trichloro-diphenylphosphorane afforded 1,2,3,5-tetraza-3-phosphorine **2.9**, which was oxidized by I_2 to yield phosphaverdazyl **2.10** (Scheme 2.4).[163] Phosphorus has also been incorporated into the bis-hydrazide moiety providing an alternative pathway to phosphaverdazyls.[163, 164] Phenylphosphonic acid bis(1-methylhydrazide) **2.11** was reacted with trimethyl orthobenzoate to yield 1,2,4,5-tetraza-6-phosphorine **2.12**. Oxidation with tetrabutylammonium periodate afforded phosphaverdazyl **2.13** (Scheme 2.5).

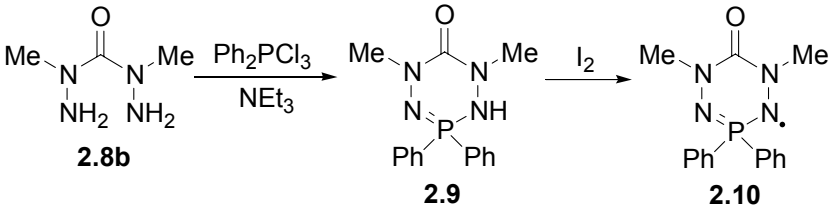

Scheme 2.4. Synthesis of phosphaverdazyls from carbonic acid bis(1-methylhdrazide).

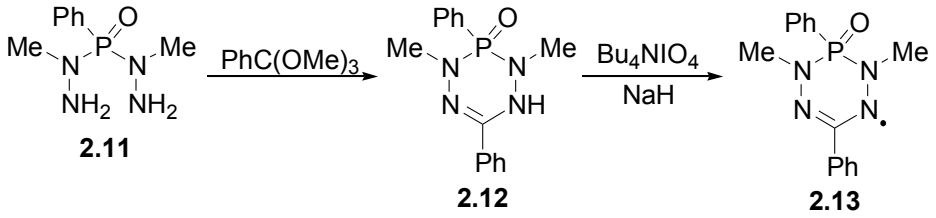

2.11 **2.12** **2.13**

Scheme 2.5. Synthesis of phosphaverdazyls from phenylphosphonic acid bis(1-methylhydrazide).

Results and discussion

2.3 Synthesis and characterization of triarylformazans

Triarylformazans **2.1**, known for their use as dyes,[205, 206] were discovered over a century ago and have been studied extensively since 1941.[207] The blood red compounds exist as *pseudo* six-membered rings with a bridging proton acting to enhance delocalization of the π-system through resonance. Although more than 1000 derivatives have been reported, there are few reports of subsequent chemistry. Formazans have been used sporadically as ligands, e.g., bis-formazan complexes of palladium **2.14a** and nickel **2.14b**,[208, 209] and the conversion of formazans to tetrazolium salts **2.15** has been studied extensively, due to their utility as redox-based stains for cell biology.[210]

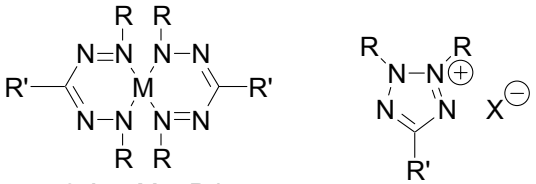

2.14a M = Pd
2.14b M = Ni

2.15

The most common method used to produce triarylformazans is the action of diazonium salts on diarylhydrazones **2.5** under basic conditions (Scheme 2.6).[211] Diarylhydrazones are prepared via the reaction of ayrlhydrazines and arylaldehydes in alcoholic solution. The diazonium salts are generated *in situ* via the reaction of the

appropriate amine with nitrous acid. The utility of this route is limited by the availability and stability of the specific arylhydrazine and aryldiazonium reagents.

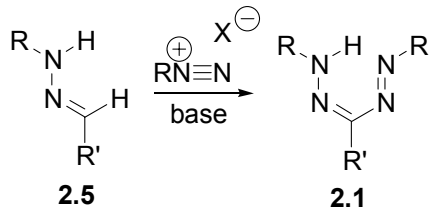

2.5 **2.1**

Scheme 2.6. The action of diazonium salts on diarylhydrazones.

Alternative syntheses do not rely on the use of diazonium salts, for example, the reaction of halogenated hydrazones **2.16** with arylhydrazines to afford formazans **2.1** (Scheme 2.7).[212] Similarly the reaction of two equivalents of arylhydrazine with benzotrichloride **2.17** has been reported to produce triarylformazans (Scheme 2.8).[213, 214]

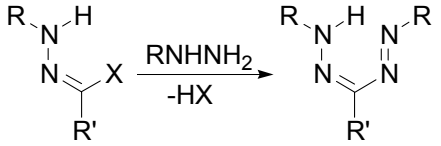

2.16 **2.1**

Scheme 2.7. The action of hydrazines on chlorinated hydrazones.

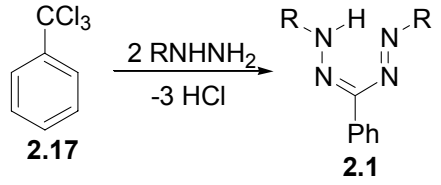

2.17 **2.1**

Scheme 2.8. The action of hydrazines on benzotrichloride.

Most reports on formazans originate in the early 1900s, preceding modern characterization techniques. As a result, there is relatively little known about their properties. However, the common feature of all formazans is their intense colour, which allowed chemists to identify them over 100 years ago. The formazans reported here were

studied primarily for their utility as precursors to type I verdazyl radicals, but also provide an opportunity to update their characterization. The properties of type I verdazyl radicals synthesized from formazans were studied in detail, and compared to a variety of type II verdazyls. Particular emphasis was placed on their electrochemical properties and electronic structure.

The triarylformazans described here (Scheme 2.9) were synthesized according to literature procedures under biphasic conditions via the coupling reaction of an aryldiazonium chloride salt with arylhydrazones in the presence of base.[211] Many of these compounds have been reported previously, however their characterization was often incomplete or incorrect.

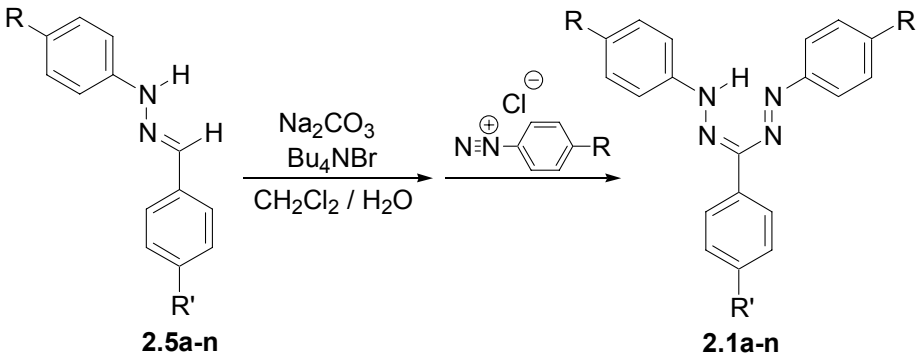

a R = H, R' = H
b R = OMe, R' = Me
c R = Me, R' = Me
d R = H, R' = Me
e R = Cl, R' = Me
f R = CN, R' = Me
g R = NO_2, R' = Me
h R = CF_3, R' = Me
i R = Me, R' = OMe
j R = Me, R' = H
k R = Me, R' = Cl
l R = Me, R' = CN
m R = Me, R' = NO_2
n R = Me, R' = CF_3

Scheme 2.9. Synthesis of triarylformazans **2.1a-n**.

This method proved versatile in establishing a family of formazans **2.1a-n**. However, derivative **2.1g** could not be isolated as a pure compound, perhaps due to reactivity associated with the electron-withdrawing nature of the N-substituents.

2.3.1 Solution properties of triarylformazans

Triarylformazans are easily identified in solution by their ^{1}H NMR and electronic spectra. The bridging proton has a characteristic chemical shift between δ 14.69 and 15.81 ppm for **2.1a-n**. The delocalized nature of triarylformazans in solution renders the two N-substituents equivalent (when they are the same). A representative ^{1}H NMR spectrum for **2.1j** is shown in Figure 2.2.

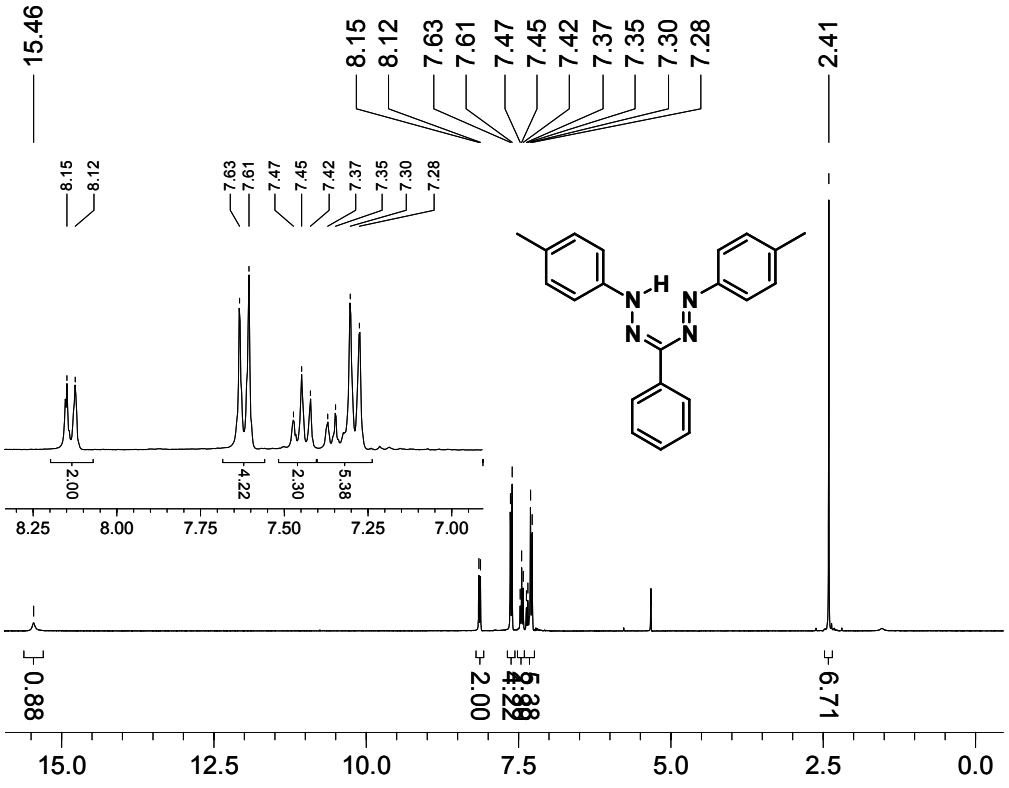

Figure 2.2. ^{1}H NMR of **2.1j** in CD_2Cl_2.

The electronic spectra of formazans have absorption maxima in the region of 483-538 nm for **2.1a-n** corresponding to intramolecular charge transfer processes that likely involve π-π* transitions between the formazan chromophore and aryl substituents. The λ_{max} values for **2.1a-n** do not follow a predictable trend with the donor/acceptor ability

through the entire range of aryl substituents. However, it is worth noting that electron rich formazans such as **2.1b** (λ_{max} = 538 nm) are red shifted compared to electron poor formazans such as **2.1h** (λ_{max} = 497 nm). The electronic spectrum for **2.1j** is shown in Figure 2.3 as a representative example.

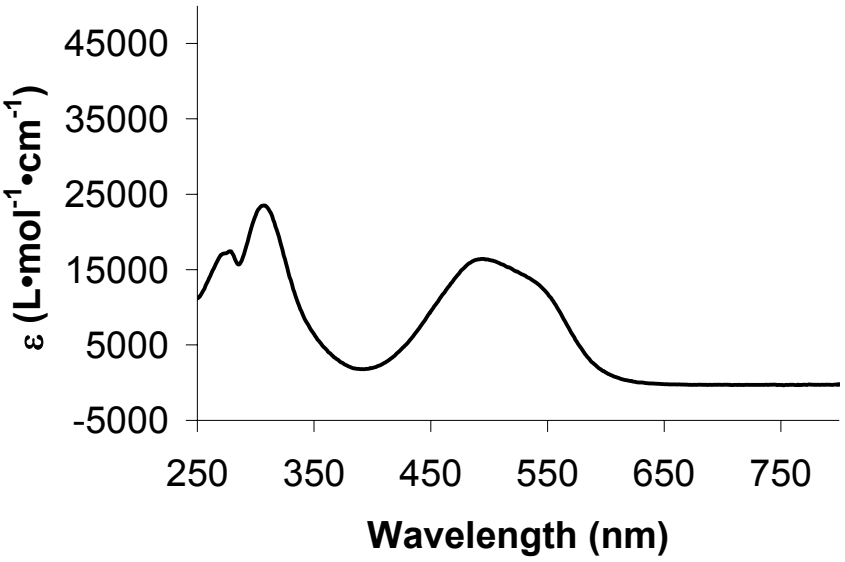

Figure 2.3. Electronic spectrum of **2.1j** in CH_2Cl_2.

2.3.2 Solid-state properties of triarylformazans

Few crystal structures of 1,3,5-triarylformazans have been reported. Existing examples possess heteroatoms in their N-substituents,[215-217] or fixed orientation.[218] The molecular structures of **2.1d** and **2.1j**, presented in Figure 2.4, are the first crystallographically characterized triphenylformazans. **2.1j** exists as a *pseudo* six-member ring with the N2-N1-C1-N3-N4 backbone significantly delocalized (N2-N1 1.318(4) Å, N3-N4 1.311(4) Å, N1-C1 1.350(4) Å, and N3-C1 1.364(5) Å), i.e., the bond lengths are between those expected for N-N and C-N single and double bonds (N-N ~ 1.40 Å, N=N ~ 1.24 Å, C-N ~ 1.49 Å, and C=N ~ 1.28 Å).[219] The 1,3,5-aryl substituents

are nearly coplanar with torsion angles of 6.61º (ring attached to N4), 2.64º (ring attached to N2), and 2.81º (ring attached to C1). The structure of **2.1d** has similar structural features (see Table 2.1), however the proton attached to N2 was allowed to refine freely in **2.1d**, differing from the crystallographically located N-H in **2.1j**. The crystallographic properties observed here are consistent with those reported in other structurally characterized 1,3,5-triarylformazans.[215-218]

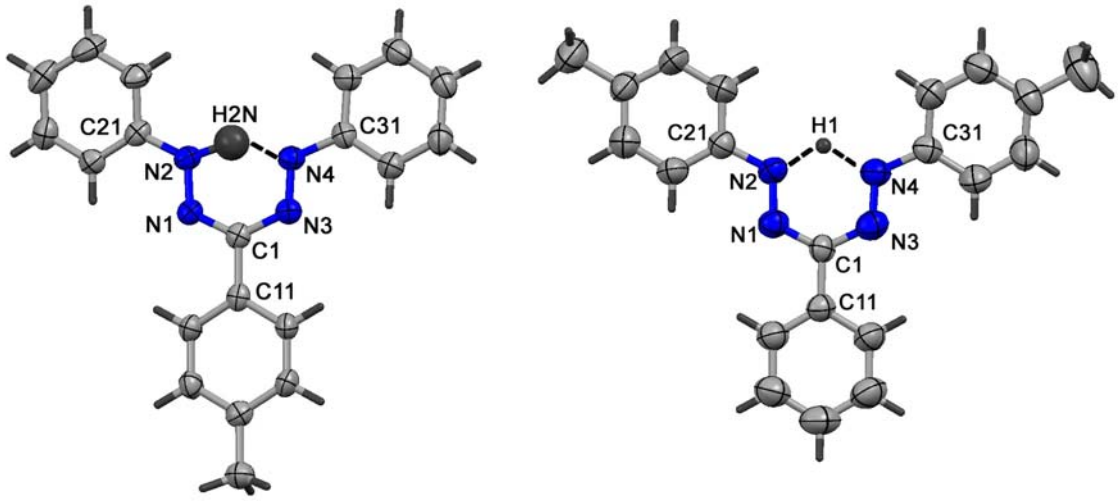

Figure 2.4. Molecular structure of **2.1d** (left) and **2.1j** (right). Thermal ellipsoids shown at 50% probability level.

Table 2.1. Selected bond lengths (Å) and bond angles (deg) for **2.1d** and **2.1j**.

Atoms	**2.1d**	**2.1j**	Atoms	**2.1d**	**2.1j**
N1-N2	1.3123(19)	1.318(4)	C21-N2-N1	118.78(15)	118.1(3)
N3-N4	1.2859(19)	1.311(4)	C31-N4-N3	116.09(15)	117.9(3)
C1-N1	1.338(2)	1.350(4)	N2-N1-C1	118.65(15)	118.4(3)
C1-N3	1.373(2)	1.364(5)	N4-N3-C1	118.36(14)	119.2(3)
			N1-C1-N3	128.39(15)	127.0(3)

2.4 Synthesis and characterization of type I verdazyl radicals

The 1,3,5-triarylverdazyls reported here were prepared according to literature procedures via the reaction of formazans with formaldehyde in the presence of base,

followed by spontaneous air-oxidation of the *leuco*-verdazyl (Scheme 2.10).[204] Although this proved to be a versatile synthesis, there were some limitations. Verdazyl radicals could not be made when electron withdrawing substituents (e.g., cyano, nitro, and trifluoromethyl) were introduced. There are two possible reasons behind the failure to make verdazyls with strong electron withdrawing substituents: either molecular oxygen is not a strong enough to oxidize the *leuco*-verdazyl, or the *leuco*-verdazyl species is not formed in the first place. Addition of oxidizing agents such as sodium periodate did not result in the production of verdazyls, supporting the latter hypothesis.

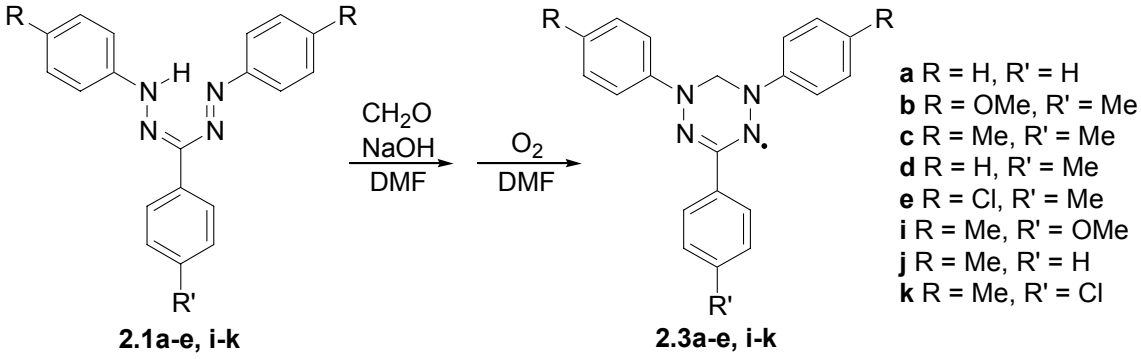

Scheme 2.10. Synthesis of triarylverdazyls **2.3a-e, i-k**.

2.4.1. Crystal structure of verdazyl 2.3j

The molecular structure of **2.3j** is shown in Figure 2.5. **2.3j** has a mirror plane down the center of the molecule along the axis formed by C1-C2-C21. The alkyl bridge (C1) lies 0.614 Å above the plane of the verdazyl (N1-N2-C2-N2*-N1*) causing the N-substituents to bend out of the plane of the verdazyl by 33.43º. These structural features are consistent with other reports on the structure of type I verdazyls.[220-223]

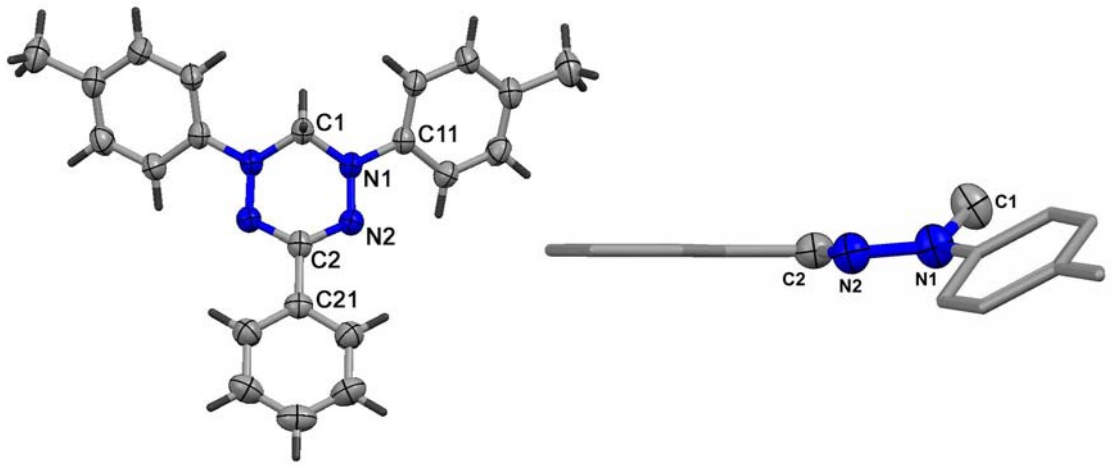

Figure 2.5. Molecular structure of **2.3j**. Top view (left) and side view (right). Thermal ellipsoids shown at 50% probability level.

Table 2.2. Selected bond lengths (Å) and angles (deg) for **2.3j**.

Atoms	**2.3j**	Atoms	**2.3j**
C2-N2	1.3351(19)	N2-C2-N2'	127.0(3)
N2-N1	1.355(2)	C2-N2-N1	114.71(17)
N1-C1	1.453(2)	N2-N1-C1	117.93(17)
		N2-N1-C11	117.08(15)
		C1-N1-C11	121.89(17)

2.4.2 Magnetic properties of verdazyl 2.3j

The magnetic properties of **2.3j** were investigated from 2-300 K on several independent samples, confirming the reproducibility of the data. Inspection of Figure 2.6 reveals a room temperature magnetic moment of 0.398 emu•K•mol^{-1}, slightly higher than the spin only value of 0.375 emu•K•mol^{-1}. As the temperature is lowered, the χT product gradually decreases near room temperature, before increasing to a value of 0.392 emu•K•mol^{-1} at 182 K. This behavior may be indicative of structural changes, although a room temperature crystal structure (from the same batch of crystals) of **2.3j** was isostructural to that determined at 193 K.

When the use of a specific magnetic model cannot be justified—dimers, chains, or other obvious repeating patterns are not present—the Curie-Weiss law (Equation 2.1) is employed in order to describe structurally unspecified intermolecular interactions between radicals.[224] The Curie-Weiss law (and all other magnetic models from this point forward) incorporates Avagadro's number (N), the g factor (g), the Bohr magneton (β), the Boltzmann constant (k), temperature (T), and spin quantum number (S).

$$\chi = \frac{Ng^2\beta^2}{3k(T-\theta)}\big(S(S+1)\big) \qquad (2.1)$$

The constants are combined to yield Equation 2.2 where C is the Curie constant ($Ng^2\beta^2/3k$) and θ is the Weiss constant used to account for intermolecular interactions.

$$\chi = \frac{C}{(T-\theta)} \qquad (2.2)$$

The straight line obtained yielded C = 0.392 emu•K•mol^{-1}, θ = -0.58 K and R^2 = 0.9998. The small negative Weiss constant is consistent with weak antiferromagnetic coupling between radicals, common to organic radicals with no appreciable mechanism for magnetic coupling.[224]

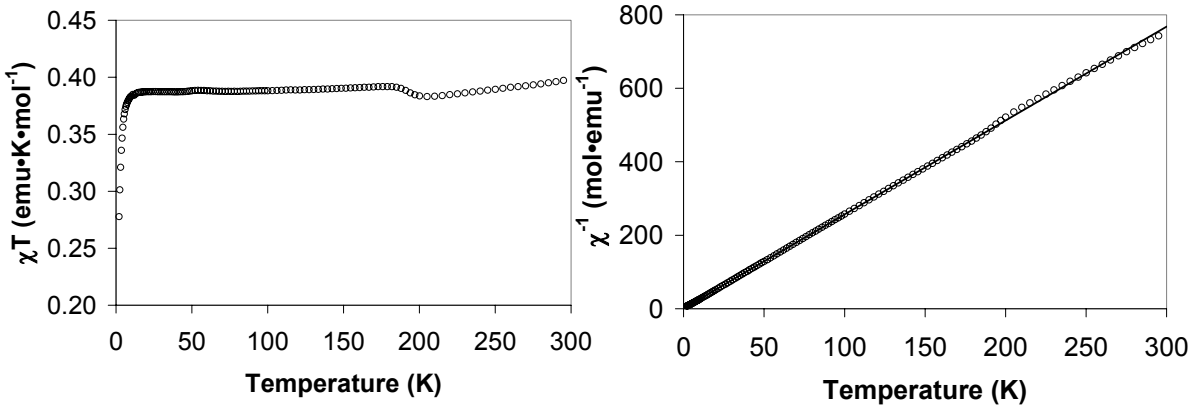

Figure 2.6. Magnetic data of **2.3j**. χT vs T (left) and χ^{-1} (right). Experimental data (○) and data fit (black line).

2.5 Electrochemistry of triarylverdazyls (type I) verdazyl radicals

The electrochemical properties of verdazyl radicals **2.3a-e**, **i-k** were studied using cyclic voltammetry; data is summarized in Table 2.3. The oxidation ($E_{ox}°$) and reduction ($E_{red}°$) half potentials are the average of the related anodic and cathodic peaks for a given redox process, and the cell potential (E_{cell}) is the difference between the oxidation and reduction half potentials. The cyclic voltammograms (CVs) of verdazyl radicals are generally comprised of two reversible waves, the higher potential wave corresponding to the oxidation of the verdazyl radical, and the lower potential wave the reduction. The reversibility of the waves is a testament to the stability of the cationic species (6π *e*-) present at more positive potentials and the anionic species (8π *e*-) present at more negative potentials (Figure 2.7).

Table 2.3. Electrochemical properties of verdazyl radicals reported in V vs Fc/Fc^+. [a]Irreversible process, cathodic peak potential reported.

Compound	$E_{ox}°$	$E_{red}°$	E_{cell}
2.3a	-0.22	-1.23	1.01
2.3b	-0.39	-1.33	0.94
2.3c	-0.31	-1.29	0.99
2.3d	-0.24	-1.26	1.02
2.3e	-0.15	-1.14	0.98
2.3i	-0.30	-1.26[a]	n.a.
2.3j	-0.29	-1.27	0.98
2.3k	-0.26	-1.26	1.00

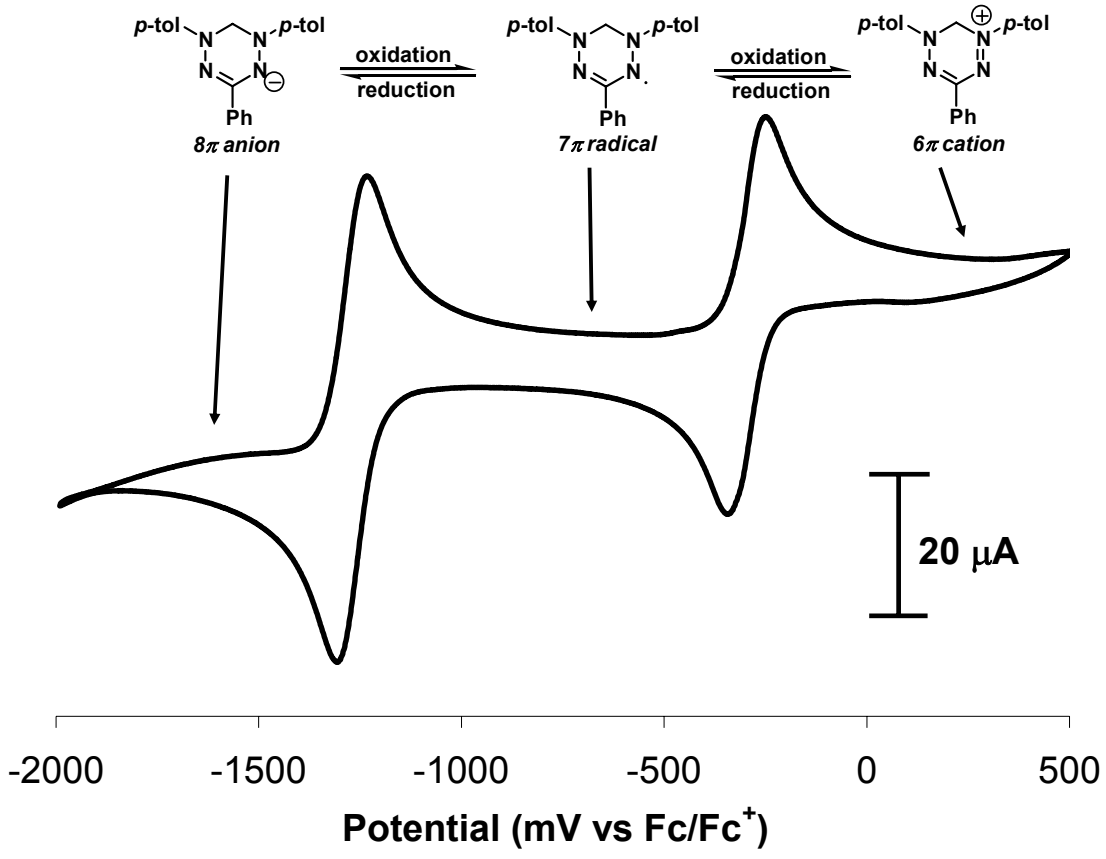

Figure 2.7. Cyclic voltammogram of **2.3j** in CH_3CN containing 0.1 M $Bu_4N^+BF_4^-$ (electrolyte). Scan rate 100 mV/s.

The reversibility of electrochemical processes was confirmed by the following observations: (i) the anodic:cathodic peak current ratios were approximately 1; (ii) peak potentials were independent of scan rate (Figure 2.8); and (iii) the peak separations were consistent with the ferrocene/ferrocenium redox couple under analogous conditions. The processes were also confirmed to involve single electron transfer by comparison of peak heights with those of equimolar quantities of ferrocene.

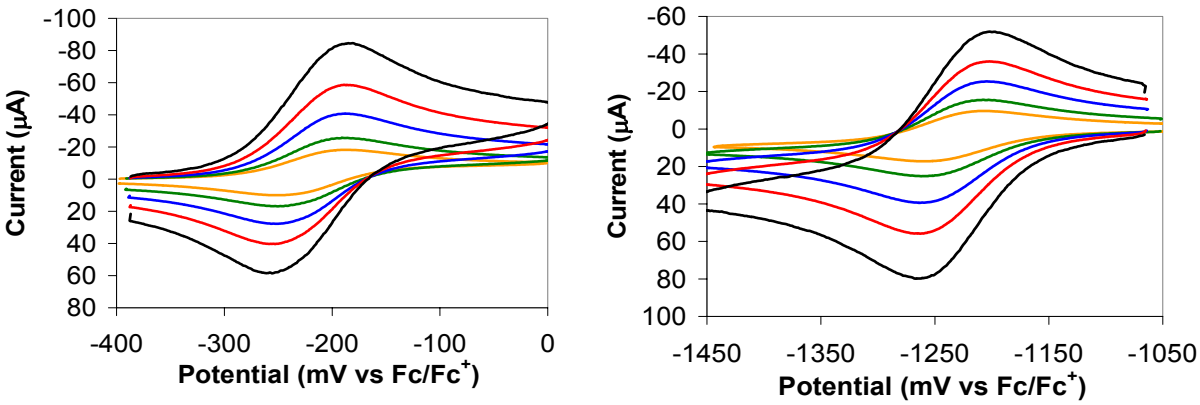

Figure 2.8. Cyclic voltammograms of **2.3a** in CH_3CN containing 0.1 M $Bu_4N^+BF_4^-$ (electrolyte): reduction (left) and oxidation (right). Scan rate 1000 mV/s (black), 500 mV/s (red), 250 mV/s (blue), 100 mV/s (green), 50 mV/s (orange).

2.5.1 Substituent effects

The oxidation potentials of type I verdazyls **2.3a-e**, **i-k** occur between -0.39 and -0.15 V vs Fc/Fc^+. Their relatively low oxidation potentials make these compounds good electron donors, as evidenced by their use in charge transfer chemistry.[225] Substituent effects are qualitatively predictable. For example, the series **2.3b→2.3c→2.3d→2.3e** consists of verdazyls containing the same substituent at the 3 position (R' = Me) and progressively more electron withdrawing substituents at the 1,5-positions (R = OMe, Me, H, Cl). The oxidation potentials rise from -0.39 V for **2.3b** to -0.15 V for **2.3e**, a range spanning nearly 0.25 V. This can be compared to a range of nearly 0.10 V for a wider

range of electron donating/withdrawing substituents in 4-substituted phenyl-1,2,3,5-dithiadiazolyl radicals **2.18**.[182, 226] The reduction potentials of **2.3b→2.3c→2.3d→2.3e** follow the same trend, and are effected qualitatively by roughly the same magnitude, with a low of -1.33 V for **2.3b** and a high of -1.14 V for **2.3e**.

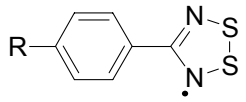

2.18

Substituent effects arising from changes in R' are smaller than those observed from changing R. The series **2.3i→2.3c→2.3j→2.3k** have fixed 1,5-substituents (R = Me) with the substituent at the 3-position following the same substituent progression (R' = OMe, Me, H, Cl). The oxidation potentials rise from -0.30 V for **2.3i** to -0.26 V for **2.3k**, a range spanning only 0.04 V. The trend in reduction potentials is similar to that observed above, ranging from -1.29 V for **2.3c** to -1.26 V for **2.3k**. However, the range is much smaller spanning only 0.02 V. The reduction potential for compound **2.3i** was not included in this range as its reduction wave was irreversible.

The smaller substituent effects observed at the 3-position may simply reflect the fact that there are two 1,5-substituents (vs. one subsituent at the 3-position) that may effect the redox properties. Furthermore, the 1,5-substituents are attached directly to a site of primary spin density, whereas the 3-substituents are attached at a site of negligible spin density due to a nodal plane in the verdazyl π-SOMO (see Figure 2.15 and 2.16). The "per-substituent" effects can be deduced for the series **2.3a→2.3d→2.3j→2.3c**, where each verdazyl has an additional *para*-methyl substituent ranging from triphenylformazan **2.3a** to tri-*para*-tolylformazan **2.3c**. Inspection of the CVs reveals that

both the oxidation and reduction processes are lowered by ~0.02 V with the addition of each *para*-methyl substituent.

2.6 Synthesis and characterization of type II verdazyl radicals

Several 6-oxoverdazyls were synthesized according to literature procedures (Figure 2.9). 1,3,5-Triphenyl-6-oxoverdazyl **2.4a** has been reported previously,[150, 155] and was prepared with modification of Milcent's method[150] using Fetison's reagent as an oxidant (see Scheme 2.2).[227-230] 1,5-Dialkyl-6-oxoverdazyls **2.4b-h** were prepared by modification of literature procedures, using *para*-benzoquinone or sodium periodate as oxidants (see Scheme 2.3).[149, 231] It has recently been reported that verdazyl radicals bearing *iso*-propyl N-substituents have increased stability relative to their methyl analogues, thus they were chosen for the electrochemical studies reported here.[149]

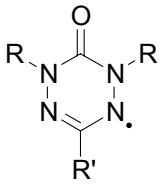

2.4a-h

a R = phenyl, R' = phenyl
b R = iPr, R' = phenyl
c R = iPr, R' = pyridyl
d R = iPr, R' = 2-imidazolyl
e R = iPr, R' = 2'-methylimidazol-5'-yl
f R = Me, R' = phenyl
g R = Me, R' = pyridyl
h R = Me, R' = 2'-methylimidazol-5'-yl

Figure 2.9. 1,5-Dialkyl-6-oxoverdazyls **2.4a-h**.

2.6.1 Crystal structure of verdazyl 2.4c

The crystal structure of **2.4c** is shown in Figure 2.10. Internally, the bonds within the verdazyl skeleton are consistent with other 1,5-dialkyl-6-oxoverdazyls structures of 1,5-dimethyl-6-oxoverdazyls.[148, 155, 232] The *iso*-propyl groups are oriented such that the methine protons on C3 and C6 are *syn* to the carbonyl moiety. The pyridine ring attached at C1 is twisted by 26.8° with respect to the plane of the verdazyl, contrasting the coplanar structure observed in the N,N-dimethyl analogue.[148]

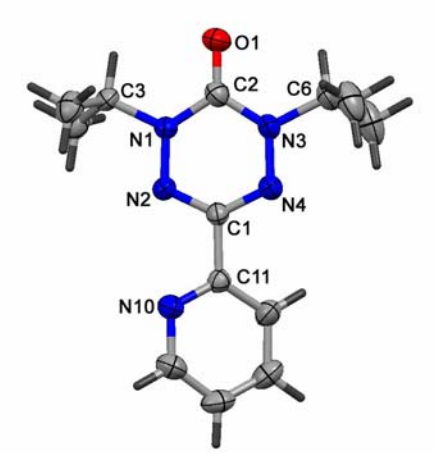

Figure 2.10. Molecular structure of **2.4c**. Thermal ellipsoids shown at 50% probability level.

Table 2.4. Selected bond lengths (Å) and angles (deg) for **2.4c**.

Atoms	**2.4c**	Atoms	**2.4c**
C2-O1	1.216(2)	N2-C1-N4	127.81(18)
N1-N2	1.365(2)	C1-N4-N3	114.95(16)
N3-N4	1.365(2)	C1-N2-N1	114.33(15)
N1-C2	1.373(2)	N2-N1-C2	124.62(16)
N3-C2	1.374(3)	N4-N3-C2	123.99(16)
N2-C1	1.324(2)	N3-C2-N1	114.30(18)
N4-C1	1.322(2)		

Inspection of the crystal packing of **2.4c** reveals one-dimensional slipped stacks parallel to *a* in which the verdazyl ring of one molecule is partially superimposed over the pyridine of neighboring molecules (Figure 2.11). The distances between radicals within the stack are outside the van der Waals radii (3.3-3.4 Å), and vary from 3.6-3.9 Å. There are no significant intermolecular contacts between the slipped stacks.

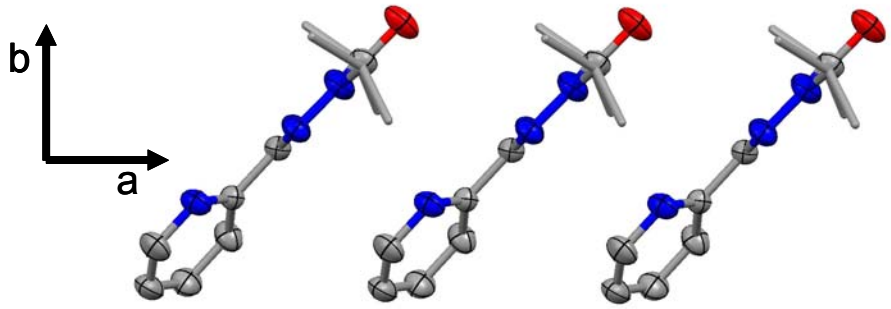

Figure 2.11. Intermolecular interactions for **2.4c**. Hydrogen atoms omitted for clarity.

2.6.2 Magnetic properties of verdazyl 2.4c

The Bonner-Fisher model ($\mathbf{H} = -J\mathbf{S}_{rad}\mathbf{S}_{rad+1}$) has been developed for 1-dimensional antiferromagnetically coupled chains where x = |J|/kT (Equation 2.3).[233] In this equation (and all other magnetic models from this point forward) ρ is used as a purity factor. This factor does not necessarily represent the purity of the compound, but rather the purity with respect to the number of magnetic spins within the sample that obey the magnetic model employed.

$$\chi = \rho\frac{Ng^2\beta^2}{kT}\frac{0.25+0.074975x+0.075235x^2}{1.0+0.9931x+0.172135x^2+0.757825x^3} \qquad (2.3)$$

The magnetic data for **2.4c** is presented in Figure 2.12 as both χ vs T and χT vs T plots. The value of χ increases with decreasing temperature, reaching a maximum value of 0.021 emu•mol^{-1} at 6 K. The data was fit using the Bonner-Fisher model with g = 2.00 fixed, yielding J = -6.66 ± 0.06 cm^{-1}, and ρ = 0.95 with a goodness of fit value R = 0.001 ($R = [\Sigma(\chi_{obs}-\chi_{calc})^2/\Sigma\chi_{obs}^2]^{1/2}$). These values are indicative of weak intermolecular antiferromagnetic coupling, consistent with the lack of close contacts between neighboring radicals.

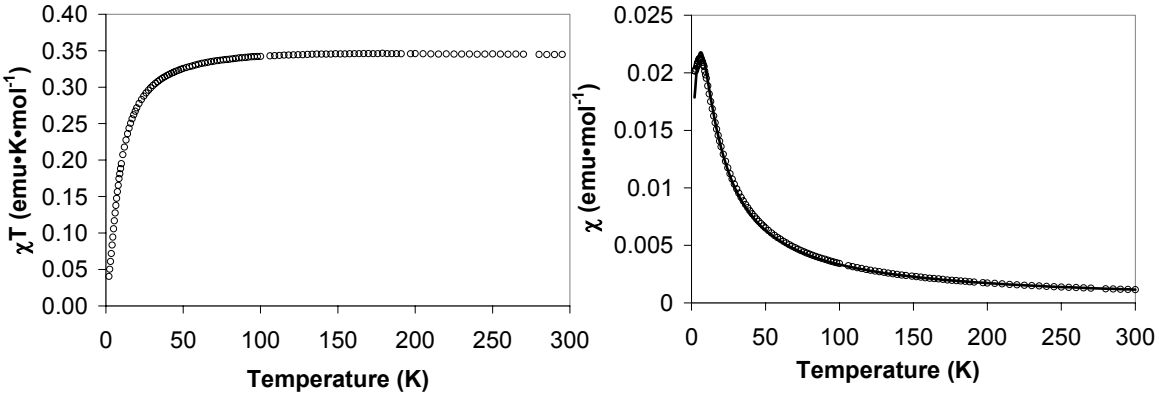

Figure 2.12. Magnetic properties of **2.4c**. χT vs T (left) and χ vs T (right). Experimental data (○) and data fit (black line).

2.6.3 Electrochemical properties of type II verdazyls

The electrochemical data for type II verdazyls **2.4a-f** is summarized in Table 2.5. Type II verdazyls **2.4a-f** have similar electrochemical properties to type I verdazyls **2.3a-e, i-k** described above, i.e., reversible oxidation and reduction waves. Within the type II verdazyls, replacement of the N-substituents has the expected effects, i.e., they become easier to oxidize and harder to reduce as the donating nature of the N-substituents is varied from phenyl (**2.4a**) to methyl (**2.4f**), and *iso*-propyl (**2.4b**). Within the limited series of derivatives of **2.4**, it is clear that the effects of the C3-substituent are similar to those previously described for type I verdazyls. Verdazyls bearing electron-withdrawing groups are slightly more easily reduced and slightly more difficult to oxidize (e.g., **2.4b** → **2.4c** → **2.4d**).

Table 2.5. Electrochemical properties of verdazyl radicals reported in V vs Fc/Fc^+. [a]Irreversible process, cathodic peak potential reported.

Compound	$E_{ox}°$	$E_{red}°$	E_{cell}
2.4a	+0.44	-0.94	1.38
2.4b	+0.18	-1.38	1.56
2.4c	+0.20	-1.36	1.55
2.4d	+0.24	-1.25[a]	n.a.
2.4e	+0.23	-1.31	1.54
2.4f	+0.27	-1.28	1.55

2.7 Comparison of type I and type II verdazyls

The CVs of verdazyls **2.3a** and **2.4a**, which vary only by the presence of a carbonyl group, are presented in Figure 2.13. Verdazyl radical **2.3a** is easier to oxidize (-0.22 V vs. 0.44 V) and harder to reduce (-1.23 V vs. -0.94 V) than **2.4a**, due to the addition of an electron withdrawing carbonyl group in **2.4a**.

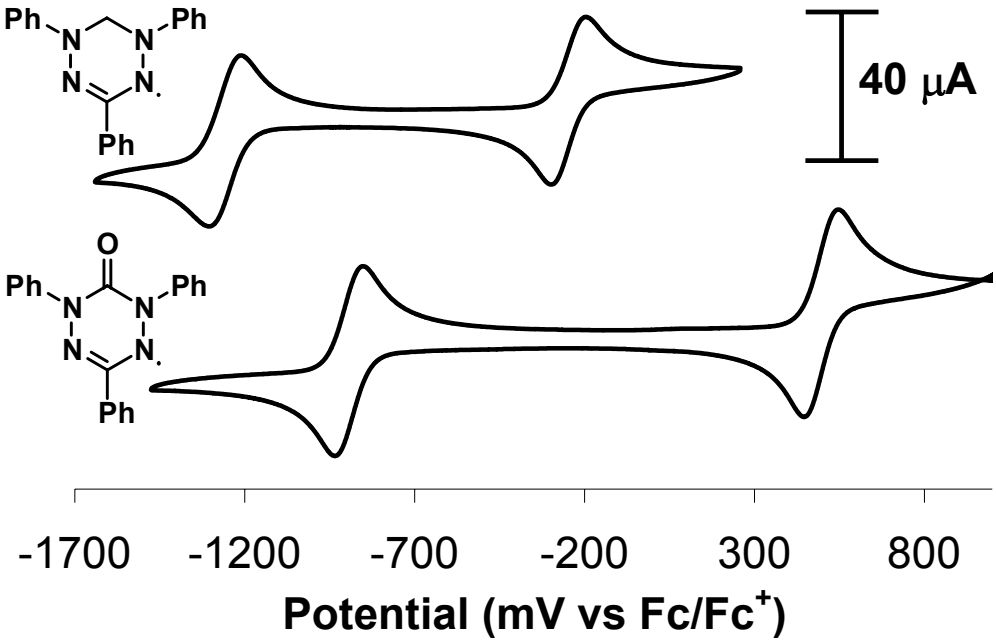

Figure 2.13. Cyclic voltammogram of **2.3a** (top) and **2.4a** (bottom) in CH_3CN containing 0.1 M $Bu_4N^+BF_4^-$ (electrolyte). Scan rate 100 mV/s.

The cell potentials are of interest because they are believed to correlate with gas phase IP-EA and/or disproportionation energies (the energy associated with $2R\bullet \rightarrow R^+ + R^-$) and are important in the design of neutral radical-based conductors.[130, 181, 182] Kaszynski has noted that "larger" (more delocalized) radicals have lower disproportionation energy and smaller cell potentials,[234] thus delocalization in verdazyl radicals will play an important role in understanding their properties.

The cell potentials vary predictably in the series of 6-oxoverdazyls, as the introduction of 1,5-alkyl substituents decreases delocalization compared to 1,5-aromatic substituents, causing the cell potentials to increase from 1.38 V in **2.4a** to 1.56 and 1.55 V in **2.4b** and **2.4f**. The cell potentials for **2.3a** and **2.4a** are, at first glance, more difficult to rationalize. The cell potential for **2.4a** might be expected to be smaller than that of **2.3a** due to the presence of an additional double bond in the verdazyl backbone, implying a relative increase in the extent of delocalization. However, the cell potential of **2.3a** (1.01 V) is significantly lower than that of **2.4a** (1.38 V), prompting further investigation into the electronic structure of these radicals.

2.7.1 DFT calculations and crystal structures of 2.3a and 2.4a

The crystal structures of **2.3a**[220, 221] and **2.4a**[155] (Figure 2.14) have been determined previously and may offer some insight into the differences in cell potentials. Verdazyl **2.3a** has a methylene bridge 0.62 Å above the verdazyl plane (N1-N2-C3-N4-N5). The non-planar structure is due to the lack of π-conjugation at sp^3 carbon (C6), and accommodation of the relatively small N1-C6-N5 angle (106.12°) at tetrahedral carbon compared to that expected in a planar six-membered ring (120°). The N-aryl substituents are twisted by 28.2° with respect to the verdazyl plane (N1-N2-C3-N4-N5), and by 13.1°

relative to the plane of the 1,5-nitrogen atoms (e.g., N2-N1-C6-C7) illustrating near coplanarity with the p orbital on the 1,5-nitrogen atoms. The crystal structure of **2.4a** reveals the carbonyl group to be coplanar with the verdazyl backbone, with an N1-C6-N5 angle of 114.38°. The N-substituents are twisted by 38.1° with respect to the verdazyl (N1-N2-C3-N4-N5) and nitrogen (e.g., N2-N1-C6-C7) planes due to steric interaction between the *ortho*-protons of the N-substituents and the carbonyl moiety.

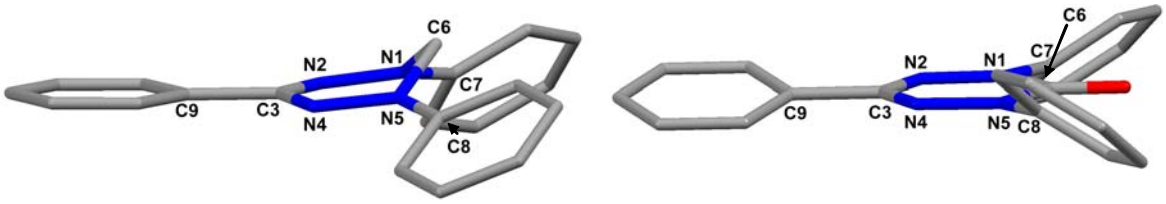

Figure 2.14. Crystal structures of **2.3a** (left) and **2.4a** (right).
Hydrogen atoms removed for clarity.

DFT calculations (UB3LYP 6-31G (d,p)) have been used to establish the π-SOMO and spin density plots for **2.3a** (Figure 2.15) and **2.4a** (Figure 2.16) in order to further understand their properties.

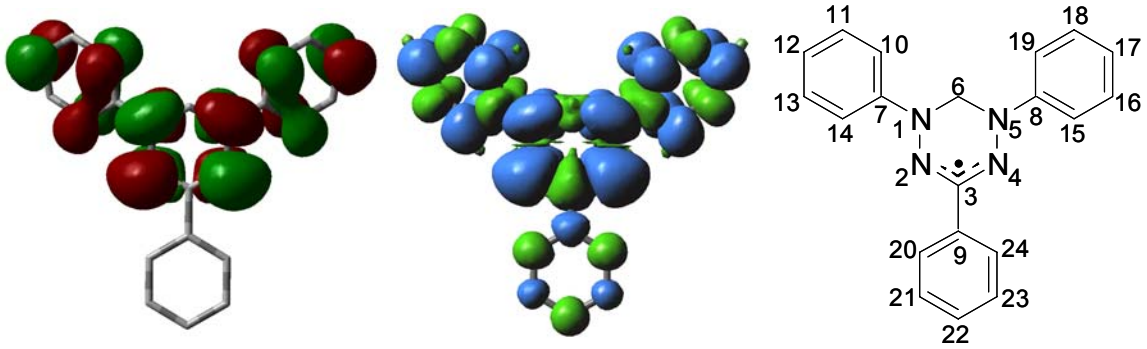

Figure 2.15. Calculated singly occupied orbital (left), spin density plot (middle), and atom labeling scheme (right) for **2.3a**.

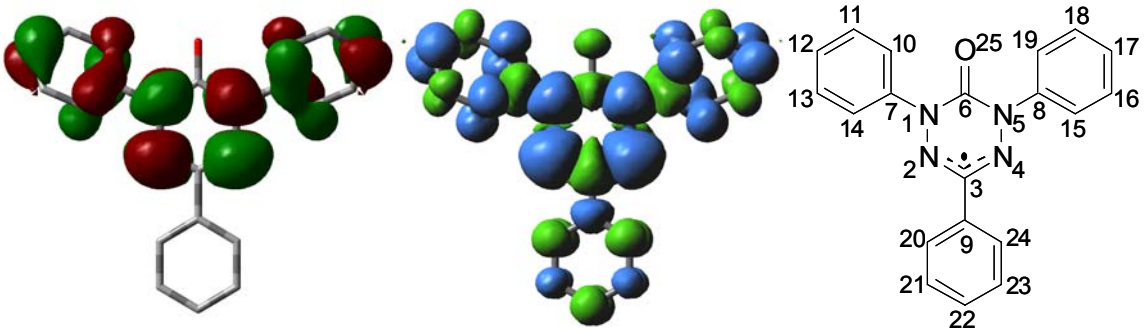

Figure 2.16. Calculated singly occupied orbital (left), spin density plot (middle), and atom labeling scheme (right) for **2.4a**.

Table 2.6. Atomic Spin Densities for **2.3a** and **2.4a**.

Atom	**2.3a**	**2.4a**
N5, N1	0.167	0.180
N2, N4	0.350	0.384
C3	-0.144	-0.149
C6	-0.011	-0.030
C9	0.0317	0.030
C7, C8	-0.049	-0.034
C10, C19	0.061	0.038
C11, C18	-0.035	-0.020
C12, C17	0.066	0.039
C13, C16	-0.034	-0.020
C14, C15	0.064	0.039
C20, C24	-0.028	-0.027
C21, C23	0.018	0.017
C22	-0.028	-0.025
O25	-	-0.011

The π-SOMO for both verdazyl radicals are consistent with other calculations on similar species,[235] with the largest spin densities found on the nitrogen atoms. The optimized structures are in close agreement with the crystal structures previously discussed, i.e., the N-phenyl substituents are twisted by 21.4° with respect to N1-N2-C3-N4-N5 and 13.8° with respect to N2-N1-C6-C7 in **2.3a**, and by 39.6° with respect to N1-N2-C3-N4-N5 in **2.4a**.

There are significant differences in the calculated spin densities in **2.3a** and **2.4a**. The differences are found primarily on the N-phenyl substituents, where the spin density coefficients in **2.3a** are roughly double those found in **2.4a** (see Table 2.6). The increased spin density in **2.3a** compared to **2.4a** relates directly to the overlap between the π-orbitals on the N-aryl substituents with the p-orbital on the 1,5-nitrogen atoms, which is greater in **2.3a** compared to **2.4a**. These computational results are consistent with EPR and ENDOR studies of these radicals, showing hyperfine coupling to aryl protons (a_H) to be roughly double in magnitude for **2.3a** compared to **2.4a**.[155] The decreased delocalization observed in **2.4a** compared to **2.3a** accounts for the difference in cell potentials, and is in agreement with Kaszynski's hypothesis that increased delocalization leads to lower disproportionation energies and cell potentials.[234]

2.8 Summary

This work represents the first systematic study of the electrochemical properties of verdazyl radicals. The ease of derivatization of triarylformazans allowed for the synthesis of a number of type I verdazyls, which were used to study substituent effects on electrochemical properties. The reversible one-electron oxidation and reduction of such radicals were shifted to higher potential in the presence of electron withdrawing groups and lower potential in the presence of electron donating groups. The relationship between electronic structure and cell potential was explored by comparing type I and type II verdazyls. The type II verdazyls studied displayed similar substituent-based properties to type I verdazyls, and had larger cell potentials than type I analogues. The relatively low cell potentials of type I verdazyl radicals was explained on the basis of crystal

structure and computational data, which illustrated that increased delocalization leads to smaller cell potentials.

2.9 Experimental

2.9.1 Synthesis and characterization

Previously reported compounds:

Formazans **2.1a**,[211] **2.1c**,[236] **2.1d**,[237] **2.1i**,[238] **2.1j**[237] and verdazyl radicals **2.3a**,[202] **2.3c**,[236] **2.3i**,[239] **2.3j**[237] have been reported previously, however, their characterization was incomplete or they were produced via different synthetic routes. Carbonic acid bis(1-alkylhydrazide)s **2.8a**[149] and **2.8b**,[143] tetrazane **2.7a**,[150] and verdazyls **2.4c**,[149] **2.4d**,[149] **2.4f**,[143] and **2.4g**,[148] were prepared using literature procedures. Their identity and purity were confirmed using appropriate spectroscopic methods (i.e., ^{1}H NMR, IR, UV-vis) through comparison with literature values.

^{13}C NMR Spectra

In several cases, quaternary carbon atoms were not observed in ^{13}C NMR due to lack of Nuclear Overhauser Enhancement (NOE) from surrounding nuclei.

General procedure for the synthesis of triarylformazans 2.1a-f, h-l, n : 1,3,5-triphenylformazan (2.1a). In a typical procedure, phenylhydrazine (3.54 g, 33 mmol) was combined with ethanol (50 mL) and benzaldehyde (3.50 g, 33 mmol). After stirring for 2 h a yellow crystalline precipitate formed. The reaction mixture was treated with sodium carbonate hydrate (16.5 g, 133 mmol), tetrabutylammonium bromide (1.25 g, 4 mmol), water (60 mL), and dichloromethane (100 mL) before being stirred at 0°C for 1 h. A solution of diazonium salt made from stirring aniline (3.52 g, 38 mmol), sodium nitrite

(3.15 g, 46 mmol), water (10 mL), and hydrochloric acid (10 mL) for 30 min at 0°C was then added dropwise. Upon addition, the organic phase in the biphasic reaction mixture turned blood red. After stirring for 2 h at RT the organic layer was collected, washed with water (3 x 100 mL) and taken to dryness *in vacuo*. Column chromatography (neutral alumina, dichloromethane) followed by trituration of the solid with methanol afforded **2.1a** as a dark purple microcrystalline solid, yield 6.50 g (65.6 %). Mp. 148-150°C. ^{1}H NMR (300 MHz, CD_2Cl_2): δ 15.36 (s, 1H), 8.16 (d, 2H, ^{3}J = 8 Hz), 7.73 (d, 4H, ^{3}J = 8 Hz), 7.60-7.25 (m, 9H) ppm. ^{13}C NMR (75 MHz, CD_2Cl_2): δ 148.5, 141.7, 138.0, 130.0, 129.0, 128.2, 128.1, 126.4, 119.3 ppm. FT-IR (KBr): 1597 (s), 1510 (s), 1492 (s), 1232 (s), 1017 (s), 752 (s) cm^{-1}. UV-vis (CH_2Cl_2): λ_{max} 270 nm (ε = 17250 L•mol^{-1}•cm^{-1}), 300 nm (ε = 22000 L•mol^{-1}•cm^{-1}), 488 nm (ε = 14250 L•mol^{-1}•cm^{-1}). MS (EI): *m/z* 300 (M^+, 35 %). Anal. Calcd for $C_{19}H_{16}N_4$: C, 75.98; H, 5.37; N, 18.65. Found: C, 76.16; H, 5.54; N, 18.36.

1,5-di-*para*-methoxyphenyl-3-*para*-tolylformazan (2.1b). Yield 26.2 %. Mp. 131-133°C. ^{1}H NMR (300 MHz, CD_2Cl_2): δ 15.40 (s, 1H), 8.01 (d, 2H, ^{3}J = 8 Hz), 7.66 (d, 4H, ^{3}J = 9 Hz), 7.25 (d, 2H, ^{3}J = 8 Hz), 7.00 (d, 4H, ^{3}J = 9 Hz), 3.86 (s, 6H), 2.41 (s, 3H) ppm. ^{13}C NMR (75 MHz, CD_2Cl_2): δ 159.8, 142.5, 141.2, 137.7, 135.6, 129.6, 126.1, 120.5, 115.2, 56.2, 21.5 ppm. FT-IR (KBr): 1599 (s), 1507 (s), 1255 (s), 1230 (s), 1033 (s), 819 (s) cm^{-1}. UV-vis (CH_2Cl_2): λ_{max} 314 nm (ε = 20750 L•mol^{-1}•cm^{-1}), 538 nm (ε = 17000 L•mol^{-1}•cm^{-1}). MS (EI): *m/z* 374 (M^+, 30 %). Anal. Calcd for $C_{22}H_{22}N_4O_2$: C, 70.57; H, 5.92; N, 14.96. Found: C, 70.19; H, 6.16; N, 15.08.

1,3,5-tri-*para*-tolylformazan (2.1c). Yield 56.7 %. Mp. 170-172°C. ^{1}H NMR (300 MHz, CD_2Cl_2): δ 15.35 (s, 1H), 8.02 (d, 2H, ^{3}J = 8 Hz), 7.61 (d, 4H, ^{3}J = 8 Hz), 7.35-7.25

(m, 6H, ^{3}J = 8 Hz), 2.40 (s, 9H) ppm. ^{13}C NMR (75 MHz, CD_2Cl_2): δ 146.4, 141.5, 138.3, 138.2, 137.9, 135.4, 130.6, 129.6, 126.2, 119.1, 21.5 ppm. FT-IR (KBr): 1598 (m), 1508 (s), 1226 (s), 816 (s) cm^{-1}. UV-vis (CH_2Cl_2): λ_{max} 279 nm (ε = 19000 $L•mol^{-1}•cm^{-1}$), 307 nm (ε = 26750 $L•mol^{-1}•cm^{-1}$), 498 nm (17000 $L•mol^{-1}•cm^{-1}$). MS (EI): *m/z* 342 (M^+, 100 %). Anal. Calcd for $C_{22}H_{22}N_4$: C, 77.16; H, 6.48; N, 16.36. Found: C, 76.66; H, 6.51; N, 16.04.

1,5-diphenyl-3-*para*-tolylformazan (2.1d). Yield 47.8 %. Mp. 154-156°C. ^{1}H NMR (300 MHz, CD_2Cl_2): δ 15.24 (s, 1H), 8.03 (d, 2H, ^{3}J = 8 Hz), 7.72 (d, 4H, ^{3}J = 8 Hz), 7.49 (t, 4H, ^{3}J = 8 Hz), 7.33-7.27 (m, 4H), 2.42 (s, 3H) ppm. ^{13}C NMR (75 MHz, CD_2Cl_2): δ 148.6, 141.9, 138.2, 135.1, 130.0, 129.7, 128.0, 126.3, 119.2, 21.5 ppm. FT-IR (KBr): 1597 (s), 1511 (s), 1497 (s), 1453 (s), 1353 (m), 1232 (s), 1035 (s), 1014 (s), 821 (s), 502 (m) cm^{-1}. UV-vis (CH_2Cl_2): λ_{max} 274 nm (ε = 20000 $L•mol^{-1}•cm^{-1}$), 301 nm (ε = 26250 $L•mol^{-1}•cm^{-1}$), 491 nm (ε = 15000 $L•mol^{-1}•cm^{-1}$). MS (LSIMS): *m/z* 315 ($M+1^+$, 75 %). Anal. Calcd for $C_{20}H_{18}N_4$: C, 76.40; H, 5.77; N, 17.82. Found: C, 76.71; H, 5.64; N, 17.97.

1,5-di-*para*-chlorophenyl-3-*para*-tolylformazan (2.1e). Yield 61.5 %. Mp. 198-200°C. ^{1}H NMR (300 MHz, CD_2Cl_2): δ 15.07 (s, 1H), 7.98 (d, 2H, ^{3}J = 8 Hz), 7.65 (d, 4H, ^{3}J = 9 Hz), 7.45 (d, 4H, ^{3}J = 9 Hz), 7.26 (d, 2H, ^{3}J = 8 Hz), 2.41 (s, 3H) ppm. ^{13}C NMR (75 MHz, CD_2Cl_2): δ 147.1, 142.2, 138.5, 134.7, 133.3, 130.1, 129.7, 126.4, 120.5, 21.5 ppm. FT-IR (KBr): 1509 (s), 1488 (s), 1479 (s), 1406 (s), 818 (s) cm^{-1}. UV-vis (CH_2Cl_2): λ_{max} 303 nm (ε = 28250 $L•mol^{-1}•cm^{-1}$), 503 nm (ε = 17000 $L•mol^{-1}•cm^{-1}$). MS (EI): *m/z* 382 (M^+, 10 %). Anal. Calcd for $C_{20}H_{16}Cl_2N_4$: C, 62.67; H, 4.21; N, 14.62. Found: C, 62.67; H, 4.29; N, 14.65.

1,5-di-*para*-cyanophenyl-3-*para*-tolylformazan (2.1f). Yield 43.3 %. Mp. 214-216°C. ^{1}H NMR (300 MHz, CD_2Cl_2): δ 14.69 (s, 1H), 7.97 (d, 2H, ^{3}J = 8 Hz), 7.78 (s (br), 8H), 7.29 (d, 2H, ^{3}J = 8 Hz), 2.42 (s, 3H) ppm. ^{13}C NMR (75 MHz, CD_2Cl_2): δ 151.1, 143.8, 139.5, 134.2, 133.8, 129.8, 126.8, 119.4, 114.6, 21.6 ppm. FT-IR (KBr): 2223 (s), 1509 (s), 1223 (s) cm^{-1}. UV-vis (CH_2Cl_2): λ_{max} 297 nm (ε = 46250 L•mol^{-1}•cm^{-1}), 513 nm (ε = 17250 L•mol^{-1}•cm^{-1}). MS (EI): *m/z* 364 (M^+, 15 %). Anal. Calcd for $C_{22}H_{16}N_6$: C, 72.51; H, 4.43; N, 23.06. Found: C, 72.49; H, 4.49; N, 23.19.

3-*para*-tolyl-1,5-di-*para*-trifluoromethylphenylformazan (2.1h). Yield 44.6 %. Mp. 164-166°C. ^{1}H NMR (300 MHz, CD_2Cl_2): δ 14.87 (s, 1H), 7.96 (d, 2H, ^{3}J = 8 Hz), 7.76 (d, 4H, ^{3}J = 9 Hz), 7.72 (d, 4H, ^{3}J = 9 Hz), 7.26 (d, 2H, ^{3}J = 8 Hz), 2.41 (s, 3H) ppm. ^{13}C NMR (75 MHz, CD_2Cl_2): δ 150.8, 142.9, 139.0, 134.1, 130.8, 129.8, 129.5, 129.1, 127.3, 127.2, 126.6, 123.4, 123.0, 119.4, 114.6, 21.6 ppm. FT-IR (KBr): 1613 (s), 1511 (m), 1418 (m), 1322 (s), 1061 (s) cm^{-1}. UV-vis (CH_2Cl_2): λ_{max} 273 nm (ε = 21500 L•mol^{-1}•cm^{-1}), 297 nm (ε = 27500 L•mol^{-1}•cm^{-1}), 497 nm (ε = 14500 L•mol^{-1}•cm^{-1}). MS (EI): *m/z* 450 (M^+, 10 %). Anal. Calcd for $C_{22}H_{16}F_6N_4$: C, 58.67; H, 3.58; N, 12.44. Found: C, 58.73; H, 3.37; N, 12.41.

3-*para*-methoxyphenyl-1,5-di-*para*-tolylformazan (2.1i). Yield 59.5 %. Mp. 162-164°C. ^{1}H NMR (300 MHz, CD_2Cl_2): δ 15.24 (s, 1H), 8.06 (d, 2H, ^{3}J = 9 Hz), 7.60 (d, 4H, ^{3}J = 8 Hz), 7.28 (d, 4H, ^{3}J = 8 Hz), 6.98 (d, 2H, ^{3}J = 9 Hz), 3.87 (s, 3H), 2.40 (s, 6H) ppm. ^{13}C NMR (75 MHz, CD_2Cl_2): δ 166.1, 160.0, 146.5, 138.1, 130.9, 130.6, 127.6, 119.1, 114.2, 55.8, 21.5 ppm. FT-IR (KBr): 1605 (m), 1508 (s), 1250 (s), 1222 (s), 1025 (s), 810 (m) cm^{-1}. UV-vis (CH_2Cl_2): λ_{max} 279 nm (ε = 20750 L•mol^{-1}•cm^{-1}), 308 nm (ε = 27500 L•mol^{-1}•cm^{-1}), 522 nm (ε = 16000 L•mol^{-1}•cm^{-1}). MS (EI): *m/z* 358 (M^+, 20 %).

Anal. Calcd for $C_{22}H_{22}N_4O$: C, 73.72; H, 6.19; N, 15.63. Found: C, 73.77; H, 6.22; N, 15.71.

1,5-di-*para*-tolyl-3-phenylformazan (2.1j). Yield 30.8 %. Mp. 140-142°C. ^{1}H NMR (300 MHz, CD_2Cl_2): δ 15.46 (s, 1H), 8.14 (d, 2H, ^3J = 8 Hz), 7.62 (d, 4H, ^3J = 8 Hz), 7.45 (t, 2H, ^3J = 8 Hz), 7.36 (t, 1H, ^3J = 8 Hz), 7.29 (d, 4H, ^3J = 8 Hz), 2.41 (s, 6H) ppm. ^{13}C NMR (75 MHz, CD_2Cl_2): δ 146.4, 141.3, 138.4, 138.2, 130.6, 128.9, 128.0, 126.2, 119.2, 21.5 ppm. FT-IR (KBr): 1596 (s), 1515 (s), 1495 (s), 1240 (s), 1044 (s), 767 (s) cm^{-1}. UV-vis (CH_2Cl_2): λ_{max} 278 nm (ε = 17500 L•mol^{-1}•cm^{-1}), 308 nm (ε = 23500 L•mol^{-1}•cm^{-1}), 493 (ε = 16250 L•mol^{-1}•cm^{-1}). MS (LSIMS): *m/z* 329 (MH^+, 100 %). Anal. Calcd for $C_{21}H_{20}N_4$: C, 76.80; H, 6.14; N, 17.06. Found: C, 76.97; H, 6.12; N, 16.69.

3-*para*-chlorophenyl-1,5-di-*para*-tolylformazan (2.1k). Yield 43.7 %. Mp. 188-190°C. ^{1}H NMR (300 MHz, CD_2Cl_2): δ 15.40 (s, 1H), 8.00 (d, 2H, ^3J = 9 Hz), 7.51 (d, 4H, ^3J = 8 Hz), 7.31 (d, 2H, ^3J = 9 Hz), 7.19 (d, 4H, ^3J = 8 Hz), 2.31 (s, 6H) ppm. ^{13}C NMR (75 MHz, CD_2Cl_2): δ 146.2, 140.3, 138.6, 136.9, 133.6, 130.6, 129.0, 127.5, 119.2, 21.5 ppm. FT-IR (KBr): 1488 (s), 1396 (m), 1238 (s) cm^{-1}. UV-vis (CH_2Cl_2): λ_{max} 235 nm (ε = 16750 L•mol^{-1}•cm^{-1}), 274 nm (ε = 18000 L•mol^{-1}•cm^{-1}), 313nm (ε = 31250 L•mol^{-1}•cm^{-1}), 496 nm (ε = 20000 L•mol^{-1}•cm^{-1}). MS (EI): *m/z* 362 (M^+, 10 %). Anal. Calcd for $C_{21}H_{19}ClN_4$: C, 69.51; H, 5.28; N, 15.44. Found: C, 69.63; H, 5.25; N, 15.63.

3-*para*-cyanophenyl-1,5-di-*para*-tolylformazan (2.1l). Yield 30.1 %. Mp. 204-206°C. ^{1}H NMR (300 MHz, CD_2Cl_2): δ 15.60 (s (br), 1H), 8.16 (d, 2H, ^3J = 9 Hz), 7.61 (d, 2H, ^3J = 9 Hz), 7.51 (d, 2H, ^3J = 8 Hz), 7.20 (d, 2H, ^3J = 8 Hz), 2.32 (s, 6H) ppm. ^{13}C NMR (75 MHz, CD_2Cl_2): δ 145.9, 142.7, 139.5, 139.1, 132.8, 130.7, 126.2, 119.9, 119.4, 110.8, 21.6 ppm. FT-IR (KBr): 2221 (s), 1601 (s), 1498 (s), 1249 (s) cm^{-1}. UV-vis (CH_2Cl_2):

λ_{max} 272 nm (ε = 49250 L•mol^{-1}•cm^{-1}), 339 nm (ε = 34000 L•mol^{-1}•cm^{-1}), 488 nm (ε = 23000 L•mol^{-1}•cm^{-1}). MS (EI): *m/z* 353 (M^+, 20 %). Anal. Calcd for $C_{22}H_{19}N_5$: C, 74.77; H, 5.42; N, 19.82. Found: C, 74.59; H, 5.51; N, 19.65.

3-*para*-nitrophenyl-1,5-di-*para*-tolylformazan (2.1m). A solution of *para*-tolylhydrazine hydrochloride (1.60 g, 10 mmol) was combined with triethylamine (1.4 mL, 10 mmol) and methanol (20 mL). After 30 min of stirring 4-nitrobenzaldehyde (1.50 g, 10 mmol) was added and the mixture was stirred for 30 min at which time an orange ppt formed. The solution was then treated with sodium acetate (1.75 g, 21 mmol), sodium hydroxide (1.25 g, 31 mmol), and methanol (80 mL). After 30 min of stirring, a solution of diazonium salt prepared by stirring *para*-toluidine (1.07 g, 10 mmol), sodium nitrite (0.75 g, 11 mmol), water (10 mL), and hydrochloric acid (5 mL) at 0°C for 30 min was added. The solution immediately turned blood red and after 5 h was taken to dryness *in vacuo*. Column chromatography (neutral alumina, dichloromethane) followed by trituration with methanol afforded **2.1m** as a brick red microcrystalline solid, yield 2.1 g (56.3 %). Mp. 216-218°C. ^{1}H NMR (300 MHz, CD_2Cl_2): δ 15.81 (s, 1H), 8.31 (d, 2H, ^{3}J = 9 Hz), 8.25 (d, 2H, ^{3}J = 9 Hz), 7.62 (d, 4H, ^{3}J = 8 Hz), 7.31 (d, 4H, ^{3}J = 8 Hz), 2.42 (s, 6H) ppm. ^{13}C NMR (75 MHz, CD_2Cl_2): δ 147.3, 145.8, 144.7, 139.3, 130.7, 126.2, 124.3, 119.5, 21.6 ppm. FT-IR (KBr): 1592 (s), 1494 (s), 1334 (s), 1250 (s) cm^{-1}. UV-vis (CH_2Cl_2): λ_{max} 267 nm (ε = 20000 L•mol^{-1}•cm^{-1}), 420 nm (ε = 16500 L•mol^{-1}•cm^{-1}), 483 nm (ε = 20750 L•mol^{-1}•cm^{-1}). MS (EI): *m/z* 373 (M^+, 10 %). Anal. Calcd for $C_{21}H_{19}N_5O_2$: C, 67.55; H, 5.13; N, 18.76. Found: C, 67.12; H, 5.25; N, 18.23.

1,5-di-*para*-tolyl-3-*para*-trifluoromethylphenylformazan (2.1n). Yield 59.9 %. Mp. 188-190°C. ^{1}H NMR (300 MHz, CD_2Cl_2): δ 15.63 (s , 1H), 8.24 (d, 2H, ^{3}J = 8Hz), 7.67

(d, 2H, ^3J = 8 Hz), 7.59 (d, 4H, ^3J = 8 Hz), 7.28 (d, 4H, ^3J = 8 Hz), 2.40 (s, 6H) ppm. ^{13}C NMR (75 MHz, CD_2Cl_2): δ 146.0, 141.9, 139.8, 138.8, 130.6, 126.1, 125.8, 125.7, 119.3, 21.6 ppm. FT-IR (KBr): 1613 (m), 1506 (m), 1497 (m), 1322 (s), 1105 (s), 1067 (s) cm^{-1}. UV-vis (CH_2Cl_2): λ_{max} 268 nm (ε = 15250 $L•mol^{-1}•cm^{-1}$), 320 nm (ε = 27500 $L•mol^{-1}•cm^{-1}$), 488 nm (ε = 21000 $L•mol^{-1}•cm^{-1}$). MS (EI): *m/z* 396 (M^+, 10 %). Anal. Calcd for $C_{22}H_{19}F_3N_4$: C, 66.66; H, 4.83; N, 14.13. Found: C, 66.57; H, 4.82; N, 14.14.

General procedure for verdazyls 2.3a-e, i-k: 1,3,5-triphenylverdazyl (2.3a). In a typical procedure **2.3a** (0.46 g, 1.5 mmol) was combined with formaldehyde solution (1.7 mL, 23 mmol), 2 M sodium hydroxide (3.5 mL, 7 mmol), and dimethylformamide (25 mL) and allowed to stir in air for 3 hours at which time the color of the solution had changed from red to green. The mixture was then treated with diethyl ether (100 mL) and the organic layer collected, washed with water (5 x 100 mL) to remove dimethylformamide, dried with $MgSO_4$, and concentrated *in vacuo*. Recrystallization from a saturated methanolic solution afforded **2.3a** as a green microcrystalline solid, yield 0.26 g (54.2 %). Mp. 128-130°C. FT-IR (KBr): 1586 (s), 1490 (s), 1264 (m), 1145 (m), 752 (s) cm^{-1}. UV-vis (CH_2Cl_2): λ_{max} 273 nm (ε = 62250 $L•mol^{-1}•cm^{-1}$), 405 nm (ε = 7250 $L•mol^{-1}•cm^{-1}$), 716 nm (ε = 3500 $L•mol^{-1}•cm^{-1}$). MS (EI): *m/z* 313 (M^+, 70 %). Anal. Calcd for $C_{20}H_{17}N_4$: C, 76.65; H, 5.47; N, 17.88. Found: C, 76.25; H, 5.10; N, 17.37.

1,5-di-*para*-methoxyphenyl-3-*para*-tolylverdazyl (2.3b). Yield 75.6 %. Mp. 120-122°C. FT-IR (KBr): 1504 (s), 1248 (s), 1033 (m), 821 (m) cm^{-1}. UV-vis (CH_2Cl_2): λ_{max} 287 nm (ε = 27500 $L•mol^{-1}•cm^{-1}$), 327 nm (ε = 11750 $L•mol^{-1}•cm^{-1}$), 414 nm (ε = 8250 $L•mol^{-1}•cm^{-1}$), 736 nm (ε = 4250 $L•mol^{-1}•cm^{-1}$). MS (EI): *m/z* 387 (M^+, 100 %). Anal. Calcd for $C_{23}H_{23}N_4O_2$: C, 71.30; H, 5.98; N, 14.46. Found: C, 71.23; H, 5.97; N, 14.20.

1,3,5-tri-*para*-tolylverdazyl (2.3c). Yield 57.7%. Mp. 136-138°C. FT-IR (KBr): 1508 (s), 1397 (m), 1260 (m), 1143 (s), 825 (m), 798 (m) cm^{-1}. UV-vis (CH_2Cl_2): λ_{max} 248 nm (ε = 12500 $L•mol^{-1}•cm^{-1}$), 284 nm (ε = 22000 $L•mol^{-1}•cm^{-1}$), 325 nm (ε = 10000 $L•mol^{-1}•cm^{-1}$), 403 nm (ε = 6750 $L•mol^{-1}•cm^{-1}$), 727 nm (ε = 3250 $L•mol^{-1}•cm^{-1}$). MS (EI): *m/z* 354 ($M\text{-}1^+$, 100 %). Anal. Calcd for $C_{23}H_{23}N_4$: C, 77.72; H, 6.52; N, 15.76. Found: C, 77.13; H, 6.69; N, 15.12.

1,5-diphenyl-3-*para*-tolylverdazyl (2.3d). Yield 27.2%. Mp. 138-140°C. FT-IR (KBr): 1590 (s), 1494 (s), 1397 (m), 1143 (s), 746 (s) cm^{-1}. UV-vis (CH_2Cl_2): λ_{max} 246 nm (ε = 10000 $L•mol^{-1}•cm^{-1}$), 280 nm (ε = 23000 $L•mol^{-1}•cm^{-1}$), 320 nm (ε = 12000 $L•mol^{-1}•cm^{-1}$), 398 nm (ε = 7500 $L•mol^{-1}•cm^{-1}$), 721 nm (ε = 3500 $L•mol^{-1}•cm^{-1}$). MS (EI): *m/z* 327 (M^+, 80 %). Anal. Calcd for $C_{21}H_{19}N_4$: C, 77.04; H, 5.85; N, 17.11. Found: C, 76.43; H, 5.57; N, 16.64.

1,5-di-*para*-chlorophenyl-3-*para*-tolylverdazyl (2.3e). Yield 83.7%. Mp. 122-124°C. FT-IR (KBr): 1584 (m), 1488 (s), 1091 (s), 818 (s) cm^{-1}. UV-vis (CH_2Cl_2): λ_{max} 283 nm (ε = 25000 $L•mol^{-1}•cm^{-1}$), 327 nm (ε = 13250 $L•mol^{-1}•cm^{-1}$), 395 nm (ε = 9000 $L•mol^{-1}•cm^{-1}$), 730 nm (ε = 4050 $L•mol^{-1}•cm^{-1}$) . MS (EI): *m/z* 396 (M^+, 40 %). Anal. Calcd for $C_{21}H_{17}Cl_2N_4$: C, 63.65; H, 4.32; N, 14.14. Found: C, 63.73; H, 4.41; N, 14.17.

3-*para*-methoxyphenyl-1,5-di-*para*-tolylverdazyl (2.3i). Yield 74.3 %. Mp. 56-58°C (dec). FT-IR (KBr): 1709 (m), 1610 (m), 1507 (s), 1249 (s) cm^{-1}. UV-vis (CH_2Cl_2): λ_{max} 283 nm (ε = 26000 $L•mol^{-1}•cm^{-1}$), 323 nm (ε = 11500 $L•mol^{-1}•cm^{-1}$), 391 nm (ε = 7000 $L•mol^{-1}•cm^{-1}$), 738 nm (ε = 3250 $L•mol^{-1}•cm^{-1}$). MS (EI): *m/z* 370 ($M\text{-}H^+$, 10 %).

Elemental Analysis was not attempted as **2.6i** was observed to decompose over a period of several hours.

3-phenyl-1,5-di-*para*-tolylverdazyl (2.3j). Yield 50.2 %. Mp. 122-124°C. FT-IR (KBr): 1599 (m), 1504 (s), 1262 (s), 1143 (s) cm^{-1}. UV-vis (CH_2Cl_2): λ_{max} 247 nm (ε = 13750 $L \cdot mol^{-1} \cdot cm^{-1}$), 286 nm ($\varepsilon$ = 24000 $L \cdot mol^{-1} \cdot cm^{-1}$), 323 nm ($\varepsilon$ = 13000 $L \cdot mol^{-1} \cdot cm^{-1}$), 410 nm ($\varepsilon$ = 8500 $L \cdot mol^{-1} \cdot cm^{-1}$), 725 nm ($\varepsilon$ = 4500 $L \cdot mol^{-1} \cdot cm^{-1}$). MS (EI): *m/z* 341 ($M^+$, 65 %). Anal. Calcd for $C_{22}H_{21}N_4$: C, 77.39; H, 6.20; N, 16.41. Found: C, 77.49; H, 6.43; N, 16.60.

3-*para*-chlorophenyl-1,5-di-*para*-tolylverdazyl (2.3k). Yield 68.1 %. Mp. 117-119°C. FT-IR (KBr): 1599 (s), 1563 (s), 1509 (s), 1088 (s) cm^{-1}. UV-vis (CH_2Cl_2): λ_{max} 256 nm (ε = 28000 $L \cdot mol^{-1} \cdot cm^{-1}$), 438 nm ($\varepsilon$ = 2500 $L \cdot mol^{-1} \cdot cm^{-1}$), 740 nm ($\varepsilon$ = 1250 $L \cdot mol^{-1} \cdot cm^{-1}$). MS (EI): *m/z* 374 ($M\text{-}H^+$, 100 %). Anal. Calcd for $C_{22}H_{20}ClN_4$: C, 70.30; H, 5.36; N, 14.91. Found: C, 69.93; H, 5.10; N, 14.94.

1,5-di-*iso*-propyl-3-phenyl-1,2,4,5-tetrazane-6-oxide (2.7b). 2.8a (2.39 g, 9.63 mmol), sodium acetate (1.58 g, 19.3 mmol), and benzaldehyde (0.99 ml, 9.6 mmol) were combined in ethanol (200 mL) and refluxed for 16 h. The solution was filtered and the solvent removed under reduced pressure. The crude product was recrystallized from heptane to give **2.7b** as a white microcrystalline solid, yield (1.7 g, 67 %) . Mp.126 - 128 ºC. ^{1}H NMR (300 MHz, $CDCl_3$): δ 7.57 (d, 2H, ^3J = 7 Hz), 7.38 (m, 3H), 4.66 (septet, 2H, ^3J = 7 Hz), 4.58 (t, 1H, ^3J = 12 Hz), 3.75 (d, 2H, ^3J = 12 Hz), 1.14 (d, 6H, ^3J = 7 Hz), 1.12 (d, 6H, ^3J = 7 Hz) ppm. ^{13}C NMR (75 MHz, $CDCl_3$): δ 154.5, 135.9, 129.0, 128.9, 126.4, 71.2, 48.0, 19.8, 18.6 ppm. FT-IR (KBr): 3216 (m), 2974 (m), υ(CO) 1587 (s), 1427 (m), 1143 (w), 1071 (w), 900 (w), 767 (w)cm^{-1}. MS (EI): *m/z* 262 (M^+, 23 %).

Anal. Calcd. for $C_{14}H_{22}N_4O$: C, 64.09; H, 8.45; N, 21.36. Found: C, 64.22; H, 8.24; N, 21.24.

1,5-di-*iso*-propyl-3-(2'-methylimidazol-5'-yl)-1,2,4,5-tetrazane-6-oxide (2.7e). 2.8a (1.66 g, 6.71 mmol), sodium acetate (1.289 g, 13.42 mmol), and 2-methylimidazolecarboxaldehyde (0.74 g, 6.71 mmol) were combined in ethanol (200 mL) and stirred overnight. The solvent was removed under reduced pressure and the crude product recrystallized from heptane to give **2.7e** as a white crystalline solid, yield 0.892 g (50 %) . ^{1}H NMR (300 MHz, $CDCl_3$): δ 6.96 (s, 1H), 6.89 (d, 1H, *J* = 1 Hz), 4.65 (septet, 2H, *J* = 7 Hz), 4.53 (t, 1H, *J* = 12 Hz), 4.39 (d, 2H, *J* = 12 Hz), 3.71 (s, 3H,), 1.08 (d, 6H, *J* = 7 Hz), 1.06 (d, 6H, *J* = 7 Hz) ppm. ^{13}C NMR (75 MHz, $CDCl_3$): δ 153.6, 142.5, 128.0, 122.3, 64.6, 47.7, 32.9, 19.6, 18.8 ppm. FT-IR (KBr): 3220 (m), 2983 (m), υ(CO) 1615 (s), 1495 (m), 1459 (m), 1416 (s), 1124 (m), 1102 (w), 1067 (m), 922 (m), 896 (w), 773 (w) cm^{-1}. MS (EI): *m/z* 266 (M^+, 21 %). Anal. Calcd. for $C_{12}H_{22}N_6O$: C, 54.11; H, 8.33; N, 31.55. Found: C, 54.02; H, 8.38; N, 31.55.

1,5-dimethyl-3-(2'-methylimidazol-5'-yl)-1,2,4,5-tetrazane-6-oxide (2.7h). A solution of 1-methyl-2-imidazole carboxaldehyde (2.0 g, 18.2 mmol) in 200 mL of methanol was added dropwise to a refluxing solution of **2.8b** (2.146 g, 18.2 mmol) in 10 mL of methanol. After complete addition the mixture was allowed to reflux for 10 h. Pure samples of **2.7h** were obtained via repeated trituration with ethyl acetate. Washings were treated with ether to recover **2.7h** as a colourless microcrystalline solid, yield 2.96 g (77.5 %). Mp. 176°C (dec). ^{1}H NMR (300 MHz, d6-DMSO): δ 7.14 (s, 1H), 6.83 (s, 1H), 5.58 (d, 2H, J-11Hz), 5.07 (t,1H, J=11Hz), 3.68 (s, 3H), 2.95 (s, 6H) ppm. ^{13}C NMR (75 MHz, $CDCl_3$): δ 154.6, 141.7, 128.0, 122.3, 63.0, 38.1, 32.9 ppm. FT-IR (KBr): 3259 (m), 3246

(m), υ (CO) 1599 (s) 1554 (s), 1432 (m), 1056 (m), 972 (s), 862 (m), 739 (m) 678 (m) cm^{-1}. MS (EI): *m/z* 210 (M^+, 50%). Anal.Calcd for $C_8H_{14}N_6O$: C, 45.70; H, 6.71; N, 39.97. Found: C, 45.75; H, 6.74; N, 40.41.

1,3,5-triphenyl-6-oxoverdazyl (2.4a). 2.7a (0.600 g, 1.8 mmol), silver carbonate (0.750 g, 2.7 mmol), and celite (0.500 g) were combined in methanol (25 mL) and allowed to stir for 15 hours. The celite, now plated with silver metal, was filtered off and the solvent removed *in vacuo* to afford a dark red powder. Recrystallization from a saturated methanolic solution afforded **2.7a** as red needles, yield 0.420 g (71.3 %). Mp. 206-208°C. FT-IR (KBr): υ(CO) 1695 (s), 1484 (w), 1121 (w), 691 (w), 601 (w) cm^{-1}. UV-vis (CH_2Cl_2): λ_{max} 255 nm (ε = 21250 $L•mol^{-1}•cm^{-1}$), 291 nm (ε = 8000 $L•mol^{-1}•cm^{-1}$), 320 nm (ε = 12750 $L•mol^{-1}•cm^{-1}$), 422 nm (ε = 1250 $L•mol^{-1}•cm^{-1}$), 537 nm (ε = 2500 $L•mol^{-1}•cm^{-1}$), 561 nm (ε = 2500 $L•mol^{-1}•cm^{-1}$). MS (EI): *m/z* 328 ($M+H^+$, 60 %). Anal. Calcd. for $C_{20}H_{15}N_4O$: C, 73.38; H, 4.62; N, 17.11. Found: C, 73.28; H, 4.54; N, 17.26.

1,5-di-*iso*-propyl-3-phenyl-6-oxoverdazyl (2.4b). *Para*-benzoquinone (0.66g, 6.1 mmol) was added to a solution of **2.7b** (1.07 g, 4.08 mmol) in toluene (50 mL) and the mixture was refluxed for 1 h. The solution was filtered to remove crystallized hydroquinone before the solvent was removed under reduced pressure. The oily red product was purified by flash chromatography (CH_2Cl_2, alumina) to give **2.4b** as a red oil that solidified upon sitting, yield (0.79 g, 75 %). Mp. 50 – 52 °C. FT-IR (KBr): 3034 (w), 2979 (w), 2934 (w), υ(CO) 1680 (s), 1455 (w), 1385 (m), 1371 (m), 1312 (w), 1231 (m), 1128 (w), 1024 (w), 776 (m), 722 (w), 695 (m), 660 (w) cm^{-1}. UV-vis (CH_2Cl_2): λ_{max} 249 nm (ε = 32375 $L•mol^{-1}•cm^{-1}$), 414 nm (ε = 1925 $L•mol^{-1}•cm^{-1}$). MS (EI) *m/z*

259 (M^+, 16 %). Anal. Calcd. for $C_{14}H_{19}N_4O$: C, 64.84; H, 7.38; N, 21.60. Found: C, 64.02; H, 7.21; N, 21.87.

1,5-di-*iso*-propyl-3-(2'-methylimidazol-5'-yl)-6-oxoverdazyl (2.4e). *para*-benzoquinone (0.35 g, 3.2 mmol) was added to a solution of **2.7e** (0.57 g, 2.1 mmol) in toluene (50 mL) and the mixture was refluxed for 1.5 h. Solvent was removed under reduced pressure to give an oily red product that was purified by flash chromatography (CH_2Cl_2, alumina) to give **2.4e** as a red solid, yield 0.46 g (83 %). Mp. 112 - 114°C. FT-IR (KBr): 3106 (m), 2976 (m), υ(CO) 1689 (s), 1467 (m), 1418 (w), 1242 (m), 1221 (w), 1166 (m), 1143 (m), 915 (w), 778 (m), 642 (w) cm^{-1}. UV-vis (CH_2Cl_2): λ_{max} 261 nm (ε = 18000 $L \cdot mol^{-1} \cdot cm^{-1}$), 412 nm (ε = 1200 $L \cdot mol^{-1} \cdot cm^{-1}$). MS (EI): *m/z* 263 ($M^+$, 5 %). Anal. Calcd. for $C_{12}H_{19}N_6O$: C, 54.74; H, 7.27; N, 31.92. Found: C, 54.80; H, 7.55; N, 31.89.

1,5-dimethyl-3-(2'-methylimidazol-5'-yl)-6-oxoverdazyl (2.4h). A solution of sodium periodate (0.229 g, 1.07 mmol) in 10 mL of distilled water was added to a vigorously stirred slurry of **2.7h** (0.15 g, 0.71 mmol) in 20 mL of distilled water resulting in a cherry red solution. After 10 min of stirring the solution was placed in an ice bath for 30 min resulting in the precipitation of **2.4h** as a microcrystalline red solid, yield 0.103 g (68%). Mp. 165°C (dec). FT-IR (KBr): 3131 (m), 3115 (m), υ(CO) 1674 (s), 1489 (m), 1464 (m), 1382 (m), 1147 (m), 914 (m), 728 (m), 643 (m) cm^{-1}. UV-vis (CH_2Cl_2): λ_{max} 415 nm (ε = 1100 $L \cdot mol^{-1} \cdot cm^{-1}$), 493 nm (ε = 410 $L \cdot mol^{-1} \cdot cm^{-1}$). MS (LSIMS): *m/z* 207 (MH^+, 100%), 107 (80%). Anal.Calcd for $C_8H_{11}N_6O$: C, 46.37; H, 5.35; N, 40.56. Found: C, 46.20; H, 5.38; N, 40.68.

Chapter 3 Formazans as ancillary ligands

3.1 Common ancillary ligands

Many popular ancillary ligands are chelating, anionic, π-conjugated N- or O-donors. Perhaps the most common family of such ligands are the acetylacetonates **3.1**,[240-244] which have also been derivatized to produce β-ketiminates **3.2**,[245-249] and β-diketiminates **3.3**.[250] The latter have emerged from the many classes of polyamido ligands (e.g., amidinates **3.4**,[251, 252] aminotroponiminates **3.5**,[253] and diazabutadienes **3.6**[254-258]) as the most versatile due to their ease of derivitization. The ability to tune steric and electronic properties of transition metal complexes of β-diketiminates through changes in R_1 and R_5 (as well as R_2, R_3, and R_4) substituents contributes greatly to their utility. The utility of β-diketiminates as ligands has also prompted the development of analogous ligand families such as triazapentadienes **3.7**,[259-262] bearing an additional nitrogen in the ligand backbone.

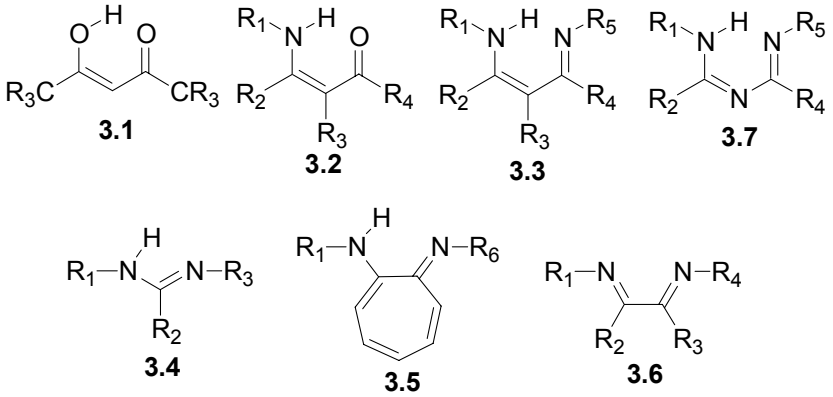

Formazans **3.8** are close structural analogues of β-diketiminates, possessing two additional nitrogen atoms in their backbone. Inorganic complexes of formazans **3.9** are ideal candidates for conversion to inorganic verdazyl radicals **3.10**. The synthesis and

conversion of such complexes to verdazyl radicals represents an alternative strategy to those used to afford phosphaverdazyls (see Chapter 1).

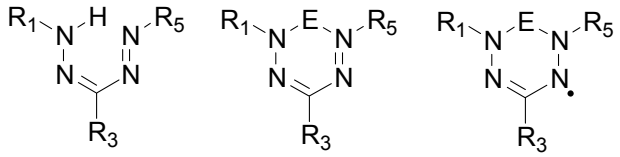

3.8 **3.9** **3.10**

The coordination chemistry of formazans has been sporadically explored over the past 60 years, but remains an undeveloped field. Examples of systematic studies of formazan complexes are rare, and include bis formazan complexes of palladium **2.14a**[208] and nickel **2.14b**[209, 263] (see section 2.2), cyclometallated ruthenium complexes **3.11**,[264] and nickel complexes of sulfur containing macrocyclic formazans **3.12**.[265-267]

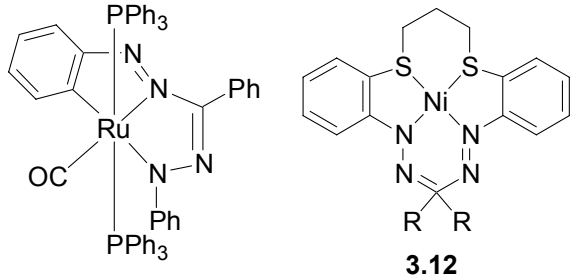

3.11 **3.12**

Several reports of crystallographic studies of transition metal complexes of formazans exist. However, in most cases these reports are not accompanied by appropriate characterization data.[268] The majority of the complexes involve asymmetric formazan ligands (e.g., **3.13**) coordinated by a similar bonding mode to that observed in **3.11**, i.e., 5 membered chelate rings are formed, and the ligand is coordinated through the 1,4-nitrogen atoms as well as the benzothiazolyl N-substituent.[269]

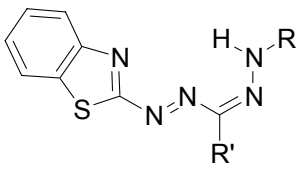

3.13

The remaining reports on transition metal complexes of formazans focus on their physical properties in the absence of structural characterization. Kawamura has reported the EPR and magnetic properties of a number of bis formazan complexes of copper (II) **3.14a**,[270-272] nickel (II) **3.14b**,[273] and cobalt (II) **3.14c**.[274] Given the novelty of formazans as ligands, and their potential to coordinate via a number of coordination modes, the importance of structural characterization cannot be overlooked. This chapter describes the synthesis and characterization of formazan ligands and their inorganic complexes, with emphasis placed on their potential utility as precursors to inorganic verdazyl radicals.

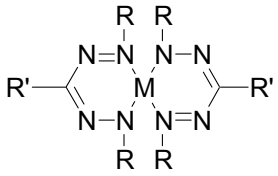

3.14a M = Cu
3.14b M = Ni
3.14c M = Co

Results and discussion

3.2 Synthesis and characterization of boratatetrazines and borataverdazyls

3.2.1 Synthesis of boratatetrazines

Existing synthetic pathways to inorganic verdazyl radicals are limited to the incorporation of phosphorus.[163-165] Group 13 complexes of formazans were attractive targets as they have potential to act as precursors to inorganic verdazyls, and to illustrate similarities between formazans and closely related β-diketiminate ligands. The known main group chemistry of formazans is limited to sporadic and incomplete reports in the Russian literature.[275, 276] Preliminary efforts to coordinate formazans to boron and

aluminum using reagents such as trimethylaluminum, trifluoroaluminum, borane, and boron trifluoride failed. The focus then turned to boron triacetate, a reagent which finds sporadic use in organic chemistry as a Lewis acid,[277-279] generated *in situ* by heating a mixture of boric acid, acetic acid, and acetic anhydride. Triarylformazans **2.1d** and **2.1j** were reacted with boron triacetate at reflux, yielding boratatetrazines **3.15d** and **3.15j** containing a four coordinate, formally anionic boron center stable to air and moisture (Scheme 3.1). The ^{1}H and ^{13}C NMR spectra of **3.15d** and **3.15j** are consistent with a delocalized boratatetrazine backbone. The ^{11}B NMR spectra consist of singlets at δ 1.32 ppm for **3.15d**, and δ 1.31 ppm for **3.15j**, consistent with examples of four coordinate, anionic boron complexes of β-diketiminates.[280] The electronic spectra of **3.15d** and **3.15j** are similar to those observed in formazans **2.1d** (λ_{max} = 491 nm) and **2.1j** (λ_{max} = 493 nm), but are redshifted in **3.15d** (λ_{max} = 558 nm) and **3.15j** (λ_{max} = 560 nm) (Figure 3.1).

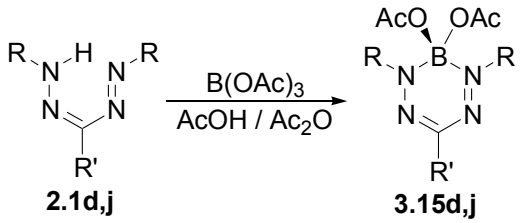

2.1d,j **3.15d,j**

Scheme 3.1. Synthesis of boratatetrazines **3.15d**, and **3.15j**.

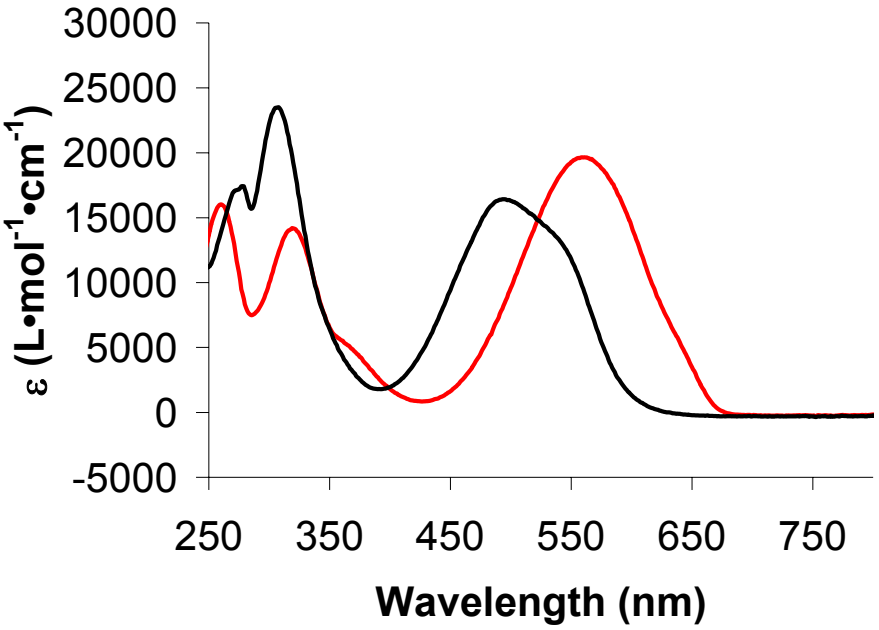

Figure 3.1. Electronic spectra of formazan **2.1j** (black line) and boratatetrazine **3.15j** (red line) in CH_2Cl_2.

3.2.2 Crystal structures of boratatetrazines 3.15d and 3.15j

The first examples of crystal structures of main group-formazan complexes (**3.15d** and **3.15j**) are shown in Figure 3.2. The structure of **3.15j** will be discussed here in detail; the structure of **3.15d** is very similar (see table 3.1). The formazan ligand is bound to tetrahedral boron in a η^2 fashion in **3.15j**. The near equivalence of the bond length pairs related by a *pseudo* mirror plane down the B1, C1, C11 axis is consistent with delocalization within the CN_4 formazan backbone (N2-N1 1.1.2976(14) Å, N4-N3 1.3025(14) Å, C1-N1 1.3376(16) Å, and C1-N3 1.3361(16) Å). The atoms making up the BCN_4 ring are nearly coplanar with the B1 atom residing 0.14 Å above the plane of the formazan. The average BN bond length is 1.561 Å, comparable to other four coordinate boron complexes of β-diketiminates ligands.[280-283]

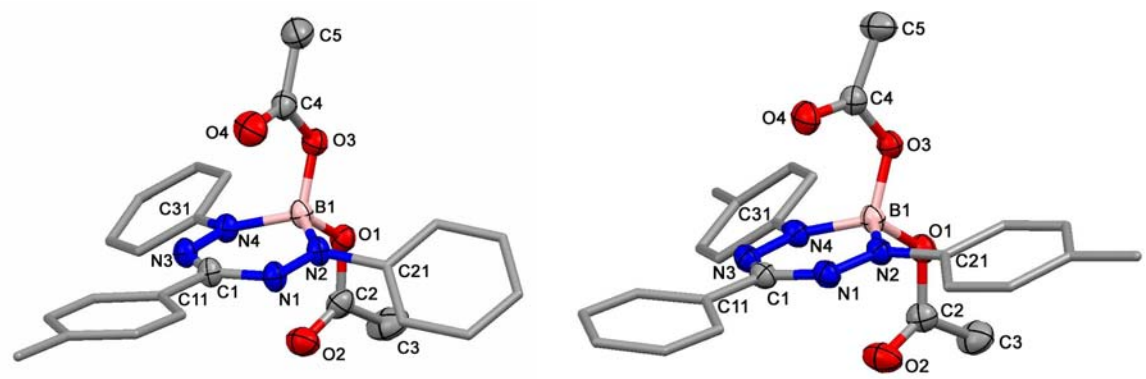

Figure 3.2. Molecular Structure of **3.15d** (molecule A, left) and **3.15j** (right). Thermal ellipsoids shown at 50% probability level. Hydrogen atoms omitted for clarity.

Table 3.1. Selected bond lengths (Å) and angles (deg) for **3.15d** and **3.15j**.

Atoms	**3.15d**[a]		**3.15j**	Atoms	**3.15d**[a]		**3.15j**
	Mol. A	Mol. B			Mol. A	Mol. B	
N1-N2	1.303(2)	1.303(2)	1.2976(14)	N3-C1-N1	126.5(2)	126.0(2)	126.47(11)
N3-N4	1.305(2)	1.304(2)	1.3025(14)	C1-N1-N2	118.11(19)	117.85(18)	119.60(10)
C1-N1	1.344(3)	1.344(3)	1.3376(16)	C1-N3-N4	118.61(18)	118.92(18)	118.33(10)
C1-N3	1.332(3)	1.341(3)	1.3361(16)	N1-N2-B1	124.82(18)	125.44(18)	123.87(10)
N2-B1	1.555(3)	1.547(3)	1.5623(16)	N3-N4-B1	124.42(18)	124.37(18)	125.03(10)
N4-B1	1.553(3)	1.548(3)	1.5601(17)	N2-B1-N4	105.51(18)	105.76(18)	105.80(9)
B1-O1	1.457(3)	1.456(3)	1.4556(16)	N2-B1-O3	113.07(19)	113.06(19)	111.00(10)
B1-O3	1.463(3)	1.464(3)	1.4683(16)	N4-B1-O3	111.34(19)	111.52(18)	112.63(10)
				N2-B1-O1	110.14(19)	110.92(19)	112.69(10)
				N4-B1-O1	111.61(19)	111.80(19)	111.12(10)
				O1-B1-O3	105.29(18)	103.94(18)	103.77(9)

[a]Two crystallographically inequivalent molecules were detected in the unit cell.

3.2.3 Electrochemistry of boratatetrazines

In order to produce stable verdazyl radicals based on boratatetrazines, their similarities to well known organic radicals must be considered. The one-electron reduction of boratatetrazines should produce borataverdazyl radical anions, isolobal to parent systems (Figure 3.3).

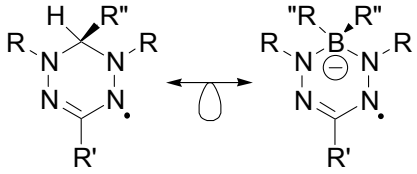

Figure 3.3. Isolobal relationship between type I verdazyls and borataverdazyl radical anions.

The cyclic voltammograms of **3.15d** and **3.15j** have reversible one-electron reduction waves at -0.86 V and -0.91 V against the ferrocene/ferrocenium redox couple (Figure 3.4). The reversible nature of the redox wave implies stability of the radical anion on the timescale of the electrochemical experiment. When the potential is decreased beyond -1.5 V, a second irreversible multielectron process is observed. The reversibility of the first reduction in the cyclic voltammograms, and the isolobal relationship between type I verdazyl radicals and borataverdazyl radical anions make **3.15d** and **3.15i** attractive precursors to borataverdazyls.

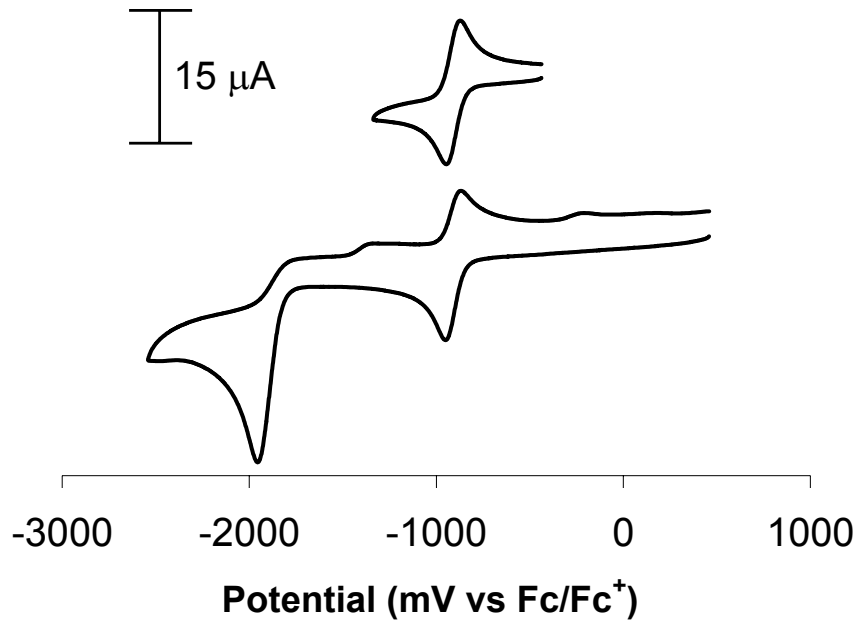

Figure 3.4. Cyclic Voltammogram of boratatetrazine **3.15j** in CH_3CN containing 0.1 M $Bu_4N^+BF_4^-$ (electrolyte). Scan rate 100 mV/s.

3.2.4 Synthesis and characterization of borataverdazyls

The low reduction potential of boratatetrazines left few choices for reducing agents strong enough to transfer an electron to boratatetrazines irreversibly.[284] Cobaltocene was chosen as it is one of few commercially available molecules with an

oxidation potential low enough to permit electron transfer to boratatetrazines **3.15d** and **3.15j**.

Green radical anion salts **3.16d** and **3.16i** precipitate from hexanes solutions upon addition of cobaltocene to a solution of boratatetrazine (Scheme 3.2). These salts were not stable when dissolved in organic solvents—they decompose to the parent boratatetrazines—including those that had been degassed via multiple freeze-pump-thaw cycles. However, radical anions **3.16d** and **3.16i** were sufficiently stable in the solid-state to allow for their characterization.

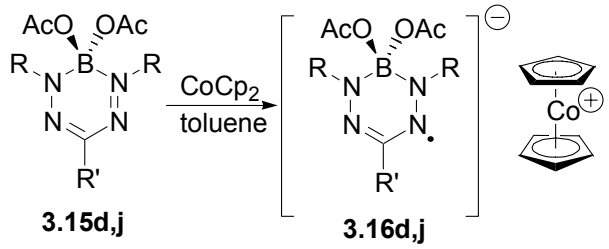

Scheme 3.2. Synthesis of borataverdazyl radical anions **3.16d** and **3.16j**.

The solid-state electronic spectrum (diffuse reflectance) of radical anion **3.16j** is shown, along with precursor compounds **2.1j** and **3.15j** in Figure 3.5. The spectrum has a low energy absorption at 744 nm, close to the longest wavelength absorption maxima in the analogous organic verdazyl (**2.3j**; λ_{max} = 725 nm). The solid-state electronic spectrum of **3.16d** is similar to that of **3.16j**, and has a low energy absorption at 743 nm. The similarity of the electronic spectra with those of isolobal type I verdazyls (see Figure 3.3) provides support for the formulation of **3.16d** and **3.16j** as borataverdazyl radical anions.

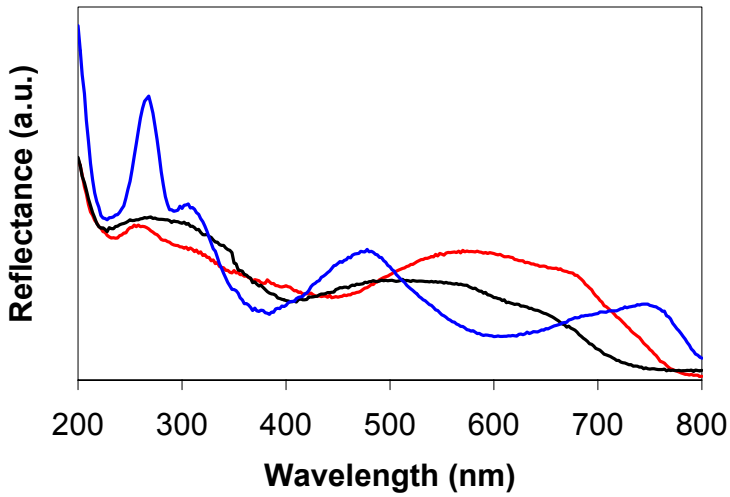

Figure 3.5. Diffuse reflectance spectra of 1.1% **2.1j** (black line), **3.15j** (red line), and **3.16j** (blue line) in $BaSO_4$.

The solid-state EPR spectra of **3.16d** and **3.16j** consist of strong featureless signals near g = 2.00, exemplified in Figure 3.6. Although little information can be gained from the shape of the spectra, the observed g-factors rule out the possibility of cobaltocene contamination as the solid-state EPR spectrum of cobaltocene is asymmetric with $g_{\|} = 1.67$ and $g_{\perp} = 1.74$.[285]

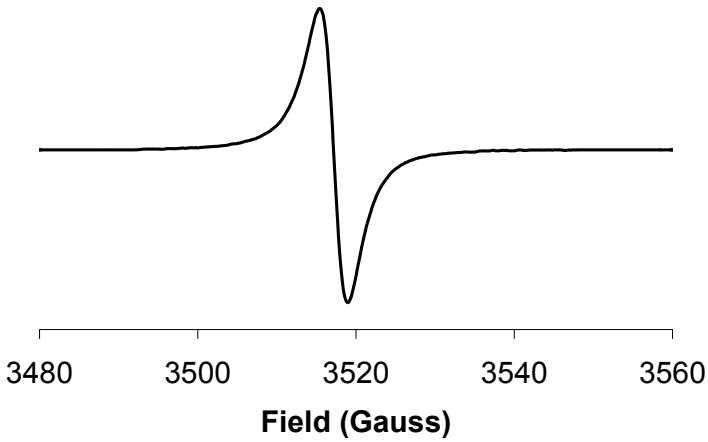

Figure 3.6. Solid-state EPR spectrum of **3.16j** at room temperature.

3.3 3-Substituted formazans

The coordination chemistry of β-diketiminates is dominated by derivatives containing bulky N-substituents (e.g., 2,6-dimethylphenyl, mesityl, and 2,6-di-*iso*-propylphenyl).[250] The synthetic pathways to most formazans do not readily allow for analogous ligands to be prepared. For example, the triarylformazans described in Chapter 2 were synthesized via coupling reactions between hydrazones and aryldiazonium salts. The hydrazones were synthesized upon condensation of aryl-aldehydes with aryl-hydrazines. However, tryiarylformazans bearing 'bulky' substituents cannot be produced via this pathway as the corresponding hydrazines and diazonium salts are often unstable.

3-Substituted formazans are not as common as triarylformazans,[207] but can be synthesized by alternative syntheses that do not rely on the synthesis of hydrazones. The 3-cyanoformazans **3.17** and 3-nitroformazans **3.18** described here were synthesized via reaction of two equivalents of aryldiazonium salts with cyanoacetic acid or nitromethane under basic conditions, avoiding the use of arylhydrazines. Although most common examples of β-diketiminates do not possess strong electron-withdrawing substituents, the chemistry of cyano- and nitro-substituted derivatives has been explored,[286-291] and their electron-withdrawing nature shown to significantly alter the catalytic activity of resulting complexes.[292-295]

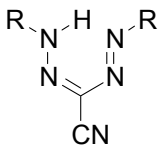

3.17

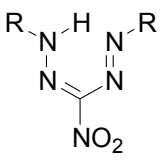

3.18

3.4 Structures of formazans

Triarylformazans exist exclusively as *pseudo* 6-membered rings in solution and the solid-state. However, other formazans with relatively small 3-substituents have been observed to adopt different structures. The conventional nomenclature used to describe the structure of formazans was established in the 1950s.[207] The orientation of substituents about the N=N bond is described using *cis/trans* nomenclature while the orientation about the C=N bond is described using *syn/anti* nomenclature. Finally, substitution of the C-N bond is described as *s-cis* or *s-trans*. To date crystal structures of three different structures have been reported (Figure 3.7), each of which can be described as *closed* (*trans-syn, s-cis*),[215, 217, 218, 296-298] *open* (*trans-syn, s-trans*),[299-301] or *linear* (*trans-anti, s-trans*).[296, 301-303] From this point forward the structures of formazans will be described using the short forms described previously, i.e., *closed*, *open*, or *linear*. Formazans existing as the *closed* structure are generally red while the *open* and *linear* formazans are orange and yellow respectively.[207] The orientation adopted is substrate dependent, and in some cases mixtures are observed. The situation is further complicated by solvatochromism of some formazans[304] and the tendency of other derivatives to interconvert photochemically.[296, 301, 305, 306]

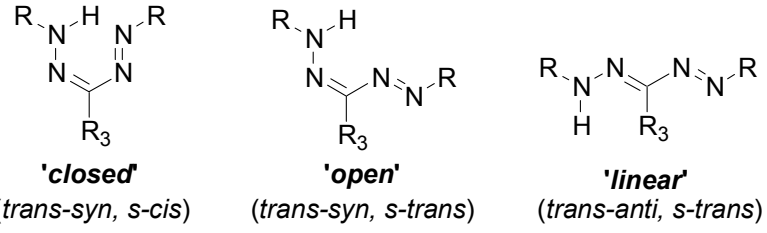

Figure 3.7. Common structures of formazans.

3.5 Synthesis and characterization of 3-cyanoformazans

3.5.1 Synthesis of 3-cyanoformazans

3-Cyanoformazans were synthesized via reaction of two equivalents of the appropriate aryldiazonium chloride salt with deprotonated cyanoacetic acid (Scheme 3.3). The reaction proceeded upon attack of the diazonium cation by the *in situ* generated carbanion of cyanoacetic acid. The hydrazone-type intermediates are then deprotonated (by hydroxide or initial carbanion) and the resulting carbanion attacks a second equivalent of aryl-diazonium cation. The carboxyl group associated with cyanoacetic acid must also be lost during the reaction (probably as CO_2), although it is not clear at which stage this occurs.

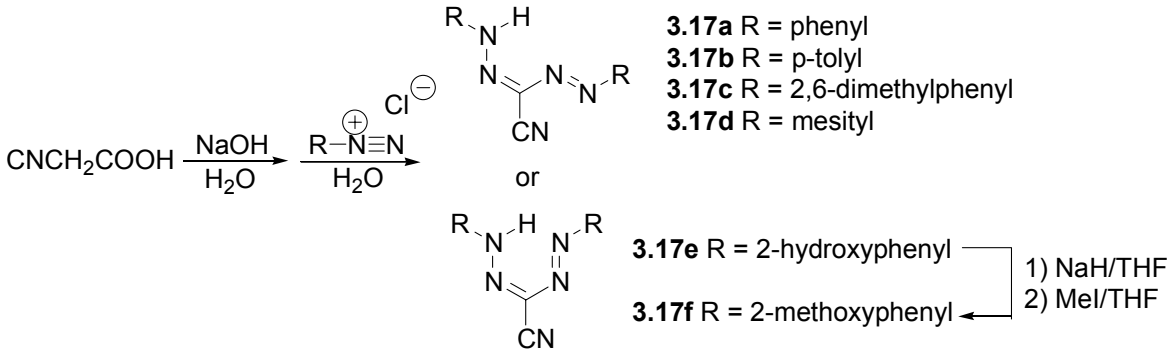

Scheme 3.3. Synthesis of 3-cyanoformazans **3.17a-f**.

This method was used to prepare 3-cyanoformazans **3.17a-f**, some of which have been reported previously.[307-310] However, the characterization of these compounds was either incomplete or incorrect. Formazan **3.17f** was also prepared by the selective methylation of **3.17e** through reaction of the corresponding trianion with an excess of methyliodide. Attempts to synthesize 3-cyanoformazans with 'bulky' aryl substituents larger than mesityl (i.e., 2,6-di-*iso*-propylphenyl or 3,5-di-*tert*-butylphenyl) were not

successful, yielding a variety of highly coloured compounds. The instability of the aryldiazonium salts involved may play a role in the failure of such reactions.

3.5.2 Solid-state properties of 3-cyanoformazans

The crystal structure of formazan **3.17d** is presented in Figure 3.8. Formazan **3.17d** adopts the *open* structure in the solid-state. The formazan backbone (N2-N1-C1-N3-N4) has greater bond alternation than triarylformazans (see section 2.3.2). However, the bond lengths observed would not be considered typical of N-N (N-N ~ 1.40 Å, N=N ~ 1.24 Å) and C-N (C-N ~ 1.49 Å, C=N ~ 1.28 Å) single and double bonds[219] (N2-N1 1.325(2) Å, N3-N4 1.269 (2) Å, N1-C1 1.304(2) Å, N3-C1 1.392(2) Å). The mesityl substituent attached to N2 is twisted with respect to the plane defined by the formazan backbone by 29.8˚, while the mesityl ring attached to N4 is twisted by 7.3˚.

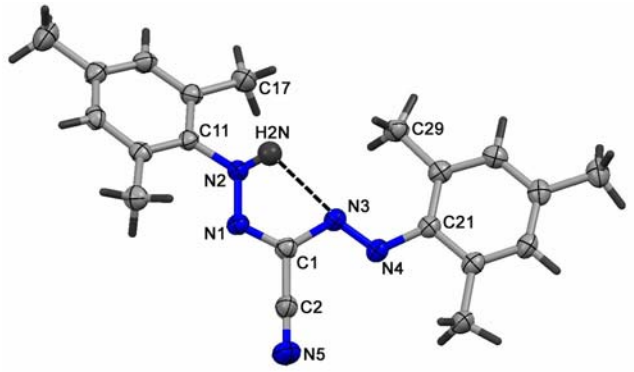

Figure 3.8. Molecular structure of **3.17d**. Thermal ellipsoids shown at the 50% probability level.

Table 3.2. Selected bond lengths (Å) and angles (deg) for **3.17d**.

Atoms	**3.17d**	Atoms	**3.17d**
N2-N1	1.325(2)	N2-N1-C1	116.38(15)
N3-N4	1.269(2)	C1-N3-N4	112.45(14)
N1-C1	1.304(2)		
C1-N3	1.392(2)		

Single crystals of **3.17a-c** were significantly disordered, precluding structural determination. Diffuse reflectance spectroscopy was employed in order to compare the solid-state structures of **3.17a-c** with that of **3.17d** (Figure 3.9). The spectrum of **3.17d** has a maximum at 453 nm, with a shoulder on the low energy side at ~530 nm. The *para*-tolyl and 2,6-dimethylphenyl derivatives **3.17b** and **3.17c** have similar spectral features that suggest all three compounds exist as the *open* structure in the solid-state. The spectrum of the phenyl derivative **3.17a** consists of a broad maximum at 407 nm and a small shoulder above 500 nm. It is not clear whether the spectral differences in **3.17a** are due to structure, or if the phenyl substituent (slightly withdrawing) plays a role as the aryl substituents in **3.17b-d** are all electron donating.

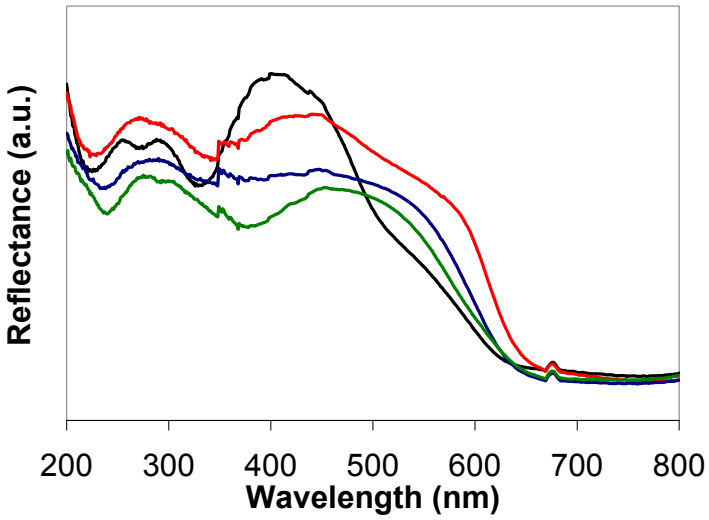

Figure 3.9. Diffuse reflectance spectra of 1.1% **3.17a** (black line), **3.17b** (red line), **3.17c** (blue line), and **3.17d** (green line) in $BaSO_4$.

The solid-state structures of **3.17e** and **3.17f** are presented in Figure 3.10. In contrast to the structure observed in **3.17d,** they exist in the *closed* orientation. In **3.17e** the formazan backbone has minimal bond alternation (N2-N1 1.3101(15) Å, N3-N4 1.2904(15) Å, N1-C1 1.3180(18) Å, C1-N3 1.3798(18) Å) while in **3.17f** no bond

alternation is observed within experimental error (N2-N1 1.292(3) Å, N3-N4 1.296(3) Å, N1-C1 1.355(4) Å, C1-N3 1.353(4) Å). Both compounds possess NH proton bridges between N2 and N4. However, their structures appear to be influenced by the presence of hydrogen bonds. Formazan **3.17e** has both intramolecular (OH2-N3) and intermolecular hydrogen bonds (OH1-N5'). The N-substituents are nearly coplanar with respect to the formazan backbone; the ring attached to N2 twisted by 3.8˚, and the ring attached to N4 twisted by 3.9˚. Formazan **3.17f** may also benefit from additional hydrogen bonding between O1 and O2 with H2N. However, these interactions are likely weak due to their relatively long OH bond distances (O-H > 2.3 Å). The N-substituents in **3.17f** are twisted with respect to the formazan backbone. The 2-methoxyphenyl attached to N2 is twisted by 27.0°, and the ring attached to N4 by 4.7°. The non-planarity of **3.17f** compared to **3.17e** results from steric interactions associated with the close proximity of the methoxy substituents.

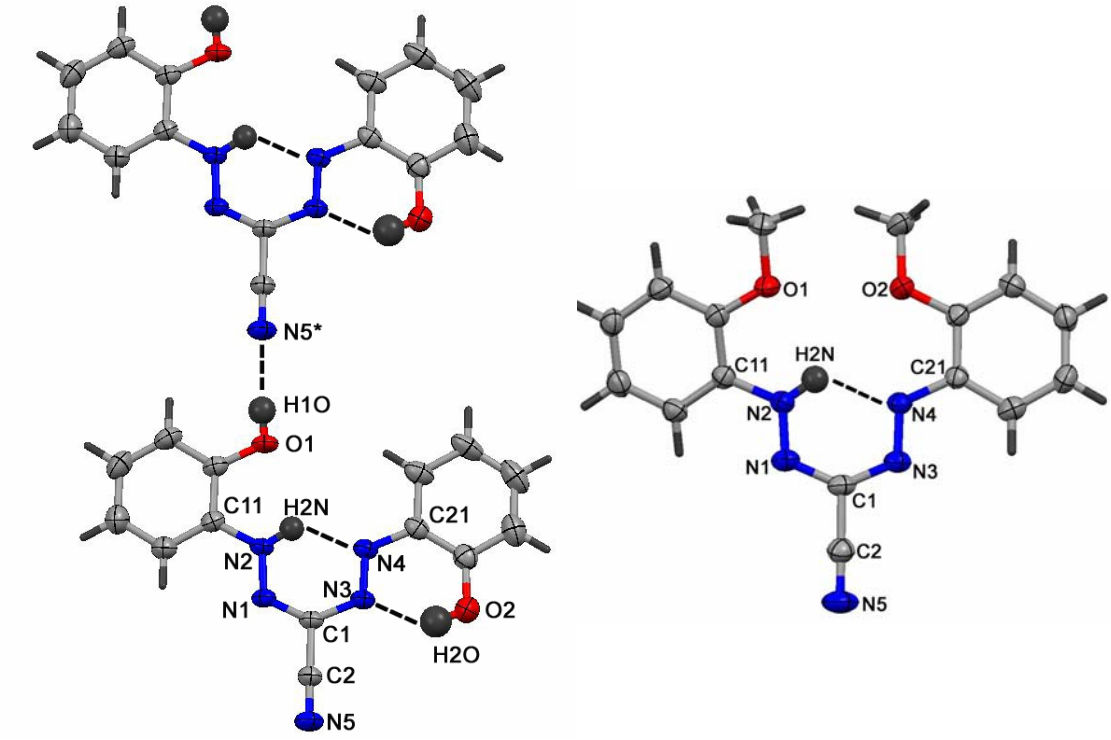

Figure 3.10. Molecular structure of **3.17e** (left) and **3.17f** (right). Thermal ellipsoids shown at 50% probability level.

Table 3.3. Selected bond lengths (Å) and angles (deg) for **3.17e** and **3.17f**.

Atoms	**3.17e**	**3.17f**	Atoms	**3.17e**	**3.17f**
N2-N1	1.3101(15)	1.292(3)	N2-N1-C1	118.13(11)	117.3(3)
N3-N4	1.2904(15)	1.296(3)	C1-N3-N4	115.11(11)	115.5(2)
N1-C1	1.3180(18)	1.355(4)			
C1-N3	1.3798(18)	1.353(4)			

3.5.3 Solution properties of 3-cyanoformazans

Many previously reported 3-cyanoformazans adopt the *closed* structure as evidenced by (i) their ^{1}H NMR shifts of the NH proton at approximately 15 ppm; (ii) the absence of NH stretches in their IR spectra due to strong intramolecular N-H bonds (exclusive to the *closed* structure); and (iii) their electronic spectra, which possess maxima near 500 nm. The *closed* structure of 3-cyanoformazans can be unequivocally

assigned by comparison of their properties with 3-cyanoformazans which are built into a macrocyclic structure, forcing the *closed* form to exist exclusively.[238, 311-314] However, other 3-cyanoformazans have been reported, and based on their ^{1}H NMR spectra (δNH 10-12 ppm), must adopt either the *open* or *linear* conformation.[307, 315]

Table 3.4 summarizes the ^{1}H NMR data for cyanoformazans **3.17a-d**. The ^{1}H NMR spectra of **3.17a-d** have two distinct resonances assigned to NH protons. The dominant resonance falls between δ 11.2 and 12.5 ppm, and the minor peak appears between δ 8.8 and 9.2 ppm. Both peaks are upfield relative to the NH resonance in formazans existing in the *closed* conformation.

Table 3.4. Ratio of formazan structures in solution for **3.17a-f**.

compound	solvent	*closed*	*open*	*linear*
3.17a	CD_2Cl_2	0	0.78	0.22
3.17b	CD_2Cl_2	0	0.85	0.15
3.17c	CD_2Cl_2	0	0.85	0.15
3.17d	CD_2Cl_2	0	0.87	0.13
3.17e	*d6*-DMSO	1.00	0	0
3.17f	*d6*-DMSO	0.88	0.12	0

The similarities in the ^{1}H NMR spectra of **3.17a-d**, i.e., the relative positions of the major and minor species, suggest that the identity of the major and minor species are also similar. A representative ^{1}H NMR spectrum for **3.17d** is shown in Figure 3.11. The ^{1}H NMR of the minor species clearly reveal the presence of inequivalent N-substituents, while in the major species the aryl substituents are equivalent. The ^{1}H NMR of other families of formazans have been studied extensively, and the *open* structure has been assigned to the symmetric set of peaks.[306, 316, 317] The equivalence of the aryl substituents arises from rapid tautomerization (Figure 3.12), perhaps via the corresponding *closed* form. In contrast, the *linear* isomer does not tautomerize rapidly, rendering the N-

substituents inequivalent. On the basis of this argument, the major species for **3.17a-d** is assigned as the *open* structure and the minor species as the *linear* structure.

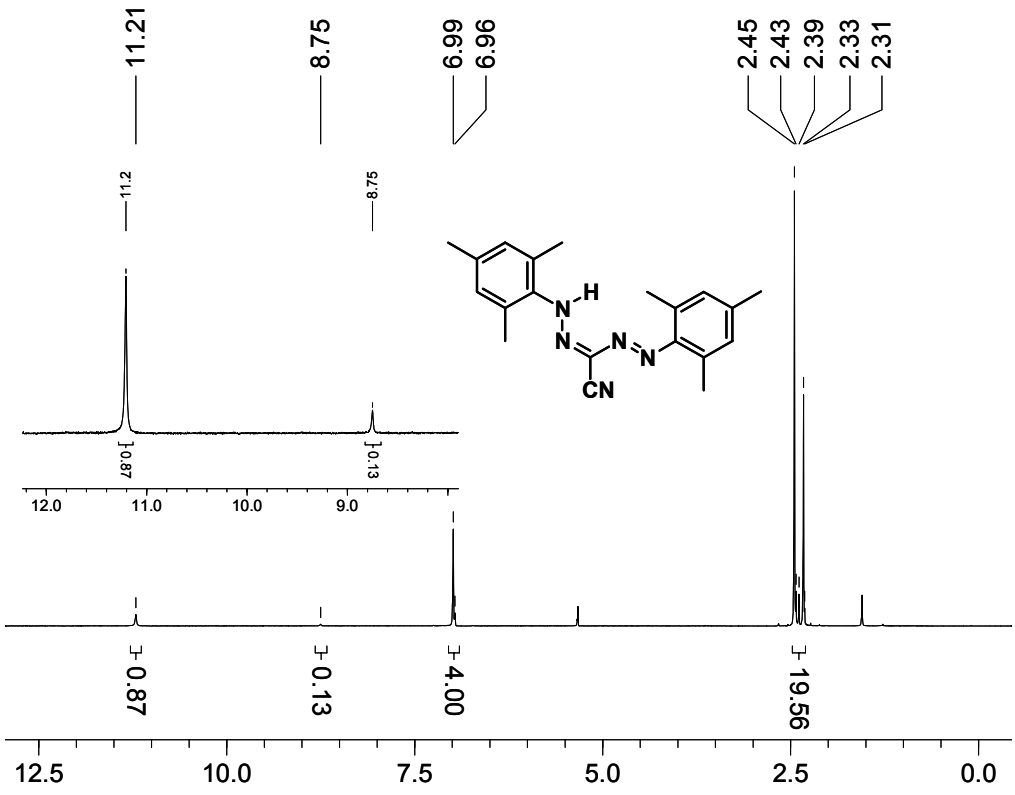

Figure 3.11. ^{1}H NMR spectrum of **3.17d** in CD_2Cl_2.

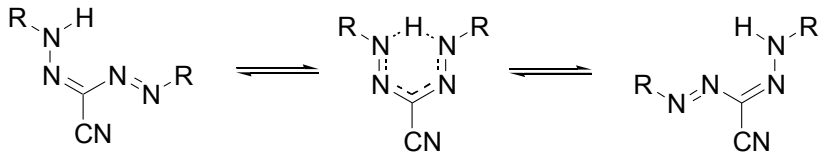

Figure 3.12. Tautomerization of open formazans.

3-Cyanoformazans **3.17e** and **3.17f** exist predominantly as the *closed* structure in solution with minor components of the *open* form. The NMR spectra of these compounds were obtained in *d6*-DMSO (low solubility in CD_2Cl_2), precluding direct comparison with other 3-cyanoformazans. However, it is worth noting that related *ortho*-functionalized 3-cyanoformazans appear to be *closed* in other solvents.[238, 311-314]

The solution electronic spectra of 3-cyanoformazans **3.17a-f** are presented in Figure 3.13. Their absorptions in the visible region are highly substrate dependent. The visible bands—spanning a range of nearly 200 nm—are believed to be charge transfer in nature due to their extremely high extinction coefficients and solvatochromism.[304] The *para*-tolyl derivative **3.17b** has its lowest energy absorption at 453 nm, red shifted by 40 nm relative to the phenyl-substituted derivative **3.17a** due to its increased electron donating ability. The 2,6-dimethylphenyl groups in **3.17c** lead to a strong blue shift (λ_{max} = 381 nm) compared to **3.17a** or **3.17b**, however, the introduction of an additional *para*-methyl substituent in **3.17d** causes a red shift compared to **3.17c** (λ_{max} = 423 nm). Compounds **3.17e** and **3.17f** exist mainly in the *closed* structure and have multiple absorptions above 450 nm, redshifted substantially from other 3-cyanoformazans. The *ortho*-hydroxyphenyl derivative **3.17e** has the lowest energy absorption of all of the 3-cyanoformazans, perhaps due to increased delocalization associated with a fixed conformation resulting from multiple hydrogen bonding interactions within the *closed* (coplanar) structure.

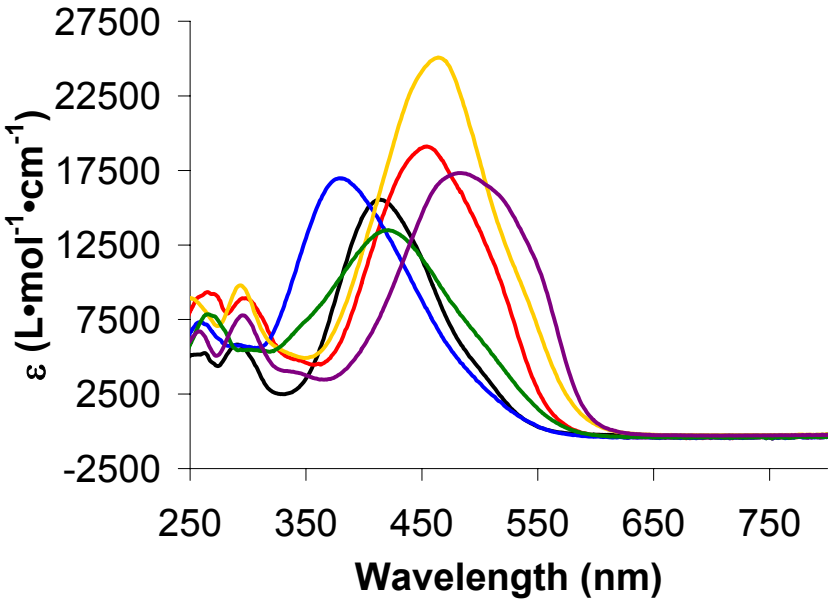

Figure 3.13. Electronic spectra of **3.17a** (black line**), 3.17b** (red line), **3.17c** (blue line), **3.17d** (green line), **3.17e** (purple line), and **3.17f** (orange line) in CH_2Cl_2.

3.6 Synthesis and characterization of 3-nitroformazans

3.6.1 Synthesis of nitroformazans

3-Nitroformazans were synthesized using similar methodologies to the synthesis of 3-cyanoformazans, using nitromethane instead of cyanoacetic acid (Scheme 3.4). This route was employed for **3.18a**, and **3.18b** which conveniently precipitate from aqueous solution. However, attempts to synthesize 3-nitroformazans bearing bulky N-subsituents this way were not successful. In the nitromethane systems even the presence of *ortho*-methyl groups causes the reaction to fail; the 2,6-dimethylphenyl derivative **3.18c** has been made previously in 1 % yield.[297]

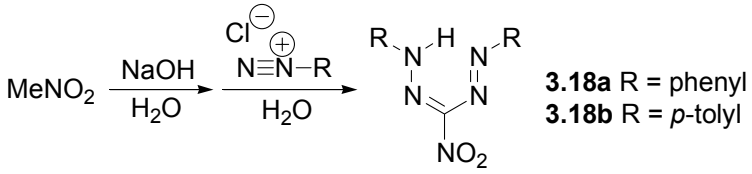

Scheme 3.4. Synthesis of 3-nitroformazans **3.18a** and **3.18b** under aqueous conditions.

In order to produce 3-nitroformazans with bulky aryl substituents (**3.18c-f**) anhydrous synthetic routes were developed. The tetrafluoroborate salts of the aryldiazonium cations[318] were stable enough under such conditions to couple with deprotonated nitromethane producing 3-nitroformazans in reasonable yields (Scheme 3.5).

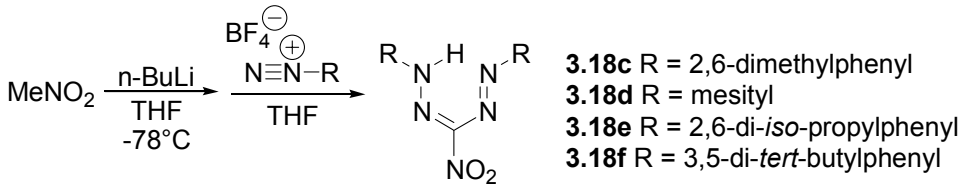

Scheme 3.5. Synthesis of 3-nitroformazans **3.18c-f** under anhydrous conditions.

3.6.2 Solid-state properties of 3-nitroformazans

The crystal structures of **3.18b** and **3.18d** are shown in Figure 3.14. Formazan **3.18d** exists as the *closed* structure in the solid-state. As is the case for other structurally characterized formazans existing as the *closed* structure, the formazan backbone is highly delocalized with minimal bond alternation observed (N1-N2 1.299(2) Å, N4-N3 1.282(2) Å, N1-C1 1.322(2) Å, N3-C1 1.357(2) Å). The mesityl substituents in **3.18d** are twisted significantly with torsion angles of 26.8˚ (ring attached to N2) and 47.2˚ (ring attached to N4) relative to the formazan backbone. The nitro group is also twisted by 14.7˚ with respect to the formazan plane. The structure of **3.18b** is similar to **3.18d** (see Table 3.5), confirming the *closed* structure. The N-substituents are twisted (17.3˚ and 3.6˚) and the nitro group is twisted by 23.4˚ with respect to the formazan plane.

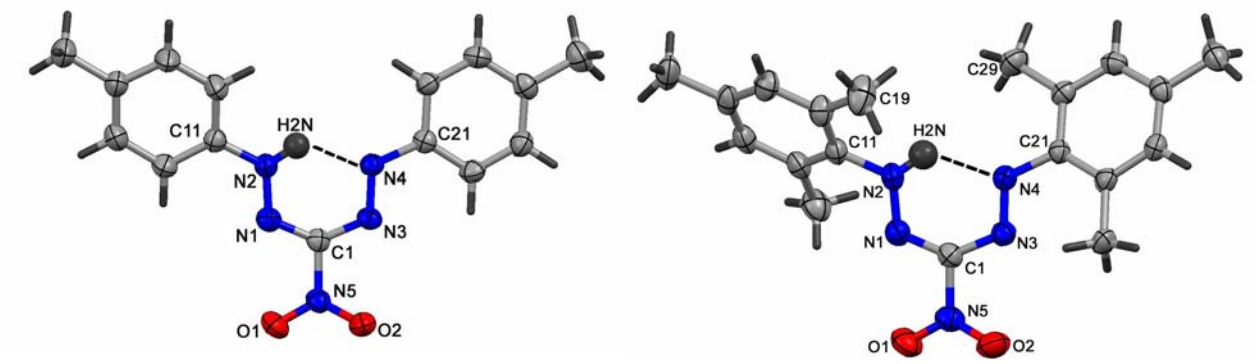

Figure 3.14. Molecular structure of **3.18b** (left) and **3.18d** (right). Thermal Ellipsoids shown at 50% probability level.

Table 3.5. Selected bond lengths (Å) and angles (deg) for **3.18b** and **3.18d**.

Atoms	**3.18b**	**3.18d**	Atoms	**3.18b**	**3.18d**
N2-N1	1.305(2)	1.299(2)	N2-N1-C1	117.19(15)	117.81(15)
N3-N4	1.2877(19)	1.282(2)	C1-N3-N4	114.59(15)	114.44(15)
N1-C1	1.320(2)	1.322(2)			
C1-N3	1.357(2)	1.357(2)			

3.6.3 Solution properties of 3-nitroformazans

A representative ^{1}H NMR spectrum of **3.18d** is presented in Figure 3.15. The ^{1}H NMR spectra of 3-nitroformazans are similar to those of triarylformazans (see section 2.3.1), i.e., the N-substituents are equivalent, and the bridging N-H proton is deshielded (δ 14.42-15.43 ppm for **3.18a-f**).

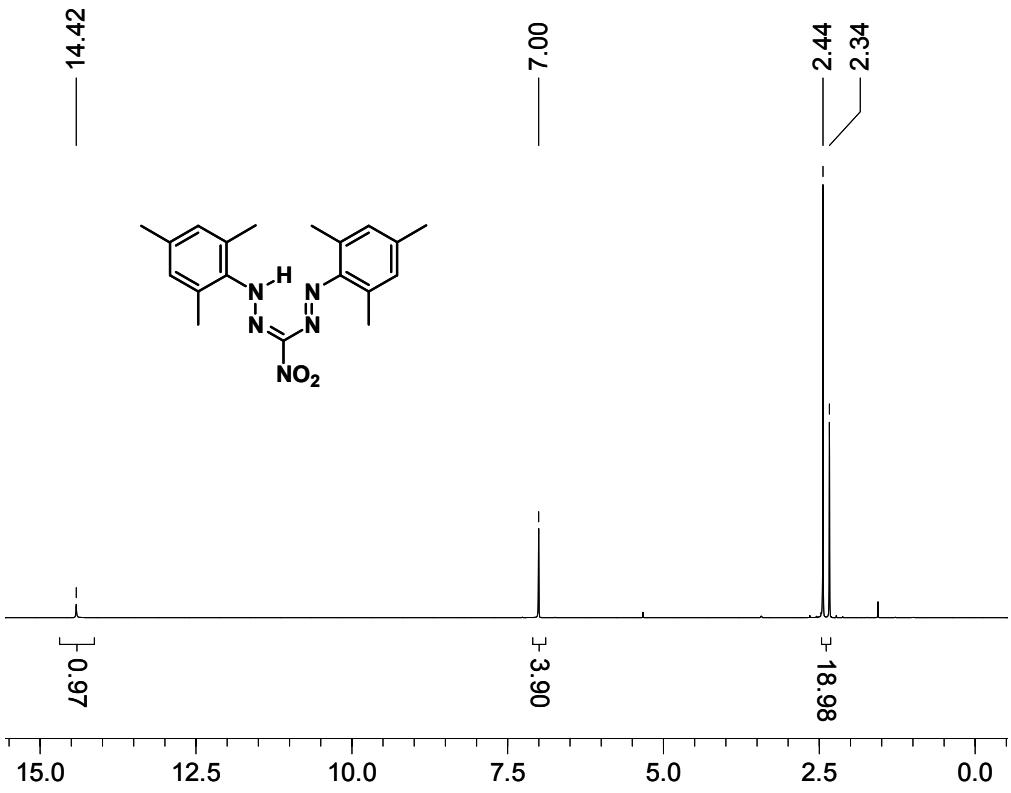

Figure 3.15. ^{1}H NMR spectrum of **3.18d** in CD_2Cl_2.

The electronic spectra of **3.18a-f** are presented in Figure 3.16. Within the series, there is little substrate dependence observed for the high energy absorption (λ_{max} = 325-342 nm). The primary visible absorption maxima fall between 398-464 nm, with additional shoulders observed on the low energy size of the maxima in most cases. In contrast to 3-cyanoformazans, direct comparison of substituent effects in 3-nitroformazans is possible as they all adopt the *closed* conformation. For 3-nitroformazans that do no possess *ortho*-substituted phenyl substituents, the λ_{max} of the visible maxima increases with electron donating ability of the aromatic group (**3.18a**, λ_{max} = 452; **3.18b**, λ_{max} = 464; **3.18f**, λ_{max} = 470 nm). The formazans with *ortho*-methyl substituents are considerably blue-shifted (**3.18c**, λ_{max} = 425; **3.18d**, λ_{max} = 432 nm) while the 2,6-di-*iso*-propylphenyl derivative **3.18e** is further blue shifted (λ_{max} = 398 nm),

suggesting that the N-substituents in **3.18c**, **3.18d**, and **3.18e** are twisted relative to the formazan backbone, with twisting in **3.18e** having the greatest effect due to increased steric bulk on the N-substituents.

.

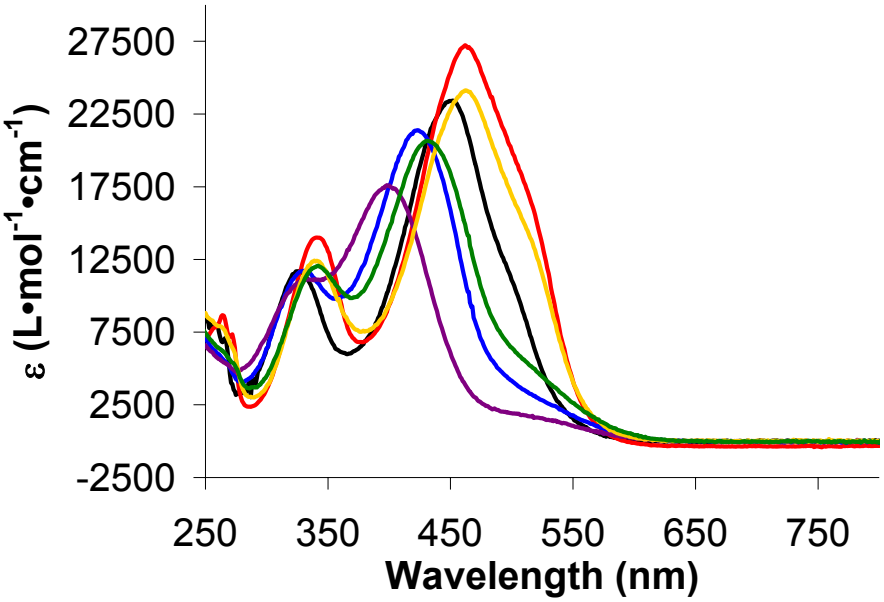

Figure 3.16. Electronic spectra of **3.18a** (black line), **3.18b** (red line), **3.18c** (blue line), **3.18d** (green line), **3.18e** (purple line), and **3.18f** (orange line) in CH_2Cl_2.

3.7 Transition metal complexes of formazans

3.7.1 Synthesis and characterization of a copper(II) complex of 3.10f

Copper (II) complex **3.19** was synthesized via deprotonation of cyanoformazan **3.17f** with NaH to afford the sodium salt, followed by addition of $CuCl_2$ (Scheme 3.6). After several hours the solution changed from red-brown to dark purple, and a small amount of NaCl was present as a precipitate.

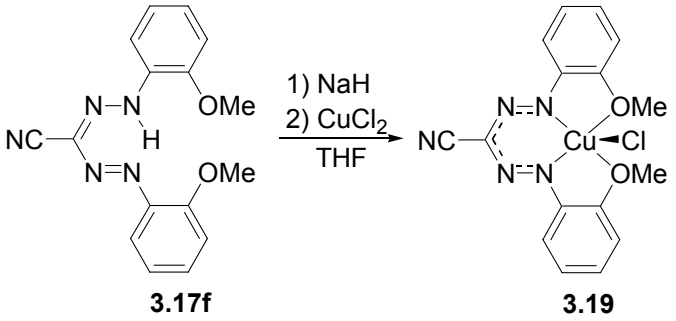

Scheme 3.6. Synthesis of copper (II) complex **3.19**.

The room temperature EPR spectrum of **3.19**, collected from a microcrystalline sample, is consistent with the unpaired electron occupying the d_{x2-y2} orbital[319] with $g_{\|}$ = 2.174, and $g_{\perp}$= 2.064. The room temperature magnetic moment of 2.08 μ_B is consistent with a copper (II) ion with g > 2. The IR spectrum of **3.19** has υ(CN) = 2225 cm^{-1} which is unchanged relative to free ligand **3.17f** (2224 cm^{-1}).

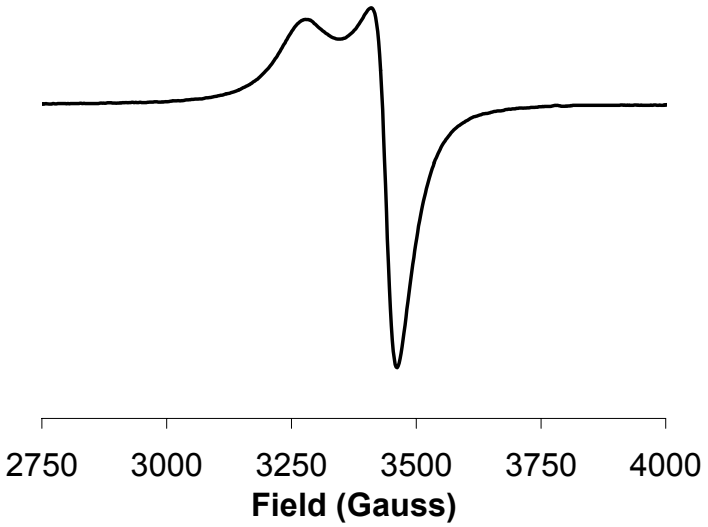

Figure 3.17. Solid-state EPR spectrum of copper (II) complex **3.19** at room temperature.

X-ray quality crystals of **3.19** were grown via diffusion of hexanes into a dichloromethane solution. The molecular structure of **3.19** is shown in Figure 3.18. The formazan ligand backbone is delocalized (N2-N1 1.297(4) Å, N4-N3 1.286(4) Å, N1-C1

1.340(5) Å, N3-C1 1.354(5) Å). The 2-methoxyphenyl substituents are twisted with respect to the N1, N2, N3, N4 formazan plane by 23.76° (ring attached to N2) and 25.61° (ring attached to N3). The geometry around the copper ion is unusual, and can only be described as *pseudo* five coordinate (Cu-O2 2.479(2) Å). The copper atom lies above the plane of the formazan ring by 0.487 Å, while O1 and O2 lay 0.188 Å and 1.237 Å out of the plane of the formazan. Cl1 points away from the formazan ligand, rather than perpendicular to the formazan ligand as in conventional geometries.

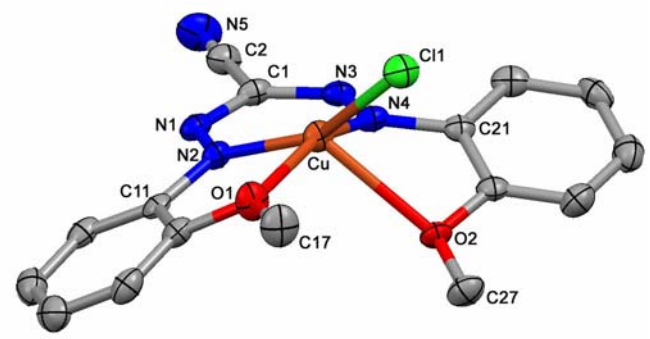

Figure 3.18. Molecular structure of **3.19**. Thermal ellipsoids shown at 50% probability level. Hydrogen atoms removed for clarity.

Table 3.6. Selected bond lengths (Å) and angles (deg) for **3.19**.

Atoms	**3.19**	Atoms	**3.19**
N2-N1	1.297(4)	N2-N1-C1	118.9(3)
N3-N4	1.286(4)	N4-N3-C1	118.5(3)
N1-C1	1.340(5)	N1-N2-M	127.8(3)
N3-C1	1.354(5)	N3-N4-M	127.8(3)
N2-M	1.928(3)	N2-M-O1	80.10(12)
N4-M	1.946(3)	N4-M-O2	71.26(10)
M-O1	2.068(3)	N2-M-N4	87.62(13)
M-O2	2.479(2)	O2-M-O1	97.47(9)
M-Cl1	2.2147(10)	N2-M-Cl1	155.37(9)
		N4-M-Cl1	103.61(10)

The electronic spectra of **3.17f** and **3.19** are presented in Figure 3.19. Compound **3.19** has a large ligand-based absorption at λ_{max} = 547 nm. Comparison with free ligand **3.17f** reveals a red shift from λ_{max} = 464 nm.

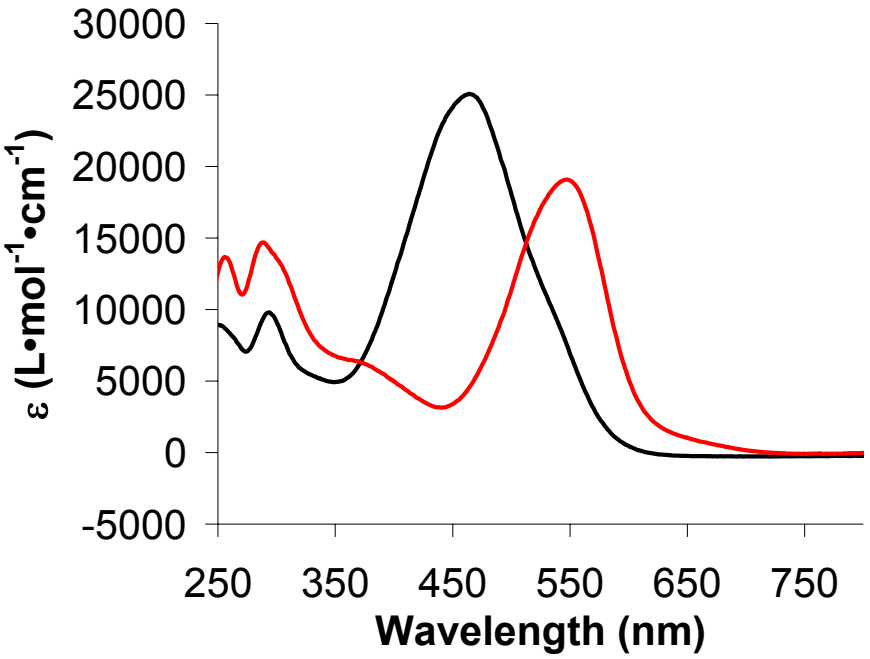

Figure 3.19. Electronic spectra of **3.17f** (black line) and **3.19** (red line) in CH_2Cl_2.

3.7.2 Synthesis and characterization of metal complexes of 3.17e.

3-Cyano-1,5-(2-hydroxyphenyl)formazan **3.17e** and two equivalents of pyridine were complexed to iron (III) and cobalt (III) to afford complexes **3.20a** and **3.20b** respectively (Scheme 3.7). **3.20a** was prepared via deprotonation of ligand **3.17e** with 3 equivalents of NaH to afford the trisodium salt, followed by the addition of $FeCl_3$ and an excess of pyridine producing three equivalents of NaCl and complex **3.20a**. Complex **3.20b** was prepared similarly, however, upon treatment with $CoCl_2$ and pyridine the reaction flask was exposed to air, allowing oxidation from cobalt (II) to cobalt (III) affording complex **3.20b**.

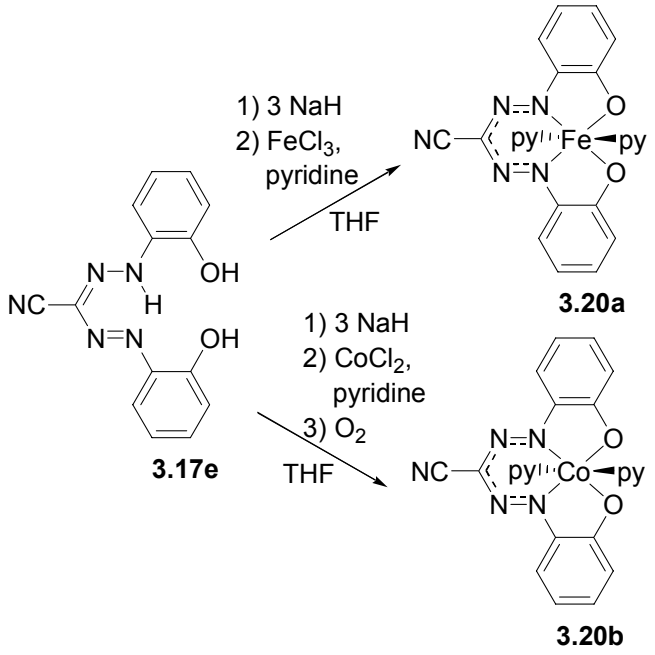

Scheme 3.7. Synthesis of iron (III) and cobalt (III) complexes **3.20a** and **3.20b**.

At room temperature, **3.20a** did not yield an EPR signal in solution or the solid-state. The room temperature magnetic moment was 1.82 μ_B, indicating the iron (III) ion is low-spin. The IR spectrum of **3.20a** has υ(CN) = 2225 cm^{-1}, lower than that of the free ligand (2236 cm^{-1}). The IR spectrum of **3.20b** has υ(CN) = 2219 cm^{-1}, once again shifted to lower energy than the free ligand. It is not immediately obvious why the nitrile stretch decreases in energy for **3.20a** and **3.20b**, although it does illustrate that a lower nitrile stretching frequency confirms the coordination of a metal to **3.17e**. The ^1H NMR spectrum of **3.20b** is consistent with a single pyridine environment, as well as a single aromatic environment for ligand **3.17e**. The equivalent pyridine rings give rise to a triplet at 7.41 ppm, a doublet at 7.37 ppm, and a triplet at 6.91 ppm. The aromatic environment of the phenol rings of the ligand gives rise to a doublet of doublets at 7.99 ppm, a doublet of doublets at 7.14 ppm, a triplet of doublets at 6.98 ppm, and a triplet of doublets at 6.53 ppm.

X-ray quality crystals of **3.20a** and **3.20b** were grown via solvent diffusion of hexanes into dichloromethane solutions. Both complexes crystallize as dichloromethane solvates. Compounds **3.20a** and **3.20b** were isostructural, and as such only **3.20a** (Figure 3.20) will be discussed in detail here. Within experimental error, the formazan ligand backbone has no bond alternation (N2-N1 1.310(3) Å, N4-N3 1.310(3) Å, N1-C1 1.352(4) Å, N3-C1 1.347(4) Å), and the N-substituents are coplanar with the N1, N2, N3, N4 formazan plane (ring attached to N2 twisted by 1.45°, and ring attached to N4 twisted by 3.65°). The iron (III) center lies within a nearly perfect octahedral field, slightly above the plane of the formazan (0.007 Å above). The two pyridine substituents are nearly coplanar (twisted by 4.87°) and are perpendicular to the plane of the formazan (89.61° and 89.84°).

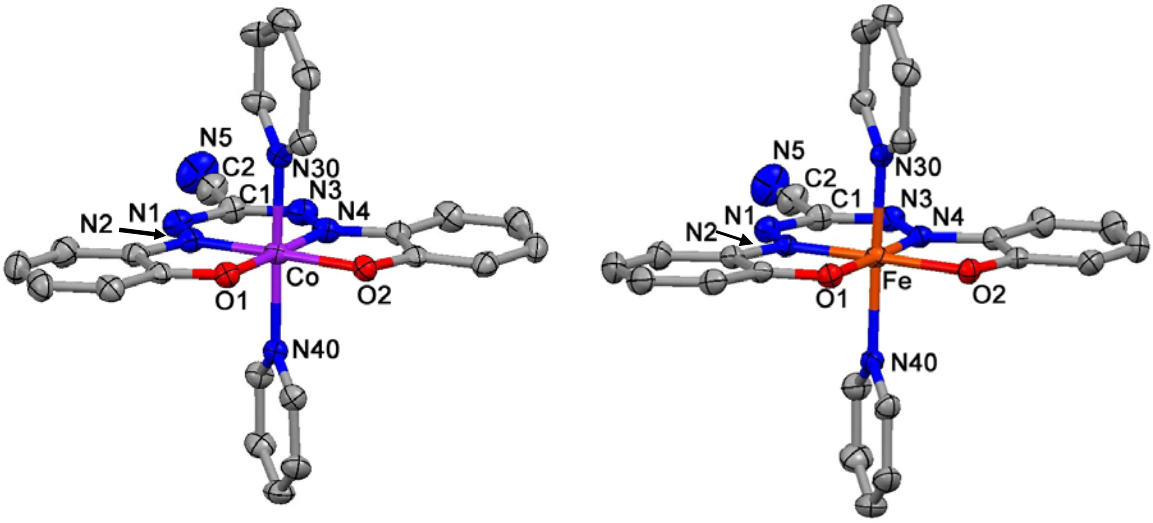

Figure 3.20. Molecular structure of **3.20a** and **3.20b**. Thermal ellipsoids shown at 50% probability level. Hydrogen atoms removed for clarity.

Table 3.7. Selected bond lengths (Å) and angles (deg) for **3.20a** and **3.20b**.

Atoms	**3.20a (M = Fe)**	**3.20b (M = Co)**	Atoms	**3.20a (M = Fe)**	**3.20b (M = Co)**
N2-N1	1.310(3)	1.288(3)	N2-N1-C1	117.6(2)	117.5(2)
N3-N4	1.310(3)	1.286(3)	N4-N3-C1	118.0(2)	117.8(2)
N1-C1	1.352(4)	1.357(4)	N1-N2-M	128.83(17)	128.17(17)
N3-C1	1.347(4)	1.358(4)	N3-N4-M	128.45(18)	127.79(19)
N2-M	1.846(2)	1.856(2)	N2-M-O1	86.29(8)	86.42(9)
N4-M	1.849(2)	1.860(2)	N4-M-O2	86.08(8)	85.97(9)
M-O1	1.9121(17)	1.8979(17)	N2-M-N4	93.49(9)	94.22(10)
M-O2	1.9218(18)	1.9075(18)	O2-M-O1	94.17(7)	93.41(8)
M-N30	2.010(2)	1.966(2)	N30-M-N40	175.96(8)	177.26(8)
M-N40	1.997(2)	1.954(2)			

The electronic spectra of **3.17e**, **3.20a**, and **3.20b** are presented in Figure 3.21. Complexes **3.20a** and **3.20b** have ligand-based transitions at λ_{max} = 484 nm for **3.20a** and λ_{max} = 483 and 503 nm for **3.20b**. Complexes **3.20a** and **3.20b** also have multiple charge transfer bands in their electronic spectra. For **3.20a,** these bands occur at λ_{max} = 592 nm and 631 nm, and for **3.20b** the charge transfer bands occur at λ_{max} = 608 nm and 658 nm. Comparison to the UV-vis spectrum of **3.17e** confirms that these bands must be associated with the transition metal (d-d, LMCT or MLCT) as similar transitions are not observed in the spectrum of the free ligand **3.17e**.

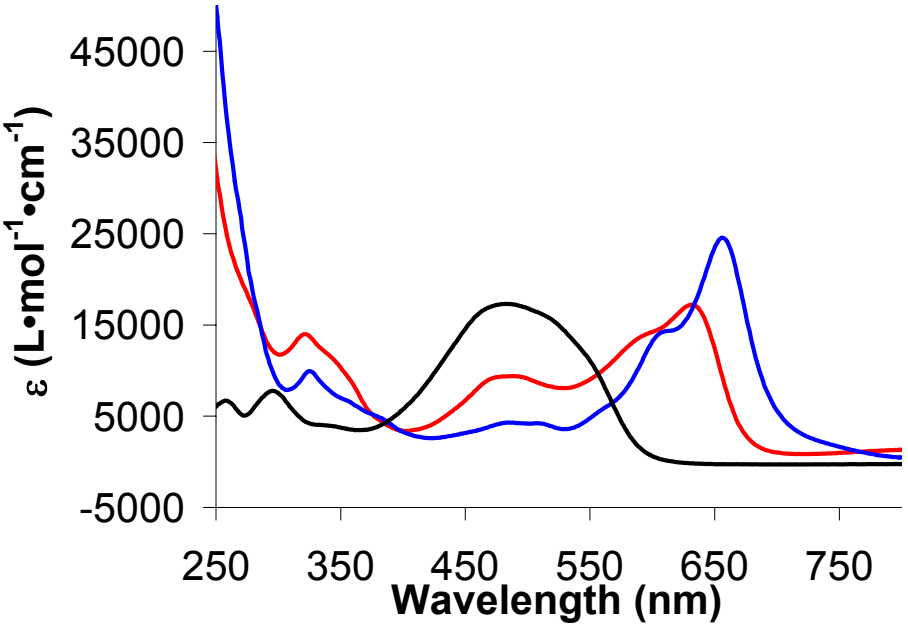

Figure 3.21. Electronic spectra of **3.17e** (black line), **3.20a** (red line), and **3.20b** (blue line) in CH_2Cl_2.

3.7.3 Synthesis and characterization of nickel (II) complexes of formazans.

Hydroxide-bridged nickel (II) complex **3.21** was the major product when one or two equivalents of **3.17c** were reacted with $Ni(OAc)_2{\cdot}4H_2O$ at gentle reflux in EtOH (Scheme 3.8). The structure of the complex confirms ligand isomerization in solution to form a 6-membered ring upon coordination as opposed to coordinating directly from the *open* form of the free ligand to form a 5-membered ring.

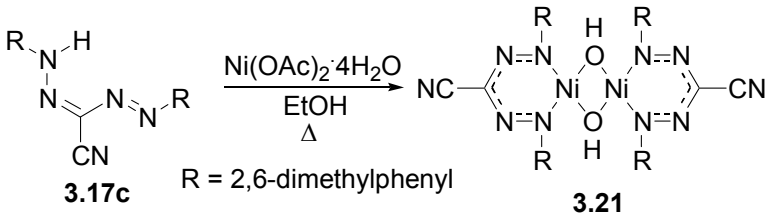

Scheme 3.8. Synthesis of nickel (II) complex **3.21**.

The IR spectrum of **3.21** has υ(CN) = 2229 cm^{-1} (shifted from 2219 cm^{-1} in the free ligand) as well as a sharp stretch at 3603 cm^{-1} due to bridging hydroxide ligands.

The bridged structure is formed as the ligand is too bulky to form a square planar homoleptic complex. Analysis of the ^{1}H NMR spectrum of **3.21** reveals high symmetry with only one resonance for methyl groups at 2.41 ppm, a doublet at 6.73 ppm and a triplet at 6.87 ppm for the aromatic protons of the equivalent aromatic rings, as well as a singlet at -6.94 ppm due to bridging hydroxides in a shielded environment. Similar chemical shifts have been observed in hydroxide bridged nickel complexes, even those in which flanking aryl substituents are not present.[320, 321] The ^{13}C NMR spectrum also supports the presence of equivalent aromatic rings.

Well formed, large crystals of **3.21** were grown via solvent diffusion of pentane into a dichloromethane solution. The crystals contain 1.25 dichloromethane molecules per complex, and are disordered with respect to the bridging oxygen atoms (O1). The asymmetric unit (Figure 3.22) consists of one quarter of the complex with the other three quarters generated by rotation about a two fold axis along b, an inversion center, and a mirror plane perpendicular to *b*. The formazan ligand backbone is delocalized, and has a mirror plane perpendicular to the formazan plane down the axis formed by N3-C2-C1-Ni. The Ni-Ni* bond distance of 2.898 Å is consistent with other bimetallic, hydroxide bridged square planar nickel complexes.[322-324] The N2-N1-C1-N1*-N2* plane tilts away from the Ni-O1-Ni*-O1* plane at an angle of 11.05°. The nickel atoms lie 0.211 Å above the N2-N1-C1-N1*-N2* plane of the formazan, and the 2,6-dimethylphenyl substituents attached to N2 are twisted perpendicular (85.39°) with respect to the plane of the formazan ligand. This twisting behavior is similar to that observed in complexes of β-diketiminates with 2,6-dimethylphenyl substituents.[291, 325-327] This behavior has not

been reported previously in formazans as very few with *ortho*-substituted N-aromatic substituents exist, and no examples of their complexes have been reported.

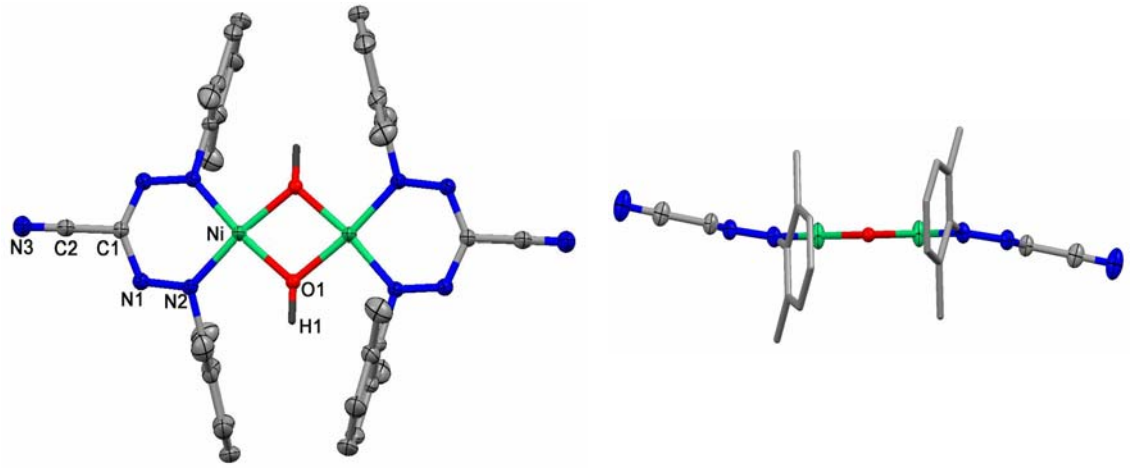

Figure 3.22. Molecular structure of **3.21**. Thermal ellipsoids shown at 50% probability level. Hydrogen atoms (excluding hydroxide protons) removed for clarity.

Table 3.8. Selected bond lengths (Å) and angles (deg) for **3.21**.

Atoms	**3.21**	Atoms	**3.21**
N2-N1	1.288(2)	N2-N1-C1	119.32(17)
N1-C1	1.3449(19)	N1-N2-Ni	128.60[a]
N2-Ni	1.8270(15)	Ni-O1-Ni*	102.81(18)
Ni-Ni*	2.898		
Ni-O1	1.854(2)		

Nickel (II) complex **3.22** was the major product when one or two equivalents of ligand **3.18b** were reacted with $Ni(OAc)_2{\cdot}4H_2O$ at gentle reflux in ethanol (Scheme 3.9). The lack of steric bulk on the *ortho*-positions of the N-substituents allows for two formazans to bind to the same metal ion. The IR spectrum of **3.22** was simplified compared to that of the free ligand. The ^{1}H NMR spectrum is consistent with a high symmetry species as all of the N-substituents are equivalent. Two doublets at 7.42 and 7.00 ppm as well as a single methyl resonance at 2.34 ppm were observed in the ^{1}H NMR, consistent with the *para*-tolyl substituted ligand. The ^{13}C NMR spectrum also

revealed a high symmetry species in solution, confirming the equivalence of the N-substituents.

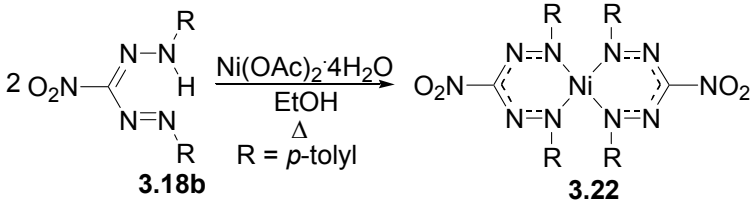

Scheme 3.9. Synthesis of nickel(II) complex **3.22**.

X-ray quality crystals were grown via the slow diffusion of pentane into a dichloromethane solution of **3.22**. The molecular structure (Figure 3.23) contains disordered methyl substituents (C27) on the *para*-tolyl ring attached to N2, and has an inversion center at the nickel (II) ion. Inspection of the formazan backbone (N2-N1 1.293(3) Å, N4-N3 1.295(3) Å, N1-C1 1.337(3) Å, N3-C1 1.330(3) Å) reveals a highly delocalized structure in the solid-state. The nickel atom lies 0.833 Å above the N2, N1, N3, N4 plane of the formazan ligands, and the ligand planes are separated by 1.666 Å. The N2, N4, Ni, N2*, N4* plane lies at an angle of 37.34° with respect to the N2, N1, N3, N4 plane of the formazan ligands. Each of the *para*-tolyl rings are significantly bent away from the metal center by 33.38° for the ring attached to N4, and 21.38° for the ring attached to N2 differing from the twisting observed in **3.21**. The side view of **3.22** reveals a metallacyclic ring in a boat conformation, with evidence of the pyramidalization of C1 ($\Sigma\theta$ = 356.7°). These features are consistent with those reported for similar nickel complexes.[263, 328]

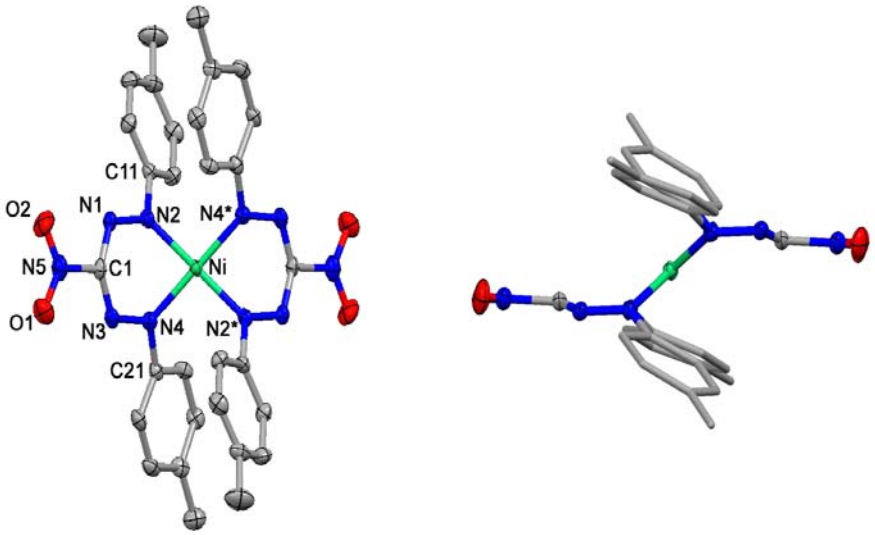

Figure 3.23. Molecular structure of **3.22**. Thermal ellipsoids shown at 50% probability level. Hydrogen atoms removed for clarity.

Table 3.9. Selected bond lengths (Å) and angles (deg) for **3.22**.

Atoms	**3.22**	Atoms	**3.22**
N2-N1	1.293(3)	N2-N1-C1	116.8(2)
N3-N4	1.295(3)	N4-N3-C1	116.8(2)
N1-C1	1.337(3)	N1-N2-Ni	122.97(18)
N3-C1	1.330(3)	N3-N4-Ni	122.79(18)
N2-Ni	1.867(2)	N2-Ni-N4	85.66(10)
N4-Ni	1.880(2)		

A palladium complex **3.23** has been reported to have similar structure.[208] In **3.23**, the palladium center lies 1.057 Å above the N2, N1, N3, N4 plane and the N2, N4, Ni, N2*, N4* plane lies at an angle of 43.16° with respect to the plane of the formazan ligand. The *para*-tolyl substituents attached to N2 and N4 are twisted by 36.34° and 21.90° respectively, similar to the structure of **3.22**. An analogous complex to **3.22** was not isolated with a cyano-substituent at the 3-position of the formazan ring as the products were not soluble in common organic solvents, perhaps indicating that an extended (polymeric) structure was generated through metal coordination of the nitrile groups.

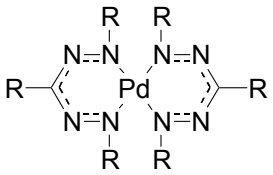

3.23
R = *p*-tolyl

The reaction of one or two equivalents of nitroformazan **3.18d** with $Ni(OAc)_2 \cdot 4H_2O$ in refluxing methanol yields complex **3.24** (Scheme 3.10). The bridging hydroxide ligands in **3.24** are confirmed by a sharp alcohol stretch at 3601 cm^{-1} in the IR spectrum, and by a singlet at -6.61 ppm in the ^1H NMR spectrum.

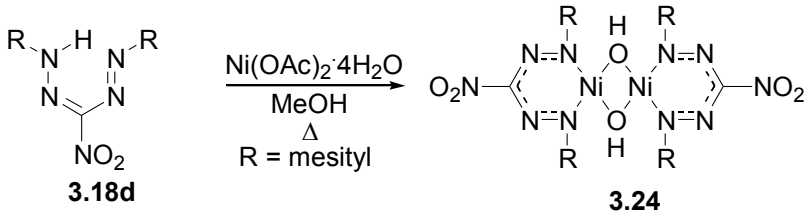

3.18d **3.24**

Scheme 3.10. Synthesis of nickel (II) complex **3.24**.

Well formed crystals of **3.24** were grown via vapor diffusion of pentane into a dichloromethane solution. The crystals contain one *n*-pentane molecule for every two complex molecules, and the bridging oxygen atoms (O1) are disordered. The formazan ligand backbone is delocalized (N2-N1 1.2882(18) Å, N4-N3 1.2860(18) Å, N1-C1 1.332(2) Å, N3-C1 1.338(2) Å), and the complex possesses an inversion center (Figure 3.24). The Ni-Ni* bond distance of 2.891 Å is consistent with that observed in **3.21**. The N2-N1-C1-N3-N4 plane is twisted at an angle of 20.19° with respect to the Ni-O1-Ni*-O1* plane, differing from **3.21** where a mirror plane runs through the molecule. This twisting causes the N-bound mesityl rings to be unique in the solid-state. The nickel (II) ion lies 0.302 Å above the N2-N1-C1-N3-N4 plane, and the mesityl groups are nearly perpendicular to it with twisting of the N2-bound mesityl ring by 77.36°, and the N4-

bound mesityl ring by 83.26°. The twisting behavior, although not as pronounced, is consistent with that observed in **3.21**, and serves as further evidence that the N-substituents of formazans readily twist when *ortho*-substituents are introduced.

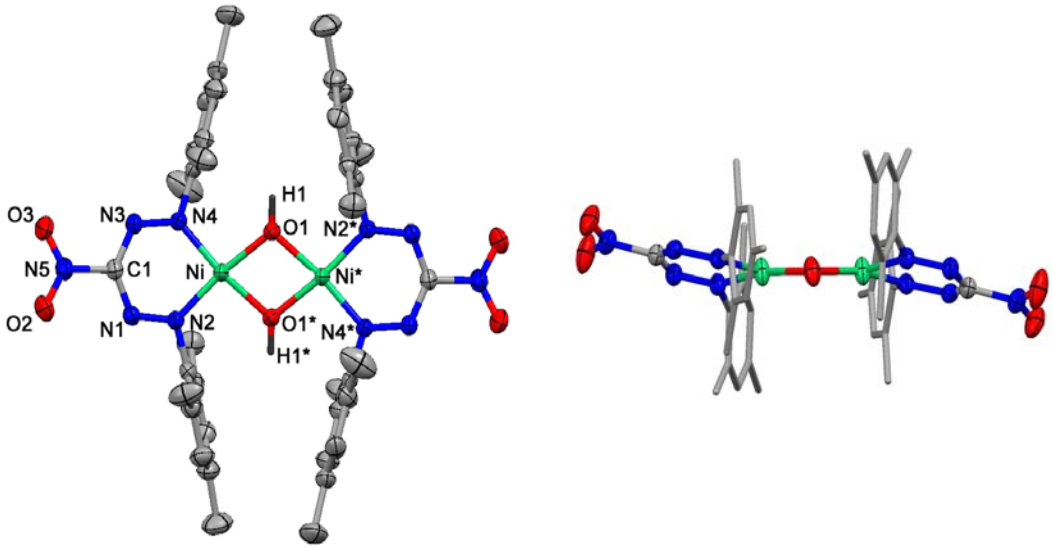

Figure 3.24. Molecular structure of **3.24**. Thermal ellipsoids shown at 50% probability level. Hydrogen atoms (excluding hydroxides) removed for clarity.

Table 3.10. Selected bond lengths (Å) and angles (deg) for **3.24**.

Atoms	**3.24**	Atoms	**3.24**
N2-N1	1.2882(18)	N2-N1-C1	118.36(13)
N3-N4	1.2860(18)	N4-N3-C1	118.22(13)
N1-C1	1.332(2)	N1-N2-Ni	127.91(11)
N3-C1	1.338(2)	N3-N4-Ni	128.20(11)
N2-Ni	1.8304(13)	N2-Ni-N4	92.54(6)
N4-Ni	1.8305(13)	Ni-O1-Ni*	100.0(2)
Ni-Ni*	2.891[a]		
Ni-O1	1.891(5)		
Ni-O1*	1.884(5)		

The electronic spectra of **3.21**, **3.22**, and **3.24** absorb in the low energy region of the visible spectrum between 620-673 nm (Figure 3.25). The origin of these absorptions is not fully understood, but is believed to involve the nickel (II) ion. The extinction coefficients between 1950-10000 $L \bullet mol^{-1} \bullet cm^{-1}$ would be considered high for d-d

transitions, and thus can be assigned to either ligand-metal (LMCT) or metal-ligand charge transfer (MLCT). The contribution from ligand-based transitions to the electronic spectra differs significantly in complexes **3.21**, **3.22**, and **3.24**. Complex **3.21** does not have any significant absorptions due to ligand-based transitions in its electronic spectrum. However, this behavior cannot be compared directly to the free ligand as it is known to exist in the *open* configuration. In contrast, for complex **3.22** absorption maxima exist at λ_{max} = 409 nm (ε = 27500 L•mol^{-1}•cm^{-1}) and in **3.24** at λ_{max} = 392 nm (ε = 14750 L•mol^{-1}•cm^{-1}). In **3.22**, the N-substituents are not twisted with respect to the plane of the formazan backbone, while in **3.24** the substituents are twisted. This twisting decreases the extent of electron delocalization as observed in the extinction coefficients of each complex, i.e., the larger extinction coefficient observed in **3.22** is directly related to increased delocalization of the π-system compared to **3.24**.

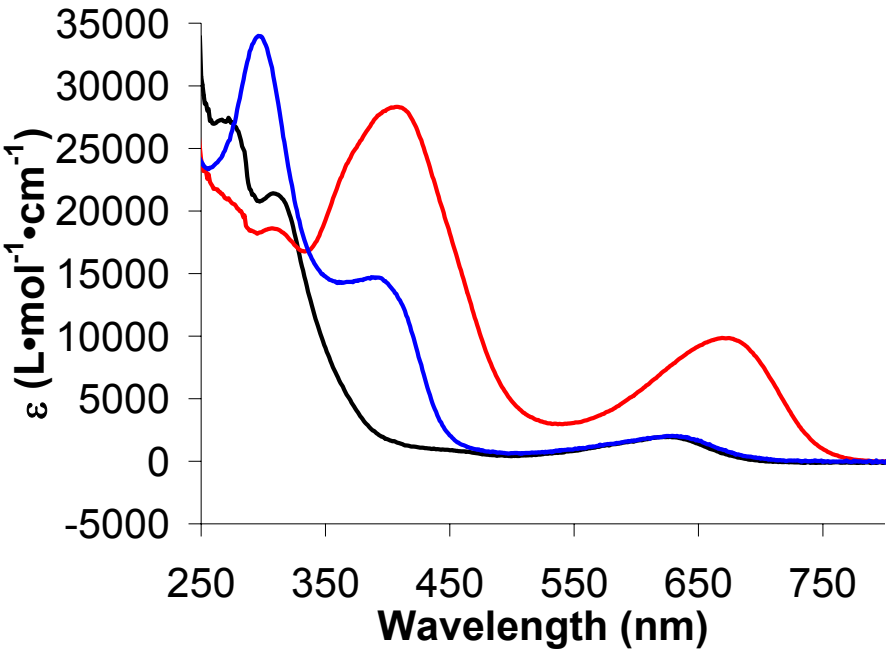

Figure 3.25. Electronic spectra of **3.21** (black line), **3.22** (red line), and **3.24** (blue line) in CH_2Cl_2.

3.8 Synthesis and characterization of palladium-formazan complexes

3.8.1 Synthesis of palladium-formazan complexes

In order to further study the coordination chemistry of formazans, a series of monometallic complexes containing redox inactive metals and one formazan ligand were targeted. The complexes described were prepared by refluxing one equivalent of the appropriate formazan with bis(1,1,1,5,5,5-hexafluoroacetylacetonato)palladium in methanol for two hours (Scheme 3.11). Similar triarylformazan complexes have been reported, but were isolated in low yields as side products during the preparation of bis(formazanato)palladium complexes.[208] Complex **3.25e** is the first formazan complex where the N-substituents of the formazan are 2,6-di-*iso*-propylphenyl groups.

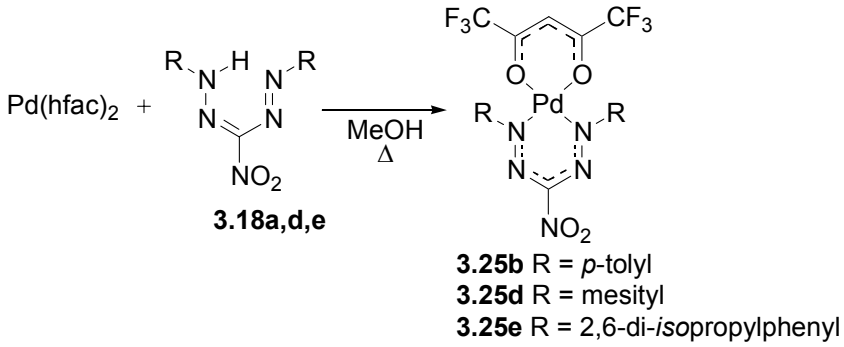

Scheme 3.11. Synthesis of palladium complexes **3.25b**, **3.25d**, and **3.25e**.

3.8.2 Solid-state properties of palladium-formazan complexes

X-ray quality crystals of **3.25b** were obtained via slow cooling of a saturated methanolic solution. The molecular structure of **3.25b** is shown in Figure 3.26. The bond lengths within the formazan backbone indicate that it is delocalized (N2-N1 1.279(2) Å, N4-N3 1.277(2) Å, N1-C1 1.333(3) Å, N3-C1 1.327(3) Å), similar to complexes of 3-nitroformazans discussed previously. The *para*-tolyl substituents are

twisted with respect to the formazan plane (N2-N1-N3-N4) at torsion angles of 21.00˚ (ring attached to N2) and 23.46˚ (ring attached to N4). The geometry around the palladium center is square planar, however, the square plane (PdN_2O_2) lies at an angle of 27.71˚ relative to the formazan ligand backbone and the palladium ion lies 0.699 Å out of the plane of the formazan as a result of steric repulsion between the hfac ligand and the 1,5-*para*-tolyl substituents of the formazan. The meso carbon (C1) is also displaced from the formazan ligand plane by 0.171 Å, as observed in other metal complexes of formazans.[208, 263]

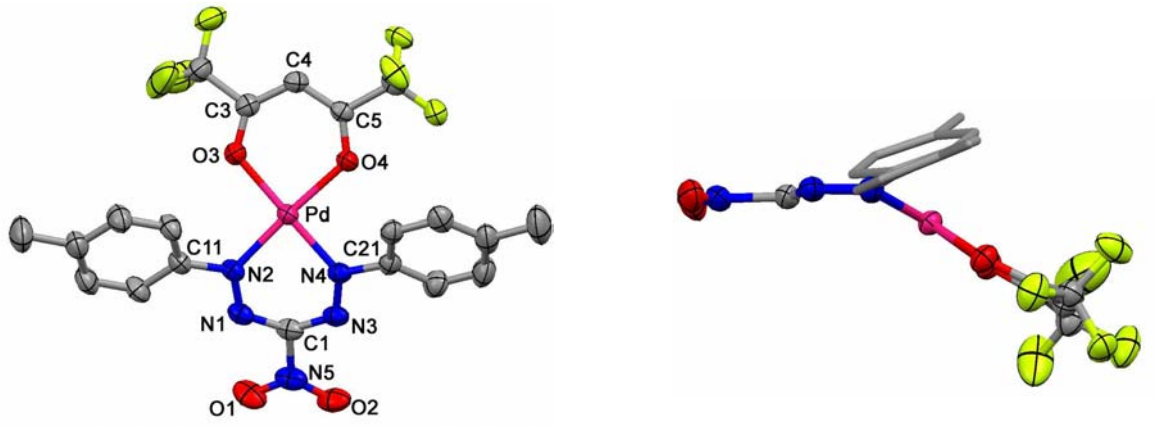

Figure 3.26. Molecular structure of **3.25b** top view (left) and side view (right). Thermal ellipsoids shown at 50% probability level.

Table 3.11. Selected bond distances (Å) and bond angles (deg) for **3.25b**.

Atoms	**3.25b**[a]		Atoms	**3.25b**[a]	
	Molecule A	Molecule B		Molecule A	Molecule B
N2-N1	1.279(2)	1.284(2)	N1-N2-Pd	122.91(13)	123.86(12)
N4-N3	1.277(2)	1.276(2)	N3-N4-Pd	123.80(13)	124.10(12)
N1-C1	1.333(3)	1.327(2)	N2-Pd-N4	86.71(6)	88.15(6)
N3-C1	1.327(3)	1.332(2)	N2-Pd-O3	93.75(6)	90.57(6)
N2-Pd	1.9859(15)	1.9912(14)	N4-Pd-O4	89.88(6)	91.12(5)
N4-Pd	1.9811(15)	1.9866(15)	O3-Pd-O4	89.42(5)	89.99(5)
O3-Pd	2.0464(13)	2.0394(12)	C4-C3-O3	129.58(18)	129.62(17)
O4-Pd	2.0310(13)	2.0460(12)	C4-C5-O4	128.78(17)	129.23(17)

[a]Two crystallographically inequivalent molecules were detected in the unit cell.

X-ray quality crystals of **3.25d** were obtained by slow evaporation of a dichloromethane solution in a NMR tube. The molecular structure of **3.25d** (Figure 3.27) is similar to **3.25a**, including (i) a delocalized ligand backbone (N2-N1 1.280(4) Å, N4-N3 1.277(4) Å, N1-C1 1.329(4) Å, N3-C1 1.339(4) Å), (ii) the palladium ion is displaced from the formazan plane (0.452 Å), (iii) the square plane of the palladium is not coplanar with the formazan ligand backbone (27.17˚), and (iv) the formazan adopts a pseudo boat conformation (C1 displaced by 0.127 Å). However, the the aryl rings are twisted with respect to the formazan plane by 62.55˚ (ring attached to N2) and 56.40˚ (ring attached to N4) in **3.25d**. The twisting behavior of the N-substituents in **3.25d** is consistent with other transition metal complexes of formazans where the N-substituents are *ortho*-substituted.

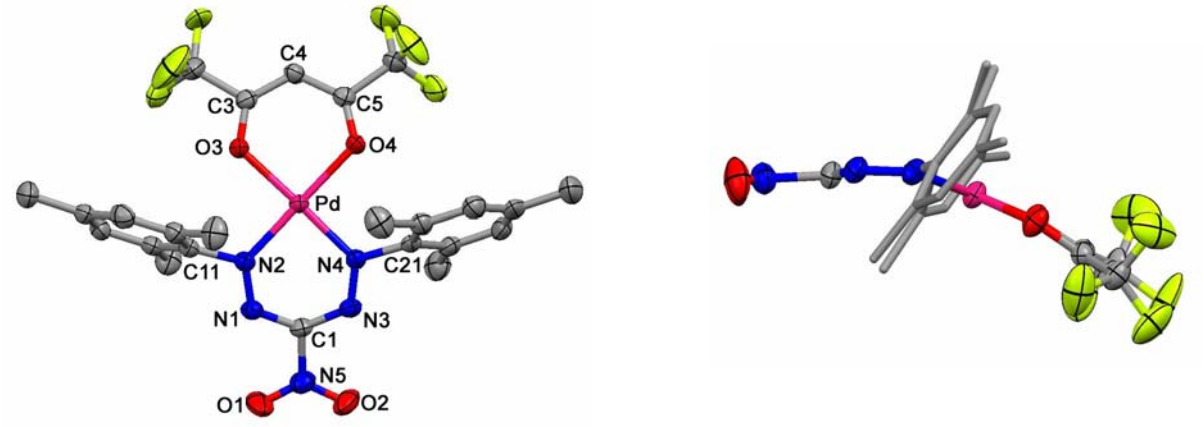

Figure 3.27. Molecular structure of **3.25d** top view (left) and side view (right). Thermal ellipsoids shown at 50% probability level.

Table 3.12. Selected bond distances (Å) and bond angles (deg) for **3.25d**.

Atoms	**3.25d**	Atoms	**3.25d**
N2-N1	1.280(4)	N1-N2-Pd	125.2(2)
N4-N3	1.277(4)	N3-N4-Pd	125.4(2)
N1-C1	1.329(4)	N2-Pd-N4	89.48(11)
N3-C1	1.339(4)	N2-Pd-O3	89.51(11)
N2-Pd	1.959(3)	N4-Pd-O4	90.46(10)
N4-Pd	1.963(3)	O3-Pd-O4	90.48(9)
O3-Pd	2.030(2)	C4-C3-O3	128.4(3)
O4-Pd	2.042(2)	C4-C5-O4	129.1(3)

3.8.3 Solution properties of palladium-formazan complexes

The NMR spectra of **3.25b**, **3.25d**, and **3.25e** all have resonances due to equivalent N-substituents. Complexes **3.25b**, **3.25d**, and **3.25e** do not isomerize in solution, as observed in a similar β-diketiminate complex **3.26**, which rapidly ring opens to form a four membered metallacycle **3.26'** at room temperature.[329] It is not clear whether the lack of isomerisation is due to increased ligand strength of the formazan compared to the β-diketiminate, or whether the introduction of the fluorine atoms into the acetyl acetonate backbone increases the electron affinity of the palladium center, thereby increasing the strength of the Pd-N bonds.

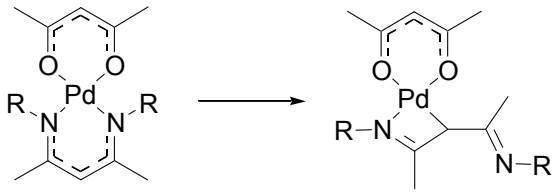

3.26 **3.26'**

The electronic spectra of **3.25b**, **3.25d**, and **3.25e** are presented in Figure 3.28. The primary electronic transition giving rise to the colour of formazans and their complexes has previously been assigned to a ligand-ligand charge transfer between the formazan chromophore and its N-substituents. The major absorption in the electronic spectra of complexes **3.25b**, **3.25d**, and **3.25e** are redshifted relative to the corresponding

free ligands due to the fixed conformation of the formazanato anion. The electronic spectrum of **3.25b** is further red shifted relative to **3.25d** and **3.25e** due to the near-planarity of the formazanato ligand and the *para*-tolyl N-substituents. The delocalization in **3.25d** and **3.25e** is thus disrupted by twisting of the *ortho*-substituted N-substituents, which is corroborated by the solid-state structures.

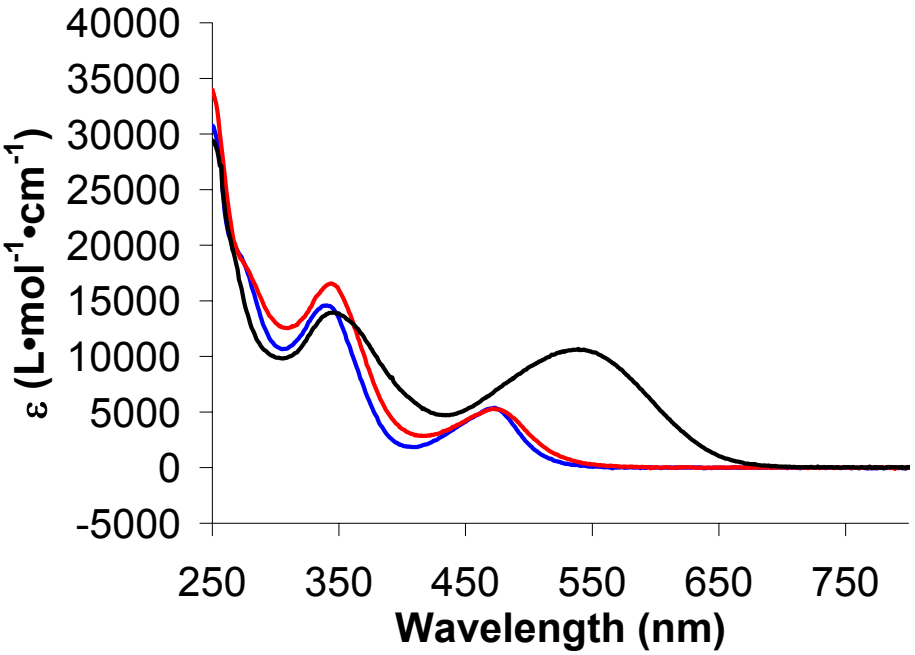

Figure 3.28. Electronic spectra of **3.25b** (black line), **3.25d** (red line), and **3.25e** (blue line) in CH_2Cl_2.

3.8.4 Electrochemical properties of palladium-formazan complexes

The CVs of **3.25b**, **3.25d**, and **3.25e** (Figure 3.29) consist of irreversible reduction waves. Complex **3.25b** is irreversibly reduced at a cathodic peak potential of -0.92 V, while **3.25d** and **3.25e** are reduced at -1.16 V and -1.18 V respectively. The irreversibility is indicative of the instability of the "palladaverdazyl" radical anions generated. Previously studied borataverdazyl radical anions exhibited reversible reduction waves under similar conditions, indicating their stability on the time scale of

the experiment. Complexes **3.25b**, **3.25d**, and **3.25e** are more difficult to reduce than borataverdazyl analogues.

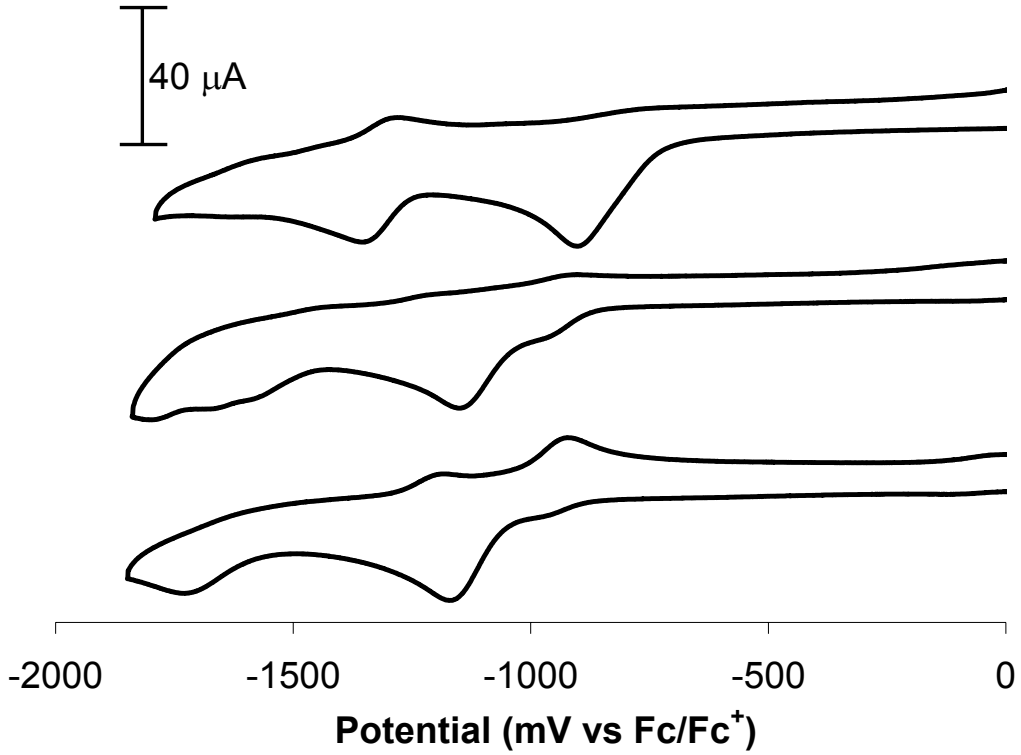

Figure 3.29. Cyclic voltammograms of **3.25b** (top), **3.25d** (middle), and **3.25e** (bottom) in CH_3CN containing 0.1 M $Bu_4N^+BF_4^-$ (electrolyte). Scan rate 100 mV/s.

The lower reduction potential for **3.25b** is consistent with the hypothesis made from the electronic spectra, whereby increased planarity leads to increased delocalization lowering the energy of the LUMO. In all three complexes instability of the reduced species precludes further investigation of electrochemical properties.

The difficulty in reduction of complexes **3.25b**, **3.25d**, and **3.25e** may seem curious given the presence of strong electron-withdrawing groups both on the formazan as well as the ancillary (hfac) ligand on the palladium ion. Boratatetrazines **3.15** do not possess strong electron-withdrawing substituents but are easier to reduce. The differences in electrochemical properties between the boratetrazines and **3.25b**, **3.25d**,

and **3.25e** may actually relate to the nature of the formazan interaction with boron or palladium. The BN bonds in **3.15** are likely to be relatively more covalent than the PdN bonds in **3.25b**, **3.25d**, and **3.25e**. As such the radical anions of **3.15** are isolobal to Type I verdazyls, and the electron deficiency of the boron center serves to accommodate the negative charge associated with chemical reduction. In contrast, the reduction of **3.25** to give a radical anion would require the additional charge to be accomodated substantially by the formazan ligand, rendering it a radical dianion. As suggested by the electrochemical data, the high negative charge associated with the reduced species does not lend itself to chemical stability despite the presence of strong electron withdrawing groups.

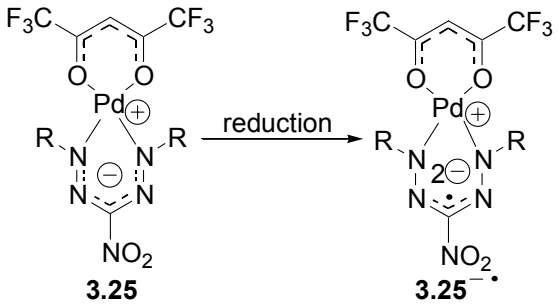

3.9 Summary

This chapter highlights significant advances in the coordination chemistry of formazans. Boratatetrazines, the first main group complexes of formazans were synthesized and structurally characterized revealing highly delocalized ligand backbones. Their electrochemistry and conversion to borataverdazyl radical anions was studied, and although the stability of the resulting radicals did not rival organic analogues, the isolobal relationship with organic verdazyls was discussed, and their properties explored. After

encountering significant challenges in the purification and crystallization of complexes of triarylformazans, 3-substituted formazans were synthesized as alternatives.

3-Substituted formazans have been shown to exist as *closed* and *open* conformers. The structural preference of each formazan appears to be governed by steric bulk associated with the 1,3,5-substituents. When the atom directly attached to C3 is small, formazans generally exist as the *open* structure, while formazans bearing relatively larger C3-substituents exist in the *closed* form. The structural preferences of 3-cyanoformazans appear to be more complex than simple steric arguments. The linear nature of the cyano-substituent allows for the *open* structure to be readily accessible, consistent with alkyl formazans previously studied.[296, 297, 301] However, in cases where heteroatoms are incorporated hydrogen bonding interactions appear to influence the structure allowing the *closed* structure to exist. 3-Nitroformazans exist exclusively in the *closed* form due to the relative bulk of the nitro-substituent. The structural properties discussed lead to the conclusion that the 3-substituent alone does not govern the preferred orientation adopted by each formazan.

The coordination chemistry of 3-cyano- and 3-nitroformazan was also described. Previous examples of metal-formazan complexes have not been well characterized, and no structurally characterized complexes of 3-cyano- or 3-nitroformazans have been reported prior to this work. All of the coordination chemistry explored produced six-membered metallacycles. This is of particular interest for 3-cyanoformazans adopting an *open* conformation as they were shown to isomerize in solution. In a broader context, this may suggest that the preferred structure of formazans may not have a significant role in its preferred mode of coordination.

Electron poor palladium complexes of 3-nitroformazans were synthesized with emphasis placed on their utility as precursors to metallaverdazyl radical anions. Such complexes were irreversibly reduced electrochemically, and palladaverdazyls were not isolated. In order to achieve metallaverdazyls, it is now apparent that the covalent nature of the metal-nitrogen bonds must be increased, perhaps through the choice of metal, or through variation of the ancillary ligand.

3.10 Experimental

3.10.1 Synthesis and characterization

General procedure for the synthesis of 3.15d and 3.15j: 1,1-diacetato-2,6-diphenyl-3-*para*-tolylboratatetrazine (3.15d). Boric acid (0.8 g, 13 mmol) was combined with acetic acid (3.5 mL) and acetic anhydride (3.5 mL) and stirred at 80ºC for 15 minutes until dissolution was observed. **2.1d** (1.0 g, 3.2 mmol) was then added as a solution in acetic acid (2.1 mL) and acetic anhydride (7.5 mL). The mixture was left to stir at 80ºC for 16 h at which time the mixture was extracted with hexanes (5 x 100 mL). The hexanes was combined and washed with water (5 x 100 mL), dried with anhydrous magnesium sulfate and concentrated *in vacuo*. Compound **3.15d** was isolated as a dark purple solid, yield 0.420 g (29.7 %). X-ray quality crystals were grown via slow evaporation of concentrated hexanes solutions of **3.15d**. Mp. 178-180°C. ^{1}H NMR (300 MHz, CD_2Cl_2): δ 8.01 (d, 2H, ^{3}J = 8 Hz), 7.95 (d of d, 4H, ^{3}J = 8 Hz), 7.48 (m, 6H), 7.32 (d, 2H, ^{3}J = 8 Hz), 2.43 (s, 3H), 1.82 (s, 6H) ppm. ^{13}C NMR (75 MHz, CD_2Cl_2): δ 171.7, 145.3, 139.4, 138.8, 132.3, 130.0, 129.5, 125.6, 123.4, 22.7, 21.6 ppm. ^{11}B NMR (115 MHz, CD_2Cl_2): δ 1.32 ppm. FT-IR (KBr): 1724 (s), 1715 (s), 1305 (s), 1250 (s), 1054 (s),

966 (s), 764 (s), 688 (s), 506 (m) cm^{-1}. UV-vis (CH_2Cl_2): λ_{max} 256 nm (ε = 20000 $L \bullet mol^{-1} \bullet cm^{-1}$), 311 nm ($\varepsilon$ = 11500 $L \bullet mol^{-1} \bullet cm^{-1}$), 558 ($\varepsilon$ = 6500 $L \bullet mol^{-1} \bullet cm^{-1}$). MS (EI): *m/z* 442 ($MH^+$, 65 %). Anal. Calcld for $C_{24}H_{23}N_4O_4B$: C, 65.18; H, 5.24; N, 12.67. Found: C, 65.31; H, 5.56; N, 12.46.

1,1-diacetato-2,6-di-*para*-tolyl-3-phenylboratatetrazine (3.15j). Yield 28.1 %. Mp. 170-172°C. ^1H NMR (CD_2Cl_2): 8.11 (d, 2H, ^3J = 8 Hz), 7.85 (d, 4H, ^3J = 8 Hz), 7.51-7.42 (m, 3H), 7.27 (d, 4H, ^3J = 8 Hz), 2.42 (s, 6H), 1.82 (s, 6H) ppm. ^{13}C NMR (CD_2Cl_2): δ 171.7, 143.1, 140.6, 135.3, 130.2, 129.2, 129.1, 125.6, 123.2, 22.7, 21.6 ppm. ^{11}B NMR (115 MHz, CD_2Cl_2): δ 1.31 ppm. FT-IR (KBr): 1717 (s), 1602 (m), 1371 (s), 1303 (s), 1251 (s), 1176 (m), 1042 (s), 971 (s), 817 (s), 504 (s) cm^{-1}. UV-vis (CH_2Cl_2): λ_{max} 260 nm (ε = 15750 $L \bullet mol^{-1} \bullet cm^{-1}$), 320 nm ($\varepsilon$ = 14250 $L \bullet mol^{-1} \bullet cm^{-1}$), 560 ($\varepsilon$ = 19750 $L \bullet mol^{-1} \bullet cm^{-1}$). MS (EI): *m/z* 456 ($MH^+$, 100 %). Anal. Calcld for $C_{25}H_{25}N_4O_4B$: C, 65.80; H, 5.52; N, 12.28. Found: C, 65.41; H, 5.66; N, 11.87.

General procedure for the synthesis of borataverdazyl radical anions 3.16d and 3.16j: 1,1-diacetato-2,6-diphenyl-3-*para*-tolylborataverdazyl radical anion (3.16d). Under argon, **3.15d** (0.085 g, 0.2 mmol) was dissolved in hexanes (50 mL) and stirred for 30 min at which time cobaltocene (0.039 mg, 0.2 mmol) in hexanes (50 mL) was added via cannula. Upon addition a green precipitate formed and after 10 min of stirring the mixture was filtered *in vacuo*, washed with hexanes (2 x 50 mL) and dried *in vacuo* for 1 hour. Compound **3.16d** was isolated as a dark green solid and was handled in the glovebox, yield 0.040 g (31.6 %). Mp. 96-98ºC (dec). FT-IR (KBr): 1707 (s), 1690 (s), 1587 (s), 1485 (s), 1267 (s), 1172 (m), 1104 (m), 1014 (m), 755 (m), 692 (m) cm^{-1}. Anal.

Calcld for $C_{34}H_{33}N_4O_4BCo$: C, 64.68; H, 5.27; N, 8.87. Found: C, 64.51; H, 5.23; N, 8.24.

1,1-diacetato-2,6-di-*para*-tolyl-3-phenylborataverdazyl radical anion (3.16j). Yield (38.8 %) Mp. 100-102ºC (dec). FT-IR (KBr): 1707 (s), 1690 (s), 1606 (m), 1505 (s), 1414 (m), 1367 (m), 1279 (m), 1172 (m), 823 (s), 698 (m), 646 (m) cm^{-1}. Anal. Calcld for $C_{35}H_{35}N_4O_4BCo$: C, 65.13; H, 5.47; N, 8.68. Found: C, 64.28; H, 5.67; N, 8.08.

Synthesis of 3-cyano-1,5-phenylformazan (3.17a). To a solution of aniline (3.72 g, 40 mmol), 12 M concentrated hydrochloric acid (10 mL), and water (10 mL) at -5˚ C was added sodium nitrite (3.00 g, 43 mmol) in small portions over a 10 min period. After 15 min of stirring, the mixture was added to a second solution containing cyanoacetic acid (1.70 g, 20 mmol), sodium hydroxide (8.00 g , 200 mmol), and water (100 mL) at 0˚ C over a 30 min period. The resulting solution was filtered to remove a black solid, and the organics extracted into dichloromethane (3 x 250 mL). After removal of the solvent the resulting dark orange solid was purified via column chromatography (neutral alumina, dichloromethane). The eluate was concentrated *in vacuo* to afford **3.17a** as an orange microcrystalline solid, yield (2.45 g, 49.1 %). Mp. 134-136ºC (dec). ^{1}H NMR (300 MHz, CD_2Cl_2): *open* δ 12.47 (s, 1H, NH), 7.68 (d, 4H, J = 7 Hz), 7.51 (t, 4H, J = 7 Hz), 7.45-7.30 (m, 2H, J = 7 Hz). *linear* δ 9.22 (s, 0.3H, NH), 7.95-7.85 (m, 0.5H), 7.35-7.15 (m, 0.4H). ^{13}C NMR (75 MHz, CD_2Cl_2): δ 152.6, 147.0, 141.5, 132.5, 130.4, 130.2, 129.9, 129.7, 126.2, 125.6, 123.6, 120.0, 116.1, 114.5 ppm. FT-IR (KBr): 2226 (m) (CN), 1527 (s), 1272 (m) cm^{-1}. UV-vis (CH_2Cl_2): λ_{max} 257 nm (ε = 5250 L•mol^{-1}•cm^{-1}), 291 nm (ε = 5750 L•mol^{-1}•cm^{-1}), 413 nm (ε = 15500 L•mol^{-1}•cm^{-1}). MS (EI): *m/z* 249

(M^+, 25 %). Anal. Calcd for $C_{14}H_{11}N_5$: C, 67.46; H, 4.45; N, 28.10. Found C, 67.46; H, 4.44; N, 28.11.

General procedure for the synthesis of formazans 3.17b-f: 3-cyano-1,5-*para*-tolylformazan (3.17b). To a solution of *para*-toluidine (4.30 g, 40 mmol), 12 M concentrated hydrochloric acid (10 mL), and water (10 mL) at -5˚ C was added sodium nitrite (3.00 g, 43 mmol) in small portions over a 10 min period. After 15 min of stirring, the mixture was added to a second solution containing cyanoacetic acid (1.70 g, 20 mmol), sodium hydroxide (8.00 g , 200 mmol) and water (100 mL) at 0˚ C over a 30 min period. The resulting orange solid was isolated via filtration and purified via column chromatography (neutral alumina, dichloromethane). The eluate was concentrated *in vacuo* to afford **3.17b** as a dark orange solid, yield (2.70 g, 48.7 %). Mp. 198-200^{o}C (dec). ^{1}H NMR (300 MHz, CD_2Cl_2): *open* δ 12.60 (s, 1H, NH), 7.58 (d, 4H, J = 7 Hz), 7.22 (d, 4H, J = 7 Hz), 2.32 (s, 6H). *linear* δ 9.04 (s, 0.2H, NH), 7.69 (s, 0.5H), 2.35 (s, 0.8H), 2.28 (s, 0.9H). ^{13}C NMR (125 MHz, CD_2Cl_2): δ 150.8, 145.0, 143.5, 140.4, 139.3, 135.5, 130.9, 130.8, 130.6, 130.4, 130.4, 125.8, 123.5, 119.9, 115.9, 114.9, 21.9, 21.6, 21.2 ppm. FT-IR (KBr): 2224 (CN), 1530, 1264 cm^{-1}. UV-vis (CH_2Cl_2): λ_{max} 265 nm (ε = 9250 L•mol^{-1}•cm^{-1}), 299 nm (ε = 9500 L•mol^{-1}•cm^{-1}), 453 nm (ε = 19000 L•mol^{-1}•cm^{-1}). MS (EI): *m/z* 277 (M^+, 35 %). Anal. Calcd for $C_{16}H_{15}N_5$: C, 69.29; H, 5.45; N, 25.25. Found C, 69.31; H, 5.40; N, 24.25.

3-cyano-1,5-(2,6-dimethylphenyl)formazan (3.17c). Yield 81.9 %. Mp. 118-120^{o}C. ^{1}H NMR (500 MHz, CD_2Cl_2): *open* δ 11.41 (s, 1H, NH), 7.18 (s, 6H), 2.48 (s, 12H), 2.33 (s, 6H). *linear* δ 8.87 (s, 0.2H, NH), 7.15 (s, 0.9H), 2.45 (s, 1H), 2.43 (s, 1H). ^{13}C NMR (125 MHz, CD_2Cl_2): δ 150.1, 144.0, 138.1, 133.0, 132.6, 131.7, 131.3, 130.3, 130.1,

129.9, 129.2, 127.9, 127.4, 125.4, 124.8, 122.5, 118.5, 114, 108.3 ppm. FT-IR (KBr): 2219 (m) (CN), 1525 (s), 1281 (m) cm^{-1}. UV-vis (CH_2Cl_2): λ_{max} 260 nm (ε = 7500 $L \bullet mol^{-1} \bullet cm^{-1}$), 381 nm ($\varepsilon$ = 17000 $L \bullet mol^{-1} \bullet cm^{-1}$). MS (EI): *m/z* 305 ($M^+$, 20 %). Anal. Calcd for $C_{18}H_{19}N_5$: C, 70.80; H, 6.27; N, 22.93. Found C, 70.53; H, 6.19; N, 22.47.

3-cyano-1,5-mesitylformazan (3.17d). Yield 60.1 %. X-ray quality crystals were grown by slow evaporation of a dichloromethane solution in an NMR tube. Mp. 180-182°C. ^1H NMR (500 MHz, CD_2Cl_2): *open* δ 11.21 (s, 1H, NH), 6.99 (s, 4H), 2.45 (s, 12H), 2.33 (s, 6H). *linear* δ 8.75 (s, 0.2H, NH), 6.94 (s, 0.5H), 2.43 (s, 1H), 2.39 (s, 1H). ^{13}C NMR (125 MHz, CD_2Cl_2): δ 147.7, 141.8, 140.8, 139.7, 133.6, 132.9, 130.9, 130.8, 130.4, 127.4, 114.2, 21.5,21.4, 21.2, 20.2, 18.8 ppm. FT-IR (KBr): 2224 (m) (CN), 1524 (s), 1273 (m) cm^{-1}. UV-vis (CH_2Cl_2): λ_{max} 265 nm (ε = 7500 $L \bullet mol^{-1} \bullet cm^{-1}$), 423 nm ($\varepsilon$ = 13500 $L \bullet mol^{-1} \bullet cm^{-1}$). MS (EI): *m/z* 333 ($M^+$, 25 %). Anal. Calcd for $C_{20}H_{23}N_5$: C, 72.04; H, 6.95; N, 21.00. Found C, 71.90; H, 7.05; N, 21.08.

3-cyano-1,5-dihydroxyphenylformazan (3.17e). Purified via column chromatography (silica gel, ethyl acetate). Yield 77.0 %. X-ray quality crystals were grown via slow evaporation of a toluene/hexanes solution in glass tubes (5 mm diameter). Mp. 182-184°C. ^1H NMR (300 MHz, d_6-DMSO): δ 13.12 (s, 1H, NH), 10.45 (s, 2H, OH), 7.61 (d of d, 2H, J = 8 Hz, 2 Hz), 7.24 (t of d, 2H, J = 8 Hz, 2 Hz), 7.02 (d, 2H, 8 Hz), 6.94 (t, 2H, 8 Hz) ppm. ^{13}C NMR (125 MHz, d_6-DMSO): δ 151.0, 134.3, 130.3, 125.0, 120.1, 117.2, 117.1, 115.2 ppm. FT-IR (KBr): 3309 (m, br) (OH), 2240 (m) (CN), 1611 (m), 1512 (s), 1475 (s), 1230 (s), 742 (s) cm^{-1}. UV-vis (CH_2Cl_2): λ_{max} 258 nm (ε = 6750 $L \bullet mol^{-1} \bullet cm^{-1}$), 296 nm ($\varepsilon$ = 7750 $L \bullet mol^{-1} \bullet cm^{-1}$), 484 nm ($\varepsilon$ = 17250 $L \bullet mol^{-1} \bullet cm^{-1}$). Anal.

Calcd for $C_{14}H_{18}N_5O_2$: C, 59.78; H, 3.94; N, 24.90. MS (EI): *m/z* 281 (M^+, 40 %). Found C, 59.74; H, 4.11; N, 24.55.

3-cyano-1,5-dimethoxyphenylformazan (3.17f). Yield 66.6 %. X-ray quality crystals were grown via slow evaporation of a dichloromethane solution in glass tubes (5 mm diameter). Mp. 140-142°C. ^{1}H NMR (300 MHz, d_6-DMSO): *closed* δ 13.68 (s, 1H, NH), 7.68 (d of d, 2H, J = 8 Hz, 1 Hz), 7.43 (t of d , 2H, J = 8 Hz, 2Hz), 7.24 (d, 2H, 8Hz), 7.07 (t, 2H, J = 8 Hz), 3.97 (s, 6H) ppm. *open* δ 10.24 (s, 0.1 H, NH), 7.53 (d, 0.4H, 8 Hz), 3.95 (s, 1H) ppm. ^{13}C NMR (75 MHz, d_6-DMSO): δ 152.4, 135.3, 131.1, 130.7, 125.0, 121.2, 116.2, 115.6, 112.8, 56.3, 56.1 ppm. FT-IR (KBr): 2224 (m) (CN), 1506 (s), 1485 (s) cm^{-1}. UV-vis (CH_2Cl_2): λ_{max} 250 nm (ε = 9000 L•mol^{-1}•cm^{-1}), 293 nm (ε = 9750 L•mol^{-1}•cm^{-1}), 464 nm (ε = 25000 L•mol^{-1}•cm^{-1}). MS (EI): m/z 309 (M^+, 70 %). Anal. Calcd for $C_{16}H_{15}N_5O_2$: C, 62.13; H, 4.89; N, 22.64. Found C, 62.28 H, 4.86; N, 22.32.

Method (b). Sodium hydride (0.50 g, 20 mmol) was added to a blood-red solution of **3.17e** (1.405 g, 5 mmol) in dry tetrahydrofuran (200 mL) at –78°C. The mixture was allowed to warm slowly to room temperature with stirring under argon overnight resulting in a purple solution. The mixture was once again cooled to –78°C and treated with methyl iodide (17.1 g, 7.5 mL, 120 mmol) before it was allowed to warm slowly to room temperature with stirring under argon overnight resulting in a dark-violet solution. The solvent was removed *in vacuo* yielding a dark-violet solid. Treatment with water (150 mL) at room temperature for 2 h produced red solid. The solid was filtered, before being rinsed with water and pentane. Recrystallization from a saturated methanolic solution afforded **3.10f** as a microcrystalline red solid, yield (1.42 g, 91 %).

General procedure for the synthesis of formazans 3.18a,b: 3-nitro-1,5-phenylformazan (3.18a). To a solution of aniline (8.61 g, 92 mmol), 12 M concentrated hydrochloric acid (25 mL), and water (50 mL) at 0˚ C was added sodium nitrite (7.52 g, 109 mmol) in small portions over a 10 min period. After 30 min of stirring, the mixture was added to a second solution containing nitromethane (2.82 g, 46 mmol), sodium hydroxide (8.00 g , 100 mmol) and water (100 mL) at 0˚ C over a 60 min period. The resulting solution was filtered, and the solid triturated with methanol. The solid was then purified via recrystallization from hot methanolic solution affording **3.18a** as a poppy red microcrystalline solid, yield (6.20 g, 50.1 %). It should be noted that rapid addition of the diazonium salt to the nitromethane solution results in the production of a brown oil. Purification of **3.18a** was complicated by the presence of this oil, and repeated crystallizations were often necessary to obtain pure samples of **3.18a**, decreasing the isolated yield. Mp. 138-140^{o}C. ^{1}H NMR (500 MHz, CD_2Cl_2): δ 15.16 (s, 1H, NH), 7.66 (d, 4H, J = 8 Hz), 7.45 (t, 4H, J = 7 Hz), 7.35 (t, 2H, J = 7 Hz). ^{13}C NMR (125 MHz, CD_2Cl_2): δ 146.8, 146.1, 130.6, 130.4, 120.4 ppm. FT-IR (KBr): 1551 (s), 1354 (s), 1281 (s), 754 (s) cm^{-1}. UV-vis (CH_2Cl_2): λ_{max} 325 nm (ε = 11500 L•mol^{-1}•cm^{-1}), 452 nm (ε = 23750 L•mol^{-1}•cm^{-1}). MS (EI): *m/z* 269 (M^+, 25 %). Anal. Calcd for $C_{13}H_{11}N_5O_2$: C, 57.99; H, 4.12; N, 26.01. Found C, 58.02; H, 3.85; N, 26.16.

3-nitro-1,5-*para*-tolylformazan (3.18b). Yield 47.5 %. It should be noted that rapid addition of the diazonium salt to the nitromethane solution results in the production of a brown oil. Purification of **3.18b** was complicated by the presence of this oil, and repeated crystallizations were often necessary to obtain pure samples of **3.18b**, decreasing the isolated yield. X-ray quality crystals were grown via slow cooling of a

saturated methanolic solution of **3.18b**. Mp. 124-126°C (dec). ^{1}H NMR (500 MHz, CD_2Cl_2): δ 15.34 (s, 1H, NH), 7.64 (d, 4H, J = 8 Hz), 7.33 (d, 4H, J = 8 Hz), 2.43 (s, 6H). ^{13}C NMR (125 MHz, CD_2Cl_2): δ 146.1, 144.7, 141.4, 131.0, 120.3, 21.7 ppm. FT-IR (KBr): 1547 (s), 1351 (m), 1282 (s), 816 (m) cm^{-1}. UV-vis (CH_2Cl_2): λ_{max} 265 nm (ε = 8250 $L•mol^{-1}•cm^{-1}$), 340 nm (ε = 14000 $L•mol^{-1}•cm^{-1}$), 464 nm (ε = 27500 $L•mol^{-1}•cm^{-1}$). MS (EI): *m/z* 297 (M^+, 15 %). Anal. Calcd for $C_{15}H_{15}N_5O_2$: C, 60.60; H, 5.09; N, 23.56. Found C, 60.61; H, 5.06; N, 23.43.

General procedure for the synthesis of formazans 3.18c-f: Synthesis of 1,5-(2,6-dimethylphenyl)-3-nitroformazan (3.18c). To a solution of nitromethane (1.4 mL, 26 mmol) in tetrahydrofuran (25 mL) at -78°C was added 1.6 M n-BuLi in hexanes (9.6 mL, 15 mmol) over a 5 min period. The resulting slurry was allowed to stir at -78°C for 1 h before a slurry of 2,6-dimethylphenyldiazonium tetrafluoroborate[318] (2.82 g, 13 mmol) in tetrahydrofuran (100 mL) was added causing the appearance of a red colour. The cold bath was then removed, and the mixture left to stir overnight slowly darkening to a blood red colour as it warmed. The mixture was filtered, concentrated, and purified via flash chromatography (alumina, dichloromethane). The dark solid was then recrystallized from a saturated methanolic solution to afford **3.18c** as large red needles, yield 1.17 g (55.2 %). Mp. 122-124°C. ^{1}H NMR (500 MHz, CD_2Cl_2): δ 14.51 (s, 1H, NH), 7.26-7.14 (multiplet, 6H), 2.48 (s, 6H). ^{13}C NMR (125 MHz, CD_2Cl_2): δ 146.3, 144.1, 132.4, 130.4, 129.6, 20.1 ppm. FT-IR (KBr): 1544 (s), 1474 (m), 1356 (m), 1334 (m), 778 (m) cm^{-1}. UV-vis (CH_2Cl_2): λ_{max} 330 nm (ε = 11750 $L•mol^{-1}•cm^{-1}$), 425 nm (ε = 21250 $L•mol^{-1}•cm^{-1}$). MS (EI): *m/z* 325 (M^+, 10 %). Anal. Calcd for $C_{17}H_{19}N_5O_2$: C, 62.75; H, 5.89; N, 21.52. Found C, 62.74; H, 5.86; N, 21.72.

1,5-mesityl-3-nitroformazan (3.18d). X-ray quality crystals were grown via slow cooling of a saturated methanolic solution. Yield 60.0 %. Mp. 136-138°C. ^{1}H NMR (500 MHz, CD_2Cl_2): δ 14.42 (s, 1H, NH), 7.00 (s, 4H), 2.44 (s, 12H), 2.34 (s, 6H). ^{13}C NMR (125 MHz, CD_2Cl_2): δ 146.4, 142.2, 140.1, 132.6, 131.1, 21.4, 20.2 ppm. FT-IR (KBr): 1607 (m), 1533 (s), 1354 (m), 1334 (m), 1271 (m), 845 (m), 744 (m) cm^{-1}. UV-vis (CH_2Cl_2): λ_{max} 342 nm (ε = 12000 $L•mol^{-1}•cm^{-1}$, 432 nm (ε = 20750 $L•mol^{-1}•cm^{-1}$). MS (EI): *m/z* 353 (M^+, 10 %). Anal. Calcd for $C_{19}H_{23}N_5O_2$: C, 64.57; H, 6.56; N, 19.82. Found C, 64.10; H, 6.53; N, 19.84.

1,5-(2,6-di-*iso*-propylphenyl)-3-nitroformazan (3.18e). Yield 36.5 %. Mp. 96-98°C. ^{1}H NMR (500 MHz, CD_2Cl_2): δ 14.53 (s, 1H, NH), 7.35-7.18 (m, 6H), 3.07 (septet, 4H, J = 7 Hz), 1.15 (d, 24H, J = 7 Hz). ^{13}C NMR (125 MHz, CD_2Cl_2): δ 146.9, 142.9, 142.7, 130.1, 124.7, 29.2, 24.1 ppm. FT-IR (KBr): 2962 (s), 1547 (s), 1503 (m), 1470 (m), 1327 (m), 1283 (m), 746 (m) cm^{-1}. UV-vis (CH_2Cl_2): λ_{max} 334 nm (ε = 11000 $L•mol^{-1}•cm^{-1}$), 398 nm (ε = 17500 $L•mol^{-1}•cm^{-1}$), 532 nm (ε = 1250 $L•mol^{-1}•cm^{-1}$). MS (EI): *m/z* 437 (M^+, 5 %). Anal. Calcd for $C_{25}H_{35}N_5O_2$: C, 68.62; H, 8.06; N, 16.00. Found C, 67.83; H, 8.21; N, 15.84.

1,5-(3,5-di-*tert*-butylphenyl)-3-nitroformazan (3.18f). Yield 17.2 %. Mp. 178-180°C. ^{1}H NMR (500 MHz, CD_2Cl_2): δ 15.43 (s, 1H, NH), 7.48 (d, 4H, J = 2 Hz), 7.44 (t, 2H, J = 2 Hz), 1.30 (s, 36H). ^{13}C NMR (125 MHz, CD_2Cl_2): δ 153.5, 146.6, 146.4, 125.2, 114.8, 35.6, 31.6 ppm. FT-IR (KBr): 2967 (s), 1604 (w), 1544 (s), 1363 (m), 1355 (m), 1299 (m), 1280 (m), 878 (w), 800 (w), 695 (w) cm^{-1}. UV-vis (CH_2Cl_2): λ_{max} 340 nm (ε = 12250 $L•mol^{-1}•cm^{-1}$), 432 nm (ε = 24000 $L•mol^{-1}•cm^{-1}$). MS (EI): *m/z* 493 (M^+, 15 %).

Anal. Calcd for $C_{29}H_{43}N_5O_2$: C, 70.55; H, 8.78; N, 14.19. Found C, 70.42; H, 8.88; N, 13.69.

copper(3-cyano-1,5-(2-methoxyphenylformazanato)chloride (3.19). 3.17f (1.00 g, 3.2 mmol) was combined with freshly distilled tetrahydrofuran (100 mL) under argon and treated with sodium hydride (0.080 g, 3.3 mmol) before it was allowed to stir for 16 h changing colour from red to brown-red. Copper (II) chloride (0.432 g, 3.3 mmol) was added and the reaction was once again left to stir for 16 h. The solvent was then removed and the solid triturated with hexanes (100 mL). The solid was then dissolved in dichloromethane (3 x 150 mL) leaving behind a small amount of brown solid byproduct. The solution was filtered before being concentrated *in vacuo* affording **3.19** as a dark purple solid (green reflex), yield 1.00 g (75.9 %). X-ray quality crystals were grown from solvent diffusion of hexanes into a dichloromethane solution of **3.19**. Mp. 180-182°C (dec., brown). FT-IR (KBr): 2225 (m) (CN), 1587 (m), 1483 (m), 1344 (s), 752 (s) cm^{-1}. UV-vis (CH_2Cl_2): λ_{max} 256 nm (ε = 13750 $L \bullet mol^{-1} \bullet cm^{-1}$), 288 nm ($\varepsilon$ = 14750 $L \bullet mol^{-1} \bullet cm^{-1}$), 371 nm ($\varepsilon$ = 6250 $L \bullet mol^{-1} \bullet cm^{-1}$), 547 nm ($\varepsilon$ = 19250 $L \bullet mol^{-1} \bullet cm^{-1}$). Anal. Calcld for $C_{19}H_{16}N_4$: C, 47.18; H, 3.46; N, 17.19. Found: C, 47.21; H, 3.81; N, 16.87.

iron(3-cyano-1,5-(2-hydroxyphenylformazanato)-bis-pyridine (3.20a). 3.17e (0.250 g, 0.88 mmol) was combined with freshly distilled tetrahydrofuran (100 mL) under argon and treated with sodium hydride (0.064 g, 2.7 mmol) before being left to stir for 16 h changing color from red to dark blue. Iron (III) chloride (0.144 g, 0.88 mmol) and pyridine (0.36 mL, 4.5 mmol) were added and the reaction was left to stir for 16 h at which time the solution was a dark blue color. The mixture was then filtered and the solvent was removed *in vacuo*. Trituration with hexanes allowed for **3.20a** to be isolated

as a dark blue solid (bronze reflex), yield 0.317 g (72.9 %). X-ray quality crystals were grown from solvent diffusion of hexanes into a dichloromethane solution of **3.20a**. Mp. 270-272°C. FT-IR (KBr): 2225 (m) (CN), 1577 (m), 1459 (s), 1448 (s), 1300 (s) cm^{-1}. UV-vis (CH_2Cl_2): λ_{max} 234 nm (ε = 32500 $L \bullet mol^{-1} \bullet cm^{-1}$), 320 nm ($\varepsilon$ = 14000 $L \bullet mol^{-1} \bullet cm^{-1}$), 484 nm ($\varepsilon$ = 9250 $L \bullet mol^{-1} \bullet cm^{-1}$), 592 nm ($\varepsilon$ = 13750 $L \bullet mol^{-1} \bullet cm^{-1}$), 631 nm ($\varepsilon$ = 17250 $L \bullet mol^{-1} \bullet cm^{-1}$). Anal. Calcld for $FeC_{24}H_{18}N_7O_2$: C, 58.55; H, 3.69; N, 19.92. Found: C, 57.63; H, 3.82; N, 19.36.

cobalt(3-cyano-1,5-(2-hydroxyphenylformazanato)-bis-pyridine (3.20b). 3.17e (0.250 g, 0.88 mmol) was combined with freshly distilled tetrahydrofuran (100 mL) under argon and treated with sodium hydride (0.064 g, 2.7 mmol) before being left to stir for 16 h changing color from red to dark blue. Cobalt (II) chloride (0.115 g, 0.88 mmol) and pyridine (0.36 mL, 4.5 mmol) were added and the reaction was left to stir for 16 h at which time the solution had changed to a red-brown color. The mixture was then allowed to stir open to air changing color to dark blue before the solution was filtered and the solvent removed *in vacuo*. Trituration with hexanes allowed for **3.20b** to be isolated as a dark blue solid (bronze reflex), yield 0.325 g (74.3 %). X-ray quality crystals were grown from solvent diffusion of hexanes into a dichloromethane solution of **3.20b**. Mp. 262-264°C . ^{1}H NMR (300 MHz, CD_2Cl_2): δ 7.99 (d of d, 2H, ^3J = 7 Hz, ^4J = 1 Hz), 7.41 (t, 2H, ^3J = 7 Hz), 7.37 (d, 4H, ^3J = 7 Hz), 7.14 (d of d, 2H, ^3J = 8 Hz, ^4J = 1 Hz), 6.98 (t of d, 2H, ^3J = 7 Hz, ^4J = 1 Hz), 6.91 (t, 4H, ^3J = 7 Hz), 6.53 (t of d, 2H, ^3J = 7 Hz, ^4J = 1 Hz). ^{13}C NMR (75 MHz, CD_2Cl_2): δ 168.4, 151.6, 147.5, 139.2, 130.4, 125.1, 119.4, 116.4, 116.2 ppm. FT-IR (KBr): 2219 (m) (CN), 1462 (s), 1448 (s), 1234 (s) cm^{-1}. UV-vis (CH_2Cl_2): λ_{max} 242 nm (ε = 42500 $L \bullet mol^{-1} \bullet cm^{-1}$), 325 nm ($\varepsilon$ = 10000 $L \bullet mol^{-1} \bullet cm^{-1}$),

483 nm (ε = 4250 L•mol^{-1}•cm^{-1}), 509 nm (ε = 4250 L•mol^{-1}•cm^{-1}), 608 nm (ε = 14500 L•mol^{-1}•cm^{-1}), 658 nm (ε = 24750 L•mol^{-1}•cm^{-1}). Anal. Calcd for $CoC_{24}H_{18}N_7O_2$: C, 58.19; H, 3.66; N, 19.79. Found C, 57.78; H, 3.79; N, 19.39.

bis-(3-cyano-1,5-(2,6-dimethylphenyl)formazanato)-bis-μ-hydroxonickel (3.21). **3.17c** (0.540 g, 1.8 mmol), nickel acetate tetrahydrate (0.440 g, 1.8 mmol), and 95 % ethanol (100 mL) were combined and allowed to reflux open to air for 16 h. After cooling to room temperature the mixture was filtered and the solid washed with 95 % ethanol (3 x 10 mL) affording **3.21** as a dark green microcrystalline solid, yield 0.440 g (32.2 %). X-ray quality crystals were grown via diffusion of pentane into a solution of **3.21** in dichloromethane. Mp. 266-268^{o}C (dec). ^{1}H NMR (300 MHz, CD_2Cl_2): δ 6.87 (t, 4H, ^{3}J = 7 Hz), 6.73 (d, 8H, ^{3}J = 8 Hz), 2.41 (s, 24H), -6.94 (s, 2H, μ-OH). ^{13}C NMR (75 MHz, CD_2Cl_2): δ 145.2, 130.9, 129.2, 129.1, 18.3 ppm. FT-IR (KBr): 3603 (m) (OH), 2229 (m) (CN), 1358 (s) cm^{-1}. UV-vis (CH_2Cl_2): λ_{max} 271 nm (ε = 27500 L•mol^{-1}•cm^{-1}), 307 nm (ε = 21500 L•mol^{-1}•cm^{-1}), 620 nm (ε = 1950 L•mol^{-1}•cm^{-1}). Anal. Calcd for $Ni_2C_{36}H_{38}N_{10}O_2$: C, 56.88; H, 5.04; N, 18.43. Found C, 56.99; H, 5.13; N, 18.32.

bis(3-nitro-1,5-*para*-tolylformazanato)nickel (3.22). **3.18b** (0.400 g, 1.3 mmol), nickel acetate tetrahydrate (0.167 g, 0.67 mmol), and 95 % ethanol (50 mL) were combined and allowed to reflux open to air for 16 h. After cooling to room temperature the mixture was filtered and the solid washed with 95 % ethanol (3 x 10 mL) affording **3.22** as a dark green microcrystalline solid, yield 0.362 g (85.5 %). X-ray quality crystals were grown via diffusion of pentane into a solution of **3.22** in dichloromethane. Mp. 358-360^{o}C. ^{1}H NMR (300 MHz, CD_2Cl_2): δ 7.42 (d, 4H, ^{3}J = 8 Hz), 7.00 (d, 4H, ^{3}J = 8 Hz), 2.34 (s, 6H). ^{13}C NMR (75 MHz, CD_2Cl_2): δ 148.7, 140.5, 129.9, 123.6, 21.5 ppm. FT-IR (KBr): 1525

(m), 1355 (s), 1275 (s), 819 (m) cm^{-1}. UV-vis (CH_2Cl_2): λ_{max} 310 nm (ε = 18500 $L \bullet mol^{-1} \bullet cm^{-1}$), 409 nm ($\varepsilon$ = 27500 $L \bullet mol^{-1} \bullet cm^{-1}$), 673 nm ($\varepsilon$ = 10000 $L \bullet mol^{-1} \bullet cm^{-1}$). Anal. Calcd for $NiC_{30}H_{28}N_{10}O_4$: C, 55.32; H, 4.33; N, 21.51. Found C, 55.06; H, 4.22; N, 20.97.

bis-(1,5-mesityl-3-nitroformazanato)-bis-μ-hydroxonickel (3.24). 3.18d (0.610 g, 1.7 mmol), nickel acetate tetrahydrate (0.430 g, 1.7 mmol), and methanol (100 mL) were combined and allowed to reflux open to air for 16 h. After cooling to room temperature the mixture was filtered and the solid washed with methanol (3 x 10 mL) affording **3.24** as a dark green microcrystalline solid, yield 0.431 g (59.2 %). X-ray quality crystals were grown via vapor diffusion of pentane into a solution of **3.24** in dichloromethane. Mp. 276-278°C (dec). ^{1}H NMR (300 MHz, CD_2Cl_2): δ 6.61 (s, 8H), 2.41 (s, 24H), 2.26 (s, 12H), -6.61 (s, 2H, μ-OH). ^{13}C NMR (75 MHz, CD_2Cl_2): δ 143.1, 138.4, 130.8, 129.6, 21.5, 18.5 ppm. FT-IR (KBr): 3601 (m) (OH), 1537 (s), 1371 (s), 1355 (s), 1294 (s), 761 (s) cm^{-1}. UV-vis (CH_2Cl_2): λ_{max} 298 nm (ε = 34000 $L \bullet mol^{-1} \bullet cm^{-1}$), 392 nm ($\varepsilon$ = 14750 $L \bullet mol^{-1} \bullet cm^{-1}$), 635 nm ($\varepsilon$ = 2000 $L \bullet mol^{-1} \bullet cm^{-1}$). Anal. Calcd for $Ni_2C_{38}H_{46}N_{10}O_2$: C, 53.30; H, 5.42; N, 16.36. Found C, 53.30; H, 5.48; N, 16.45.

General procedure for the synthesis of palladium complexes 3.18b,d,e: palladium(3-nitro-1,5-*para*-tolylformazanato)(1,1,1,6,6,6-hexafluroacetylacetonato) (3.25b). 3.18b (0.240 g, 0.81 mmol), bis-(1,1,1,6,6,6-hexafluoroacteylacetonato)palladium (0.420 g, 0.81 mmol), and methanol (30 mL) were combined and allowed to reflux in air for 2 h. The solvent was removed *in vacuo*, and the complex was recrystallized from saturated methanolic solution. **3.25b** was isolated by filtration as a dark purple microcrystalline solid, yield 0.233 g (47.2 %). X-ray quality crystals were obtained by cooling a dilute methanolic solution of **3.25b** in a -20ºC freezer for 72 hours. Mp. 186-188°C. ^{1}H NMR

(500 MHz, CD_2Cl_2): δ 7.82 (d, 4H, ^3J = 8 Hz), 7.26 (d, 4H, ^3J = 8 Hz), 6.12 (s, 1H), 2.42 (s, 6H). ^{13}C NMR (125 MHz, CD_2Cl_2): δ 176.1 (q, ^2J = 36 Hz), 146.7, 141.3, 129.9, 125.3, 116.9 (q, ^1J = 285 Hz), 92.7, 21.6 ppm. FT-IR (KBr): 1631 (s), 1601 (w), 1533 (s), 1458 (s), 1394 (s), 1293 (s), 1257 (s), 1152 (s), 817 (m), 802 (m) cm^{-1}. UV-vis (CH_2Cl_2): λ_{max} 250 nm (ε = 30000 L•mol^{-1}•cm^{-1}), 344 nm (ε = 14000 L•mol^{-1}•cm^{-1}), 540 nm (ε = 10500 L•mol^{-1}•cm^{-1}). Anal. Calcd for $PdC_{20}H_{15}F_6N_5O_4$: C, 39.39; H, 2.48; N, 11.49. Found C, 39.39; H, 2.46; N, 11.57.

palladium(1,5-mesityl-3-nitroformazanato)(1,1,1,6,6,6-hexafluroacetylacetonato) (3.25d). X-ray quality crystals were obtained via slow evaporation of a dichloromethane solution of **3.25d** in an NMR tube. Yield 0.220 g (86.9 %). Mp. 198-200°C. ^1H NMR (500 MHz, CD_2Cl_2): δ 6.93 (s, 4H), 6.06 (s, 1H), 2.31 (s, 6H), 2.26 (s, 12H). ^{13}C NMR (125 MHz, CD_2Cl_2): δ 177.0 (q, ^2J = 36 Hz), 151.5, 144.7, 139.6, 131.9, 129.4, 116.9 (q, 1J = 285 Hz), 92.6, 21.3, 18.5 ppm. FT-IR (KBr): 1631 (s), 1610 (s), 1544 (s), 1452 (s), 1402 (s), 1307 (s), 1254 (s), 1220 (s), 1149 (s) cm^{-1}. UV-vis (CH_2Cl_2): λ_{max} 250 nm (ε = 33750 L•mol^{-1}•cm^{-1}), 344 nm (ε = 16750 L•mol^{-1}•cm^{-1}), 473 nm (ε = 5250 L•mol^{-1}•cm^{-1}). Anal. Calcd for $PdC_{24}H_{23}F_6N_5O_4$: C, 43.29; H, 3.48; N, 10.52. Found C, 43.74; H, 3.71; N, 10.53.

palladium(1,5-(2,6-di-*iso*-propylphenyl)-3-nitroformazanato)(1,1,1,6,6,6-hexafluroacetylacetonato) (3.25e). Yield 0.270 g (62.1 %). Mp. 222-224°C (dec). ^1H NMR (500 MHz, CD_2Cl_2): δ 7.42 (t, 2H, ^3J = 8 Hz), 7.24 (d, 4H, ^3J = 8 Hz), 6.05 (s, 1H), 3.21 (septet, 4H, ^3J = 7 Hz), 1.29 (d, 12H, ^3J = 7 Hz), 1.21 (d, 12H, ^3J = 7 Hz). ^{13}C NMR (125 MHz, CD_2Cl_2): δ 176.9 (q, ^2J = 36 Hz), 144.4, 142.7, 130.2, 124.3, 116.8 (q, ^1J = 285 Hz), 92.7, 29.7, 24.7, 23.1 ppm. FT-IR (KBr): 2966 (w), 1630 (s), 1549 (s), 1466 (s),

1407 (s), 1310 (s), 1257 (s), 1214 (s), 1150 (s), 786 (m) cm^{-1}. UV-vis (CH_2Cl_2): λ_{max} 248 nm (ε = 30750 $L \bullet mol^{-1} \bullet cm^{-1}$), 341 nm ($\varepsilon$ = 14750 $L \bullet mol^{-1} \bullet cm^{-1}$), 473 nm ($\varepsilon$ = 5250 $L \bullet mol^{-1} \bullet cm^{-1}$). Anal. Calcd for $PdC_{30}H_{35}F_6N_5O_4$: C, 48.04; H, 4.70; N, 9.34. Found C, 48.28; H, 4.71; N, 9.38.

Chapter 4 Magnetostructural studies of verdazyl-based spin dimers

4.1 Stable radicals and molecular magnetism

As outlined in Chapter 1, there are three widespread approaches to molecular magnetism which incorporate stable radicals as a source of unpaired electrons (spins). Whether bound to paramagnetic transition metal ions, incorporated into polymers, or as radical crystals, radicals play an important role in the properties of molecule-based magnets.

Verdazyl radicals are good candidates for use in molecule-based magnets as they (i) are extremely stable in both solution and the solid-state, (ii) are produced via synthetic pathways amenable to derivatization, and (iii) have been shown to give rise to strong magnetic interactions in a variety of systems.[53]

As the field of molecular magnetism continues to advance, there is still much room for improvement, which ultimately must begin with the study of model compounds. It is important to further understanding of magnetic interactions in metal-metal, metal-radical, and radical-radical model systems. This chapter describes two different classes of spin dimers, i.e., molecules containing two unpaired electrons. Verdazyl diradicals were synthesized and studied in order to understand the interaction between radicals bridged by *para*- and *meta*-benzene. Copper (II) complexes of verdazyls were also synthesized, and their magnetostructural properties studied.

4.2 Magnetic coupling in two-spin systems

The simplest magnetic system involves the interaction of two unpaired electrons. For two-spin systems there are two possible modes of magnetic coupling between unpaired electrons (Figure 4.1). The nature of the coupling depends on interactions between half filled molecular orbitals (magnetic orbitals). Antiferromagnetic coupling, is by far the most common, and involves the alignment of unpaired electrons antiparallel to one another (S = 0 ground state). Ferromagnetic coupling, involves parallel alignment of unpaired electrons (S = 1 ground state).

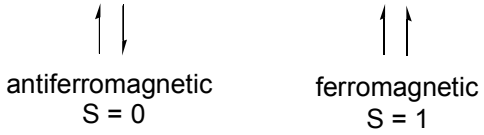

Figure 4.1. Ground state orientations of spin dimers.

The energy gap between the S = 0 and S = 1 spin states is known as the magnetic coupling parameter (J) (Equation 4.1). By convention this equation yields J > 0 when electrons are ferromagnetically coupled, and J < 0 when unpaired electrons are antiferromagnetically coupled.

$$J = E\,(S = 0) - E(S = 1) \qquad (4.1)$$

Inspection of the temperature dependence of the magnetic moment allows for qualitative analysis of magnetic coupling (Figure 4.2). The magnetic moment of a paramagnetic sample does not change with variation in temperature in the presence of a magnetic field; in other words there is no interaction between the unpaired electrons. Systems in which unpaired electrons are antiferromagnetically coupled (J < 0) show a decrease in magnetic moment with decreasing temperature, and ferromagnetically coupled (J > 0) systems show an increase in moment with decreasing temperature.[224] The

Bleaney-Bowers equation is generally used to model such systems in order to extract the magnetic coupling parameter (see later for details).[330]

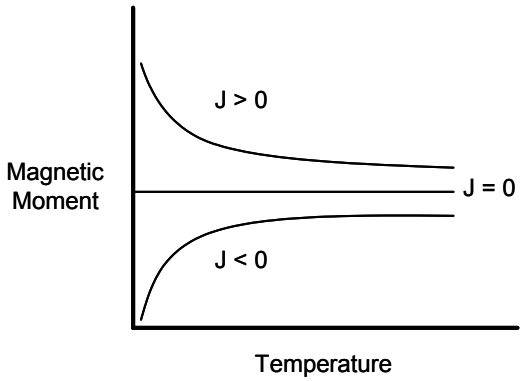

Figure 4.2. Qualitative magnetic behavior of spin dimers.

Results and discussion

4.3 Benzene-bridged diradicals

The intramolecular magnetic interactions in organic diradicals have been studied extensively.[331-340] Among the most common classes of diradicals are those bridged by benzene. In molecules attached to the benzene spacer at a nodal plane of the radical, e.g., **4.1**[341, 342] and **4.2**[343] , the interactions between unpaired electrons are understood to arise from a phenomenon known as spin polarization.

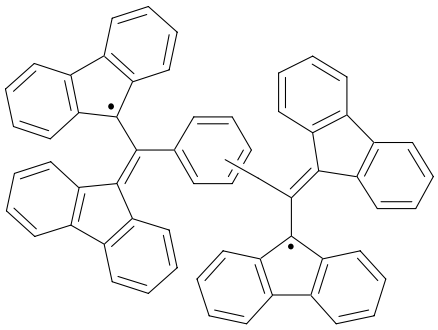

4.1

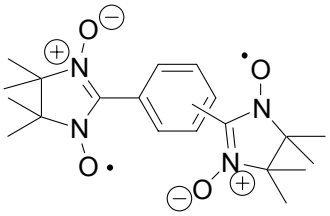

4.2

Spin polarization results from the ability of unpaired electrons to polarize conjugated π-systems. The alternation of polarity around the benzene spacer accounts for the type of interaction observed. In order for alternation of polarity to be maintained through a *para*-benzene spacer the radicals must be antiferromagnetically coupled (Figure 4.3, left). In contrast, radicals coupled through a *meta*-benzene spacer must be ferromagnetically coupled in order to maintain alternation of polarity around the benzene ring (Figure 4.3, right). The predicted trends based on spin polarization arguments are consistent with most examples in the literature where the radical units are coplanar with the aromatic spacer. However, deviations from planarity and substituent effects have been shown to cause substantial changes in the magnitude of the coupling.[344]

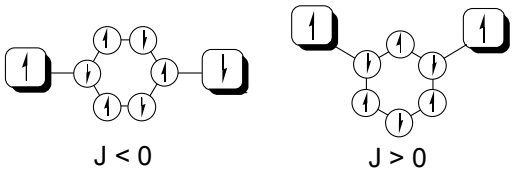

Figure 4.3. Spin polarization in para- (left) and meta- (right) benzene-bridged diradicals.

4.4 Syntheis and characterization of verdazyl diradicals

Few reports of verdazyl diradicals exist, and in most cases the results are incomplete or incorrect. Early studies of *para*- and *meta*-benzene bridged diradicals **4.3a** and **4.3b** provided a qualitative assessment of the interaction between radicals,[345-347] while the only attempt to quantify the magnitude of the interactions[348] incorrectly concluded ferromagnetic coupling for both.[53] Poor stability has hampered the study of other verdazyl diradicals including N-methyl-substituted diradicals **4.4a-c**[349] and bis-verdazyls **4.5a**[350] and **4.5c.**[349] However, diradical **4.5b** was sufficiently stable to allow

for its magnetic characterization. The two radicals couple antiferromagnetically with a singlet-triplet gap of J = -760 cm^{-1}.[232]

The methylene bridged diradical **4.6** has recently been synthesized. Although it possesses a saturated linker, the radicals have been shown to interact antiferromagnetically with a singlet triplet gap of J = -150 cm^{-1}.[351] The *iso*-propyl substituents incorporated in **4.6**, and other monoradicals have been shown to greatly enhance the stability of oxoverdazyl radicals,[149] subsequently opening the door to several diradical systems previously unattainable due to their inherent instability. In this vein, analogues of **4.4a** and **4.4b** bearing *iso*-propyl substituents were prepared in order to further study the electronic communication of verdazyl radicals through benzene spacers.

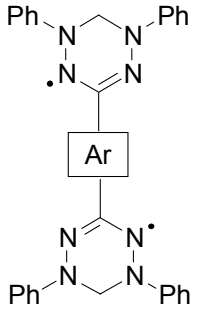

4.3a Ar = 1,4-C_6H_4
4.3b Ar = 1,4-C_6H_4

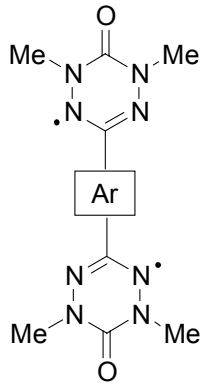

4.4a Ar = 1,4-C_6H_4
4.4b Ar = 1,3-C_6H_4
4.4c Ar = 2,5-C_4H_2S

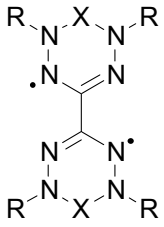

4.5a R = Ph, X = CH_2
4.5b R = Me, X = CO
4.5c R = Me, X = CS

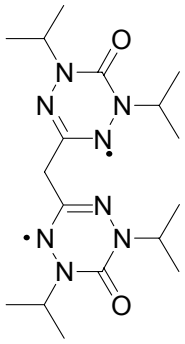

4.6

4.4.1 Synthesis of benzene-bridged verdazyl diradicals

Benzene bridged diradicals **4.7a** and **4.7b** were obtained by slight modification of established procedures (Scheme 4.1).[149] Reaction of two equivalents of carbonic acid bis(1-*iso*-propylhydrazide) **2.8a** with the appropriate dialdehyde affords tetrazanes **4.8a** and **4.8b**, which have a tendancy to form solvates (in most organic solvents). The off white solids were desolvated by heating *in vacuo* and then oxidized with *para*-

benzoquinone to afford diradicals **4.7a** and **4.7b** in good yield. Recrystallization of the diradicals via slow cooling of saturated ethyl acetate solutions afforded well formed crystals suitable for X-ray diffraction.

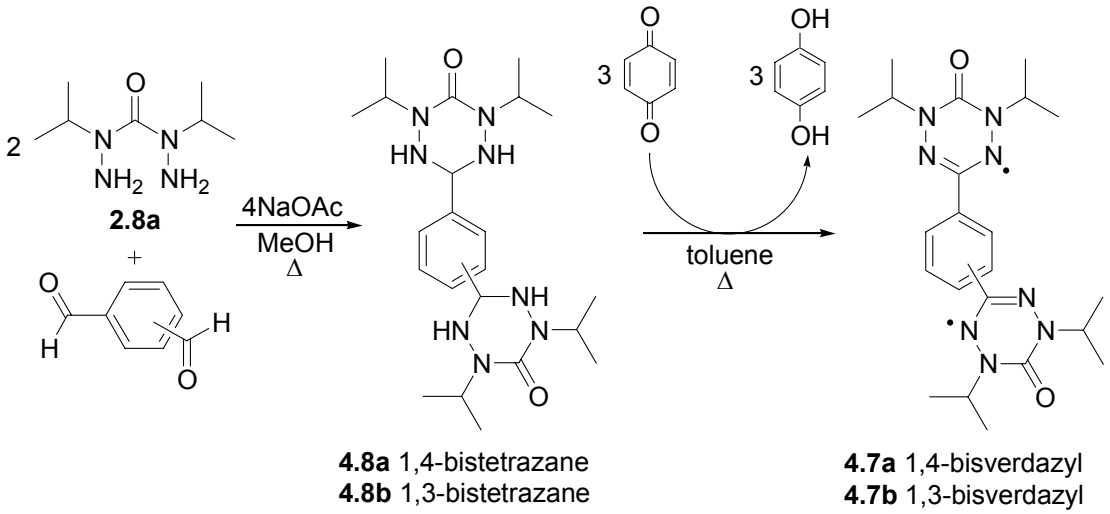

Scheme 4.1. Synthesis of diradicals **4.7a** and **4.7b**.

4.4.2 Phenyl-substituted monoverdazyl 2.4b as a model system

Diradicals **4.7a** and **4.7b** are the first examples of verdazyl diradicals exhibiting sufficient stability properties to allow their reliable and comprehensive characterization. The diradicals were compared to **2.4b** (Chapter 2) in order to probe the effects of electronic communication between the unpaired electrons on their electrochemistry, electronic spectra, and EPR spectra. In order to gain further insight into the spin density found within diradicals **4.7a** and **4.7b** as well as monoradical **2.4b**, calculations were performed on **2.4b** (Figure 4.4).

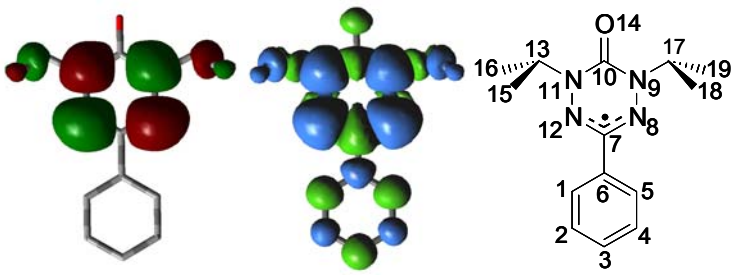

Figure 4.4. Calculated singly occupied molecular orbital (left), spin density plot (middle), and atom labeling scheme (right) for **2.4b**.

Table 4.1. Atomic spin densities for **2.4b**.

Atom	Spin density	Atom	Spin density
C1, C5	-0.029	N9, N11	0.207
C2, C4	0.018	C10	-0.033
C3	-0.027	O14	-0.123
C6	0.032	C13, C17	-0.0123
C7	-0.155	C15, C16, C18, C19	0.0112
N8, N12	0.393		

The verdazyl radical SOMO is well established[235] as a π* orbital spanning the four nitrogens with minor contributions on the N-substituents. The orbital contains two nodal planes, one passing through the C6-C7-C10 axis, and the second bisecting the N-N bonds. The overall spin density alternates via spin-polarization around the molecule with the highest spin densities found on the two coordinate (N8, N12; 0.393) and three coordinate nitrogens (N9, N11; 0.207) consistent with the SOMO. Two other atoms possess significant spin density (C7 (-0.155) and O14 (-0.123)). The spin density on C7 is of particular importance, as it is the position which determines the amount of spin allowed to 'leak' onto the phenyl substituent, and directly relates to spin polarization in the diradicals. Furthermore, the alternating sign of the spin density around the phenyl ring (C1-C2-C3-C4-C5-C6) confirms the spin polarization pattern described in section 4.3. The non-negligible spin density found on C13, C15, C16, C17, C18, C19, and O14

may also be important when considering intermolecular interactions between diradicals in the solid-state.

4.4.3 Electronic spectra of 4.7a, and 4.7b

The electronic spectra of **2.4b**, **4.7a**, and **4.7b** are presented in Figure 4.5. All three compounds have maxima at 417 nm as well as a broader, weaker absorption at 450-470 nm, typical of 3-aryl-6-oxoverdazyl radicals.[144, 352, 353] The minor differences between the monoradical and the diradicals suggest limited intramolecular communication between verdazyls in **4.7a** and **4.7b**. The apparent lack of communication is consistent with the symmetry properties of verdazyl radicals, which possess a node at the substituted carbon (C3) (see Figure 4.4). The presence of the node does not permit significant overlap with the aromatic substituent (phenyl) in **2.4b**, **4.7a**, and **4.7b**. However, upon closer inspection of the high energy region of the spectra it is apparent that a mechanism for conjugation must be operational, perhaps involving other molecular orbitals (LUMO, NHOMO, etc.). The monoradical **2.4b** and the 1,3-diradical **4.7b** have an absorption at 250 nm, and the 1,4-diradical **4.7a** is redshifted to 280 nm. These observations are consistent with cross conjugation of the 1,3-derivative and conjugation of the 1,4-derivative.

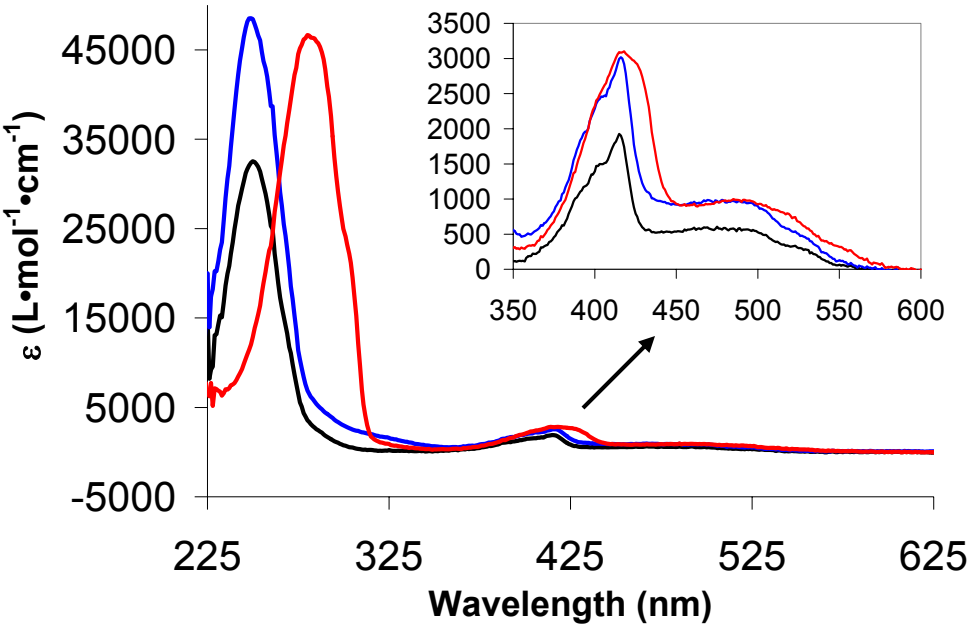

Figure 4.5. Electronic spectra of **2.4b** (black line), **4.7a** (red line), and **4.7b** (blue line) in CH_2Cl_2.

4.4.4 Electrochemistry of 4.7a, and 4.7b

Electrochemical studies of previously reported verdazyl diradicals **4.4a** and **4.4b** were hampered by their instability.[349] Two reversible waves were observed in their cyclic voltammograms, and described as two-electron processes. However, the authors did not indicate how they distinguished between two closely related one electron processes, and one two electron process.[349] In order to assess the nature of each electrochemical transition cyclic voltammetry studies were carried out for **4.7a**, and **4.7b** as well as Osteryoung square wave voltammetry (OSWV).

The cyclic voltammograms of **4.7a**, **4.7b**, and monoverdazyl **2.4b** are presented in Figure 4.6. The electrochemical features of the two diradicals are nearly identical to one another; both species can be reversibly oxidized to dications and reduced to dianions. The diradicals have slightly higher oxidation and reduction potentials than **2.4b**,

indicating that the verdazyl moiety is slightly electron withdrawing as a substituent. The similarities in the CVs of **4.7a** and **4.7b** also indicate that the substituent effects are inductive, as the different substitution patterns do not vary significantly. The CV and OSWV traces for **4.7a** and **4.7b** clearly have two distinguishable one-electron reduction processes while the oxidation waves appear to be made up of two overlapping one-electron processes based on the width and height of the peak heights compared to that of equimolar octamethylferrocene (Me_8Fc) shown in Figure 4.7.

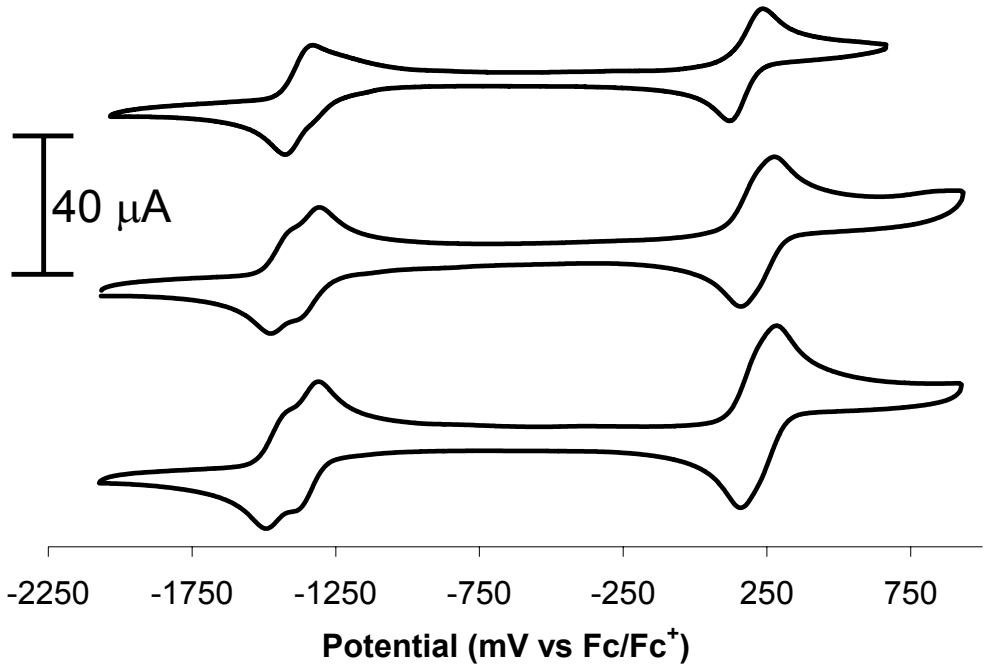

Figure 4.6. Cyclic voltammograms of **2.4b** (top), **4.7a** (middle), and **4.7b** (bottom) in CH_3CN containing 0.1 M $Bu_4N^+BF_4^-$ (electrolyte). Scan rate 250 mV/s.

Table 4.2. Electrochemical properties of **2.4b**, **4.7a**, and **4.7b** reported in V vs. Fc/Fc^+.

Compound	$E_{ox}°$	$E_{red1}°$	$E_{red2}°$
2.4b	+0.18	-1.38	-
4.7a	+0.22	-1.34	-1.44
4.7b	+0.22	-1.35	-1.45

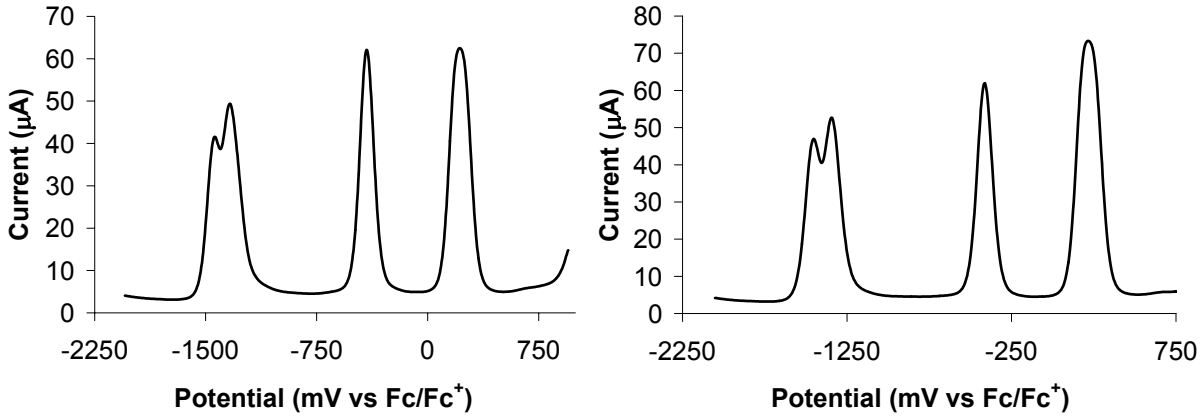

Figure 4.7. OSWV of **4.7a** (left) and **4.7b** (right) in CH_3CN containing 0.1 M $Bu_4N^+BF_4^-$ (electrolyte). Scan rate 250 mV/s. The wave at -410 mV is due to Me_8Fc/Me_8Fc^+ internal reference.

4.4.5 EPR studies of 4.7a and 4.7b

The low temperature EPR spectra of diradicals **4.7a** and **4.7b** are presented in Figures 4.8 and 4.9 respectively. Both spectra are consistent with randomly oriented triplets. Although simulation of the spectra did not reproduce the peak intensities well, the position of the peaks could be well reproduced, which allows for determination of zero field splitting (ZFS) parameters. The distance between the outer peaks is 2D, while the distance between the innermost peaks is D + 3E (where D and E are zero field splitting parameters).[354] Simulation of the spectra yielded g = 2.0049, $|D/hc|$ = 0.00210 cm^{-1}, and $|E/hc|$ = 0.000047 cm^{-1} for **4.7a** and g = 2.0056, $|D/hc|$ = 0.00348 cm^{-1}, and $|E/hc|$ = 0.000116 cm^{-1} for **4.7b**. Zero field splitting parameter D is inversely proportional to the cube of the distance between unpaired electrons, while E is related to the molecular symmetry of a diradical.[354] To this accord the smaller value of D for **4.7a** relative to **4.7b** can be rationalized as the distance between unpaired electrons is larger for a *para*-benzene spacer than a *meta*-benzene spacer.

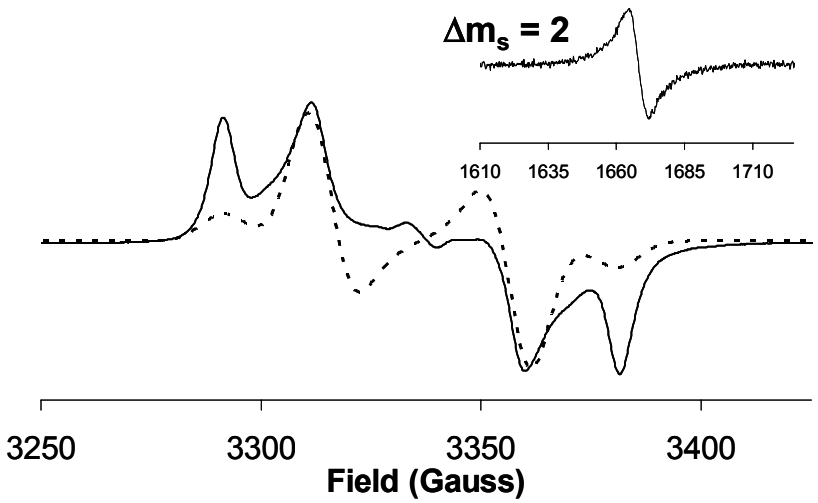

Figure 4.8. X-band EPR spectrum of **4.7a** (black line), simulation (dashed line), and half-field signal (inset) in degassed toluene at 77 K.

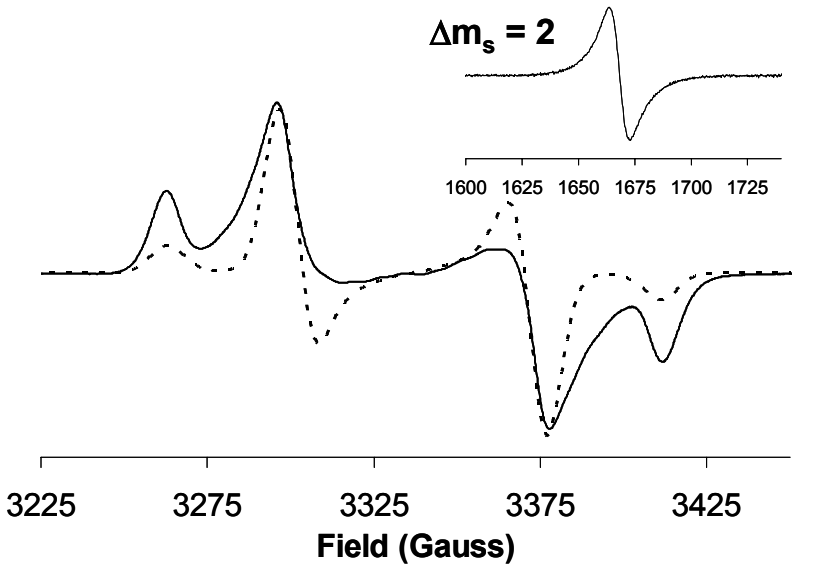

Figure 4.9. X-band EPR spectrum of **4.7b** (black line), simulation (dashed line), and half-field signal (inset) in degassed toluene at 77 K.

The $\Delta m_s = 2$ transitions arising due to the presence of the triplet state for both diradicals are shown as insets in Figures 4.13 and 4.14 respectively. The triplet signal, found at half the field of the randomly oriented triplet signal is generally small as the transition between $m_s = -1$ and $m_s = +1$ is formally forbidden, violating the $\Delta m_s = \pm 1$

selection rule governing transitions between spin states (Figure 4.10). The spectrum of **4.7a** has a lower signal to noise ratio as it possesses a singlet ground state (see below).

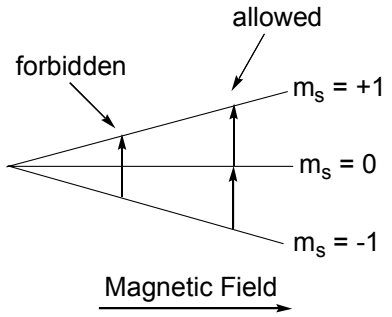

Figure 4.10. "EPR active" transitions.

Variable-temperature EPR data was collected for **4.7a** and **4.7b** in frozen toluene solution by monitoring the intensity of the $\Delta m_s = 2$ signal intensity. A plot of the signal intensity against inverse temperature (Curie Plot) allows for quantitative analysis of the singlet-triplet gap in **4.7a** (Figure 4.11). The data was fit using a variation on the Bleaney-Bowers dimer model,[224, 354] where C is a normalization parameter to account for arbitrary intensity units (Equation 4.2).

$$I = \frac{C}{T}\frac{3[\exp(-J/RT)]}{1+3[\exp(-J/RT)]} \qquad (4.2)$$

The best fit yields J = -30.0 ± 1.4 cm^{-1}, consistent with a ground state singlet containing a relatively weak magnetic interaction. Qualitatively, the fit is not of particularly high quality (R = 0.02), however it is consistent with other studies of this nature, where data collection is often hampered by non-uniformity in the toluene glass.[344] The variable-temperature data for **4.7b** (Figure 4.12) is consistent with a ferromagnetically coupled diradical (J > 0).[354]

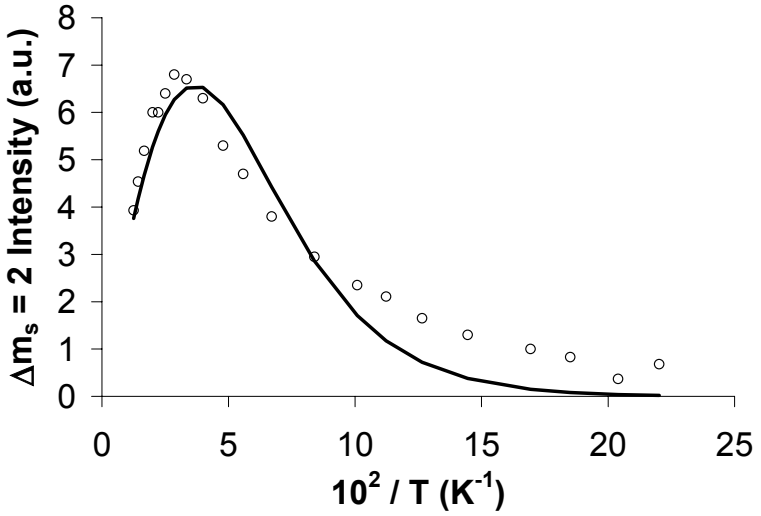

Figure 4.11. Curie plot for **4.7a** (○), and calculated fit (black line).

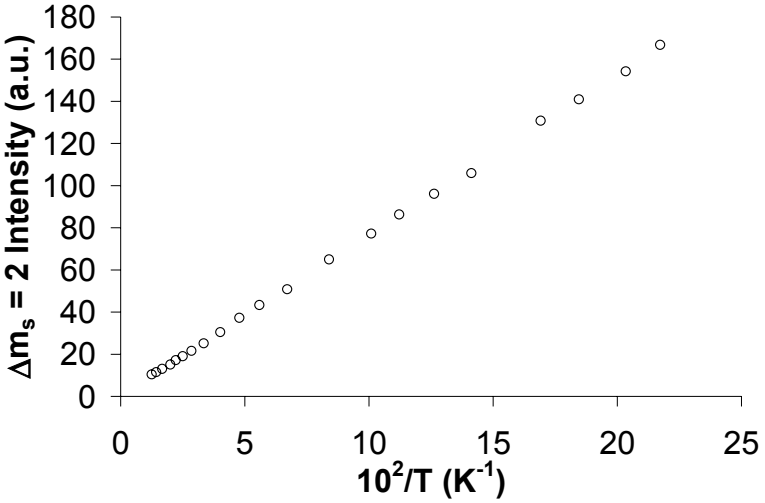

Figure 4.12. Curie plot of the $\Delta m_s = 2$ signal intensity for **4.7b**.

4.4.6 Crystal structures of benzene-bridged verdazyl diradicals

Diradical **4.7a** crystallizes in the *C2/c* space group, and has a crystallographic mirror plane passing through the central benzene ring (Figure 4.13). The *iso*-propyl groups in **4.7a** are oriented such that the methine protons are oriented *syn* to the carbonyl group, consistent with other 1,5-di-*iso*-propyl-6-oxoverdazyls. The two verdazyl rings are twisted by 27.5º relative to the benzene spacer. The bond lengths within the verdazyl

skeleton do not support any quinoidal contributions to the electronic structure, as observed in **4.9**, which is best represented as the closed shell structure **4.9'**.[355] The lack of quinoidal contributions in **4.7a** can be rationalized on the basis that, unlike compound **4.9**, there are no sites of primary spin density in the π-SOMO directly bound to the benzene spacer in **4.7a** (see Figure 4.4).

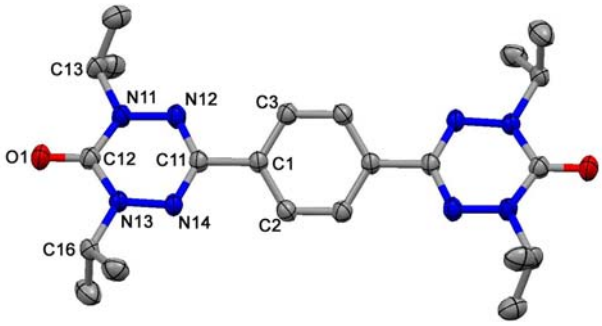

Figure 4.13. Molecular structure of **4.7a**. Thermal ellipsoids shown at 50% probability level. Hydrogen atoms removed for clarity.

Table 4.3. Selected bond lengths (Å) and angles (deg) for **4.7a**.

Atoms	**4.7a**	Atoms	**4.7a**
N11-N12	1.368(3)	N14-C11-N12	127.0(2)
N13-N14	1.365(3)	C11-N12-N11	114.9(2)
C11-N12	1.329(4)	N12-N11-C12	124.4(2)
C11-N14	1.330(4)	C12-N13-N14	124.0(2)
C12-N11	1.371(4)	N13-N14-C11	115.2(2)
C12-N13	1.378(4)		
C12-O1	1.222(3)		

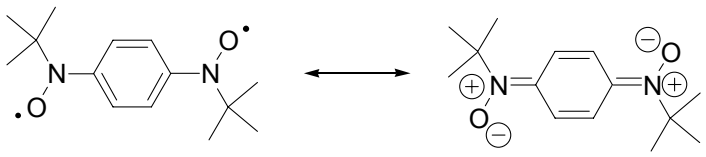

4.9 **4.9'**

Diradical **4.7b** crystallizes in the *I2/a* space group, with each verdazyl ring slightly twisted relative to the benzene ring (Figure 4.14). The radical attached to C1 is twisted by 15.3º while the radical attached to C3 is twisted by 6.0º. The bond lengths and

angles of each verdazyl ring are typical, and the possibility of quinoidal contributions in **4.7b** is precluded by cross conjugation associated with the *meta*-substitution pattern.

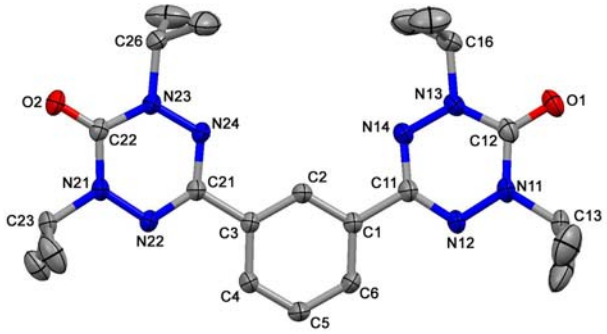

Figure 4.14. Molecular structure of **4.7b**. Thermal ellipsoids shown at 50% probability level. Hydrogen atoms removed for clarity.

Table 4.4. Selected bond lengths (Å) and angles (deg) for **4.7b**.

Atoms	**4.7b**	Atoms	**4.7b**
C11-N14	1.3276(14)	N12-C11-N14	127.06(13)
N14-N13	1.3659(13)	C11-N14-N13	115.05(12)
N13-C12	1.3770(19)	N14-N13-C12	124.53(12)
C12-N11	1.376(2)	N13-C12-N11	113.98(12)
N11-N12	1.3705(16)	C12-N11-N12	124.35(12)
N12-C11	1.3313(18)	N11-N12-C11	114.91(12)
C12-O1	1.2229(17)	N22-C21-N24	127.10(12)
C21-N24	1.3288(18)	C21-N24-N23	114.93(11)
N24-N23	1.3626(16)	N24-N23-C22	124.76(12)
N23-C22	1.3777(18)	N23-C22-N21	113.65(11)
C22-N21	1.3793(18)	C22-N21-N22	124.51(11)
N21-N22	1.3662(15)	N21-N22-C21	114.96(11)
N22-C21	1.3276(17)		
C22-O2	1.2176(12)		

The crystal packing of **4.7b** consists of diradical units interacting in a side-on fashion as linear chains in the *a*-*c* plane. Two separate sets of interactions are observed in Figure 4.15, each having implications on intermolecular magnetic coupling.

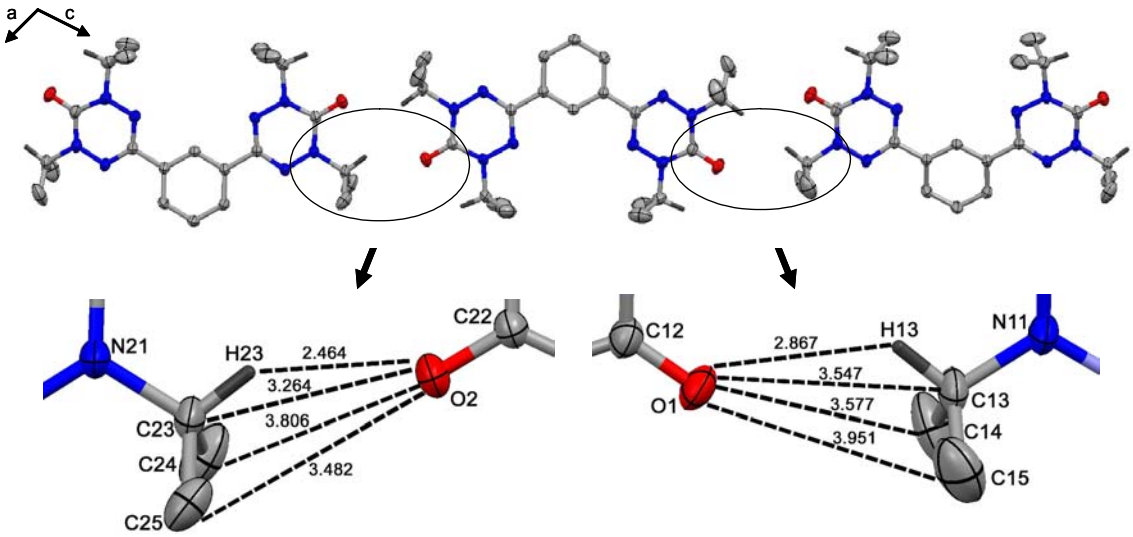

Figure 4.15. Intermolecular interactions in **4.7b**.

4.4.7 Magnetic properties of 4.7a and 4.7b

The magnetic susceptibilities of crystalline samples of **4.7a** and **4.7b** were recorded between 2 and 300 K. The χT vs. T plot for **4.7a** (Figure 4.16) has a value of 0.733 emu•K•mol^{-1}, slightly less than the value expected for two non-interacting unpaired electrons (0.750 emu•K•mol^{-1}). The shape of the plot is indicative of weak antiferromagnetic interactions as it gradually approaches a value of 0 emu•K•mol^{-1} as the temperature approaches 2 K. The susceptibility of **4.7a** (Figure 4.16) increases as the temperature is lowered to a maximum value of 0.014 emu•mol^{-1} at 26 K. Further cooling results in a rapid decrease in χ, until at cryogenic temperatures a small upturn is observed due to a small amount of paramagnetic impurity. The data was modeled using the Bleaney-Bowers dimer model (**H** = -J**S**$_1$·**S**$_2$) (Equation 4.3).[224, 330]

$$\chi = \frac{2Ng^2\beta^2}{kT[3+\exp(-J/kT)]} \qquad (4.3)$$

It was necessary to add a Curie term to Equation 4.3 in order to account for paramagnetic impurities, yielding Equation 4.4.[224]

$$\chi = \rho \frac{2Ng^2\beta^2}{kT[3+\exp(-J/kT)]} + (1-\rho)\frac{Ng^2\beta^2}{3k}\frac{S(S+1)}{T} \qquad (4.4)$$

Fitting the data with fixed g = 2.00 yields ρ = 0.99, and J = -29.73 ± 0.03 cm^{-1} with an agreement factor R = 0.0001. These results are consistent with a weakly antiferromagnetically coupled diradical. The magnitude of the intramolecular coupling is comparable to that seen in other 1,4-substituted diradicals.[356]

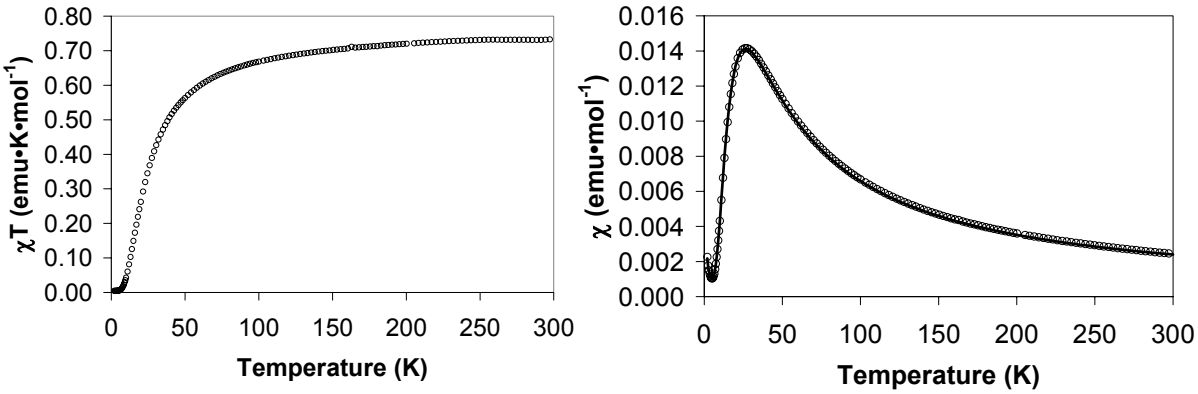

Figure 4.16. Magnetic properties of **4.7a**. χT vs. T (left) and χ vs. T (right). Experimental data (○) and data fit (black line).

The magnetic properties of **4.7b** are shown in Figure 4.17 as a χT vs. T plot. The room temperature value of 0.832 emu•K•mol^{-1} is higher than the expected value for two unpaired electrons (0.750 emu•K•mol^{-1}), consistent with ferromagnetic coupling. As the temperature decreases, the χT value reaches a maximum at 1.44 emu•K•mol^{-1} at 9 K before decreasing again at cryogenic temperatures. The maximum value is higher than the maximum value for two ferromagnetically coupled spins (1.00 emu•K•mol^{-1}), indicating the presence of both intra- and intermolecular ferromagnetic interactions. This behaviour is consistent with the intermolecular contacts observed between *iso*-propyl

groups previously shown to possess significant spin density, giving rise to additional ferromagnetic interactions (see Figure 4.15).

Complex systems containing multiple magnetic interactions such as this are difficult (sometimes impossible) to model. For these reasons a spin-dilution approach was employed. Diradical **4.7b** was suspended in polyvinyl chloride (PVC) film (~10 wt % of diradical) by slow evaporation of a dichloromethane solution of PVC and diradical. The dilution is expected to suppress the intermolecular contacts, allowing for the intramolecular interaction between diradicals to be considered exclusively.[340] The magnetic data for the diluted sample of **4.7b** (Figure 4.17) has a maximum χT value of 0.82 emu•K•mol^{-1} at 17 K. The decrease at cryogenic temperatures is consistent with intermolecular antiferromagnetic coupling, implying aggregation of the diradicals in the PVC medium. Although intermolecular interactions still exist, the ferromagnetic interactions complicating the initial data set have been attenuated. The Bleaney-Bowers model with a mean-field approximation[357] added to account for unspecified intermolecular interactions (Equation 4.5) was used to model the magnetic data where χ is taken from equation 4.4. In the mean field approximation the intermolecular interactions are described by 2zJ' where z is the number of molecules involved in the interaction, and J' is the molecular exchange parameter of the interactions.

$$\chi' = \rho \frac{\chi}{1 - (2zJ'/Ng^2\beta^2)\chi} \qquad (4.5)$$

Data fitting with g = 2.00 fixed gave $\rho = 0.97$, J = 19.3 ± 1.7 cm^{-1}, and zJ' = -1.01 ± 0.03 cm^{-1}. The agreement factor for this data was not good (R = 0.02), reflecting the differences between fit and experimental data associated with an overcorrection for the

diamagnetism of the PVC film. The magnetic studies reported confirm weakly ferromagnetically coupled spins in **4.7b**, and the magnitude of the coupling is consistent with other diradicals bridged by *meta*-benzene spacers.[356]

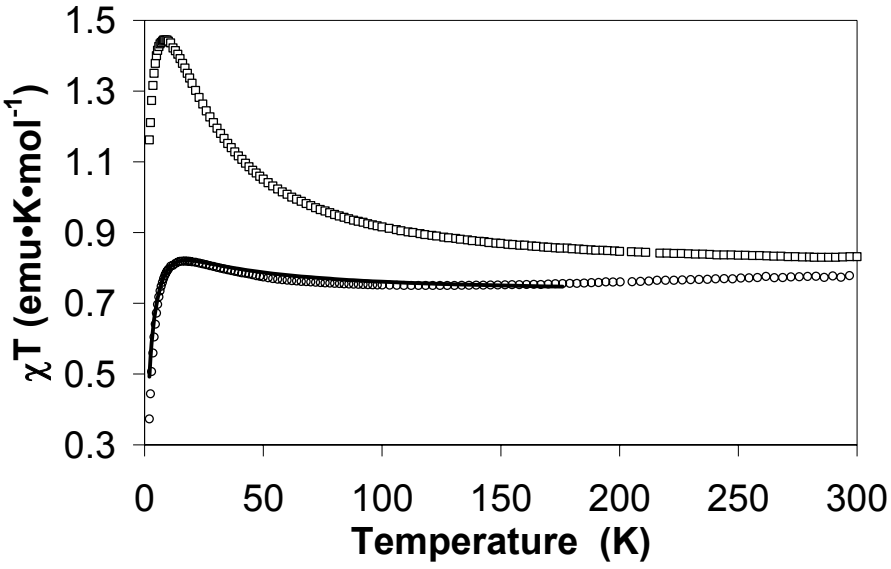

Figure 4.17. Magnetic properties of **4.7b**. χT vs. T (□), diluted in PVC (○), and data fit (black line).

4.5 Copper (II)-radical complexes

Copper (II) is often incorporated into model systems for molecule-based magnets as its simple salts are readily available, and copper (II) possesses one unpaired electron, confined to the d_{x2-y2} or d_{z2} orbitals in most coordination geometries. It has been widely shown that copper (II) complexes of nitroxides and nitronyl nitroxides (e.g., **4.10**,[358] **4.11**,[359] and **4.12**[360]) exhibit ferromagnetic metal-radical coupling.[358-364]

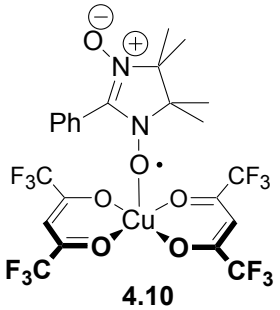

4.10

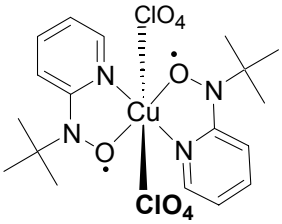

4.11

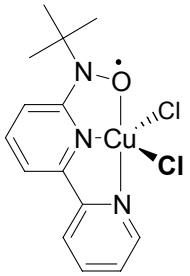

4.12

The origin of the ferromagnetic coupling in these and other systems is rationalized on the basis of orbital orthogonality arguments.[224] When net overlap between magnetic orbitals is observed, the result is generally antiferromagnetic coupling. When net overlap between magnetic orbitals is not observed ferromagnetic coupling is generally observed. The magnitude of the coupling in each case is highly dependent on spatial parameters, i.e., distances and angles that describe the interaction of magnetic orbitals. An orbital representation of the interactions between magnetic orbitals in transition metal ions and a simplified π-SOMO (p-orbital) are shown in Figure 4.18. As previously mentioned, the lack of orbital overlap observed when the magnetic interaction involves the $d_{x^2-y^2}$ or d_{z^2} orbital allows for the prediction of ferromagnetic coupling, while the overlap observed when d_{xy}, d_{xz}, or d_{yz} orbitals are involved should give rise to antiferromagnetic coupling.

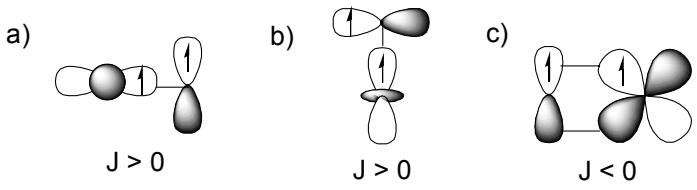

Figure 4.18. Simplified magnetic orbital interactions: (a) $d_{x^2-y^2}$ and π-SOMO, (b) d_{z^2} and π-SOMO, and (c) d_{xy}, d_{xz}, or d_{yz} and π-SOMO.

4.6 Synthesis and characterization of copper (II)-verdazyl complexes

4.6.1 Synthesis of copper (II)-verdazyl complexes

6-Oxoverdazyl radicals have been shown to coordinate to a variety of transition metal ions when the substituent at the 3-position contains a heteroatom allowing for metal chelation.[147, 166, 167, 169, 170, 352, 365-367] Verdazyl radicals have previously been shown to couple strongly with octahedral nickel(II) ions in a ferromagnetic fashion.[166, 167, 170] The ferromagnetic coupling in nickel(II) verdazyl complexes and the established trends in copper (II) nitroxide complexes prompted the synthesis of a number of copper (II) complexes of verdazyls as models for molecule-based magnets.

Reaction of readily available hydrated copper (II) chloride, or 1,1,1,6,6,6-hexafluoroacetylacetonato (hfac) salts with one equivalent of chelating radical afford the following complexes (Scheme 4.2).

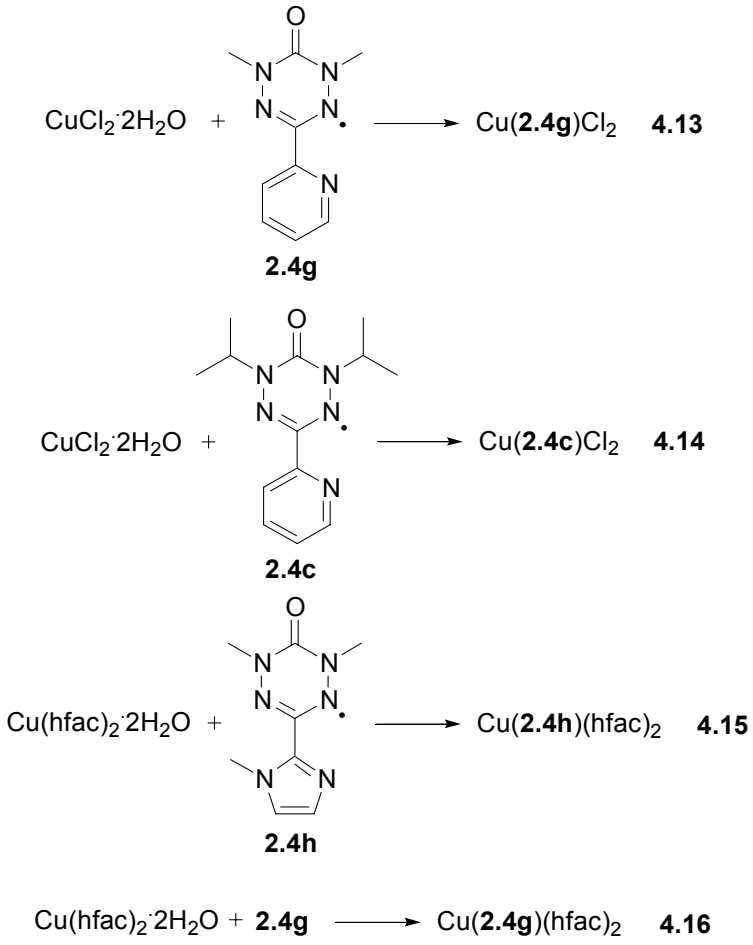

Scheme 4.2. Synthesis of copper (II)-verdazyl complexes.

4.6.2 Structure and magnetism of copper (II)-verdazyl complexes 4.13 and 4.14

The crystal structure of **4.13** is presented in Figure 4.19. The complex crystallizes in the *Pbca* space group, and has an ambiguous geometry at the copper center. The angle between the Cl1-Cu-Cl2 and the N2-Cu-N10 planes is 47.80°, between that expected for square planar (0˚) and tetrahedral (90˚) geometries. The copper atom lies in the same plane as the pyridine, but is 0.84 Å above the plane of the verdazyl. The verdazyl ring is twisted 19.00° with respect to the pyridine ring, and the C1-N4 (1.306 Å) and C1-N2 (1.358 Å) are substantially different. The distortion of the ligand in **4.13** has not been observed previously in complexes of **2.4g** which are essentially planar and symmetric

with respect to the ligand, i.e., the C1-N2 and C1-N4 bond lengths are equivalent within experimental error.[169, 170]

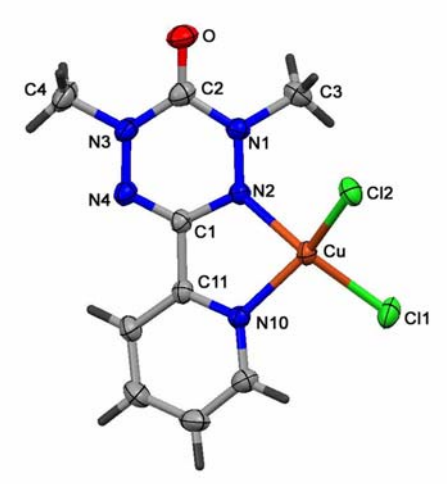

Figure 4.19. Molecular structure of **4.13**. Thermal ellipsoids shown at 50% probability level.

Table 4.5. Selected bond lengths (Å) and angles (deg) for **4.13**.

Atoms	**4.13**	Atoms	**4.13**
Cu-Cl1	2.2234(5)	Cl1-Cu-Cl2	102.02(2)
Cu-Cl2	2.1965(5)	N2-Cu-N10	81.34(6)
Cu-N2	1.9992(14)	N2-N1-C2	124.09(15)
Cu-N10	1.9921(15)	Cu-N2-C1	111.77(11)
O1-C2	1.210(2)	N1-N2-C1	114.34(14)
N1-N2	1.349(2)	N4-N3-C2	124.11(15)
N1-C2	1.385(2)	N3-N4-C1	115.90(15)
N2-C1	1.385(2)	Cu-N10-C11	114.56(12)
N3-N4	1.342(2)	N2-C1-N4	126.96(16)
N3-C2	1.379(3)		
N4-C1	1.306(2)		
Cu--N2’	3.889		

Molecules of **4.13** weakly associate in the solid-state (Figure 4.20). The intermolecular Cu-N2 contacts of 3.89 Å are slightly longer than the sum of the van der Waals distances for Cu and N. This relatively ‘long’ intermolecular distance is not expected to give rise to significant magnetic coupling as the overlap between the magnetic orbitals on Cu and N2 will be minimal.

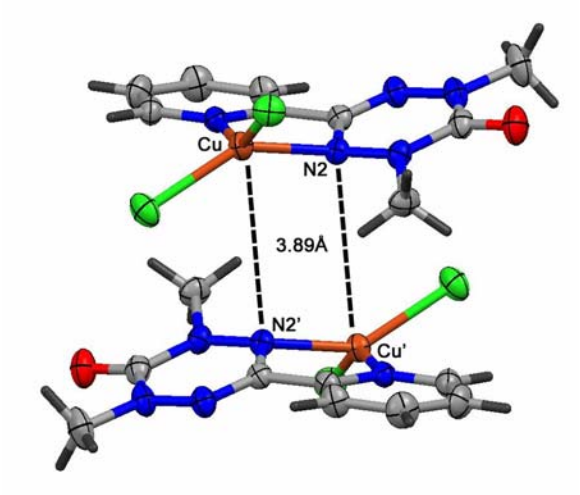

Figure 4.20. Intermolecular contacts in the structure of **4.13**.

The magnetic properties of **4.13** are represented as both χT vs. T and χ vs. T plots in Figure 4.21. The χT product has a maximum value of 0.34 emu•K•mol^{-1}, significantly lower then the spin only (0.750 emu•K•mol^{-1}). The room temperature value of χT and the observed decrease in χT with decreased temperature are both consistent with strong antiferromagnetic coupling. The χT vs. T data was modeled with the Bleaney-Bowers model ($\mathbf{H} = -J\mathbf{S}_{Cu}\cdot\mathbf{S}_{rad}$), incorporating a mean field term to account for intermolecular interactions as well as a Curie-Weiss term to account for S = ½ impurity (Equation 4.6).[224, 330, 357] Where χ is the Bleaney-Bowers dimer model (equation 4.3).

$$\chi' = \rho\frac{\chi}{1-(2zJ'/Ng^2\beta^2)\chi} + (1-\rho)\frac{Ng^2\beta^2}{3k(T-\theta)}(S(S+1)) \qquad (4.6)$$

The best fit with g = 2.1 fixed, looks good qualitatively (black line, Figure 4.21), yielding ρ = 0.97, J = -204.0 ± 0.9 cm^{-1}, J' = -130.2 ± 1.0 cm^{-1}, θ = -2.3 K, and R = 0.011. However, within the magnetism community, there exists an unwritten rule regarding the mean field approximation. It is assumed that the approximation is used to model intermolecular interactions where the value of J' is less then 10 % of J. The red line

shown in Figure 4.21 represents the line generated by a similar system where J = -200 cm^{-1} and J' = -20 cm^{-1}. Clearly, the fit of the χT data cannot be used for more than a qualitative picture of strong antiferromagnetic coupling. The lack of curvature in the χT vs. T plot may play a role in the data fitting results, as fits of this type benefit from the presence of a well-defined maximum in the data.

The χ vs. T data was also fit using the Bleaney-Bowers dimer model (**H** = $-J\mathbf{S}_{Cu}\cdot\mathbf{S}_{rad}$) with a Curie term (equation 4.4). The modest fit obtained by modeling of the data with equation 4.5 with g = 2.10 fixed gave ρ = 0.91, and J = -250.0 ± 6.9 cm^{-1} with a goodness of fit value of R = 0.14. Although the data fit is modest, the values obtained are consistent with strong antiferromagnetic coupling. The coupling is attributed to the strong overlap between Cu and N2. The p-orbital on N2 appears to point towards the Cu center as a result of ligand distortion (see Figure 4.20), allowing magnetic orbitals to overlap, resulting in strong antiferromagnetic coupling. The observed properties are consistent with copper (II) complexes of nitroxides where equatorially bound nitroxides lead to strong antiferromagnetic coupling.[48]

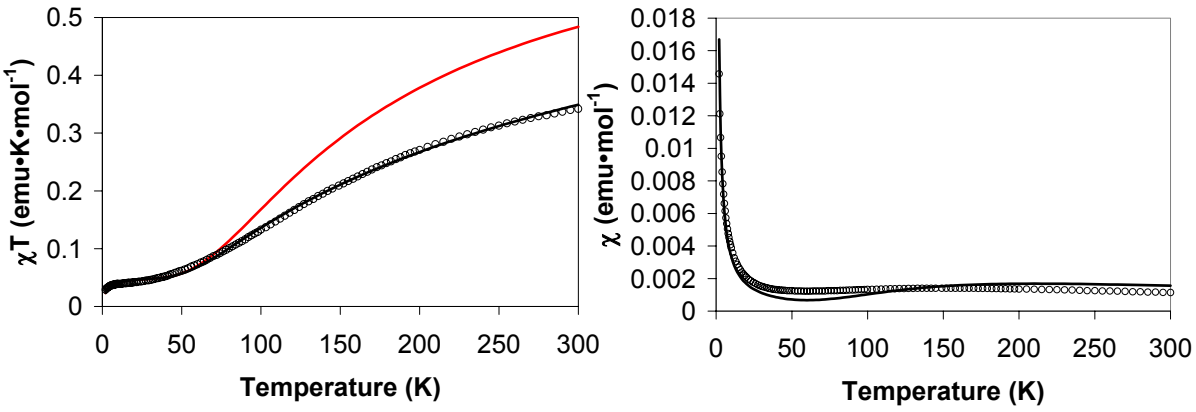

Figure 4.21. Magnetic properties of **4.13**. χT vs. T (left) and χ vs. T (right). Experimental data (○), data fits (black lines), and theoretical fit (red line).

The interpretation of the behavior observed in **4.13** is further corroborated by the properties of complex **4.14**. The crystal structure of **4.14** is shown in Figure 4.22. The complex crystallizes as a chloride bridged binuclear structure related by an inversion center, and has a distorted square pyramidal geometry around each copper (II) ion. The structural features related to the metal-radical interactions are quite similar to those observed in **4.13**: the Cu atom lies 1.11 Å out of the plane of the verdazyl, the verdazyl and pyridine rings are twisted by 21.5°, and there is substantial asymmetry in the C1-N2 (1.351 Å) and C1-N4 (1.313 Å) bonds. The *iso*-propyl groups are oriented with the methine protons *anti* to the carbonyl moiety, opposite to what was observed for free verdazyl **2.4c**.

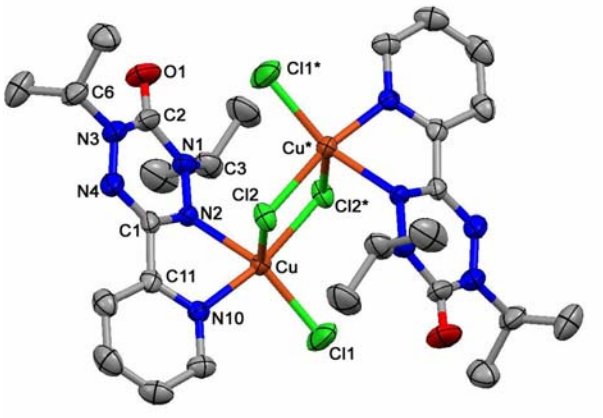

Figure 4.22. Molecular structure of **4.14**. Thermal ellipsoids shown at 50% probability level. Hydrogen atoms omitted for clarity.

Table 4.6. Selected bond lengths (Å) and angles (deg) for **4.14**.

Atoms	**4.14**	Atoms	**4.14**
Cu-Cl1	2.2136(13)	Cl1-CuCl2	96.46(5)
Cu-Cl2	2.2140(11)	Cl1-Cu-N10	95.27(10)
Cu-Cl2’	2.933(13)	Cl2-Cu-N2	94.63(9)
Cu-N2	2.058(3)	Cl2-Cu-Cl2’	86.42(9)
Cu-N10	2.009(3)	N2-Cu-N10	78.98(13)
O1-C2	1.219(6)	N2-N1-C2	121.9(4)
N1-N2	1.355(5)	Cu-N2-N1	128.8(3)
N1-C2	1.402(6)	N1-N2-C1	115.2(3)
N2-C1	1.351(5)	N4-N3-C2	123.2(4)
N3-N4	1.348(6)	N3-N4-C1	115.4(4)
N3-C2	1.375(8)		
N4-C1	1.313(5)		

The magnetic data for **4.14** is shown as a χ vs. T plot in Figure 4.23. Copper (II) complex **4.14** is diamagnetic at room temperature, but becomes weakly paramagnetic at cryogenic temperatures due to the presence of paramagnetic impurities. The strong antiferromagnetic copper (II)-verdazyl coupling occurs as a result of orbital overlap associated with the Cu-N2 bond, which involves the π-orbital on N2 pointing towards the Cu as observed in **4.13**. Magnetostructural studies of a wide range of bimetallic copper (II) complexes containing a Cu_2Cl_2 core have led to an understanding of the relationship between the exchange interaction between copper (II) centers and structural parameters. Specifically the ratio θ/r, where θ represents the Cu-Cl-Cu angle and r is the longer of the two Cu-Cl bonds has been correlated to the nature of the exchange interaction.[368, 369] For **4.14**, the ratio is 31.9°/Å which, when compared to existing compounds, leads to a predicted exchange interaction near zero or very weakly antiferromagnetic.[368, 369] The diamagnetism in **4.14** must therefore arise from very strong antiferromagnetic coupling between each of the verdazyl radical-copper (II) units.

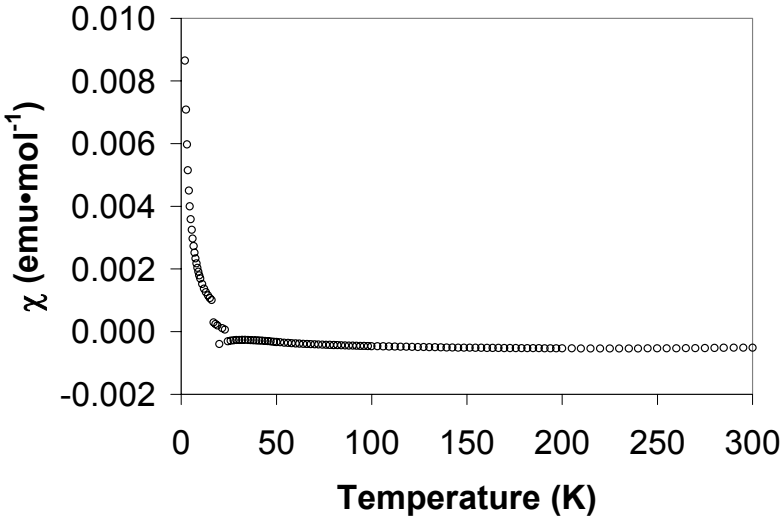

Figure 4.23. Magnetic properties of **4.14** (χ vs. T). The discontinuity in the data between 10-30 K is due to instrumental error associated with the crossover from diamagnetic to paramagnetic.

4.6.3 Structure and magnetism of copper (II)-verdazyl complexes 4.15 and 4.16

The molecular structure of copper (II) complex **4.15** is presented in Figure 4.24. **4.15** crystallizes in the $P\bar{1}$ space group, and has a copper (II) ion residing in an octahedral ligand field exhibiting a significant Jahn-Tellar distortion (Cu-N2 = 2.544 Å and Cu-O22 = 2.234 Å (axial), Cu-N11 1.961 Å and Cu-O21 1.971 Å (equatorial)). The verdazyl ligand, which occupies one of the axial coordination sites is essentially planar, with a torsion angle of 4.8° between the verdazyl and imidazolyl rings, and the bond lengths and angles within the verdazyl skeleton are close to that of uncoordinated verdazyls, consistent with other complexes where structure effects of coordination are minimal.[166, 167, 169]

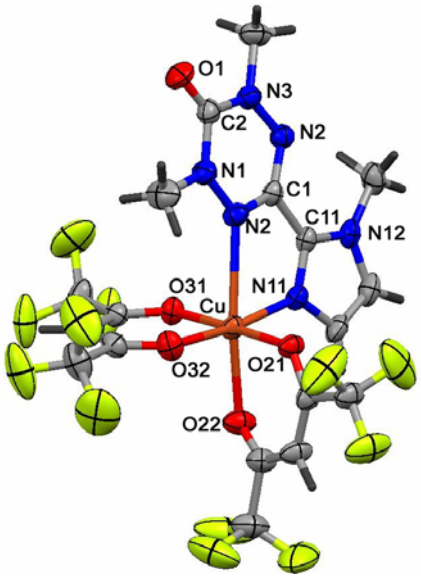

Figure 4.24. Molecular structure of **4.15**. Thermal ellipsoids shown at 50% probability level.

Table 4.7. Selected bond lengths (Å) and angles (deg) for **4.15**.

Atoms	**4.15**	Atoms	**4.15**
Cu-O21	1.971(2)	O21-Cu-O22	88.65(9)
Cu-O22	2.234(2)	O31-Cu-O32	91.04(9)
Cu-O31	1.985(2)	N2-Cu-N11	71.92(10)
Cu-O32	1.948(2)	N1-N2-C1	115.0(3)
Cu-N2	2.544(3)	N3-N4-C1	114.0(3)
Cu-N11	1.961(3)	Cu-N11-C11	124.1(2)
N1-N2	1.361(4)	N2-C1-N4	127.8(3)
N2-C1	1.327(4)	N2-N1-C2	124.1(3)
N3-N4	1.359(4)	N4-N3-C2	125.3(3)
N4-C1	1.328(4)	N1-C2-N3	113.8(3)
N1-C2	1.381(4)		
N3-C2	1.376(4)		

The solid-state packing of **4.15** (Figure 4.25) contains close intermolecular contacts between verdazyls with an interplanar distance of 3.30 Å. The closest contacts between spin-bearing atoms are N1-N3’ and N3-N1’ (3.389 Å).

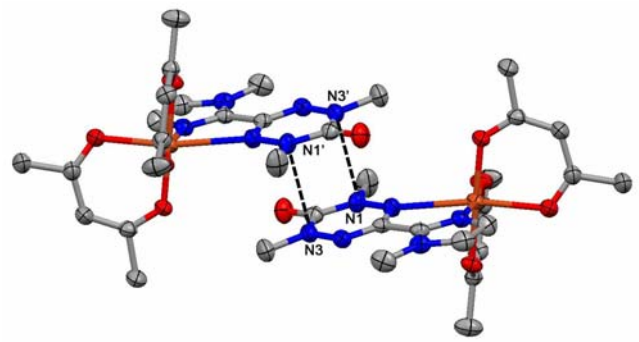

Figure 4.25. Intermolecular interactions in **4.15**.
Hydrogen and fluorine atoms omitted for clarity.

The variable temperature magnetic data of **4.15** is represented as a χT vs. T plot in Figure 4.29. The room temperature value of χT is 0.81 emu•K•mol^{-1}, which is slightly higher then the spin-only value of 0.750 emu•K•mol^{-1} due to the increased g-factor for copper (II) centers (~2.1) relative to organic radicals (~2.0). The value of χT remains relatively constant down to a temperature of 100 K below which it decreases rapidly before plateauing near 20 K at a value of roughly 0.5 emu•K•mol^{-1}. The value decreases further at cryogenic temperatures. The data was modeled using a four-spin system ($\mathbf{H} = -J_1\mathbf{S}_{rad1}\cdot\mathbf{S}_{rad2} - J_2(\mathbf{S}_{rad1}\cdot\mathbf{S}_{Cu1} + \mathbf{S}_{rad2}\cdot\mathbf{S}_{Cu2})$) to account for coupling between the copper centers and the radical ligands, as well as intermolecular radical-radical interactions (Figure 4.26).[370, 371]

$$S_{Cu1} \overset{J_2}{\text{——}} S_{rad1} \overset{J_1}{\text{——}} S_{rad2} \overset{J_2}{\text{——}} S_{Cu2}$$

Figure 4.26. Relevant magnetic exchange interactions in four spin model.

The model used for this system is presented in Equation 4.7. A Curie-Weiss term was included to account for S = ½ impurities. It should also be noted that the data has been processed assuming two spins per mole (one Cu-radical complex), and thus the first term of the equation has been multiplied by ½.

$$\chi = (\rho)\frac{Ng^2\beta^2}{2kT}\frac{A}{B} + (1-\rho)\frac{Ng^2\beta^2}{3k(T-\theta)}\big(S(S+1)\big) \qquad (4.7)$$

$$A = 10\exp(-E_1/kT) + 2\exp(-E_2/kT) + 2\exp(-E_3/kT) + 2\exp(-E_4/kT)$$

$$B = 5\exp(-E_1/kT) + 3[\exp(-E_2/kT) + \exp(-E_3/kT) + \exp(-E_4/kT)] + \exp(-E_5/kT) + \exp(-E_6/kT)$$

$$E_1 = -J_2 - J_1/2$$

$$E_2 = J_2 - J_1/2$$

$$E_3 = J_1/2 + (J_2^2 + J_1^2)^{1/2}$$

$$E_4 = J_1/2 - (J_2^2 + J_1^2)^{1/2}$$

$$E_5 = J_2 + J_1/2 + (4J_2^2 - 2J_2J_1 + J_1^2)^{1/2}$$

$$E_6 = J_2 + J_1/2 - (4J_2^2 - 2J_2J_1 + J_1^2)^{1/2}$$

The quantitative fit of the data in Figure 4.27 does not appear to be particularly good visually, however the qualitative trends were reproduced by the fit. From the model with g = 2.1 fixed we obtain ρ = 0.95, J_1 = -39.5 ± 1.2 cm^{-1}, J_2 = +6.0 ± 1.5 cm^{-1} and θ = +0.6 K with a goodness of fit value of R = 0.024. It is worth noting that the fit is relatively insensitive to the magnitude of the copper (II)-radical coupling. However, the magnitude of the copper (II)-radical coupling is consistent with weak ferromagnetic coupling associated with the long Cu-N2 bond length due to Jahn-Tellar distortions. The magnetic behavior of **4.15** is dominated by antiferromagnetic intermolecular interactions between π-stacked verdazyl radicals.

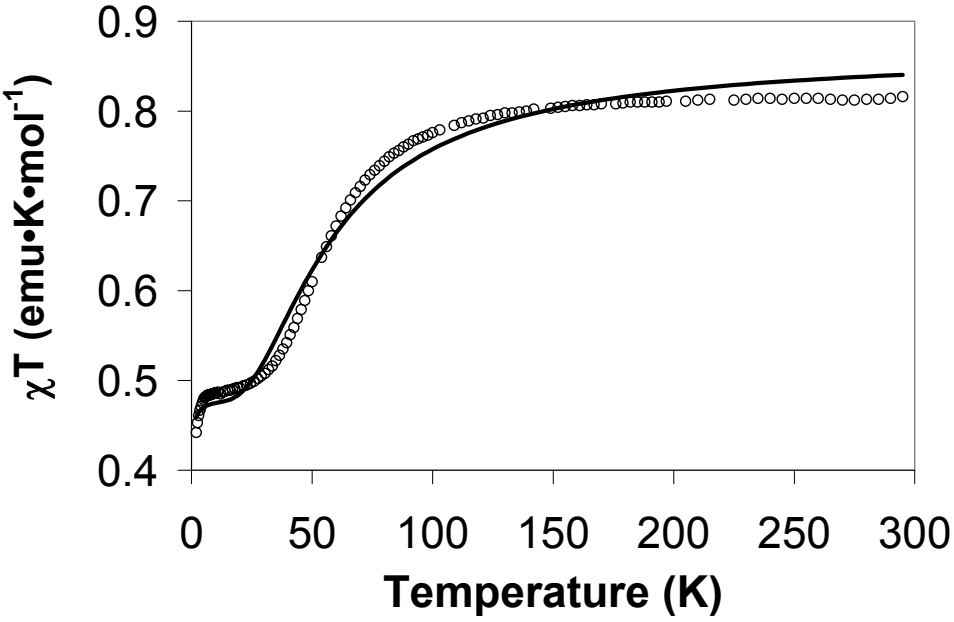

Figure 4.27. Molecular properties of **4.15**. χT vs. T (○) and data fit (black line).

Single crystals of **4.16** suitable for X-ray diffraction could not be obtained. The magnetic data for **4.16** is shown as both χT vs. T and χ^{-1} vs. T plots in Figure 4.28. The χT vs. T plot has a maximum value of 0.81 emu•K•mol^{-1}, consistent with g ~ 2.1. Below 100 K the value of χT decreases gradually, consistent with weak antiferromagnetic interactions. Equation 4.6 was used to fit the magnetic data with g = 2.1 fixed, yielding ρ = 0.99, J = 4.0 ± 0.5 cm^{-1}, 2zJ' = -8.0 ± 0.1 cm^{-1}, and θ = 1.5 K with a goodness of fit value of R = 0.0011. The small intramolecular coupling parameter obtained form the fit is consistent with an axially bound verdazyl radical in a Jahn-Tellar distorted octahedral field, and thus the coordination environment in **4.16** is assumed to be similar to that observed in **4.15**.

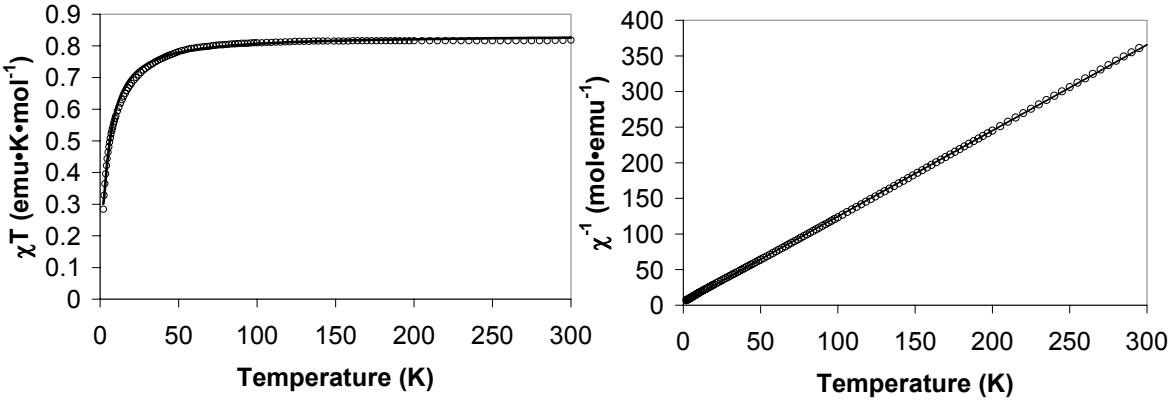

Figure 4.28. Magnetic properties of **4.16**. χT vs. T (left) and χ^{-1} vs. T (right). Experimental data (○) and data fit (black line).

As previously discussed J' is assumed to be less than 10 % of J. In this case, unless there are numerous molecules involved in the intermolecular interaction, the assumption is violated. Thus, the magnetic data qualitatively is consistent with weak or no ferromagnetic coupling between copper and radical, with the dominant features arising due to antiferromagnetic intermolecular interactions at low temperature. The magnitude of the interactions need only be considered as estimated values.

A second approach was taken to 'quantify' the magnetic properties of **4.16**. Ignoring intramolecular interactions allows the data to be fit to the Curie-Weiss law where intermolecular interactions are considered exclusively. Using equation 2.2, the χ^{-1} vs. T plot yields C = 0.83 emu•K•mol^{-1} and θ = -3.5 K with an R^2 value of 0.9999. The success of the Curie-Weiss equation in fitting the 1/χ vs. T data may suggest that the intramolecular copper (II)-verdazyl interaction is less significant than initially believed, and that intermolecular interactions alone account for the magnetic behavior observed in **4.15** and **4.16**. Both approaches to fitting the magnetic data allow for the conclusion that the copper (II)-radical coupling is very small, consistent with Jahn-Tellar distortion of the

Cu-N bond attached to the verdazyl. However, this interpretation follows the assumption that the verdazyl radical in **4.16** is bound to an axial coordination site, and the Cu-N2 bond is elongated by Jahn-Tellar distortion.

4.7 Summary

As a result of the instability of early examples, verdazyl diradicals have not received much attention compared to analogous nitroxide systems. Diradicals **4.7a** and **4.7b** have, for the first time, allowed for the quantitative and comprehensive study of the interactions between verdazyls through *para*- and *meta*-benzene spacers. The electronic spectra of diradicals **4.7a** and **4.7b** were similar to monoverdazyl **2.4b**. However, conjugation in **4.7a** caused slight red shifting of absorption maxima, a feature that was not observed in cross-conjugated diradical **4.7b**. The electrochemical properties of diradicals **4.7a** and **4.7b** showed little dependence on the topology of the organic spacer, although the CVs did reveal that their oxidation and reduction occurred via two separate one-electron processes, contradicting previous reports.[349] The antiferromagnetic coupling observed in **4.7a**, and ferromagnetic coupling in **4.7b** follow the predicted trends for diradicals of this type.[356]

The copper (II)-verdazyl complexes presented here have added to the 'database' of metal-radical systems. It was found that equatorially coordinated verdazyl radicals are strongly antiferromagnetically coupled to copper (II), while axially coordinated verdazyls are weakly ferromagnetically coupled to copper (II) due to Jahn-Tellar distortions lengthening the copper (II)-verdazyl bond. Copper (II) was chosen for these studies as the magnetostructural properties of envisioned complexes were anticipated to be relatively simple compared to other metal ions containing more than one unpaired

electron. In reality, the flexibility of the coordination geometry of copper (II) ions and the presence of significant Jahn-Tellar distortions caused the magnetostructural properties of the reported complexes to be quite complicated.

The magnetic properties of several spin-dimers based on verdazyl radicals have been modeled in this work, and served to highlight one of the fundamental arguments surrounding magnetochemistry; Should data fits match experimental values exactly, or should data fitting be used only to gain a qualitative picture of the magnetic coupling? Both approaches have been employed with emphasis placed on qualitative properties, i.e., the data fitting parameters were used to 'estimate' the magnitude of magnetic coupling interactions. Ultimately, the magnetic models used are not specific to each system, and, although convenient, their generalization limits their utility in reproducing magnetic properties.

4.8 Experimental

4.8.1 Synthesis and characterization

1,4-bis(1,5-di-*iso*-propyl-6-oxo-2,3,4,5-tetrazan-3-yl)benzene (4.8a). To a refluxing solution of **2.8a** (1.00 g, 4 mmol), sodium acetate (0.67 g, 8 mmol), and methanol (75 mL) was added terephthaldicarboxaldehyde (0.273 g, 2 mmol) in methanol (100 mL) dropwise over a period of 3 h. The solution was refluxed in air for a further 20 h at which time a pale yellow solution remained. The solvent was removed *in vacuo*, and the residue dissolved in dichloromethane (5 x 50 mL). The dichloromethane fractions were then washed with distilled water (3 x 100 mL), dried with magnesium sulphate, and concentrated *in vacuo* yielding a pale yellow solid. The solid was then triturated with a minimal amount of ethyl acetate, ground into a fine powder, and heated *in vacuo*

overnight at 90ºC affording **4.8a** as a white powder, yield (0.655 g, 73 %). Mp. 162-164^{o}C (dec.). ^{1}H NMR (300 MHz, d6-DMSO): δ 7.56 (s, 4H), 4.98 (d, 4H, ^{3}J = 11 Hz), 4.49 (sep, 4H, ^{3}J = 8 Hz), 4.34 (t, 2H, ^{3}J = 11 Hz), 1.05 (d, 12H, ^{3}J = 7 Hz), 1.03 (d, 12H, ^{3}J = 7 Hz). ^{13}C NMR (75 MHz, d6-DMSO): δ 153.5, 136.6, 126.7, 71.5, 46.8, 19.6, 18.4 ppm. FT-IR (KBr): 3245 (m), 1610 (s) υ(CO) cm^{-1}. MS (LSIMS): *m/z* 447 (MH^{+}, 100 %). Anal. Calcd for $C_{22}H_{38}N_{8}O_{2}$: C, 59.17; H, 8.58; N, 25.09. Found C, 59.26, H, 8.22; N, 24.86.

1,3-bis(1,5-di-*iso*-propyl-6-oxo-2,3-4,5-tetrazan-3-yl)benzene (4.8b). To a refluxing solution of **2.8a** (1.00 g, 4 mmol), sodium acetate (0.67 g, 8 mmol), and methanol (75 mL) was added isophthaldicarboxaldehyde (0.273 g, 2 mmol) in methanol (100 mL) dropwise over a period of 3 h. The solution was refluxed in air for a further 20 h at which time a pale yellow solution remained. The solvent was removed *in vacuo*, and the residue dissolved in dichloromethane (5 x 50 mL). The dichloromethane fractions were then washed with distilled water (3 x 100 mL), dried with magnesium sulphate, and concentrated *in vacuo* yielding a pale yellow solid. The solid was then triturated with a minimal amount of ethyl acetate, ground into a fine powder, and heated *in vacuo* overnight at 90ºC affording **4.8b** as a white powder, yield (0.857 g, 95 %). Mp. 180-182^{o}C (dec.). ^{1}H NMR (300 MHz, d6-DMSO): δ 7.77 (s, 1H), 7.55 (d, 2H, ^{3}J = 8 Hz), 7.42 (t, 1H, ^{3}J = 7 Hz), 5.01 (d, 4H, ^{3}J = 11 Hz), 4.49 (sep, 4H, ^{3}J = 8 Hz), 4.39 (t, 2H, ^{3}J = 11 Hz), 1.06 (d, 12H, ^{3}J = 7 Hz), 1.04 (d, 12H, ^{3}J = 7 Hz). ^{13}C NMR (75 MHz, d6-DMSO): δ 153.5, 136.7, 128.3, 126.4, 125.5, 71.5, 46.7, 19.6, 18.5 ppm. FT-IR (KBr): 3245 (m), 1606 (s) υ(CO) cm^{-1}. MS (LSIMS): *m/z* 447 ($M+H^{+}$, 100 %). Anal. Calcd for $C_{22}H_{38}N_{8}O_{2}$: C, 59.17; H, 8.58; N, 25.09. Found C, 59.09; H, 8.42; N, 24.83.

1,4-bis(1,5-di-*iso*-propyl-6-oxo-3-verdazyl)benzene (4.7a). A solution of **4.8a** (0.300 g, 0.67 mmol), benzoquinone (0.220 g, 2.0 mmol), and toluene (20 mL) was allowed to reflux for 30 min in air before being taken to dryness *in vacuo*. The residue was purified via column chromatography (5 cm x 20 cm neutral alumina, dichloromethane) before it was once again taken to dryness. The purified residue was recrystallized via slow cooling of a saturated ethyl acetate solution affording **4.7a** as well formed orange-red crystals suitable for X-ray crystallography, yield (0.194 g, 66 %). Mp. 160-162^{o}C. FT-IR (KBr): 1678 (s) υ(CO) cm^{-1}. UV-vis (CH_2Cl_2): λ_{max} 280 nm (ε = 46300 L•mol-1•cm^{-1}), 417 nm (ε = 3090 L•mol^{-1}•cm^{-1}), 485 nm (ε = 1000 L•mol^{-1}•cm^{-1}). MS (EI): *m/z* 440 (M^+, 100 %). Anal. Calcd for $C_{22}H_{32}N_8O_2$: C, 59.98; H, 7.32; N, 25.44. Found C, 60.00; H, 7.10; N, 25.51.

1,3-bis(1,5-di-*iso*-propyl-6-oxo-3-verdazyl)benzene (4.7b). A solution of **4.8b** (0.300 g, 0.67 mmol), benzoquinone (0.220 g, 2.0 mmol), and toluene (20 mL) was allowed to reflux for 30 min in air before being taken to dryness *in vacuo*. The residue was purified via column chromatography (5 cm x 20 cm neutral alumina, dichloromethane) before it was once again taken to dryness. The purified residue was recrystallized via slow cooling of a saturated ethyl acetate solution affording **4.7b** as well formed orange-red crystals suitable for X-ray crystallography, yield (0.184 g, 62 %). Mp. 134-136^{o}C (dec.). FT-IR (KBr): 1675 (s) υ(CO) cm^{-1}. UV-vis (CH_2Cl_2): λ_{max} 248 nm (ε = 48500 L•mol^{-1}•cm^{-1}), 417 nm (ε = 3018 L•mol^{-1}•cm^{-1}), 480 nm (ε = 980 L•mol^{-1}•cm^{-1}). MS (EI): *m/z* 440 (M^+, 100 %). Anal. Calcd for $C_{22}H_{32}N_8O_2$: C, 59.98; H, 7.32; N, 25.44. Found C, 60.21; H, 7.26; N, 25.51.

[1,5-dimethyl-3-(2'-pyridyl)-6-oxoverdazyl]copper (II) chloride (4.13). A solution of **2.4g** (freshly separated from hydroquinone by flash chromatography; (0.072 g , 0.35 mmol) in 2 mL of ethanol was added to a solution of $CuCl_2 \cdot 2H_2O$ (0.060 g, 0.35 mmol) in 2 mL ethanol. The solution immediately turned dark red, and after 5 min of gentle heating was placed in a -15°C freezer overnight resulting in the precipitation of **4.13** as a dark red crystalline solid, yield 0.095 g (80%). Single crystals were grown by solvent diffusion of hexane into a dichloromethane solution of **4.13**. Mp. 102-104°C (dec). FT-IR (KBr): 1697 (s) υ(CO) cm^{-1}. UV-vis (CH_2Cl_2): λ_{max} 280 nm (ε = 7500 $L \cdot mol^{-1} \cdot cm^{-1}$), 492 nm (ε = 3750 $L \cdot mol^{-1} \cdot cm^{-1}$). Anal.Calcd for $C_9H_{10}N_5OCuCl_2$: C, 31.92; H, 2.98; N, 20.68. Found: C, 32.05; H, 3.13; N, 19.95.

[1,5-di-*iso*-propyl-3-(2'-pyridyl)6-oxoverdazyl]copper (II) chloride dimer (4.14). A solution of **2.13c** (0.050 g , 0.19 mmol) in 2 mL of ethanol was added to a solution of $CuCl_2 \cdot 2H_2O$ (0.032 g, 0.19 mmol) in 1 mL of ethanol. The solution immediately turned red-purple, and after 5 min of gentle heating was placed in a -15°C freezer overnight resulting in the precipitation of **4.14** as a dark red crystalline solid, yield 0.054 g (72%). Single crystals were grown by slow evaporation of a saturated 1:1 solution of **4.14** in dichloromethane and hexane. Mp. 112-114°C (dec). FT-IR (KBr): 1702 (s) υ(CO) cm^{-1}. UV-vis (CH_2Cl_2): λ_{max} 281 nm (ε = 12750 $L \cdot mol^{-1} \cdot cm^{-1}$), 500 nm (ε = 5750 $L \cdot mol^{-1} \cdot cm^{-1}$). Anal.Calcd for $C_{13}H_{18}N_5OCuCl_2$: C, 39.55; H, 4.60; N, 17.74. Found: C, 39.54; H, 4.61; N, 17.87.

1,5-dimethyl-3-(2'-methylimidazol-5'-yl)-6-oxoverdazylbis-(1,1,1,5,5,5-hexafluoroacetylacetonato)copper (II) (4.15). A solution of **2.4h** (0.090 g, 0.44 mmol) in 10 mL dichloromethane was added to a slurry of $Cu(hfac)_2 \cdot 2H_2O$ (0.224 g, 0.44 mmol)

in 20 mL heptane. The solution immediately turned pink, and upon refluxing for 1 h turned dark red. The solvent was removed *in vacuo* leaving a microcrystalline red solid. Recrystallization from ethanol afforded **4.15** as single crystals, yield 0.195 g (65%). Mp. 86-88°C (dec). FT-IR (KBr): 1712 (s) υ(CO) cm^{-1}. UV-vis (CH_2Cl_2): λ_{max} 422 nm (ε = 3100 $L•mol^{-1}•cm^{-1}$). Anal.Calcd for $C_{19}H_{17}N_6O_5F_{12}Cu$: C, 31.57; H, 1.91; N, 12.27. Found: C, 31.53; H, 2.03; N, 12.27.

1,5-dimethyl-3-(2'-pyridyl)-6-oxoverdazylbis-(1,1,1,5,5,5-hexafluoroacetylacetonato)copper (II) (4.16). A solution of **2.4g**:hydroquinone (0.216 g, 0.68 mmol) in 10 mL dichloromethane was added to a slurry of $Cu(hfac)_2{\cdot}2H_2O$ (0.328 g, 0.64 mmol) in 30 mL heptane. The solution immediately turned a light brown colour, and after 30 min a white precipitate was observed in the dark brown solution. The solution was filtered and the solvent was removed *in vacuo* leaving a microcrystalline brown solid. Recrystallization from hexanes yielded **4.16** as gold needles, yield 0.330 g (76%). Mp. 94-97°C (dec). FT-IR (KBr): 1705 (s) υ(CO) cm^{-1}. UV-vis (CH_2Cl_2): λ_{max} 421 nm (ε = 2800 $L•mol^{-1}•cm^{-1}$). Anal.Calcd for $C_{19}H_{12}N_5O_5F_{12}Cu$: C, 33.47; H, 1.77; N, 10.27. Found: C, 33.60; H, 1.60; N, 10.59.

Chapter 5 General conclusions and future work

Stable radicals have been widely studied as a result of their utility as ligands for transition metals, spin labels, and as components of magnetic and conducting materials. However, most stable radicals were discovered by accident, and very little effort has been made towards the systematic design of stable radicals. Verdazyl radicals are the only class of organic radicals whose stability rivals that of the nitroxides, and the synthetic pathways used to produce verdazyls make them amenable to derivatization. Significant advances in the design, synthesis, and chemistry of verdazyl radicals have been made in this work, including (i) the systematic study of the electrochemistry of verdazyl radicals, (ii) the development of formazans as ancillary ligands *en route* to inorganic verdazyl radicals, and (iii) magnetostructural studies of verdazyl diradicals and copper (II) verdazyl complexes.

The electrochemical properties of stable radicals have significant implication on their use in a number of applications, including their use in charge transfer chemistry, organic-radical batteries, and single-component molecular conductors. The systematic study of the electrochemical properties of verdazyl radicals was reported. Most verdazyl radicals were reversibly oxidized and reduced, highlighting their potential utility as building blocks in organic-radical batteries. Furthermore, the relatively low oxidation potentials observed for type I verdazyl radicals may allow for their use as electron donors in charge transfer salts, a property that may also be exploited in transition metal complexes of verdazyl radicals where valence tautomerism is of considerable interest. The tunability of the electrochemical properties of verdazyl radicals was illustrated by

studying their substituent effects. The presence of electron-withdrawing substituents rendered verdazyl radicals harder to oxidize and easier to reduce, while the introduction of electron-donating substituents had the opposite effect. The properties reported also rule out the possibility of their use as radical conductors. The large cell potentials (~ 1 V) observed for verdazyl radicals implies a high energy barrier associated with related charged states (anions and cations), theoretically rendering them ineffective charge carriers.

The similarities between formazans and benchmark ancillary ligands, including β-diketiminates was explored. Although formazans have been widely studied—mainly for their use as dyes—very little was known about their inorganic chemistry at the outset of this work. Triarylformazans were reacted with boron triacetate to form boratatetrazines, the first examples of main group formazan complexes, which were reduced to yield borataverdazyl radical anions. 3-Substituted formazans were synthesized as alternatives to triarylformazans, allowing for the first time, bulky N-aryl substituents to be incorporated into the formazan backbone. The coordination chemistry of 3-substituted formazans was explored, and a correlation between steric bulk at the ligand and complex structure was established. The development of formazans as ancillary ligands has opened the door to a number of spin-off projects. In particular, the coordination chemistry of compound **3.18e** is of interest as the β-diketiminate analogue **5.1** has been used extensively as a ligand.[286, 288-290] The increased electrophilicity of formazans relative to β-diketiminates is expected to play a significant role in the reactivity of their complexes. The ability of copper (I) complexes of β-diketiminates **5.2** to bind molecular oxygen has lead to their use as mimics for metalloproteins.[372] Similar copper (I) complexes of

formazans **5.3** should also bind molecular oxygen allowing for the effects of additional nitrogen atoms in the ligand backbone to be studied.

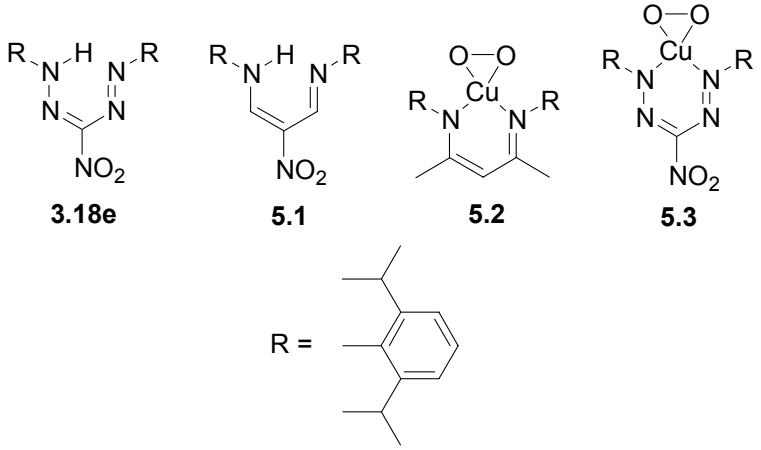

The incorporation of *iso*-propyl substituents to type II verdazyls has allowed for significant enhancement of their stability in solution and the solid-state. This increased stability allowed for the first stable verdazyl diradicals to be studied. The magnetic properties of diradicals **4.7a** and **4.7b** were consistent with other benzene-bridged diradicals, as the origin of magnetic coupling through benzene spacers is well known. In addition, this work served to highlight the use of verdazyl radicals as redox active chromophores. Future work in this area will likely involve type I verdazyl diradicals bridged through the 1,5-positions of the verdazyl backbone. Unlike diradicals **4.7a** and **4.7b**, diradicals **5.4a** and **5.4b** are substituted at a site of primary spin density (see Figure 4.4), potentially giving rise to significant enhancement of the communication between verdazyl radicals, and drastic changes in their magnetic and electronic properties.

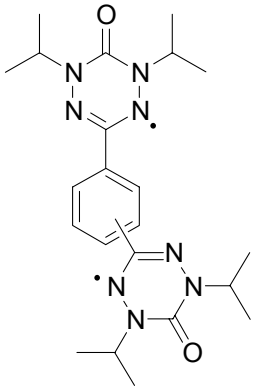

4.7a,b

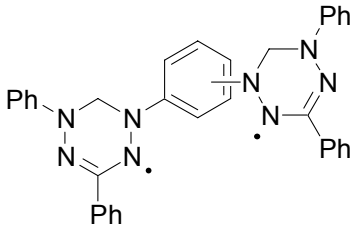

5.4a,b

Copper (II) complexes of verdazyl radicals were expected to exhibit ferromagnetic coupling. The coordinative flexibility of copper (II) ions and Jahn-Tellar distortions in octahedral copper (II) verdazyl complexes did not allow for complexes with significant ferromagnetic coupling interactions to be observed. However, when coupled with previous studies,[53] the magnetic interactions of verdazyl radicals and most first row transition metals have been reported, and their potential as building blocks for molecule-based magnets assessed. Future work in this area may incorporate the coordination chemistry and electrochemistry of verdazyl radicals in the form of redox active cobalt complexes, which may exhibit valence tautomeric behavior. Valence tautomerism has been reported in 2,2'-bipyridine (bipy) complexes of cobalt where electron transfer from cobalt (II) to a semiquinone (SQ) ligand in complex **5.5** gives rise to cobalt (III) complex **5.6**, bearing one catecholate (Cat) and one semiquinone ligand at low temperatures (Figure 5.1).[373] Similarly, when bipy is replaced by a verdazyl radical (vd), valence tautomerism between complexes **5.7** and **5.8** may occur. In addition, the possibility of metal-mediated electron transfer from the verdazyl radical in complex **5.7** to one of the semiquinone ligands yielding complex **5.9** also exists (Figure 5.2), making complexes of this type attractive targets.

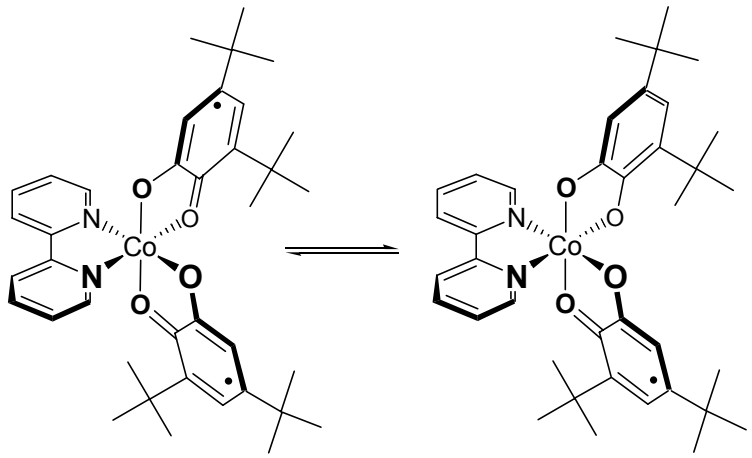

Figure 5.1. Valence tautomerism observed for Co(bipy)$(SQ)_2$ complex **5.5**.

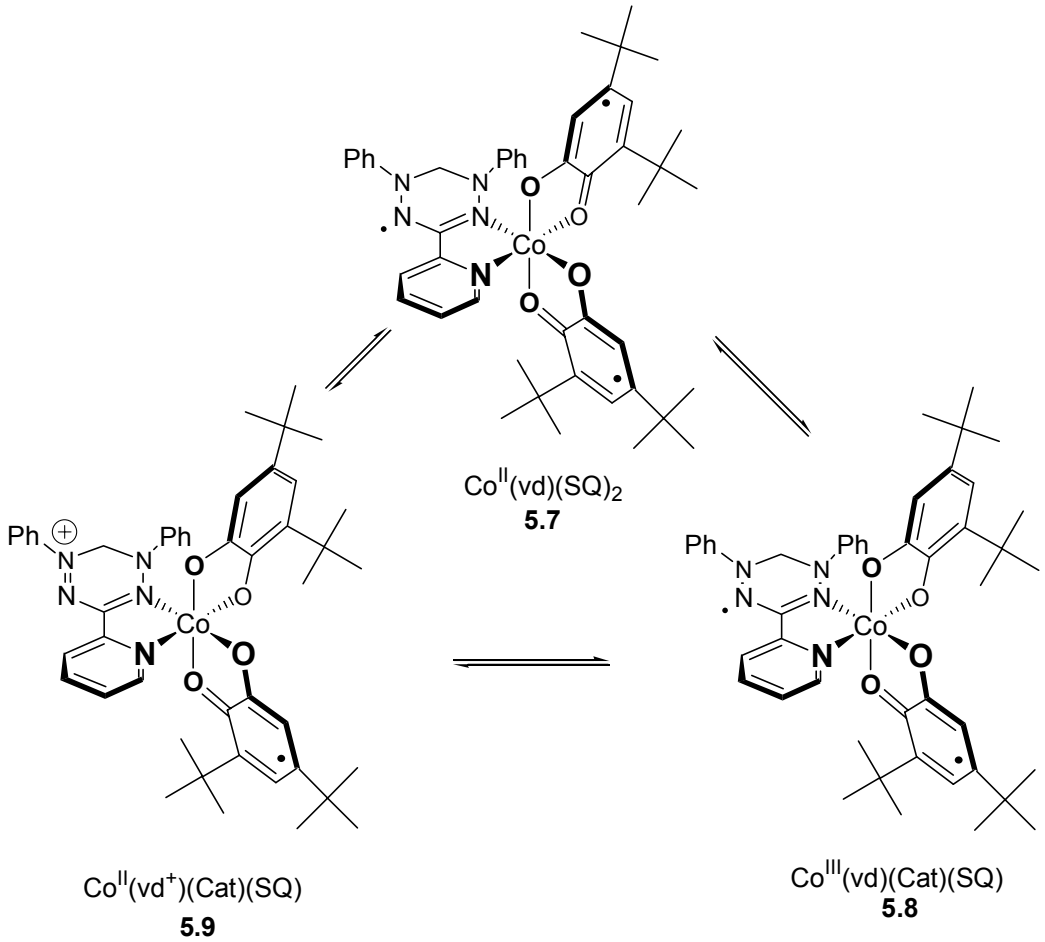

Figure 5.2. Potential valence tautomerism observed for Co(vd)$(SQ)_2$ complex **5.7**.

References

1. Gomberg, M. *J. Am. Chem. Soc.* **1900**, *22*, 757.
2. Griller, D.; Ingold, K. U. *Acc. Chem. Res.* **1976**, *9*, 13.
3. Bunce, N. J. *J. Chem. Educ.* **1987**, *64*, 907.
4. Beckwith, A. L. J.; Bowry, V. W.; Ingold, K. U. *J. Am. Chem. Soc.* **1992**, *114*, 4983.
5. Bowry, V. W.; Ingold, K. U. *J. Am. Chem. Soc.* **1992**, *114*, 4992.
6. Rehorek, D. *Chem. Soc. Rev.* **1991**, *20*, 341.
7. Evans, C. A. *Aldrichimica Acta* **1979**, *12*, 23.
8. Riesz, P.; Rosenthal, I. *Can. J. Chem.* **1982**, *60*, 1474.
9. Rosenthal, I.; Mossoba, M. M.; Riesz, P. *Can. J. Chem.* **1982**, *60*, 1486.
10. Janzen, E. G.; Blackburn, B. J. *J. Am. Chem. Soc.* **1969**, *91*, 4481.
11. Janzen, E. G.; Evans, C. A.; Liu, J. I. P. *J. Mag. Res.* **1973**, *9*, 513.
12. Janzen, E. G.; Liu, J. I. P. *J. Mag. Res.* **1973**, *9*, 510.
13. Berliner, L. J., *Spin Labelling: Theory and Applications*. Academic Press: New York, 1979.
14. Swartz, H. M.; Bolton, J. R.; Borg, D. C., *Biological Applications of Electron Spin Resonance*. Wiley-Interscience: New York, 1972.
15. Zweier, J. L.; Kuppusamy, P. *Proc. Natl. Acad. Sci. U.S.A.* **1988**, *85*, 5703.
16. Zweier, J. L.; Kuppusamy, P.; Lutty, G. A. *Proc. Natl. Acad. Sci. U.S.A.* **1988**, *85*, 4046.
17. Haney, C.; Parasca, A.; Pelizzari, C. *Med. Phys.* **2005**, *32*, 2135.
18. Golder, W. *Onkologie* **2007**, *27*, 304.
19. Lauterbur, P. C. *Nature* **1973**, *242*, 190.
20. Rosen, Y.; Lenkinski, R. E. *Neurotherapeutics* **2007**, *4*, 330.
21. Blundell, S. J.; Pratt, F. L. *J. Phys.: Condens. Matter* **2004**, *16*, R771.

22. Takeda, K.; Yoshida, Y.; Inanaga, Y.; Kawae, T.; Shiomi, D.; Ise, T.; Kozaki, M.; Okada, K.; Sato, K.; Takui, T. *Phys. Rev. B* **2005**, *72*.

23. Robertson, C. M.; Myles, D. J. T.; Leitch, A. A.; Reed, R. W.; Dooley, B. M.; Frank, N. L.; Dube, P. A.; Thompson, L. K.; Oakley, R. T. *J. Am. Chem. Soc.* **2007**, *129*, 12688.

24. Mitani, M.; Yamaki, D.; Yoshioka, Y.; Yamaguchi, K. *J. Chem. Phys.* **1999**, *111*, 2283.

25. Miyasaka, M.; Yamazaki, T.; Tsuchida, E.; Nishide, H. *Macromolecules* **2000**, *33*, 8211.

26. Nishide, H.; Miyasaka, M.; Doi, R.; Araki, T. *Macromolecules* **2002**, *35*, 690.

27. Takahashi, M.; Nishide, H.; Tsuchida, E.; Lahti, P. M. *Chem. Mater.* **1997**, *9*, 11.

28. Rajca, A.; Rajca, S.; Wongsriratanakul, J. *J. Am. Chem. Soc.* **1999**, *121*, 6308.

29. Rajca, A.; Wongsriratanakul, J.; Rajca, S. *Science* **2001**, *294*, 1503.

30. Utamapanya, S.; Kakegawa, H.; Bryant, L.; Rajca, A. *Chem. Mater.* **1993**, *5*, 1053.

31. Jain, R.; Kabir, K.; Gilroy, J. B.; Mitchell, K. A. R.; Wong, K. C.; Hicks, R. G. *Nature* **2007**, *445*, 291.

32. Manriquez, J. M.; Yee, G. T.; McLean, R. S.; Epstein, A. J.; Miller, J. S. *Science* **1991**, *252*, 1415.

33. Miller, J. S. *Inorg. Chem.* **2000**, *39*, 4392.

34. Miller, J. S.; Manson, J. L. *Acc. Chem. Res.* **2001**, *34*, 563.

35. Haddon, R. C. *Nature* **1975**, *256*, 394.

36. Brusso, J. L.; Derakhshan, S.; Itkis, M. E.; Kleinke, H.; Haddon, R. C.; Oakley, R. T.; Reed, R. W.; Richardson, J. F.; Robertson, C. M.; Thompson, L. K. *Inorg. Chem.* **2006**, *45*, 10958.

37. Leitch, A. A.; Reed, R. W.; Robertson, C. M.; Britten, J. F.; Yu, X. Y.; Secco, R. A.; Oakley, R. T. *J. Am. Chem. Soc.* **2007**, *129*, 7903.

38. Mandal, S. K.; Samanta, S.; Itkis, M. E.; Jensen, D. W.; Reed, R. W.; Oakley, R. T.; Tham, F. S.; Donnadieu, B.; Haddon, R. C. *J. Am. Chem. Soc.* **2006**, *128*, 1982.

39. Pal, S. K.; Itkis, M. E.; Tham, F. S.; Reed, R. W.; Oakley, R. T.; Donnadieu, B.; Haddon, R. C. *J. Am. Chem. Soc.* **2007**, *129*, 7163.

40. Rawson, J. M.; Alberola, A.; Whalley, A. *J. Mater. Chem.* **2006**, *16*, 2560.

41. deNooy, A. E. J.; Besemer, A. C.; vanBekkum, H. *Synthesis* **1996**, 1153.

42. Sheldon, R. A.; Arends, I.; Ten Brink, G. J.; Dijksman, A. *Acc. Chem. Res.* **2002**, *35*, 774.

43. Zimmer, H.; Lankin, D. C.; Horgan, S. W. *Chem. Rev.* **1971**, *71*, 229.

44. Font-Sanchis, E.; Aliaga, C.; Focsaneanu, K. S.; Scaiano, J. C. *Chem. Commun.* **2002**, 1576.

45. Scaiano, J. C.; Martin, A.; Yap, G. P. A.; Ingold, K. U. *Org. Lett.* **2000**, *2*, 899.

46. Wright, J. S.; Carpenter, D. J.; McKay, D. J.; Ingold, K. U. *J. Am. Chem. Soc.* **1997**, *119*, 4245.

47. Wright, J. S.; Johnson, E. R.; DiLabio, G. A. *J. Am. Chem. Soc.* **2001**, *123*, 1173.

48. Caneschi, A.; Gatteschi, D.; Rey, P. *Prog. Inorg. Chem.* **1991**, *39*, 331.

49. Pierpont, C. G.; Lange, C. W. *Prog. Inorg. Chem.* **1994**, *41*, 331.

50. Preuss, K. E. *Dalton Trans.* **2007**, 2357.

51. Chaudhuri, P.; Wieghardt, K. *Prog. Inorg. Chem.* **2001**, *50*, 151.

52. Kaim, W. *Coord. Chem. Rev.* **1987**, *76*, 187.

53. Koivisto, B. D.; Hicks, R. G. *Coord. Chem. Rev.* **2005**, *249*, 2612.

54. Hawker, C. J. *Acc. Chem. Res.* **1997**, *30*, 373.

55. Patten, T. E.; Matyjaszewski, K. *Acc. Chem. Res.* **1999**, *32*, 895.

56. Hawker, C. J.; Bosman, A. W.; Harth, E. *Chem. Rev.* **2001**, *101*, 3661.

57. Chen, E. K. Y.; Teertstra, S. J.; Chan-Seng, D.; Otieno, P. O.; Hicks, R. G.; Georges, M. K. *Macromolecules* **2007**, *40*, 8609.

58. Georges, M. K.; Veregin, R. P. N.; Kazmaier, P. M.; Hamer, G. K. *Macromolecules* **1993**, *26*, 2987.

59. Veregin, R. P. N.; Georges, M. K.; Kazmaier, P. M.; Hamer, G. K. *Macromolecules* **1993**, *26*, 5316.

60. Power, P. P. *Chem. Rev.* **2003**, *103*, 789.

61. Hicks, R. G. *Org. Biomol. Chem.* **2007**, *5*, 1321.

62. Neumann, W. P.; Uzick, W.; Zarkadis, A. K. *J. Am. Chem. Soc.* **1986**, *108*, 3762.

63. Maki, A. H.; Allendoe.Rd; Danner, J. C.; Keys, R. T. *J. Am. Chem. Soc.* **1968**, *90*, 4225.

64. Neumann, W. P.; Penenory, A.; Stewen, U.; Lehnig, M. *J. Am. Chem. Soc.* **1989**, *111*, 5845.

65. Dunnebacke, D.; Neumann, W. P.; Penenory, A.; Stewen, U. *Chem. Ber.* **1989**, *122*, 533.

66. Kahr, B.; Vanengen, D.; Gopalan, P. *Chem. Mater.* **1993**, *5*, 729.

67. Ballester, M.; Riera, J.; Castaner, J.; Badia, C.; Monso, J. M. *J. Am. Chem. Soc.* **1971**, *93*, 2215.

68. Ballester, M. *Acc. Chem. Res.* **1985**, *18*, 380.

69. Armet, O.; Veciana, J.; Rovira, C.; Riera, J.; Castaner, J.; Molins, E.; Rius, J.; Miravitlles, C.; Olivella, S.; Brichfeus, J. *J. Phys. Chem.* **1987**, *91*, 5608.

70. Carilla, J.; Fajari, L.; Julia, L.; Riera, J.; Viadel, L. *Tetrahedron Lett.* **1994**, *35*, 6529.

71. Carilla, J.; Fajari, L.; Julia, L.; Sane, J.; Rius, J. *Tetrahedron* **1996**, *52*, 7013.

72. Reid, D. H. *Tetrahedron* **1958**, *3*, 339.

73. Sogo, P. B.; Nakazaki, M.; Calvin, M. *J. Chem. Phys.* **1957**, *26*, 1343.

74. Goto, K.; Kubo, T.; Yamamoto, K.; Nakasuji, K.; Sato, K.; Shiomi, D.; Takui, T.; Kubota, M.; Kobayashi, T.; Yakusi, K.; Ouyang, J. Y. *J. Am. Chem. Soc.* **1999**, *121*, 1619.

75. Lu, J. M.; Rosokha, S. V.; Kochi, J. K. *J. Am. Chem. Soc.* **2003**, *125*, 12161.

76. Small, D.; Rosokha, S. V.; Kochi, J. K.; Head-Gordon, M. *J. Phys. Chem. A* **2005**, *109*, 11261.

77. Small, D.; Zaitsev, V.; Jung, Y. S.; Rosokha, S. V.; Head-Gordon, M.; Kochi, J. K. *J. Am. Chem. Soc.* **2004**, *126*, 13850.

78. Zaitsev, V.; Rosokha, S. V.; Head-Gordon, M.; Kochi, J. K. *J. Org. Chem.* **2006**, *71*, 520.

79. Koutentis, P. A.; Chen, Y.; Cao, Y.; Best, T. P.; Itkis, M. E.; Beer, L.; Oakley, R. T.; Cordes, A. W.; Brock, C. P.; Haddon, R. C. *J. Am. Chem. Soc.* **2001**, *123*, 3864.

80. Altwicke, E. R. *Chem. Rev.* **1967**, *67*, 475.

81. Coppinger, G. M. *J. Am. Chem. Soc.* **1957**, *79*, 501.

82. Dietz, F.; Tyutyulkov, N.; Baumgarten, M. *J. Phys. Chem. B* **1998**, *102*, 3912.

83. Novak, I.; Kovac, B. *Chem. Phys. Lett.* **2005**, *413*, 351.

84. Miura, Y.; Asada, H.; Kinoshita, M. *Chem. Lett.* **1978**, 1085.

85. Miura, Y.; Isogai, M.; Kinoshita, M. *Bull. Chem. Soc. Jpn.* **1985**, *58*, 751.

86. Miura, Y.; Isogai, M.; Kinoshita, M. *Bull. Chem. Soc. Jpn.* **1987**, *60*, 3065.

87. Miura, Y.; Katsura, Y.; Kinoshita, M. *Chem. Lett.* **1977**, 409.

88. Miura, Y.; Katsura, Y.; Kinoshita, M. *Bull. Chem. Soc. Jpn.* **1979**, *52*, 1121.

89. Miura, Y.; Kinoshita, M. *Bull. Chem. Soc. Jpn.* **1977**, *50*, 1142.

90. Miura, Y.; Kurokawa, S.; Nakatsuji, M.; Ando, K.; Teki, Y. *J. Org. Chem.* **1998**, *63*, 8295.

91. Miura, Y.; Tanaka, A. *J. Chem. Soc., Chem. Commun.* **1990**, 441.

92. Miura, Y.; Tanaka, A.; Hirotsu, K. *J. Org. Chem.* **1991**, *56*, 6638.

93. Miura, Y.; Yamamoto, A.; Katsura, Y.; Kinoshita, M. *J. Chem. Soc., Chem. Commun.* **1980**, 37.

94. Clarke, C. S.; Haynes, D. A.; Rawson, J. M.; Bond, A. D. *Chem. Commun.* **2003**, 2774.

95. Cordes, A. W.; Bryan, C. D.; Davis, W. M.; Delaat, R. H.; Glarum, S. H.; Goddard, J. D.; Haddon, R. C.; Hicks, R. G.; Kennepohl, D. K.; Oakley, R. T.; Scott, S. R.; Westwood, N. P. C. *J. Am. Chem. Soc.* **1993**, *115*, 7232.

96. Cordes, A. W.; Haddon, R. C.; Hicks, R. G.; Oakley, R. T.; Palstra, T. T. M. *Inorg. Chem.* **1992**, *31*, 1802.

97. Cordes, A. W.; Haddon, R. C.; Hicks, R. G.; Kennepohl, D. K.; Oakley, R. T.; Palstra, T. T. M.; Schneemeyer, L. F.; Scott, S. R.; Waszczak, J. V. *Chem. Mater.* **1993**, *5*, 820.

98. Cordes, A. W.; Haddon, R. C.; Hicks, R. G.; Kennepohl, D. K.; Oakley, R. T.; Schneemeyer, L. F.; Waszczak, J. V. *Inorg. Chem.* **1993**, *32*, 1554.

99. Vegas, A.; Perezsalazar, A.; Banister, A. J.; Hey, R. G. *J. Chem. Soc., Dalton Trans.* **1980**, 1812.

100. Hofs, H. U.; Bats, J. W.; Gleiter, R.; Hartmann, G.; Mews, R.; Eckertmaksic, M.; Oberhammer, H.; Sheldrick, G. M. *Chem. Ber.* **1985**, *118*, 3781.

101. Cordes, A. W.; Goddard, J. D.; Oakley, R. T.; Westwood, N. P. C. *J. Am. Chem. Soc.* **1989**, *111*, 6147.

102. Banister, A. J.; Hansford, M. I.; Hauptman, Z. V.; Wait, S. T.; Clegg, W. *J. Chem. Soc., Dalton Trans.* **1989**, 1705.

103. Barclay, T. M.; Cordes, A. W.; George, N. A.; Haddon, R. C.; Itkis, M. E.; Oakley, R. T. *Chem. Commun.* **1999**, 2269.

104. Alberola, A.; Less, R. J.; Pask, C. M.; Rawson, J. M.; Palacio, F.; Oliete, P.; Paulsen, C.; Yamaguchi, A.; Farley, R. D.; Murphy, D. M. *Angew. Chem., Int. Ed.* **2003**, *42*, 4782.

105. Banister, A. J.; Bricklebank, N.; Lavender, I.; Rawson, J. M.; Gregory, C. I.; Tanner, B. K.; Clegg, W.; Elsegood, M. R. J.; Palacio, F. *Angew. Chem., Int. Ed.* **1996**, *35*, 2533.

106. Antorrena, G.; Davies, J. E.; Hartley, M.; Palacio, F.; Rawson, J. M.; Smith, J. N. B.; Steiner, A. *Chem. Commun.* **1999**, 1393.

107. Banister, A. J.; Batsanov, A. S.; Dawe, O. G.; Herbertson, P. L.; Howard, J. A. K.; Lynn, S.; May, I.; Smith, J. N. B.; Rawson, J. M.; Rogers, T. E.; Tanner, B. K.; Antorrena, G.; Palacio, F. *J. Chem. Soc., Dalton Trans.* **1997**, 2539.

108. Banister, A. J.; Bricklebank, N.; Clegg, W.; Elsegood, M. R. J.; Gregory, C. I.; Lavender, I.; Rawson, J. M.; Tanner, B. K. *J. Chem. Soc., Chem. Commun.* **1995**, 679.

109. Aherne, C.; Banister, A. J.; Luke, A. W.; Rawson, J. M.; Whitehead, R. J. *J. Chem. Soc., Dalton Trans.* **1992**, 1277.

110. Burford, N.; Passmore, J.; Schriver, M. J. *J. Chem. Soc., Chem. Commun.* **1986**, 140.

111. Passmore, J.; Sun, X. P. *Inorg. Chem.* **1996**, *35*, 1313.

112. Passmore, J.; Sun, X. P.; Parsons, S. *Can. J. Chem.* **1992**, *70*, 2972.

113. Awere, E. G.; Burford, N.; Haddon, R. C.; Parsons, S.; Passmore, J.; Waszczak, J. V.; White, P. S. *Inorg. Chem.* **1990**, *29*, 4821.

114. Brownridge, S.; Du, H. B.; Fairhurst, S. A.; Haddon, R. C.; Oberhammer, H.; Parsons, S.; Passmore, J.; Schriver, M. J.; Sutcliffe, L. H.; Westwood, N. P. C. *J. Chem. Soc., Dalton Trans.* **2000**, 3365.

115. Awere, E. G.; Burford, N.; Mailer, C.; Passmore, J.; Schriver, M. J.; White, P. S.; Banister, A. J.; Oberhammer, H.; Sutcliffe, L. H. *J. Chem. Soc., Chem. Commun.* **1987**, 66.

116. Wolmershauser, G.; Kraft, G. *Chem. Ber.* **1990**, *123*, 881.

117. Chung, Y. L.; Sandall, J. P. B.; Sutcliffe, L. H.; Joly, H.; Preston, K. F.; Johann, R.; Wolmershauser, G. *Magn. Reson. Chem.* **1991**, *29*, 625.

118. Chung, Y. L.; Fairhurst, S. A.; Gillies, D. G.; Kraft, G.; Krebber, A. M. L.; Preston, K. F.; Sutcliffe, L. H.; Wolmershauser, G. *Magn. Reson. Chem.* **1992**, *30*, 774.

119. Chung, Y. L.; Fairhurst, S. A.; Gillies, D. G.; Preston, K. F.; Sutcliffe, L. H. *Magn. Reson. Chem.* **1992**, *30*, 666.

120. Harrison, S. R.; Pilkington, R. S.; Sutcliffe, L. H. *J. Chem. Soc., Faraday Trans. I* **1984**, *80*, 669.

121. Fairhurst, S. A.; Pilkington, R. S.; Sutcliffe, L. H. *J. Chem. Soc., Faraday Trans. I* **1983**, *79*, 925.

122. Barclay, T. M.; Beer, L.; Cordes, A. W.; Oakley, R. T.; Preuss, K. E.; Taylor, N. J.; Reed, R. W. *Chem. Commun.* **1999**, 531.

123. Barclay, T. M.; Cordes, A. W.; Haddon, R. C.; Itkis, M. E.; Oakley, R. T.; Reed, R. W.; Zhang, H. *J. Am. Chem. Soc.* **1999**, *121*, 969.

124. Beer, L.; Cordes, A. W.; Haddon, R. C.; Itkis, M. E.; Oakley, R. T.; Reed, R. W.; Robertson, C. M. *Chem. Commun.* **2002**, 1872.

125. Cordes, A. W.; Mingie, J. R.; Oakley, R. T.; Reed, R. W.; Zhang, H. Z. *Can. J. Chem.* **2001**, *79*, 1352.

126. Oakley, R. T.; Reed, R. W.; Robertson, C. M.; Richardson, J. F. *Inorg. Chem.* **2005**, *44*, 1837.

127. Beer, L.; Britten, J. F.; Clements, O. P.; Haddon, R. C.; Itkis, M. E.; Matkovich, K. M.; Oakley, R. T.; Itkis, M. E. *Chem. Mater.* **2004**, *16*, 1564.

128. Beer, L.; Britten, J. F.; Brusso, J. L.; Cordes, A. W.; Haddon, R. C.; Itkis, M. E.; MacGregor, D. S.; Oakley, R. T.; Reed, R. W.; Robertson, C. M. *J. Am. Chem. Soc.* **2003**, *125*, 14394.

129. Beer, L.; Brusso, J. L.; Cordes, A. W.; Godde, E.; Haddon, R. C.; Itkis, M. E.; Oakley, R. T.; Reed, R. W. *Chem. Commun.* **2002**, 2562.

130. Beer, L.; Brusso, J. L.; Cordes, A. W.; Haddon, R. C.; Itkis, M. E.; Kirschbaum, K.; MacGregor, D. S.; Oakley, R. T.; Pinkerton, A. A.; Reed, R. W. *J. Am. Chem. Soc.* **2002**, *124*, 9498.

131. Boere, R. T.; Oakley, R. T.; Reed, R. W.; Westwood, N. P. C. *J. Am. Chem. Soc.* **1989**, *111*, 1180.

132. Cordes, A. W.; Hayes, P. J.; Josephy, P. D.; Koenig, H.; Oakley, R. T.; Pennington, W. T. *J. Chem. Soc., Chem. Commun.* **1984**, 1021.

133. Hayes, P. J.; Oakley, R. T.; Cordes, A. W.; Pennington, W. T. *J. Am. Chem. Soc.* **1985**, *107*, 1346.

134. Forrester, A. R.; Hay, J. M.; Thomson, R. H., *Organic Chemistry of Stable Free Radicals*. Academic Press: London, 1968.

135. Rozanstev, E. G., *Free Nitroxyl Radicals*. Plenum: New York, 1970.

136. Keana, J. F. W. *Chem. Rev.* **1978**, *78*, 37.

137. Fremy, E. *Ann. Chim. Phys.* **1845**, *15*, 408.

138. Piloty, O.; Scherwin, B. G. *Ber.* **1901**, *34*, 1870.

139. Ullman, E. F.; Siecki, J. H.; Boocock, D. G. B.; Darcy, R. *J. Am. Chem. Soc.* **1972**, *94*, 7049.

140. Dooley, B. M.; Bowles, S. E.; Storr, T.; Frank, N. L. *Org. Lett.* **2007**, *9*, 4781.

141. Zakrassov, A.; Shteiman, V.; Sheynin, Y.; Tumanskii, B.; Botoshansky, M.; Kapon, M.; Keren, A.; Kaftory, M.; Vos, T. E.; Miller, J. S. *J. Mater. Chem.* **2004**, *14*, 1827.

142. Kuhn, R.; Trischmann, H. *Angew. Chem., Int. Ed.* **1963**, *8*, 520.

143. Neugebauer, F. A.; Fischer, H. *Angew. Chem. Int. Ed.* **1980**, *19*, 724.

144. Neugebauer, F. A.; Fischer, H.; Siegel, R. *Chem. Ber.* **1988**, *121*, 815.

145. Koivisto, B. D.; Ichimura, A. S.; McDonald, R.; Lemaire, M. T.; Thompson, L. K.; Hicks, R. G. *J. Am. Chem. Soc.* **2006**, *128*, 690.

146. Barclay, T. M.; Hicks, R. G.; Lemaire, M. T.; Thompson, L. K.; Xu, Z. Q. *Chem. Commun.* **2002**, 1688.

147. Hicks, R. G.; Koivisto, B. D.; Lemaire, M. T. *Org. Lett.* **2004**, *6*, 1887.

148. Hicks, R. G.; Lemaire, M. T.; Ohrstrom, L.; Richardson, J. F.; Thompson, L. K.; Xu, Z. Q. *J. Am. Chem. Soc.* **2001**, *123*, 7154.

149. Pare, E. C.; Brook, D. J. R.; Brieger, A.; Badik, M.; Schinke, M. *Org. Biomol. Chem.* **2005**, *3*, 4258.

150. Milcent, R.; Barbier, G.; Capelle, S.; Catteau, J. P. *J. Heterocycl. Chem.* **1994**, *31*, 319.

151. Azuma, N.; Ohyanish.H; Yamauchi, J.; Mukai, K.; Deguchi, Y. *Bull. Chem. Soc. Jpn.* **1974**, *47*, 2369.

152. Degtyarev, L. S.; Gorlov, Y. I. *J. Struct. Chem.* **1975**, *16*, 715.

153. Degtyarev, L. S.; Stetsenko, A. A.; Gorlov, Y. I. *Chem. Phys. Lett.* **1980**, *69*, 323.

154. Mukai, K.; Azuma, N.; Shikata, H.; Ishizu, K. *Bull. Chem. Soc. Jpn.* **1970**, *43*, 3958A.

155. Neugebauer, F. A.; Fischer, H.; Krieger, C. *J. Chem. Soc., Perkin Trans. II* **1993**, 535.

156. Podenko, L. S.; Chirkov, A. K.; Petroshen, V. E.; Shchipanov, V. P. *J. Struct. Chem.* **1981**, *22*, 667.

157. Azuma, N.; Deguchi, Y.; Marumo, F.; Saito, Y. *Bull. Chem. Soc. Jpn.* **1975**, *48*, 819.

158. Azuma, N.; Deguchi, Y.; Marumo, F.; Saito, Y. *Bull. Chem. Soc. Jpn.* **1975**, *48*, 825.

159. Azuma, N.; Yamauchi, J.; Mukai, K.; Ohyanish.H; Deguchi, Y. *Bull. Chem. Soc. Jpn.* **1973**, *46*, 2728.

160. Mukai, K.; Azuma, N.; Ishizu, K. *Bull. Chem. Soc. Jpn.* **1970**, *43*, 3618.

161. Mukai, K.; Oishi, K.; Ishizu, K.; Azuma, N. *Chem. Phys. Lett.* **1973**, *23*, 522.

162. Hicks, R. G. *Austral. J. Chem.* **2001**, *54*, 597.

163. Hicks, R. G.; Hooper, R. *Inorg. Chem.* **1999**, *38*, 284.

164. Hicks, R. G.; Ohrstrom, L.; Patenaude, G. W. *Inorg. Chem.* **2001**, *40*, 1865.

165. Barclay, T. M.; Hicks, R. G.; Ichimura, A. S.; Patenaude, G. W. *Can. J. Chem.* **2002**, *80*, 1501.

166. Barclay, T. M.; Hicks, R. G.; Lemaire, M. T.; Thompson, L. K. *Chem. Commun.* **2000**, 2141.

167. Barclay, T. M.; Hicks, R. G.; Lemaire, M. T.; Thompson, L. K. *Inorg. Chem.* **2001**, *40*, 5581.

168. Barclay, T. M.; Hicks, R. G.; Lemaire, M. T.; Thompson, L. K. *Inorg. Chem.* **2001**, *40*, 6521.

169. Barclay, T. M.; Hicks, R. G.; Lemaire, M. T.; Thompson, L. K. *Inorg. Chem.* **2003**, *42*, 2261.

170. Hicks, R. G.; Lemaire, M. T.; Thompson, L. K.; Barclay, T. M. *J. Am. Chem. Soc.* **2000**, *122*, 8077.

171. Gilroy, J. B.; McKinnon, S. D. J.; Koivisto, B. D.; Hicks, R. G. *Org. Lett.* **2007**, *9*, 4837.

172. Gilroy, J. B.; Ferguson, M. J.; McDonald, R.; Patrick, B. O.; Hicks, R. G. *Chem. Commun.* **2007**, 126.

173. Gilroy, J. B.; Otieno, P. O.; Ferguson, M. J.; McDonald, R.; Hicks, R. G. *Inorg. Chem.* **2008**, *47*, 1279.

174. Gilroy, J. B.; Patrick, B. O.; McDonald, R.; Hicks, R. G. *Inorg. Chem.* **2008**, *47*, 1287.

175. Gilroy, J. B.; Ferguson, M. J.; McDonald, R.; Hicks, R. G. *Inorg. Chim. Acta* **2008**, In Press.

176. Gilroy, J. B.; McKinnon, S. D. J.; Kennepohl, P.; Zsombor, M. S.; Ferguson, M. J.; Thompson, L. K.; Hicks, R. G. *J. Org. Chem.* **2007**, *72*, 8062.

177. Gilroy, J. B.; Koivisto, B. D.; McDonald, R.; Ferguson, M. J.; Hicks, R. G. *J. Mater. Chem.* **2006**, *16*, 2618.

178. Ratera, I.; Ruiz-Molina, D.; Renz, F.; Ensling, J.; Wurst, K.; Rovira, C.; Gutlich, P.; Veciana, J. *J. Am. Chem. Soc.* **2003**, *125*, 1462.

179. Sporer, C.; Ratera, I.; Ruiz-Molina, D.; Zhao, Y. X.; Vidal-Gancedo, J.; Wurst, K.; Jaitner, P.; Clays, K.; Persoons, A.; Rovira, C.; Veciana, J. *Angew. Chem. Int. Ed.* **2004**, *43*, 5266.

180. Heckmann, A.; Lambert, C. *J. Am. Chem. Soc.* **2007**, *129*, 5515.

181. Chi, X.; Itkis, M. E.; Patrick, B. O.; Barclay, T. M.; Reed, R. W.; Oakley, R. T.; Cordes, A. W.; Haddon, R. C. *J. Am. Chem. Soc.* **1999**, *121*, 10395.

182. Boere, R. T.; Moock, K. H. *J. Am. Chem. Soc.* **1995**, *117*, 4755.

183. Nakahara, K.; Iwasa, S.; Satoh, M.; Morioka, Y.; Iriyama, J.; Suguro, M.; Hasegawa, E. *Chem. Phys. Lett.* **2002**, *359*, 351.

184. Nishide, H.; Iwasa, S.; Pu, Y. J.; Suga, T.; Nakahara, K.; Satoh, M. *Electrochim. Acta* **2004**, *50*, 827.

185. Suga, T.; Pu, Y. J.; Oyaizu, K.; Nishide, H. *Bull. Chem. Soc. Jpn.* **2004**, *77*, 2203.

186. Buhrmester, C.; Moshurchak, L. M.; Wang, R. L.; Dahn, J. R. *J. Electrochem. Soc.* **2006**, *153*, A1800.

187. Katsumata, T.; Satoh, M.; Wada, J.; Shiotsuki, M.; Sanda, F.; Masuda, T. *Macromol. Rapid Commun.* **2006**, *27*, 1206.

188. Nakahara, K.; Iwasa, S.; Iriyama, J.; Morioka, Y.; Suguro, M.; Satoh, M.; Cairns, E. J. *Electrochim Acta* **2006**, *52*, 921.

189. Li, H. Q.; Zou, Y.; Xia, Y. Y. *Electrochim. Acta* **2007**, *52*, 2153.

190. Boere, R. T.; Moock, K. H.; Parvez, M. *Z. Anorg. Allg. Chem.* **1994**, *620*, 1589.

191. Ziessel, R.; Ulrich, G.; Lawson, R. C.; Echegoyen, L. *J. Mater. Chem.* **1999**, *9*, 1435.

192. Boere, R. T.; Roemmele, T. L. *Coord. Chem. Rev.* **2000**, *210*, 369.

193. Ionita, P.; Whitwood, A. C.; Gilbert, B. C. *J. Chem. Soc., Perkin Trans. 2* **2001**, 1453.

194. Coronado, E.; Gimenez-Saiz, C.; Nicolas, M.; Romero, F. M.; Rusanov, E.; Stoeckli-Evans, H. *New J. Chem.* **2003**, *27*, 490.

195. Fish, J. R.; Swarts, S. G.; Sevilla, M. D.; Malinski, T. *J. Phys. Chem.* **1988**, *92*, 3745.

196. Malinski, T.; Fish, J. R. *J. Electrochem. Soc.* **1988**, *135*, C149.

197. Krzyczmonik, P.; Scholl, H. *J. Electroanal. Chem.* **1992**, *335*, 233.

198. Kato, Y.; Shimizu, Y.; Lin, Y. J.; Unoura, K.; Utsumi, H.; Ogata, T. *Electrochim. Acta* **1995**, *40*, 2799.

199. Baur, J. E.; Wang, S.; Brandt, M. C. *Anal. Chem.* **1996**, *68*, 3815.

200. Marx, L.; Schollhorn, B. *New J. Chem.* **2006**, *30*, 430.

201. Manda, S.; Nakanishi, I.; Ohkubo, K.; Yakumaru, H.; Matsumoto, K. I.; Ozawa, T.; Ikota, N.; Fukuzumi, S.; Anzai, K. *Org. Biomol. Chem.* **2007**, *5*, 3951.

202. Kuhn, R.; Trischmann, H. *Monatsh. Chem.* **1964**, *95*, 457.

203. Katritzky, A. R.; Belyakov, S. A.; Durst, H. D.; Xu, R. X.; Dalal, N. S. *Can. J. Chem.* **1994**, *72*, 1849.

204. Mukai, K.; Matsubara, M.; Hisatou, H.; Hosokoshi, Y.; Inoue, K.; Azuma, N. *J. Phys. Chem. B* **2002**, *106*, 8632.

205. Tezcan, H.; Can, S.; Tezcan, R. *Dyes and Pigments* **2002**, *52*, 121.

206. Tezcan, H.; Uzluk, E. *Dyes and Pigments* **2007**, *75*, 633.

207. Nineham, A. W. *Chem. Rev.* **1955**, *55*, 355.

208. Siedle, A. R.; Pignolet, L. H. *Inorg. Chem.* **1980**, *19*, 2052.

209. Irving, H.; Gill, J. B.; Cross, W. R. *J. Chem. Soc.* **1960**, 2087.

210. Seidler, E. *Prog. Histochem. Cytochem.* **1991**, *24*, 1.

211. Katritzky, A. R.; Belyakov, S. A.; Cheng, D.; Durst, H. D. *Synthesis* **1995**, 577.

212. Chattaway, F. D.; Walker, A. J. *J. Chem. Soc.* **1925**, *127*, 975.

213. Bodforss, S. *Ber.* **1926**, *59*, 670.

214. Borsche, W.; Manteuffel, R. *Ann.* **1933**, *505*, 189.

215. Klyuev, N. A.; Zhilnikov, V. G.; Aleksandrov, G. G.; Grandberg, II; Lipunova, G. N. *Russ. J. Org. Chem.* **1983**, *19*, 2615.

216. Polyakova, I. N.; Starikova, Z. A.; Olkhovikova, N. B. *Kristallografiya* **1990**, *35*, 1133.

217. Maki, H.; Goto, M.; Honda, K.; Uchiumi, A.; Kurahashi, M. *Anal. Sci.* **1993**, *9*, 567.

218. Kozlova, N. P.; Agre, V. M.; Starikova, Z. A.; Dyakonov, I. A. *J. Struct. Chem.* **1991**, *32*, 418.

219. Allen, F. H.; Kennard, O.; Watson, D. G.; Brammer, L.; Orpen, A. G.; Taylor, R. *J. Chem. Soc., Perkin Trans. 2* **1987**, S1.

220. Williams, D. E. *Acta Crystallogr., Sect. B: Struct. Sci* **1973**, *B 29*, 96.

221. Williams, D. E. *J. Am. Chem. Soc.* **1969**, *91*, 1243.

222. Azuma, N. *Bull. Chem. Soc. Jpn.* **1982**, *55*, 1357.

223. Azuma, N.; Tsutsui, K.; Miura, Y.; Higuchi, T. *Bull. Chem. Soc. Jpn.* **1981**, *54*, 3274.

224. Kahn, O., *Molecular Magnetism*. VCH: New York, 1993.

225. Nakatsuji, S.; Kitamura, A.; Takai, A.; Nishikawa, K.; Morimoto, Y.; Yasuoka, N.; Kawamura, H.; Anzai, H. *Z. Naturforsch. B.* **1998**, *53*, 495.

226. Aherne, C. M.; Banister, A. J.; Gorrell, I. B.; Hansford, M. I.; Hauptman, Z. V.; Luke, A. W.; Rawson, J. M. *J. Chem. Soc., Dalton Trans.* **1993**, 967.

227. Fetizon, M.; Golfier, M.; Milcent, R.; Papadakis, I. *Tetrahedron* **1975**, *31*, 165.

228. Fetizon, M.; Golfier, M.; Mourgues, P. *Tetrahedron Lett.* **1972**, 4445.

229. Balogh, V.; Golfier, M.; Fetizon, M. *J. Org. Chem.* **1971**, *36*, 1399.

230. Fetizon, M.; Golfier, M. *C. R. Acad. Sci. Ser. C.* **1968**, *267*, 900.

231. Neugebauer, F. A.; Fischer, H. *Angew. Chem. Int. Ed.* **1980**, *19*, 724.

232. Brook, D. J. R.; Fox, H. H.; Lynch, V.; Fox, M. A. *J. Phys. Chem.* **1996**, *100*, 2066.

233. Bonner, F. C.; Fisher, M. E. *Phys. Rev. A.* **1964**, *135*, 640.

234. Kaszynski, P. *J. Phys. Chem. A.* **2001**, *105*, 7626.

235. Jornet, J.; Deumal, M.; Ribas-Arino, J.; Bearpark, M. J.; Robb, M. A.; Hicks, R. G.; Novoa, J. J. *Chem. Eur. J.* **2006**, *12*, 3995.

236. Neugebauer, F. A.; Trischmann, H.; Taigel, G. *Monatsh. Chem.* **1967**, *98*, 713.

237. Mukai, K.; Yamamoto, T.; Kohno, M.; Azuma, N.; Ishizu, K. *Bull. Chem. Soc. Jpn.* **1974**, *47*, 1797.

238. Ibrahim, Y. A.; Elwahy, A. H. M.; Abbas, A. A. *Tetrahedron* **1994**, *50*, 11489.

239. Neugebauer, F. A.; Brunner, H. *Tetrahedron* **1974**, *30*, 2841.

240. Okada, K.; Beppu, S.; Tanaka, K.; Kuratsu, M.; Furuichi, K.; Kozaki, M.; Suzuki, S.; Shiomi, D.; Sato, K.; Takui, T.; Kitagawa, Y.; Yamaguchi, K. *Chem. Commun.* **2007**, 2485.

241. Clegg, J. K.; Bray, D. J.; Gloe, K.; Gloe, K.; Hayter, M. J.; Jolliffe, K. A.; Lawrance, G. A.; Meehan, G. V.; McMurtrie, J. C.; Lindoy, L. F.; Wenzel, M. *Dalton Trans.* **2007**, 1719.

242. Bennett, M. A.; Byrnes, M. J.; Kovacik, I. *J. Organomet. Chem.* **2004**, *689*, 4463.

243. Wong-Foy, A. G.; Bhalla, G.; Liu, X. Y.; Periana, R. A. *J. Am. Chem. Soc.* **2003**, *125*, 14292.

244. Richert, S. A.; Tsang, P. K. S.; Sawyer, D. T. *Inorg. Chem.* **1989**, *28*, 2471.

245. Tang, H. Y.; Chen, H. Y.; Huang, J. H.; Lin, C. C. *Macromolecules* **2007**, *40*, 8855.

246. Lyashenko, G.; Saischek, G.; Pal, A.; Herbst-Irmer, R.; Mosch-Zanetti, N. C. *Chem. Commun.* **2007**, 701.

247. Lee, W. Y.; Hsieh, H. H.; Hsieh, C. C.; Lee, H. M.; Lee, G. H.; Huang, J. H.; Wu, T. C.; Chuang, S. H. *J. Organomet. Chem.* **2007**, *692*, 1131.

248. Shukla, P.; Gordon, J. C.; Cowley, A. H.; Jones, J. N. *J. Organomet. Chem.* **2005**, *690*, 1366.

249. Yu, R. C.; Hung, C. H.; Huang, J. H.; Lee, H. Y.; Chen, J. T. *Inorg. Chem.* **2002**, *41*, 6450.

250. Bourget-Merle, L.; Lappert, M. F.; Severn, J. R. *Chem. Rev.* **2002**, *102*, 3031.

251. Edelmann, F. T. *Coord. Chem. Rev.* **1994**, *137*, 403.

252. Junk, P. C.; Cole, M. L. *Chem. Commun.* **2007**, 1579.

253. Roesky, P. W. *Chem. Soc. Rev.* **2000**, *29*, 335.

254. Gardiner, M. G.; Hanson, G. R.; Henderson, M. J.; Lee, F. C.; Raston, C. L. *Inorg. Chem.* **1994**, *33*, 2456.

255. Scott, P.; Hitchcock, P. B. *J. Chem. Soc. Chem. Commun.* **1995**, 579.

256. Trifonov, A. A.; Borovkov, I. A.; Fedorova, E. A.; Fukin, G. K.; Larionova, J.; Druzhkov, N. O.; Cherkasov, V. K. *Chem. Eur. J.* **2007**, *13*, 4981.

257. Trifonov, A. A.; Fedorova, E. A.; Ikorskii, V. N.; Dechert, S.; Schumann, H.; Bochkarev, M. N. *Eur. J. Inorg. Chem.* **2005**, 2812.

258. Muresan, N.; Chlopek, K.; Weyhermuller, T.; Neese, F.; Wieghardt, K. *Inorg. Chem.* **2007**, *46*, 5327.

259. Siedle, A. R.; Webb, R. J.; Behr, F. E.; Newmark, R. A.; Weil, D. A.; Erickson, K.; Naujok, R.; Brostrom, M.; Mueller, M.; Chou, S. H.; Young, V. G. *Inorg. Chem.* **2003**, *42*, 932.

260. Dias, H. V. R.; Singh, S. *Inorg. Chem.* **2004**, *43*, 7396.

261. Dias, H. V. R.; Singh, S. *Inorg. Chem.* **2004**, *43*, 5786.

262. Guo, J. P. *Eur. J. Inorg. Chem* **2006**, 3634.

263. Dale, D. *J. Chem. Soc. A.* **1967**, 278.

264. Jameson, G. B.; Muster, A.; Robinson, S. D.; Wingfield, J. N.; Ibers, J. A. *Inorg. Chem.* **1981**, *20*, 2448.

265. Alcock, N. W.; Tasker, P. A. *J. Chem. Soc., Chem. Commun.* **1972**, 1239.

266. Donaldson, P. B.; Haria, P.; Tasker, P. A. *J. Chem. Soc., Dalton Trans.* **1976**, 2382.

267. Donaldson, P. B.; Tasker, P. A.; Alcock, N. W. *J. Chem. Soc., Dalton Trans.* **1976**, 2262.

268. Sigeikin, G. I.; Lipunova, G. N.; Pervova, I. G. *Russ. Chem. Rev.* **2006**, *75*, 885.

269. Brown, D. A.; Bogge, H.; Lipunova, G. N.; Muller, A.; Plass, W.; Walsh, K. G. *Inorg. Chim. Acta* **1998**, *280*, 30.

270. Kawamura, Y.; Deguchi, Y.; Yamauchi, J.; Ohyanishiguchi, H. *Bull. Chem. Soc. Jpn.* **1988**, *61*, 181.

271. Kawamura, Y.; Ohyanishiguchi, H.; Yamauchi, J.; Deguchi, Y. *Bull. Chem. Soc. Jpn.* **1984**, *57*, 1441.

272. Kawamura, Y.; Yamauchi, J.; Ohyanishiguchi, H. *Bull. Chem. Soc. Jpn.* **1993**, *66*, 3593.

273. Kawamura, Y.; Yamauchi, J. *Bull. Chem. Soc. Jpn.* **1995**, *68*, 3041.

274. Kawamura, Y.; Yamauchi, J.; Ohyanishiguchi, H. *Chem. Lett.* **1990**, 1619.

275. Stepanov, B. I.; Avramenko, G. V. *Zh. Obshch. Khim.* **1980**, *50*, 358.

276. Kolodina, T. S.; Avramenko, G. V.; Stepanov, B. I. *Zh. Obshch. Khim.* **1983**, *53*, 1340.

277. Krohn, K.; Micheel, J.; Zukowski, M. *Tetrahedron* **2000**, *56*, 4753.

278. Feldman, K. S.; Quideau, S.; Appel, H. M. *J. Org. Chem.* **1996**, *61*, 6656.

279. Russell, R. A.; Collin, G. J.; Sterns, M.; Warrener, R. N. *Tetrahedron Lett.* **1979**, 4229.

280. Qian, B. X.; Baek, S. W.; Smith, M. R. *Polyhedron* **1999**, *18*, 2405.

281. Park, K. H.; Marshall, W. J. *J. Org. Chem.* **2005**, *70*, 2075.

282. Bandini, M.; Cozzi, P. G.; Monari, M.; Perciaccante, R.; Selva, S.; Umani-Ronchi, A. *Chem. Commun.* **2001**, 1318.

283. Kuhn, N.; Kuhn, A.; Speis, M.; Blaser, D.; Boese, R. *Chem. Ber.* **1990**, *123*, 1301.

284. Connelly, N. G.; Geiger, W. E. *Chem. Rev.* **1996**, *96*, 877.

285. Ammeter, J. H.; Swalen, J. D. *J. Chem. Phys.* **1972**, *57*, 678.

286. Yokota, S.; Tachi, Y.; Nishiwaki, N.; Ariga, M.; Itoh, S. *Inorg. Chem.* **2001**, *40*, 5316.

287. Allen, S. D.; Moore, D. R.; Lobkovsky, E. B.; Coates, G. W. *J. Organometal. Chem.* **2003**, *683*, 137.

288. Shimokawa, C.; Itoh, S. *Inorg. Chem.* **2005**, *44*, 3010.

289. Shimokawa, C.; Tachi, Y.; Nishiwaki, N.; Ariga, M.; Itoh, S. *Bull. Chem. Soc. Jpn* **2006**, *79*, 118.

290. Shimokawa, C.; Yokota, S.; Tachi, Y.; Nishiwaki, N.; Ariga, M.; Itoh, S. *Inorg. Chem.* **2003**, *42*, 8395.

291. Spencer, D. J. E.; Reynolds, A. M.; Holland, P. L.; Jazdzewski, B. A.; Duboc-Toia, C.; Pape, L. L.; Yokota, S.; Tachi, Y.; Itoh, S.; Tolman, W. B. *Inorg. Chem.* **2002**, *41*, 6307.

292. Allen, S. D.; Moore, D. R.; Lobkovsky, E. B.; Coates, G. W. *J. Am. Chem. Soc.* **2002**, *124*, 14284.

293. Moore, D. R.; Cheng, M.; Lobkovsky, E. B.; Coates, G. W. *Angew. Chem. Int. Ed.* **2002**, *41*, 2599.

294. Moore, D. R.; Cheng, M.; Lobkovsky, E. B.; Coates, G. W. *J. Am. Chem. Soc.* **2003**, *125*, 11911.

295. Byrne, C. M.; Allen, S. D.; Lobkovsky, E. B.; Coates, G. W. *J. Am. Chem. Soc.* **2004**, *126*, 11404.

296. Cunningham, C. W.; Burns, G. R.; McKee, V. *J. Chem. Soc., Perkin Trans. 2* **1989**, 1429.

297. Dijkstra, E.; Hutton, A. T.; Harry, M. N.; Irving, H. M. N. H.; Nassimbeni, L. R. *Acta Crystallogr., Sect. B: Struct. Sci* **1982**, *B38*, 535.

298. Polyakova, I. N.; Starikova, Z. A.; Sulim, O. P.; Lipunova, G. N. *Kristallographiya* **1992**, *37*, 653.

299. Preuss, J.; Gieren, A. *Acta Cryst. B* **1975**, *31*, 1276.

300. Hutton, A. T.; Irving, H. M. N. H.; Nassimbeni, L. R.; Gafner, G. *Acta Cryst. B* **1979**, *35*, 1354.

301. Burns, G. R.; Cunningham, C. W.; McKee, V. *J. Chem. Soc., Perkin Trans. 2* **1988**, 1275.

302. Guillerez, J.; Pascard, C.; Prange, T. *J. Chem. Res.* **1978**, 308.

303. Omelchen, Y. A.; Kondrash, Y. D.; Ginzburg, S. L.; Neigauz, M. G. *Kristallografiya* **1974**, *19*, 522.

304. Sherif, O. E. *Monatsh. Chem.* **1997**, *128*, 981.

305. Kuhn, R.; Weitz, H. M. *Chem. Ber.* **1953**, *86*, 1188.

306. Hutton, A. T.; Irving, H. M. N. H. *J. Chem. Soc., Perkin Trans. 2* **1982**, 1117.

307. Abdel-Ghani, N. T.; Issa, Y. M.; Mikosch, H.; Bauer, G. *Microchem. J.* **1999**, *61*, 85.

308. Shawali, A. S.; Elgalil, M. A. *Tetrahedron* **1971**, *27*, 4305.

309. Budesinsky, B. W.; Svec, J. *Inorg. Chem.* **1971**, *10*, 313.

310. Ibrahim, Y. A. *Tetrahedron* **1997**, *53*, 8507.

311. Katritzky, A. R.; Belyakova, S. A.; Durst, H. D. *Tetrahedron Lett.* **1994**, *35*, 6465.

312. Abbas, A. A.; Elwahy, A. H. M. *Synthesis* **2001**, 1331.

313. Ibrahim, Y. A.; Behbehani, H.; Ibrahim, M. R.; Abrar, N. M. *Tetrahedron Lett.* **2002**, *43*, 6971.

314. Elwahy, A. H. M.; Abbas, A. A. *Tetrahedron Lett.* **2006**, *47*, 1303.

315. Galil, F. M. A.; Khalifa, F. A.; Abdin, T. S. *Dyes and Pigments* **1990**, *12*, 49.

316. Hutton, A. T.; Irving, H. M. N. H.; R.Nassimbeni, L. *Acta Crystall., Sect. B: Struct. Sci* **1980**, *36*, 2071.

317. Hutton, A. T.; Irving, H. M. N. H. *J. Chem. Soc., Chem. Commun.* **1980**, 763.

318. Doyle, M. P.; Bryker, W. J. *J. Org. Chem.* **1979**, *44*, 1572.

319. Garribba, E.; Micera, G. *J. Chem. Ed.* **2006**, *83*, 1229.

320. Kitajima, N.; Hikichi, S.; Tanaka, M.; Morooka, Y. *J. Am. Chem. Soc.* **1993**, *115*, 5496.

321. Lopez, G.; Garcia, G.; Sanchez, G.; Garcia, J.; Ruiz, J.; Hermoso, J. A.; Vegas, A.; Martinezripoll, M. *Inorg. Chem.* **1992**, *31*, 1518.

322. Ito, M.; Sakai, K.; Tsubomura, T.; Takita, Y. *Bull. Chem. Soc. Jpn.* **1999**, *72*, 239.

323. Itoh, S.; Bandoh, H.; Nakagawa, M.; Nagatomo, S.; Kitagawa, T.; Karlin, K. D.; Fukuzumi, S. *J. Am. Chem. Soc.* **2001**, *123*, 11168.

324. Shiren, K.; Ogo, S.; Fujinami, S.; Hayashi, H.; Suzuki, M.; Uehara, A.; Watanabe, Y.; Moro-oka, Y. *J. Am. Chem. Soc.* **2000**, *122*, 254.

325. Hill, M. S.; Hitchcock, P. B.; Pongtavornpinyo, R. *Dalton Trans.* **2007**, 731.

326. Fekl, U.; Kaminsky, W.; Goldberg, K. I. *J. Am. Chem. Soc.* **2003**, *125*, 15286.

327. MacAdams, L. A.; Buffone, G. P.; Incarvito, C. D.; Rheingold, A. L.; Theopold, K. H. *J. Am. Chem. Soc.* **2005**, *127*, 1082.

328. Polyakova, I. N.; Starikova, Z. A.; Sulim, O. P.; Lipunova, G. N. *Kristallographiya* **1992**, *37*, 653.

329. Tian, X.; Goddard, R.; Porschke, K. R. *Organometallics* **2006**, *25*, 5854.

330. Bleaney, B.; Bowers, K. D. *Proc. R. Soc. London* **1952**, *A214*, 451.

331. Stroh, C.; Turek, P.; Ziessel, R. *Chem. Commun.* **1998**, 2337.

332. Hase, S.; Shiomi, D.; Sato, K.; Takui, T. *J. Mater. Chem.* **2001**, *11*, 756.

333. Schatzschneider, U.; Weyhermuller, T.; Rentschler, E. *Eur. J. Inorg. Chem.* **2001**, 2569.

334. Rajadurai, C.; Ivanova, A.; Enkelmann, V.; Baumgarten, M. *J. Org. Chem.* **2003**, *68*, 9907.

335. Hayakawa, K.; Shiomi, D.; Ise, T.; Sato, K.; Takui, T. *Chem. Lett.* **2004**, *33*, 1494.

336. Ziessel, R.; Stroh, C.; Heise, H.; Kohler, F. H.; Turek, P.; Claiser, N.; Souhassou, M.; Lecomte, C. *J. Am. Chem. Soc.* **2004**, *126*, 12604.

337. Zoppellaro, G.; Enkelmann, V.; Geies, A.; Baumgarten, M. *Org. Lett.* **2004**, *6*, 4929.

338. Stroh, C.; Ziessel, R.; Raudaschl-Sieber, G.; Kohler, F. H.; Turek, P. *J. Mater. Chem.* **2005**, *15*, 850.

339. Catala, L.; Le Moigne, J.; Kyritsakas, N.; Rey, P.; Novoa, J. J.; Turek, P. *Chem. Eur. J.* **2001**, *7*, 2466.

340. Hayakawa, K.; Shiomi, D.; Ise, T.; Sato, K.; Takui, T. *J. Mater. Chem.* **2006**, *16*, 4146.

341. Tukada, H. *J. Am. Chem. Soc.* **1991**, *113*, 8991.

342. Tukada, H.; Mutai, K. *Tet. Lett.* **1992**, *33*, 6665.

343. Caneschi, A.; Chiesi, P.; David, L.; Ferraro, F.; Gatteschi, D.; Sessoli, R. *Inorg. Chem.* **1993**, *32*, 1445.

344. Shultz, D. A.; Boal, A. K.; Lee, H.; Farmer, G. T. *J. Org. Chem.* **1999**, *64*, 4386.

345. Kuhn, R.; Neugebauer, F. A.; Trischmann, H. *Mon. Chem.* **1966**, *97*, 525.

346. Mukai, K.; Azuma, N.; Shikata, H.; Ishizu, K. *Bull. Chem. Soc. Jpn.* **1970**, *43*, 3958.

347. Kopf, P.; Morokuma, K.; Kreilick, R. *J. Chem. Phys.* **1971**, *54*, 105.

348. Azuma, N.; Ishizu, K.; Mukai, K. *J. Chem. Phys.* **1974**, *61*, 2294.

349. Fico, R. M.; Hay, M. F.; Reese, S.; Hammond, S.; Lambert, E.; Fox, M. A. *J. Org. Chem.* **1999**, *64*, 9386.

350. Neugebauer, F. A.; Fischer, H.; Meier, P. *Chem. Ber.-Recl.* **1980**, *113*, 2049.

351. Brook, D. J. R.; Yee, G. T. *J. Org. Chem.* **2006**, *71*, 4889.

352. Brook, D. J. R.; Fornell, S.; Stevens, J. E.; Noll, B.; Koch, T. H.; Eisfeld, W. *Inorg. Chem.* **2000**, *39*, 562.

353. Barr, C. L.; Chase, P. A.; Hicks, R. G.; Lemaire, M. T.; Stevens, C. L. *J. Org. Chem.* **1999**, *64*, 8893.

354. Berson, J. A., *The Chemistry of Quinonoid Compounds.* Wiley: 1988; 'Vol.' II, Chapter 10.

355. Nakazono, S.; Karasawa, S.; Koga, N.; Iwamura, H. *Angew. Chem. Int. Ed.* **1998**, *37*, 1550.

356. Rajca, A. *Chem. Rev.* **1994**, *94*, 871.

357. Carlin, R. L., *Magnetochemistry*. Springer-Verlag: New York, 1986.

358. Gatteschi, D.; Laugier, J.; Rey, P.; Zanchini, C. *Inorg. Chem.* **1987**, *26*, 938.

359. Okazawa, A.; Nogami, T.; Ishida, T. *Chem. Mater.* **2007**, *19*, 2733.

360. Osanai, K.; Okazawa, A.; Nogami, T.; Ishida, T. *J. Am. Chem. Soc.* **2006**, *128*, 14008.

361. Anderson, O. P.; Kuechler, T. C. *Inorg. Chem.* **1980**, *19*, 1417.

362. Caneschi, A.; Gatteschi, D.; Grand, A.; Laugier, J.; Pardi, L.; Rey, P. *Inorg. Chem.* **1988**, *27*, 1031.

363. Cogne, A.; Laugier, J.; Luneau, D.; Rey, P. *Inorg. Chem.* **2000**, *39*, 5510.

364. Caneschi, A.; Gatteschi, D.; Sessoli, R.; Rey, P.; Cabello, C. I. *J. Mater. Chem.* **1992**, *2*, 1283.

365. Brook, D. J. R.; Fornell, S.; Noll, B.; Yee, G. T.; Koch, T. H. *J. Chem. Soc. Dalton Trans.* **2000**, 2019.

366. Brook, D. J. R.; Lynch, V.; Conklin, B.; Fox, M. A. *J. Am. Chem. Soc.* **1997**, *119*, 5155.

367. Wu, J. Z.; Bouwman, E.; Reedijk, J.; Mills, A. M.; Spek, A. L. *Inorg. Chim. Acta* **2003**, *351*, 326.

368. Marsh, W. E.; Patel, K. C.; Hatfield, W. E.; Hodgson, D. J. *Inorg. Chem.* **1983**, *22*, 511.

369. Alves, W. A.; Santos, R.; Paduan-Filho, A.; Becerra, C. C.; Borin, A. C.; Ferreira, A. *Inorg. Chim. Acta* **2004**, *357*, 2269.

370. Liu, Z. L.; Li, L. C.; Liao, D. Z.; Jiang, Z. H.; Yan, S. P. *Cryst. Growth Des.* **2005**, *5*, 783.

371. Liu, Z.; Lu, Z.; Zhang, D.; Jiang, Z.; Li, L.; Liu, C.; Zhu, D. *Inorg. Chem.* **2004**, *43*, 6620.

372. Cramer, C. J.; Tolman, W. B. *Acc. Chem. Res.* **2007**, *40*, 601.

373. Adams, D. M.; Dei, A.; Rheingold, A. L.; Hendrickson, D. N. *J. Am. Chem. Soc.* **1993**, *115*, 8221.

Appendix A: Experimental considerations

A-1 General considerations

NMR spectra were recorded on a 300 or 500 MHz Bruker instrument. Infrared spectra were recorded as KBr pellets using a Perkin Elmer Spectrum One instrument. Electronic spectra were recorded using a Cary 50 Scan instrument. EPR spectra of microcrystalline samples were recorded in capillary tubes on a Bruker AMX360 spectrometer. Elemental analysis was carried out by Canadian Microanalytical Services Ltd., Vancouver, BC. Mass spectra were recorded using a Kratos Concept H spectrometer using electron impact (EI), or liquid secondary (LSIMS) ionization sources. Melting points were recorded (uncorrected) using a Gallenkamp melting point apparatus.

A-2 Magnetic measurements

Variable temperature magnetic data (2-300K) were collected using a Quantum Design MPMS SQUID magnetometer operating at field strengths of 1 and 5 T. Diamagnetic corrections were made by subtracting the magnetic susceptibility of the corresponding radical precursor (**4.7a** and **4.7b**), Pascal's constants (**4.13**), or the slope of the paramagnetic regime of the raw magnetic moment data (**2.3j**, **2.4e**, **4.15**, and **4.16**) from the raw magnetic susceptibility data.

A-3 Electrochemistry experiments

Cyclic voltammetry experiments were performed with a Bioanalytical Systems CV50 voltammetric analyzer. Typical electrochemical cells consisted of a three-electrode setup including a glassy carbon working electrode, platinum counter electrode, and silver reference. Acetonitrile solutions of analyte (~1 mM) and electrolyte (0.1 M

$Bu_4N^+BF_4^-$) were referenced against an internal standard (~1 mM Ferrocene/Ferrocenium) at a scan rate of 100 mV/s (Chapter 2 and 3) or 250 mV/s (Chapter 4).

A-4 Crystal structure determinations

X-ray diffraction data was collected on a Bruker PLATFORM/SMART 1000 CCD with graphite-monochromatized Mo-Kα radiation (λ = .71073Å) by Dr. Brian O. Patrick at the University of British Columbia or by Dr. Robert McDonald or Dr. Michael J. Ferguson at the University of Alberta. The crystal structures were solved by direct methods (SHELXS-97).

A-5 Variable temperature EPR experiments

Variable temperature EPR spectra were recorded in deoxygenated (three freeze-pump-thaw cycles) toluene solutions (~10^{-4}M) on a Bruker AMX360 spectrometer equipped with a helium cryostat by Dr. Pierre Kennepohl at the University of British Columbia, and spectra obtained simulated with WinEPR SimFonia.

A-6 DFT calculations

Density Functional Theory (DFT) calculations were carried out using Gaussian-03W by Mark S. Zsombor at the University of Victoria. The calculations were performed using the 6-31G(d,p) basis set at UB3LYP level of theory.

Appendix B: DFT calculation output parameters

Table B-1. Output paramaters for **2.3a.**


```
1|1|UNPC-UNK|FOpt|UB3LYP|6-31G(d,p)|C20H17N4(2)|PCUSER|03-Nov-2007|0||
 # OPT UB3LYP/6-31G(D,P) GEOM=CONNECTIVITY||Untitled-2||0,2|N,-1.149348
 2708,-0.3905263466,-0.648760176|N,-1.15059122,-0.4065582516,0.70154851
 5|C,0.0593133175,-0.4127647074,1.2812534719|N,1.2281237875,-0.19695446
 85,0.658942086|N,1.1761130982,-0.1856053445,-0.6904131572|C,0.05184838
 52,-0.8574533559,-1.3232729479|C,2.2713136462,0.3326889671,-1.40261329
 73|C,-2.3428853165,-0.0738725816,-1.3199691868|C,0.0990314703,-0.56331
 49357,2.7580876801|C,-2.5545303552,-0.4544321783,-2.656600165|C,-3.741
 6288995,-0.1080440941,-3.3002502353|C,-4.7377356874,0.5990958812,-2.62
 81498468|C,-4.5324300359,0.9597791594,-1.2933385466|C,-3.3493853208,0.
 6353216183,-0.6394629819|C,3.1619012218,1.2090074566,-0.7560777232|C,4
 .2460273787,1.7332109434,-1.4505569311|C,4.463647816,1.4098047957,-2.7
 929481241|C,3.5832269109,0.5373523227,-3.4314460785|C,2.4985806799,-0.
 0091838576,-2.747111068|C,-1.0852474445,-0.7457750304,3.4885220342|C,-
 1.0455251022,-0.8845618725,4.8741902981|C,0.1741773562,-0.8480656391,5
 .5526916089|C,1.3565833092,-0.672884429,4.8311669671|C,1.3221659274,-0
 .5336297936,3.4454037235|H,0.0092441457,-0.5876026119,-2.3741491747|H,
 0.150009679,-1.9494800103,-1.2154826309|H,-1.8188593119,-1.0420647076,
 -3.1943362861|H,-3.8888539254,-0.4098129925,-4.3330723193|H,-5.6612686
 97,0.8621958861,-3.1338201945|H,-5.2986479251,1.5107987859,-0.75572840
 02|H,-3.1803295603,0.9219619824,0.3904513131|H,2.982056937,1.464896379
 7,0.2800896305|H,4.922753562,2.4113462059,-0.9387841029|H,5.3084152293
 ,1.8286980413,-3.3302876133|H,3.7441312998,0.2627432604,-4.469791295|H
 ,1.8583064772,-0.7180271853,-3.2602130436|H,-2.0304585773,-0.778841683
 7,2.9590506|H,-1.9710855604,-1.0243009819,5.4255380718|H,0.2033113221,
 -0.9591482414,6.6327865236|H,2.3113173758,-0.6469289117,5.3488374742|H
 ,2.2391802218,-0.4025943514,2.8825786654||Version=x86-Win32-G03RevB.04
 |State=2-A|HF=-991.3246112|S2=0.775486|S2-1=0.|S2A=0.750327|RMSD=8.143
 e-009|RMSF=2.919e-006|Dipole=-0.0081014,-0.1231352,-1.0578648|PG=C01 [
 X(C20H17N4)]||@
```

Table B-2. Output parameters for **2.4a**.

1|1|UNPC-UNK|FOpt|UB3LYP|6-31G(d,p)|C20H15N4O1(2)|PCUSER|05-Nov-2007|0
||# OPT UB3LYP/6-31G(D,P) GEOM=CONNECTIVITY||Triphenyl Oxyverdizyl||0,
2|N,0.,0.,0.|N,0.0156112182,1.3662965119,0.0301960896|C,1.2195233576,1
.9383116345,0.0263762915|N,2.3927631224,1.3083220164,-0.0305610946|N,2
.3387378019,-0.0543338584,-0.120959678|C,1.1497015509,-0.7979013602,-0
.0945392339|C,3.6197143043,-0.7052526063,-0.1370040615|C,-1.3124823006
,-0.5837466296,-0.0385165052|C,1.257403261,3.422768799,0.0919750643|C,
-1.5970190366,-1.7901714748,0.6120934403|C,-2.8950105167,-2.2967610071
,0.5712585073|C,-3.9077857612,-1.6135977047,-0.1026461655|C,-3.6159520
539,-0.4074948018,-0.7416216644|C,-2.3237559344,0.1106585254,-0.712918
9512|C,4.6635045263,-0.1253811641,0.5937097314|C,5.927582157,-0.709149
5994,0.5737176064|C,6.1590929031,-1.8674864489,-0.1697871554|C,5.11438
70587,-2.4361124939,-0.8990521424|C,3.8439604879,-1.8624827854,-0.8921
518276|C,0.0858037314,4.1522163075,0.3434443646|C,0.1242838065,5.54344
11232,0.4040857929|C,1.32887775,6.2237478485,0.2157532785|C,2.49770113
61,5.5022596224,-0.0345257193|C,2.4651775624,4.1109570221,-0.096846488
8|O,1.1186673328,-2.0140862182,-0.1482834531|H,-0.8162395069,-2.325658
044,1.1329595352|H,-3.1120948238,-3.2323843815,1.0775746976|H,-4.91555
65758,-2.0166763995,-0.1288033572|H,-4.3947774698,0.1338424504,-1.2702
180405|H,-2.0882123221,1.0485245451,-1.2002507505|H,4.4749106633,0.776
6436735,1.1623478359|H,6.7317624842,-0.2568655829,1.1462229316|H,7.144
977954,-2.3220757101,-0.1815309886|H,5.2847125802,-3.333270161,-1.4863
937099|H,3.0381189998,-2.3095057499,-1.4564691089|H,-0.8461269316,3.61
98396797,0.494059441|H,-0.7888027603,6.0972066896,0.6019672256|H,1.356
5562567,7.3084273739,0.2636861677|H,3.4382350221,6.0241136802,-0.18487
46273|H,3.3691370514,3.547184936,-0.2959012874||Version=x86-Win32-G03R
evB.04|State=2-A|HF=-1065.3646033|S2=0.773115|S2-1=0.|S2A=0.750236|RMS
D=8.412e-009|RMSF=2.121e-006|Dipole=0.0043943,-0.007041,0.3171674|PG=C
01 [X(C20H15N4O1)]||@

Table B-3. Output parameters for **2.4c**.

1|1|UNPC-UNK|FOpt|UB3LYP|6-31G(d,p)|C14H19N4O1(2)|PCUSER|19-Feb-2007|0
||# OPT UB3LYP/6-31G(D,P) GEOM=CONNECTIVITY||Phenyl-Di Iso-propyl Verd
azyl Radical||0,2|C,-1.2139308474,0.0000132966,2.7944464046|C,-1.21377
98419,0.000029964,4.1874889851|C,-0.008642418,0.0000233381,4.892291626
1|C,1.1989775755,0.0000009932,4.1917515304|C,1.2040506197,-0.000012981
6,2.7987180206|C,-0.0036824188,-0.0000068509,2.0847208076|C,-0.0010569
733,-0.0000257708,0.5984915721|N,1.1892252685,-0.0001463254,-0.0073121
685|N,1.1644896041,-0.0001900507,-1.367807159|C,0.0037725817,-0.000233
6463,-2.1356773163|N,-1.1596498086,-0.0000212823,-1.3719125228|N,-1.18
91918252,0.000074645,-0.0115134227|C,-2.4795258195,0.0001907471,-2.042
2007019|O,0.0059353428,-0.000042939,-3.3599389078|C,-3.2501477571,1.27
55573881,-1.6883945966|C,-3.2505899243,-1.2748796581,-1.6882885478|C,2
.4867252921,-0.0001807119,-2.0334283751|C,3.2563355603,-1.2753736235,-
1.6768140679|C,3.2562913214,1.2750634698,-1.6768826136|H,-2.1477872396
,0.0000167039,2.2448746298|H,-2.1582601041,0.0000456057,4.7238275757|H
,-0.0105612809,0.0000357089,5.9783802039|H,2.1415569675,-0.0000025235,
4.7314238049|H,2.1398430166,-0.0000283483,2.2524493121|H,-2.2408238418
,0.0001032289,-3.1063645282|H,-4.2093461721,1.2862010536,-2.2146873627
|H,-2.6888219991,2.1667747991,-1.9838128141|H,-3.4427846674,1.32676933
61,-0.6135227746|H,-4.2097936957,-1.2852296629,-2.2145769176|H,-3.4432
4233,-1.325939001,-0.6134115232|H,-2.6895757683,-2.1663157177,-1.98363
85697|H,2.2517841166,-0.0002141868,-3.0984288361|H,4.217388955,-1.2858
671795,-2.1997143036|H,2.6962287988,-2.1667197503,-1.9741513343|H,3.44
51832887,-1.3264719919,-0.6012645792|H,4.2173466141,1.2855635915,-2.19
97798147|H,3.445136115,1.3262364201,-0.6013355665|H,2.6961521106,2.166
3707988,-1.974274793||Version=x86-Win32-G03RevB.04|State=2-A|HF=-839.1
647948|S2=0.773877|S2-1=0.|S2A=0.750199|RMSD=6.007e-009|RMSF=2.945e-00
5|Dipole=-0.0005583,-0.0000326,0.313008|PG=C01 [X(C14H19N4O1)]||@

Appendix C: Crystallographic parameters

Table C-1. Crystallographic parameters

	2.1d	**2.1j**	**2.3j**	**2.4c**
formula	$C_{20}H_{18}N_4$	$C_{21}H_{20}N_4$	$C_{22}H_{21}N_4$	$C_{13}H_{18}N_5O$
FW	314.38	328.41	341.43	260.32
Dimensions (mm)	0.30 × 0.28 × 0.28	0.10 × 0.25 × 0.50	0.65 × 0.09 × 0.06	0.68 × 0.12 × 0.10
a (Å)	11.7762 (8)	7.830(1)	8.6889 (17)	5.1997 (13)
b (Å)	13.4272 (9)	21.154(2)	22.319 (4)	26.482 (7)
c (Å)	12.0220 (8)	22.289(3)	9.4504 (19)	10.429 (3)
α (deg)	90.0	90.0	90.0	90.0
β (deg)	118.5943 (12)	90.0	90.0	103.785 (4)
γ (deg)	90.0	90.0	90.0	90.0
volume ($Å^3$)	1669.08 (19)	3691.9(8)	1832.7 (6)	1394.7 (6)
ρ_{calc} ($g \cdot cm^{-3}$)	1.251	1.182	1.237	1.240
system	monoclinic	orthorhombic	orthorhombic	monoclinic
space group	*P*2$_1$/*c* (No. 14)	*Pbca* (No. 61)	*Pnma* (No. 62)	*P*2$_1$/*c* (No. 14)
Z	4	8	4	4
μ (mm^{-1})	0.077	0.072	0.075	0.084
T (K)	193.15	296.15	193.15	193.15
$2\theta_{max}$ (deg)	52.80	45.2	52.92	52.82
unique reflections	3429 $R_{int} = 0.0310$	2431 $R_{int} = 0.055$	1926 $R_{int} = 0.0936$	2853 $R_{int} = 0.0706$
R_1[a]	0.0503	0.141	0.0451	0.0524
wR_2[b]	0.1364	0.178	0.1135	0.1187

[a] $R_1 = \Sigma\,(|F_0|-|F_c|)/\Sigma|F_0|$, [b] $wR_2 = [\Sigma w(|F_0|-|F_c|)^2/\Sigma w(|F_0|)^2]^{1/2}$

Table C-1. continued, Crystallographic parameters

	3.15d	**3.15j**	**3.17d**	**3.17e·0.5C$_7$H$_8$**
formula	$C_{24}H_{23}BN_4O_4$	$C_{25}H_{25}BN_4O_4$	$C_{20}H_{23}N_5$	$C_{17.5}H_{15}N_5O_2$
FW	442.27	456.30	333.43	327.35
Dimensions (mm)	0.52 × 0.15 × 0.13	0.38 × 0.27 × 0.23	0.42 × 0.21 × 0.10	0.36 × 0.22 × 0.13
a (Å)	10.3612 (15)	9.8688 (13)	7.1370(5)	8.3409(9)
b (Å)	14.925 (2)	10.6690 (14)	16.3529(12)	8.8321(10)
c (Å)	15.608 (2)	12.4677 (17)	30.754(2)	12.5426(14)
α (deg)	103.098 (2)	87.363 (2)	90	71.5642(18)
β (deg)	97.538 (3)	80.634 (2)	90	85.3860(18)
γ (deg)	95.549 (3)	66.5696 (18)	90	70.4702(17)
volume (Å^3)	2310.5 (6)	1188.2 (3)	3589.3(4)	825.80 (16)
ρ_{calc} (g·cm^{-3})	1.271	1.275	1.234	1.316
system	triclinic	triclinic	orthorhombic	triclinic
space group	$P\bar{1}$ (No. 2)	$P\bar{1}$ (No. 2)	*Pbca* (No. 61)	$P\bar{1}$ (No. 2)
Z	4	2	8	2
μ (mm^{-1})	0.087	0.087	0.076	0.090
T (K)	193.15	193.15	193.15	193.15
$2\theta_{max}$ (deg)	53.00	52.84	52.80	52.78
unique reflections	9430 R_{int} = 0.0505	4822 R_{int} = 0.0224	3671 R_{int} = 0.0614	3353 R_{int} = 0.0222
R_1[a]	0.0514	0.0394	0.0466	0.0410
wR_2[b]	0.1460	0.1117	0.1547	0.1219

[a] $R_1 = \Sigma\,(|F_0|-|F_c|)/\Sigma|F_0|$, [b] $wR_2 = [\Sigma w(|F_0|-|F_c|)^2/\Sigma w(|F_0|)^2]^{1/2}$

Table C-1. continued, Crystallographic parameters

	3.17f	**3.18b**	**3.18d**	**3.19**
formula	$C_{16}H_{15}N_5O_2$	$C_{15}H_{15}N_5O_2$	$C_{19}H_{23}N_5O_2$	$C_{16}H_{14}N_5O_2CuCl$
FW	309.33	297.32	353.42	407.31
Dimensions (mm)	0.52 × 0.20 × 0.10	0.52 × 0.12 × 0.06	0.63 × 0.17 × 0.12	0.02 × 0.05 × 0.50
a (Å)	7.1822 (9)	7.2118(10)	8.9215 (13)	13.328(2)
b (Å)	10.8832 (14)	9.8215(14)	9.2825 (14)	7.1885(6)
c (Å)	11.6087 (12)	11.7772(16)	12.9559 (19)	17.422(2)
α (deg)	62.139 (9)	110.419(2)	77.929 (2)	90.0
β (deg)	74.242 (8)	96.245(2)	78.539 (2)	91.044(3)
γ (deg)	72.220 (9)	105.752(2)	63.853 (2)	90.0
volume ($Å^3$)	754.90 (16)	733.01(18)	934.9 (2)	1668.8(3)
ρ_{calc} ($g \cdot cm^{-3}$)	1.361	1.347	1.256	1.621
system	triclinic	triclinic	triclinic	monoclinic
space group	$P\bar{1}$ (No. 2)	$P\bar{1}$ (No. 2)	$P\bar{1}$ (No. 2)	$P2_1/n$ (No. 14)
Z	2	2	2	4
μ (mm^{-1})	0.094	0.094	0.085	0.1489
T (K)	193.15	193.15	193.15	173.15
$2\theta_{max}$ (deg)	50.00	52.76	52.72	50.1
unique reflections	2571 $R_{int} = 0.0303$	2972 $R_{int} = 0.0289$	3766 $R_{int} = 0.0229$	2942 $R_{int} = 0.074$
R_1[a]	0.0644	0.0474	0.0496	0.073
wR_2[b]	0.1829	0.1370	0.1469	0.088

[a] $R_1 = \Sigma\,(|F_0|-|F_c|)/\Sigma|F_0|$, [b] $wR_2 = [\Sigma w(|F_0|-|F_c|)^2/\Sigma w(|F_0|)^2]^{1/2}$

Table C-1. continued, Crystallographic parameters

	3.20a·CH_2Cl_2	**3.20b·CH_2Cl_2**	**3.21·1.25CH_2Cl_2**	**3.22**
formula	$C_{25}H_{20}Cl_2FeN_7O_2$	$C_{25}H_{20}Cl_2CoN_7O_2$	$C_{37.25}H_{40.5}N_{10}O_2Ni_2Cl_{2.5}$	$C_{30}H_{28}N_{10}O_4Ni$
FW	577.23	580.31	866.34	651.33
Dimensions (mm)	0.38 × 0.34 × 0.23	0.66 × 0.42 × 0.33	0.15 × 0.25 × 0.50	0.05 × 0.12 × 0.30
a (Å)	9.0144 (6)	8.9601 (8)	15.3752(8)	12.5875(13)
b (Å)	9.3053 (6)	9.3250 (8)	16.4725(8)	7.4705(9)
c (Å)	15.8871 (11)	15.8258 (13)	10.6976(5)	16.707(2)
α (deg)	73.7154 (8)	73.4386 (10)	90.0	90.0
β (deg)	87.5893 (9)	87.6027 (10)	132.934(2)	103.689(4)
γ (deg)	87.5292 (9)	87.5323 (11)	90.0	90.0
volume ($Å^3$)	1277.36 (15)	1265.66 (19)	1983.6(2)	1526.4(3)
ρ_{calc} ($g \cdot cm^{-3}$)	1.501	1.523	1.450	1.417
system	triclinic	triclinic	monoclinic	monoclinic
space group	$P\bar{1}$ (No. 2)	$P\bar{1}$ (No. 2)	$C2/m$ (No. 12)	$P2_1/c$ (No. 14)
Z	2	2	2	2
μ (mm^{-1})	0.837	0.927	0.1164	0.0689
T (K)	193.15	193.15	173.15	173.15
$2\theta_{max}$ (deg)	52.76	52.70	55.9	50.2
unique reflections	5180 $R_{int} = 0.0178$	5083 $R_{int} = 0.0119$	2444 $R_{int} = 0.028$	2692 $R_{int} = 0.073$
R_1[a]	0.0492	0.0496	0.036	0.041
wR_2[b]	0.1510	0.1468	0.097	0.071

[a] $R_1 = \Sigma (|F_0|-|F_c|)/\Sigma|F_0|$, [b] $wR_2 = [\Sigma w(|F_0|-|F_c|)^2/\Sigma w(|F_0|)^2]^{1/2}$

Table C-1. continued, Crystallographic parameters

	3.24·0.5C_5H_{12}	**3.25b**	**3.25d**	**4.7a**
formula	$C_{40.5}H_{52}N_{10}Ni_2O_6$	$C_{20}H_{15}F_6N_5O_4Pd$	$C_{24}H_{23}F_6N_5O_4Pd$	$C_{22}H_{32}N_8O_2$
FW	892.34	609.77	665.87	440.56
Dimensions (mm)	0.54 × 0.41 × 0.16	0.53 × 0.41 × 0.30	0.35 × 0.15 × 0.06	0.29 × 0.27 × 0.07
a (Å)	11.6602 (14)	11.7149 (9)	11.8370 (17)	26.760 (6)
b (Å)	19.801 (2)	13.8658 (11)	13.2420 (19)	5.9051 (12)
c (Å)	19.807 (2)	16.2625 (13)	17.729 (3)	16.435 (3)
α (deg)	90.0	87.9598 (10)	90.0	90.0
β (deg)	92.5918 (16)	72.3284 (10)	99.234 (2)	112.993 (3)
γ (deg)	90.0	66.5383 (9)	90.0	90.0
volume ($Å^3$)	4568.5 (9)	2297.9 (3)	2743.0 (7)	2390.7 (8)
ρ_{calc} ($g \cdot cm^{-3}$)	1.297	1.763	1.612	1.224
system	monoclinic	triclinic	monoclinic	monoclinic
space group	*C*2/*c* (No. 15)	$P\bar{1}$ (No. 2)	$P2_1/c$ (No. 14)	*C*2/*c* (No. 15)
Z	4	4	4	4
μ (mm^{-1})	0.878	0.894	0.756	0.083
T (K)	193.15	193.15	193.15	193.15
$2\theta_{max}$ (deg)	55.32	54.98	55.26	50.50
unique reflections	5301 R_{int} = 0.0300	10380 R_{int} = 0.0108	12120 R_{int} = 0.000[c]	2160 R_{int} = 0.0533
R_1[a]	0.0372	0.0247	0.0545	0.0589
wR_2[b]	0.1035	0.0646	0.1335	0.1661

[a] $R_1 = \Sigma (|F_0|-|F_c|)/\Sigma|F_0|$, [b] $wR_2 = [\Sigma w(|F_0|-|F_c|)^2/\Sigma w(|F_0|)^2]^{1/2}$, [c] crystals displayed non merohedral twinning and were indexed with CELL_NOW.

Table C-1. continued, Crystallographic parameters

	4.7b	**4.13**	**4.14**	**4.15**
formula	$C_{22}H_{32}N_8O_2$	$C_9H_{10}Cl_2CuN_5O$	$C_{13}H_{18}Cl_2CuN_5O$	$C_{18}H_{13}CuF_{12}N_6O_5$
FW	440.56	338.66	394.76	684.88
Dimensions (mm)	0.57 × 0.38 × 0.20	0.45 × 0.39 × 0.33	0.52 × 0.45 × 0.37	0.46 × 0.16 × 0.07
a (Å)	25.546 (3)	14.9568 (12)	17.2769 (13)	9.8110 (9)
b (Å)	9.3143 (9)	9.9809 (8)	10.7994 (8)	10.9073 (10)
c (Å)	21.518 (2)	17.3231 (14)	17.8486 (14)	12.5202 (12)
α (deg)	90.0	90.0	90.0	78.5653 (14)
β (deg)	106.528 (2)	90.0	90.0	83.4835 (14)
γ (deg)	90.0	90.0	90.0	73.6999 (14)
volume ($Å^3$)	4908.6 (8)	2586.0 (4)	3330.2 (4)	1258.0 (2)
ρ_{calc} ($g \cdot cm^{-3}$)	1.192	1.740	1.575	1.808
system	monoclinic	orthorhombic	orthorhombic	triclinic
space group	*I*2/*a* (No. 15)	*Pbca* (No. 61)	*Pbca* (No. 61)	$P\bar{1}$
Z	8	8	8	2
μ (mm^{-1})	0.081	2.096	1.640	1.000
T (K)	193.15	193.15	193.15	193.15
$2\theta_{max}$ (deg)	52.82	52.74	52.78	52.86
unique reflections	5046 R_{int} = 0.0266	2639 R_{int} = 0.0220	3417 R_{int} = 0.0202	5142 R_{int} = 0.0305
R_1[a]	0.0462	0.0230	0.0488	0.0453
wR_2[b]	0.1376	0.0656	0.1137	0.1302

[a] $R_1 = \Sigma\,(|F_0|-|F_c|)/\Sigma|F_0|$, [b] $wR_2 = [\Sigma w(|F_0|-|F_c|)^2/\Sigma w(|F_0|)^2]^{1/2}$

Appendix D: Complete listing of bond lengths and angles

Table D-1. Bond lengths (Å) and angles (deg) for **2.1d**.

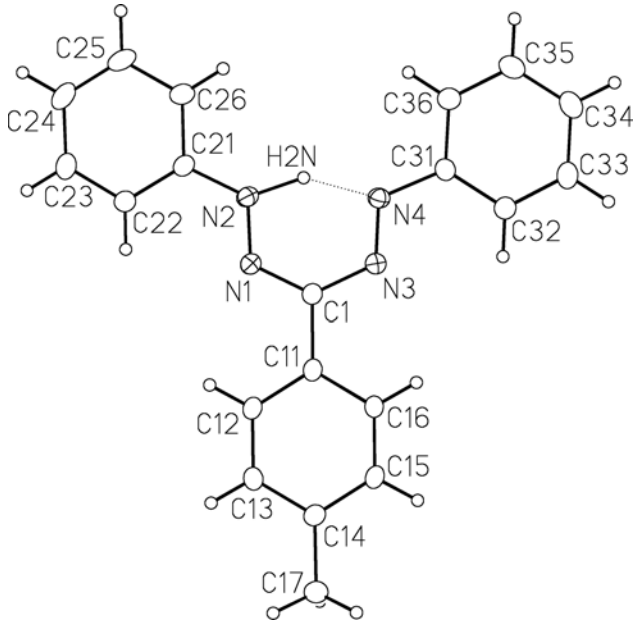

N1	N2	1.3123(19)	
N1	C1	1.338(2)	
N2	C21	1.398(2)	
N2	H2N	1.16(2)	
N3	N4	1.2859(19)	
N3	C1	1.373(2)	
N4	C31	1.412(2)	
N4	H2N	1.52(2)†	
C1	C11	1.474(2)	
C11	C12	1.392(2)	
C11	C16	1.397(2)	
C12	C13	1.377(3)	
C13	C14	1.393(2)	
C14	C15	1.389(2)	
C14	C17	1.494(2)	
C15	C16	1.374(3)	
C21	C22	1.387(2)	
C21	C26	1.390(2)	
C22	C23	1.378(2)	
C23	C24	1.378(3)	
C24	C25	1.377(3)	
C25	C26	1.375(3)	
C31	C32	1.390(3)	
C31	C36	1.392(3)	
C32	C33	1.376(3)	
C33	C34	1.383(3)	
C34	C35	1.371(3)	
C35	C36	1.376(3)	
N2	N1	C1	118.65(15)
N1	N2	C21	118.78(15)
N1	N2	H2N	106.2(12)
C21	N2	H2N	134.8(12)
N4	N3	C1	118.36(14)
N3	N4	C31	116.09(15)
N3	N4	H2N	102.2(9)†
C31	N4	H2N	141.7(9)†
N1	C1	N3	128.39(15)
N1	C1	C11	116.38(15)
N3	C1	C11	115.19(15)

C1	C11	C12	122.02(16)
C1	C11	C16	121.20(15)
C12	C11	C16	116.79(16)
C11	C12	C13	121.64(17)
C12	C13	C14	121.50(17)
C13	C14	C15	116.85(16)
C13	C14	C17	121.85(17)
C15	C14	C17	121.30(17)
C14	C15	C16	121.84(17)
C11	C16	C15	121.39(17)
N2	C21	C22	123.80(16)
N2	C21	C26	116.58(17)
C22	C21	C26	119.59(17)
C21	C22	C23	119.57(17)
C22	C23	C24	120.9(2)
C23	C24	C25	119.31(19)
C24	C25	C26	120.7(2)
C21	C26	C25	119.9(2)
N4	C31	C32	123.88(16)
N4	C31	C36	116.50(16)
C32	C31	C36	119.62(17)
C31	C32	C33	119.50(18)
C32	C33	C34	120.7(2)
C33	C34	C35	119.8(2)
C34	C35	C36	120.4(2)
C31	C36	C35	120.00(19)
N2	H2N	N4	146(2)†

Table D-2. Bond lengths (Å) and angles (deg) for **2.1j**.

C1	N1	1.350(4)
C1	N3	1.364(5)
C1	C11	1.464(5)
C11	C12	1.378(5)
C11	C16	1.403(5)
C12	C13	1.385(5)
C12	H12	0.9300
C13	C14	1.374(6)
C13	H13	0.9300
C14	C15	1.379(6)
C14	H14	0.9300
C15	C16	1.387(6)
C15	H15	0.9300

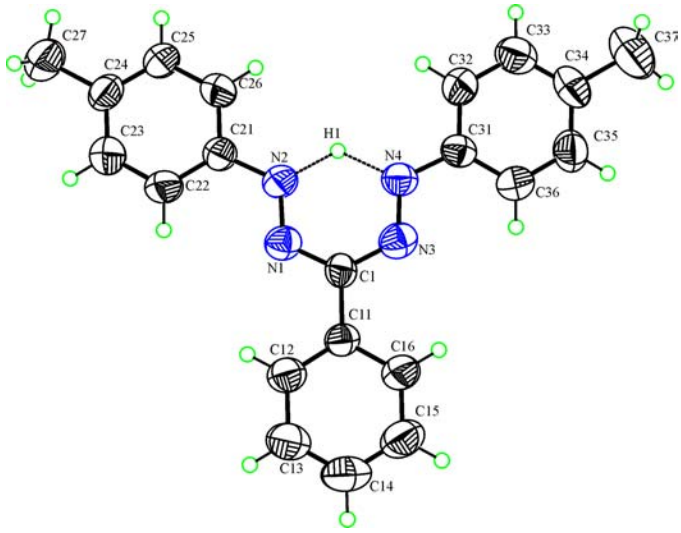

C16	H16	0.9300	
C21	C26	1.374(5)	
C21	C22	1.379(5)	
C21	N2	1.417(5)	
C22	C23	1.388(5)	
C22	H22	0.9300	
C23	C24	1.377(5)	
C23	H23	0.9300	
C24	C25	1.368(5)	
C24	C27	1.519(5)	
C25	C26	1.390(5)	
C25	H25	0.9300	
C26	H26	0.9300	
C27	H27A	0.9600	
C27	H27B	0.9600	
C27	H27C	0.9600	
C27	H27D	0.9600	
C27	H27E	0.9600	
C27	H27F	0.9600	
C31	C32	1.377(5)	
C31	C36	1.390(5)	
C31	N4	1.406(5)	
C32	C33	1.381(6)	
C32	H32	0.9300	
C33	C34	1.375(6)	
C33	H33	0.9300	
C34	C35	1.374(6)	
C34	C37	1.503(6)	
C35	C36	1.376(6)	
C35	H35	0.9300	
C36	H36	0.9300	
C37	H37A	0.9600	
C37	H37B	0.9600	
C37	H37C	0.9600	
C37	H37D	0.9600	
C37	H37E	0.9600	
C37	H37F	0.9600	
N1	N2	1.318(4)	
N2	H1	1.39(2)	
N3	N4	1.311(4)	
N4	H1	1.45(2)	
N1	C1	N3	127.0(3)
N1	C1	C11	116.4(4)
N3	C1	C11	116.6(4)
C12	C11	C16	118.1(4)
C12	C11	C1	121.7(4)

C16	C11	C1	120.2(4)
C11	C12	C13	121.2(4)
C11	C12	H12	119.4
C13	C12	H12	119.4
C14	C13	C12	120.7(5)
C14	C13	H13	119.7
C12	C13	H13	119.7
C13	C14	C15	119.0(4)
C13	C14	H14	120.5
C15	C14	H14	120.5
C14	C15	C16	120.9(4)
C14	C15	H15	119.5
C16	C15	H15	119.5
C15	C16	C11	120.1(4)
C15	C16	H16	119.9
C11	C16	H16	119.9
C26	C21	C22	119.1(4)
C26	C21	N2	116.9(4)
C22	C21	N2	124.0(4)
C21	C22	C23	119.6(4)
C21	C22	H22	120.2
C23	C22	H22	120.2
C24	C23	C22	122.0(4)
C24	C23	H23	119.0
C22	C23	H23	119.0
C25	C24	C23	117.3(4)
C25	C24	C27	121.6(4)
C23	C24	C27	121.0(4)
C24	C25	C26	121.8(4)
C24	C25	H25	119.1
C26	C25	H25	119.1
C21	C26	C25	120.1(4)
C21	C26	H26	120.0
C25	C26	H26	120.0
C24	C27	H27A	109.5
C24	C27	H27B	109.5
H27A	C27	H27B	109.5
C24	C27	H27C	109.5
H27A	C27	H27C	109.5
H27B	C27	H27C	109.5
C24	C27	H27D	109.5
H27A	C27	H27D	141.1
H27B	C27	H27D	56.3
H27C	C27	H27D	56.3
C24	C27	H27E	109.5
H27A	C27	H27E	56.3

H27B	C27	H27E	141.1
H27C	C27	H27E	56.3
H27D	C27	H27E	109.5
C24	C27	H27F	109.5
H27A	C27	H27F	56.3
H27B	C27	H27F	56.3
H27C	C27	H27F	141.1
H27D	C27	H27F	109.5
H27E	C27	H27F	109.5
C32	C31	C36	118.3(4)
C32	C31	N4	117.2(4)
C36	C31	N4	124.4(4)
C31	C32	C33	120.7(4)
C31	C32	H32	119.7
C33	C32	H32	119.7
C34	C33	C32	121.5(4)
C34	C33	H33	119.3
C32	C33	H33	119.3
C35	C34	C33	117.5(4)
C35	C34	C37	121.6(5)
C33	C34	C37	121.0(5)
C34	C35	C36	122.2(4)
C34	C35	H35	118.9
C36	C35	H35	118.9
C35	C36	C31	119.9(4)
C35	C36	H36	120.0
C31	C36	H36	120.0
C34	C37	H37A	109.5
C34	C37	H37B	109.5
H37A	C37	H37B	109.5
C34	C37	H37C	109.5
H37A	C37	H37C	109.5
H37B	C37	H37C	109.5
C34	C37	H37D	109.5
H37A	C37	H37D	141.1
H37B	C37	H37D	56.3
H37C	C37	H37D	56.3
C34	C37	H37E	109.5
H37A	C37	H37E	56.3
H37B	C37	H37E	141.1
H37C	C37	H37E	56.3
H37D	C37	H37E	109.5
C34	C37	H37F	109.5
H37A	C37	H37F	56.3
H37B	C37	H37F	56.3
H37C	C37	H37F	141.1

H37D	C37	H37F	109.5
H37E	C37	H37F	109.5
N2	N1	C1	118.4(3)
N1	N2	C21	118.1(3)
N1	N2	H1	115.5(10)
C21	N2	H1	126.3(10)
N4	N3	C1	119.2(3)
N3	N4	C31	117.9(3)
N3	N4	H1	113.5(10)
C31	N4	H1	128.6(10)

Table D-3. Bond lengths (Å) and angles (deg) for **2.3j**.

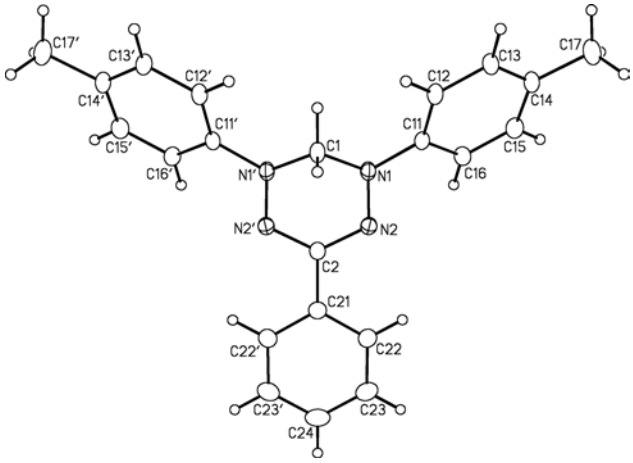

N2	C2	1.3351(19)	
C2	C21	1.484(4)	
C11	C12	1.381(2)	
C11	C16	1.387(3)	
C12	C13	1.382(3)	
C13	C14	1.382(3)	
C14	C15	1.387(3)	
C14	C17	1.506(3)	
C15	C16	1.377(3)	
C21	C22	1.384(2)	
C22	C23	1.385(3)	
C23	C24	1.373(3)	
N2	N1	C1	117.93(17)
N2	N1	C11	117.08(15)
C1	N1	C11	121.89(17)
N1	N2	C2	114.71(17)
N1	C1	N1'	105.9(2)
N2	C2	N2'	127.0(3)
N2	C2	C21	116.45(13)
N1	C11	C12	121.71(17)
N1	C11	C16	119.14(18)
C12	C11	C16	119.16(18)
C11	C12	C13	120.13(18)
C12	C13	C14	121.8(2)
C13	C14	C15	116.93(19)
C13	C14	C17	122.2(2)
C15	C14	C17	120.87(19)
C14	C15	C16	122.33(19)
C11	C16	C15	119.6(2)

C2	C21	C22	120.68(15)
C22	C21	C22'	118.6(3)
C21	C22	C23	120.6(2)
C22	C23	C24	120.1(2)
C23	C24	C23'	119.9(3)

Table D-4. Bond lengths (Å) and angles (deg) for **2.4c**.

O	C2	1.216(2)	
N1	N2	1.365(2)	
N1	C2	1.373(2)	
N1	C3	1.471(2)	
N2	C1	1.324(2)	
N3	N4	1.365(2)	
N3	C2	1.374(3)	
N3	C6	1.479(2)	
N4	C1	1.322(2)	
N10	C11	1.328(2)	
N10	C15	1.335(3)	
C1	C11	1.488(3)	
C3	C4	1.516(3)	
C3	C5	1.511(3)	
C6	C7	1.498(3)	
C6	C8	1.498(3)	
C11	C12	1.377(3)	
C12	C13	1.376(3)	
C13	C14	1.363(3)	
C14	C15	1.368(3)	
N2	N1	C2	124.62(16)
N2	N1	C3	114.77(15)
C2	N1	C3	120.57(16)
N1	N2	C1	114.33(15)
N4	N3	C2	123.99(16)
N4	N3	C6	114.84(16)
C2	N3	C6	121.09(17)
N3	N4	C1	114.95(16)
C11	N10	C15	116.89(18)
N2	C1	N4	127.81(18)
N2	C1	C11	116.88(17)
N4	C1	C11	115.29(17)
O	C2	N1	122.57(19)

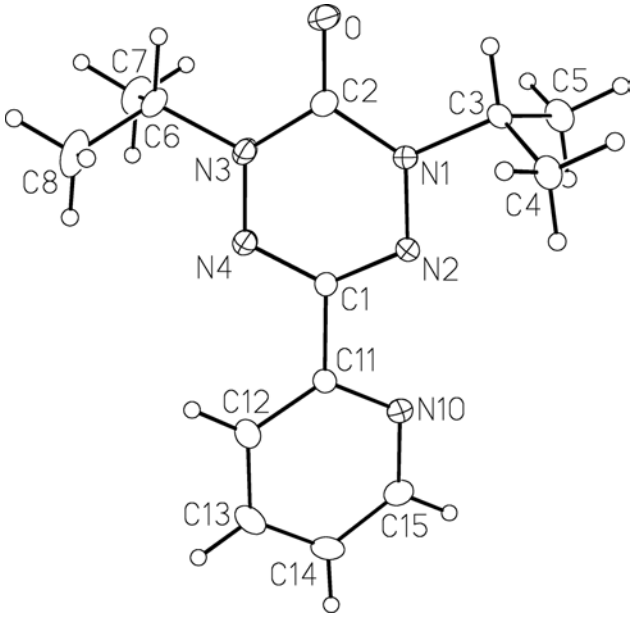

O	C2	N3	123.13(19)
N1	C2	N3	114.30(18)
N1	C3	C4	110.22(16)
N1	C3	C5	109.92(17)
C4	C3	C5	112.34(17)
N3	C6	C7	109.93(18)
N3	C6	C8	110.37(19)
C7	C6	C8	111.9(2)
N10	C11	C1	116.49(17)
N10	C11	C12	122.52(18)
C1	C11	C12	120.99(18)
C11	C12	C13	119.6(2)
C12	C13	C14	118.3(2)
C13	C14	C15	118.6(2)
N10	C15	C14	124.0(2)

Table D-5. Bond lengths (Å) and angles (deg) for **3.15d** (Molecule A).

O1	C2	1.345(3)
O1	B1	1.457(3)
O2	C2	1.206(3)
O3	C4	1.352(3)
O3	B1	1.463(3)
O4	C4	1.203(3)
N1	N2	1.303(2)
N1	C1	1.344(3)
N2	C21	1.439(3)
N2	B1	1.555(3)
N3	N4	1.305(2)
N3	C1	1.332(3)
N4	C31	1.430(3)
N4	B1	1.553(3)
C1	C11	1.484(3)
C2	C3	1.482(3)
C4	C5	1.486(3)
C11	C12	1.374(3)
C11	C16	1.382(3)
C12	C13	1.385(3)
C13	C14	1.378(4)
C14	C15	1.379(4)
C14	C17	1.503(3)
C15	C16	1.378(3)

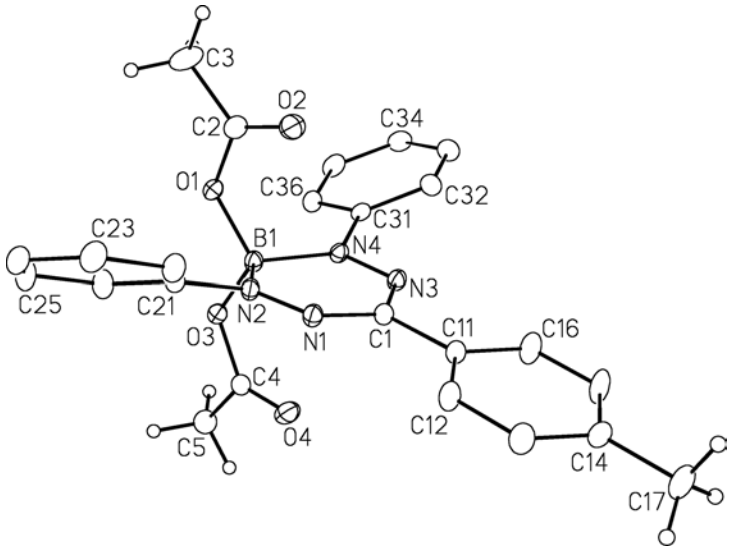

C21	C22	1.376(3)	
C21	C26	1.390(3)	
C22	C23	1.379(3)	
C23	C24	1.369(4)	
C24	C25	1.382(4)	
C25	C26	1.391(3)	
C31	C32	1.385(3)	
C31	C36	1.390(3)	
C32	C33	1.376(3)	
C33	C34	1.382(4)	
C34	C35	1.379(4)	
C35	C36	1.383(3)	
C2	O1	B1	117.73(18)
C4	O3	B1	119.66(18)
N2	N1	C1	118.11(19)
N1	N2	C21	114.55(18)
N1	N2	B1	124.82(18)
C21	N2	B1	120.34(18)
N4	N3	C1	118.61(18)
N3	N4	C31	113.83(18)
N3	N4	B1	124.42(18)
C31	N4	B1	121.64(18)
N1	C1	N3	126.5(2)
N1	C1	C11	117.0(2)
N3	C1	C11	116.39(19)
O1	C2	O2	123.1(2)
O1	C2	C3	113.1(2)
O2	C2	C3	123.9(2)
O3	C4	O4	122.7(2)
O3	C4	C5	112.3(2)
O4	C4	C5	125.1(2)
C1	C11	C12	120.5(2)
C1	C11	C16	121.8(2)
C12	C11	C16	117.7(2)
C11	C12	C13	120.5(2)
C12	C13	C14	122.3(2)
C13	C14	C15	116.5(2)
C13	C14	C17	122.2(2)
C15	C14	C17	121.3(2)
C14	C15	C16	121.7(2)
C11	C16	C15	121.2(2)
N2	C21	C22	120.8(2)
N2	C21	C26	119.0(2)

C22	C21	C26	120.2(2)
C21	C22	C23	119.4(2)
C22	C23	C24	121.1(3)
C23	C24	C25	119.8(2)
C24	C25	C26	119.8(2)
C21	C26	C25	119.6(2)
N4	C31	C32	119.8(2)
N4	C31	C36	120.0(2)

Table D-6. Bond lengths (Å) and angles (deg) for **3.15d** (Molecule B).

O1	C2	1.342(3)
O1	B1	1.456(3)
O2	C2	1.200(3)
O3	C4	1.339(3)
O3	B1	1.464(3)
O4	C4	1.206(3)
N1	N2	1.303(2)
N1	C1	1.344(3)
N2	C21	1.439(3)
N2	B1	1.547(3)
N3	N4	1.304(2)
N3	C1	1.341(3)
N4	C31	1.435(3)
N4	B1	1.548(3)
C1	C11	1.473(3)
C2	C3	1.483(3)
C4	C5	1.493(3)
C11	C12	1.388(3)
C11	C16	1.394(3)
C12	C13	1.386(3)
C13	C14	1.384(3)
C14	C15	1.388(3)
C14	C17	1.509(3)
C15	C16	1.380(3)
C21	C22	1.380(3)
C21	C26	1.384(3)
C22	C23	1.382(4)
C23	C24	1.370(4)
C24	C25	1.374(4)
C25	C26	1.378(3)
C31	C32	1.382(3)

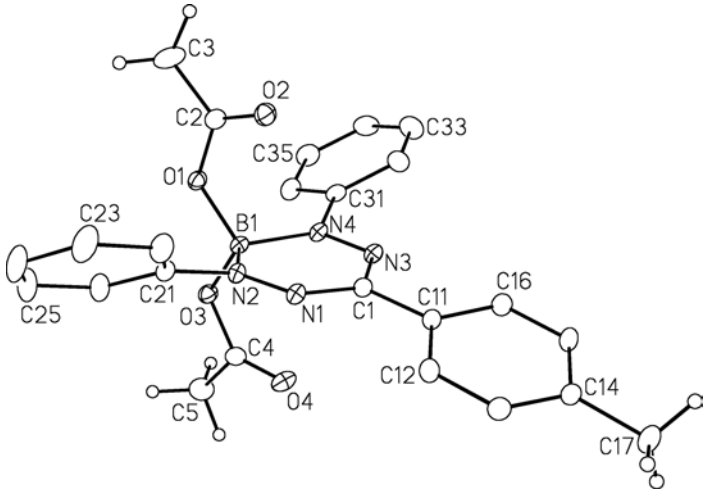

C31	C36	1.387(3)	
C32	C33	1.385(3)	
C33	C34	1.370(4)	
C34	C35	1.371(4)	
C35	C36	1.380(3)	
C2	O1	B1	119.16(18)
C4	O3	B1	120.97(18)
N2	N1	C1	117.85(18)
N1	N2	C21	114.69(18)
N1	N2	B1	125.44(18)
C21	N2	B1	119.49(18)
N4	N3	C1	118.92(18)
N3	N4	C31	114.70(18)
N3	N4	B1	124.37(18)
C31	N4	B1	120.84(18)
N1	C1	N3	126.0(2)
N1	C1	C11	117.82(19)
N3	C1	C11	116.14(19)
O1	C2	O2	123.5(2)
O1	C2	C3	112.0(2)
O2	C2	C3	124.4(2)
O3	C4	O4	123.3(2)
O3	C4	C5	111.7(2)
O4	C4	C5	125.0(2)
C1	C11	C12	121.8(2)
C1	C11	C16	120.6(2)
C12	C11	C16	117.5(2)
C11	C12	C13	120.8(2)
C12	C13	C14	121.7(2)
C13	C14	C15	117.3(2)
C13	C14	C17	121.5(2)
C15	C14	C17	121.2(2)
C14	C15	C16	121.3(2)
C11	C16	C15	121.2(2)
N2	C21	C22	120.0(2)
N2	C21	C26	119.6(2)
C22	C21	C26	120.4(2)
C21	C22	C23	118.9(3)
C22	C23	C24	121.0(3)
C23	C24	C25	119.8(3)
C24	C25	C26	120.3(3)
C21	C26	C25	119.6(3)
N4	C31	C32	120.0(2)

N4	C31	C36	119.7(2)

Table D-7. Bond lengths (Å) and angles (deg) for **3.15j**.

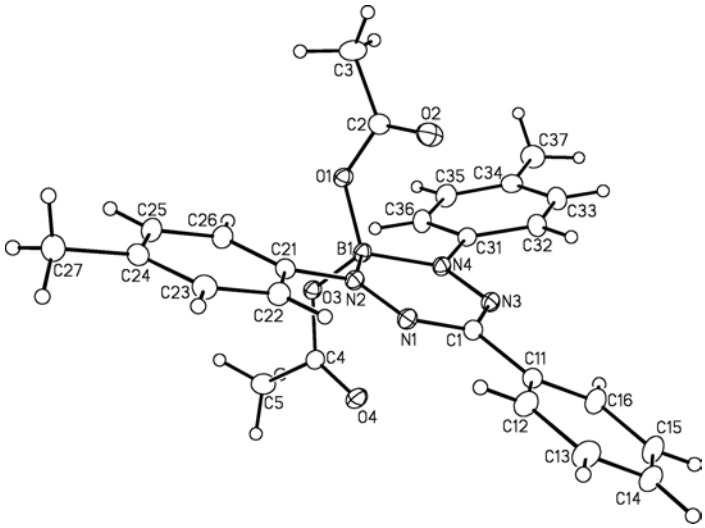

O1	C2	1.3405(16)	
O1	B1	1.4556(16)	
O2	C2	1.2013(16)	
O3	C4	1.3380(15)	
O3	B1	1.4683(16)	
O4	C4	1.2027(15)	
N1	N2	1.2976(14)	
N1	C1	1.3376(16)	
N2	C21	1.4327(16)	
N2	B1	1.5623(16)	
N3	N4	1.3025(14)	
N3	C1	1.3361(16)	
N4	C31	1.4310(16)	
N4	B1	1.5601(17)	
C1	C11	1.4791(17)	
C2	C3	1.4947(19)	
C4	C5	1.4992(19)	
C11	C12	1.3932(18)	
C11	C16	1.3869(19)	
C12	C13	1.3821(19)	
C13	C14	1.383(2)	
C14	C15	1.378(2)	
C15	C16	1.382(2)	
C21	C22	1.3952(17)	
C21	C26	1.3930(18)	
C22	C23	1.3772(19)	
C23	C24	1.388(2)	
C24	C25	1.3921(19)	
C24	C27	1.5035(19)	
C25	C26	1.3841(19)	
C31	C32	1.3893(18)	
C31	C36	1.3887(18)	
C32	C33	1.385(2)	
C33	C34	1.386(2)	
C34	C35	1.388(2)	
C34	C37	1.5058(19)	
C35	C36	1.3836(19)	
C2	O1	B1	120.10(10)

C4	O3	B1	120.41(9)
N2	N1	C1	119.60(10)
N1	N2	C21	114.04(10)
N1	N2	B1	123.87(10)
C21	N2	B1	122.03(10)
N4	N3	C1	118.33(10)
N3	N4	C31	114.19(10)
N3	N4	B1	125.03(10)
C31	N4	B1	120.69(10)
N1	C1	N3	126.47(11)
N1	C1	C11	116.59(11)
N3	C1	C11	116.92(11)
O1	C2	O2	123.41(12)
O1	C2	C3	112.40(12)
O2	C2	C3	124.19(13)
O3	C4	O4	123.63(12)
O3	C4	C5	112.38(11)
O4	C4	C5	123.99(12)
C1	C11	C12	120.92(12)
C1	C11	C16	120.63(12)
C12	C11	C16	118.45(12)
C11	C12	C13	120.14(14)
C12	C13	C14	120.75(14)
C13	C14	C15	119.44(13)
C14	C15	C16	119.99(14)
C11	C16	C15	121.21(13)
N2	C21	C22	119.84(11)
N2	C21	C26	120.92(11)
C22	C21	C26	119.19(12)
C21	C22	C23	119.78(12)
C22	C23	C24	122.00(13)
C23	C24	C25	117.61(12)
C23	C24	C27	120.63(13)
C25	C24	C27	121.75(13)
C24	C25	C26	121.49(12)
C21	C26	C25	119.91(12)
N4	C31	C32	120.51(11)
N4	C31	C36	120.08(11)
C32	C31	C36	119.41(12)
C31	C32	C33	119.84(13)
C32	C33	C34	121.62(13)
C33	C34	C35	117.63(13)
C33	C34	C37	121.68(14)

C35	C34	C37	120.69(13)
C34	C35	C36	121.81(13)
C31	C36	C35	119.67(13)
O1	B1	O3	103.77(9)
O1	B1	N2	112.69(10)
O1	B1	N4	111.12(10)
O3	B1	N2	111.00(10)
O3	B1	N4	112.63(10)
N2	B1	N4	105.80(9)

Table D-8. Bond lengths (Å) and angles (deg) for **3.17d**.

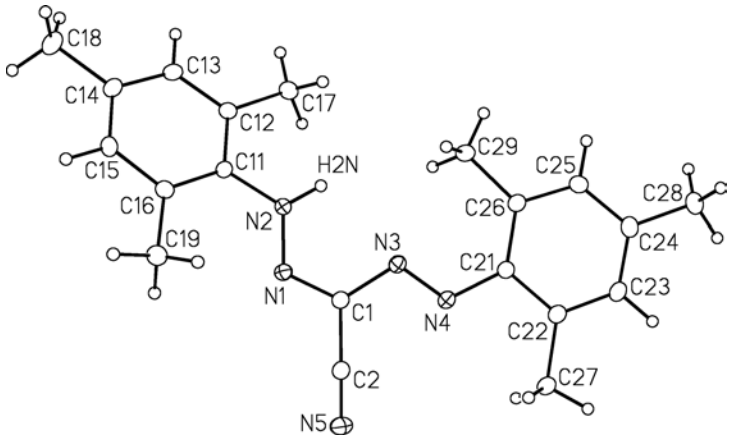

N1	N2	1.325(2)	
N1	C1	1.304(2)	
N2	C11	1.414(2)	
N3	N4	1.269(2)	
N3	C1	1.392(2)	
N4	C21	1.402(2)	
N5	C2	1.137(2)	
C1	C2	1.444(3)	
C11	C12	1.400(2)	
C11	C16	1.402(2)	
C12	C13	1.387(3)	
C12	C17	1.509(3)	
C13	C14	1.382(3)	
C14	C15	1.386(3)	
C14	C18	1.507(3)	
C15	C16	1.389(2)	
C16	C19	1.507(2)	
C21	C22	1.412(2)	
C21	C26	1.418(2)	
C22	C23	1.386(3)	
C22	C27	1.507(3)	
C23	C24	1.389(3)	
C24	C25	1.394(3)	
C24	C28	1.506(3)	
C25	C26	1.389(3)	
C26	C29	1.505(2)	
N2	N1	C1	116.38(15)
N1	N2	C11	122.54(14)
N4	N3	C1	112.45(14)

N3	N4	C21	118.04(15)
N1	C1	N3	122.24(16)
N1	C1	C2	116.55(16)
N3	C1	C2	121.19(15)
N5	C2	C1	179.7(2)
N2	C11	C12	115.99(15)
N2	C11	C16	122.43(15)
C12	C11	C16	121.48(16)
C11	C12	C13	118.28(17)
C11	C12	C17	121.61(16)
C13	C12	C17	120.10(16)
C12	C13	C14	122.25(17)
C13	C14	C15	117.62(17)
C13	C14	C18	120.98(18)
C15	C14	C18	121.38(19)
C14	C15	C16	123.31(17)
C11	C16	C15	117.03(16)
C11	C16	C19	123.96(16)
C15	C16	C19	118.97(16)
N4	C21	C22	112.51(15)
N4	C21	C26	127.04(15)
C22	C21	C26	120.44(16)
C21	C22	C23	119.17(17)
C21	C22	C27	121.20(16)
C23	C22	C27	119.63(16)
C22	C23	C24	121.77(17)
C23	C24	C25	118.06(17)
C23	C24	C28	121.57(17)
C25	C24	C28	120.38(18)
C24	C25	C26	123.05(17)
C21	C26	C25	117.51(16)
C21	C26	C29	124.45(16)
C25	C26	C29	117.99(16)

Table D-9. Bond lengths (Å) and angles (deg) for **3.17e**.

O1	C12	1.3566(18)
O2	C22	1.3457(18)
N1	N2	1.3101(15)
N1	C1	1.3180(18)
N2	C11	1.3969(18)

N3	N4	1.2904(15)	
N3	C1	1.3798(18)	
N4	C21	1.3937(19)	
N5	C2	1.1427(18)	
C1	C2	1.4403(18)	
C11	C12	1.3955(19)	
C11	C16	1.382(2)	
C12	C13	1.388(2)	
C13	C14	1.376(2)	
C14	C15	1.382(2)	
C15	C16	1.382(2)	
C21	C22	1.407(2)	
C21	C26	1.405(2)	
C22	C23	1.388(2)	
C23	C24	1.367(3)	
C24	C25	1.387(3)	
C25	C26	1.375(2)	
H2N	N4	1.91[a]	
H1O	N5[b]	2.00[a]	
H2O	N3	1.90[a]	
N2	N1	C1	118.13(11)
N1	N2	C11	120.93(12)
N4	N3	C1	115.11(11)
N3	N4	C21	115.96(12)
N1	C1	N3	132.01(12)
N1	C1	C2	114.42(12)
N3	C1	C2	113.51(12)
N5	C2	C1	179.03(16)
N2	C11	C12	115.84(13)
N2	C11	C16	123.27(13)
C12	C11	C16	120.89(14)
O1	C12	C11	116.50(13)
O1	C12	C13	124.42(13)
C11	C12	C13	119.08(14)
C12	C13	C14	119.70(15)
C13	C14	C15	121.12(15)
C14	C15	C16	119.81(16)
C11	C16	C15	119.39(15)
N4	C21	C22	126.04(14)
N4	C21	C26	114.82(14)
C22	C21	C26	119.14(14)
O2	C22	C21	122.95(14)
O2	C22	C23	118.01(15)

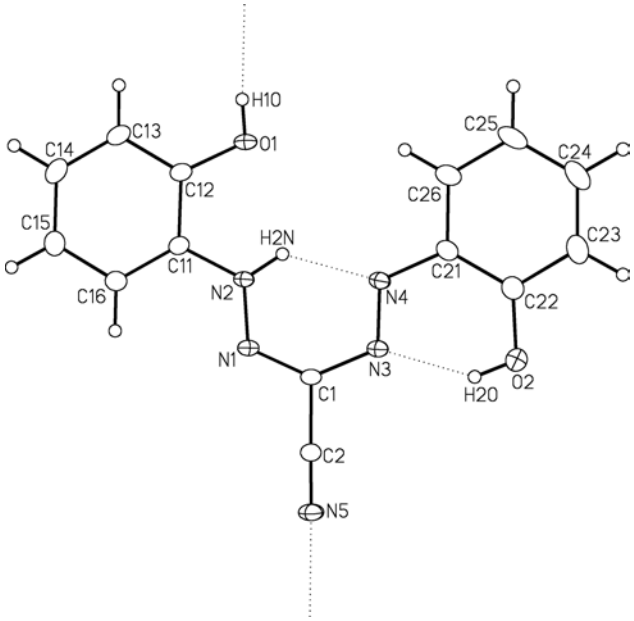

C21	C22	C23	119.04(16)
C22	C23	C24	120.79(18)
C23	C24	C25	121.03(16)
C24	C25	C26	119.34(17)
C21	C26	C25	120.65(17)

Table D-10. Bond lengths (Å) and angles (deg) for **3.17f**.

O1	C12	1.358(3)	
O1	C17	1.424(3)	
O2	C22	1.366(3)	
O2	C27	1.423(3)	
N1	N2	1.292(3)	
N1	C1	1.355(4)	
N2	N4	2.597(3)†	
N2	C11	1.413(4)	
N3	N4	1.296(3)	
N3	C1	1.353(4)	
N4	C21	1.406(4)	
N4	H2N	1.95†	
N5	C2	1.144(4)	
C1	C2	1.447(4)	
C11	C12	1.399(4)	
C11	C16	1.387(4)	
C12	C13	1.402(4)	
C13	C14	1.383(4)	
C14	C15	1.377(4)	
C15	C16	1.385(4)	
C21	C22	1.397(4)	
C21	C26	1.406(4)	
C22	C23	1.383(4)	
C23	C24	1.387(4)	
C24	C25	1.379(4)	
C25	C26	1.369(4)	
C12	O1	C17	118.2(2)
C22	O2	C27	117.4(2)
N2	N1	C1	117.3(3)
N1	N2	C11	116.9(2)
N4	N3	C1	115.5(2)
N3	N4	C21	117.1(2)
N1	C1	N3	132.3(3)

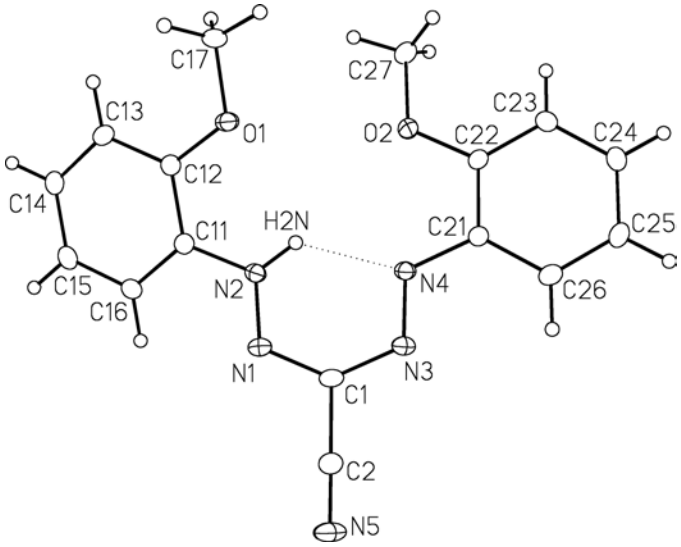

N1	C1	C2	113.4(3)
N3	C1	C2	114.3(3)
N5	C2	C1	179.6(3)
N2	C11	C12	117.5(3)
N2	C11	C16	122.1(3)
C12	C11	C16	120.4(3)
O1	C12	C11	116.4(3)
O1	C12	C13	124.5(3)
C11	C12	C13	119.1(3)
C12	C13	C14	119.5(3)
C13	C14	C15	121.0(3)
C14	C15	C16	120.1(3)
C11	C16	C15	119.8(3)
N4	C21	C22	116.5(3)
N4	C21	C26	124.1(3)
C22	C21	C26	119.4(3)
O2	C22	C21	115.2(3)
O2	C22	C23	124.6(3)
C21	C22	C23	120.2(3)
C22	C23	C24	119.5(3)
C23	C24	C25	120.7(3)
C24	C25	C26	120.6(3)
C21	C26	C25	119.7(3)
N2	H2N	N4	128.8‡

Table D-11. Bond lengths (Å) and angles (deg) for **3.18b**.

O1	N5	1.2185(19)
O2	N5	1.230(2)
N1	N2	1.305(2)
N1	C1	1.320(2)
N2	C11	1.402(2)
N2	N4	2.606(2)[a]
N3	N4	1.2877(19)
N3	C1	1.357(2)
N4	C21	1.412(2)
N4	H2N	1.94[a]
N5	C1	1.462(2)
C11	C12	1.377(3)
C11	C16	1.386(3)
C12	C13	1.378(3)

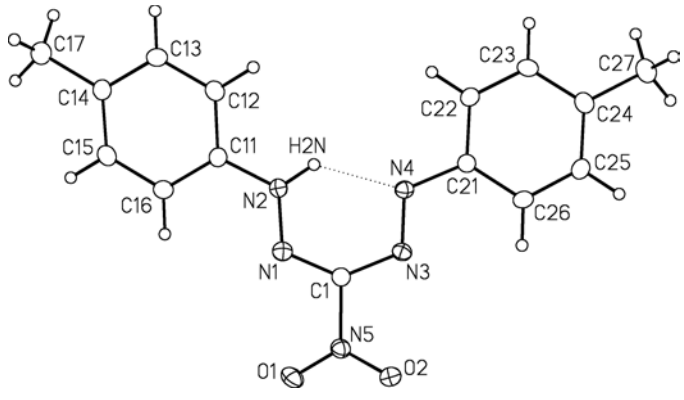

C13	C14	1.387(3)	
C14	C15	1.380(3)	
C14	C17	1.501(3)	
C15	C16	1.388(3)	
C21	C22	1.393(2)	
C21	C26	1.390(2)	
C22	C23	1.374(3)	
C23	C24	1.389(3)	
C24	C25	1.396(3)	
C24	C27	1.501(3)	
C25	C26	1.372(3)	
N2	N1	C1	117.19(15)
N1	N2	C11	120.75(15)
N4	N3	C1	114.59(15)
N3	N4	C21	115.24(15)
O1	N5	O2	123.66(16)
O1	N5	C1	119.20(16)
O2	N5	C1	117.08(15)
N1	C1	N3	134.25(17)
N1	C1	N5	113.11(16)
N3	C1	N5	112.61(15)
N2	C11	C12	117.65(17)
N2	C11	C16	122.86(17)
C12	C11	C16	119.48(18)
C11	C12	C13	120.37(19)
C12	C13	C14	121.36(19)
C13	C14	C15	117.51(18)
C13	C14	C17	120.94(19)
C15	C14	C17	121.55(19)
C14	C15	C16	122.00(19)
C11	C16	C15	119.27(18)
N4	C21	C22	116.31(16)
N4	C21	C26	124.36(16)
C22	C21	C26	119.33(17)
C21	C22	C23	120.38(18)
C22	C23	C24	121.18(18)
C23	C24	C25	117.56(18)
C23	C24	C27	120.69(19)
C25	C24	C27	121.75(19)
C24	C25	C26	122.14(19)
C21	C26	C25	119.42(17)
N2	H2N	N4	131.1[a]

Table D-12. Bond lengths (Å) and angles (deg) for **3.18d**.

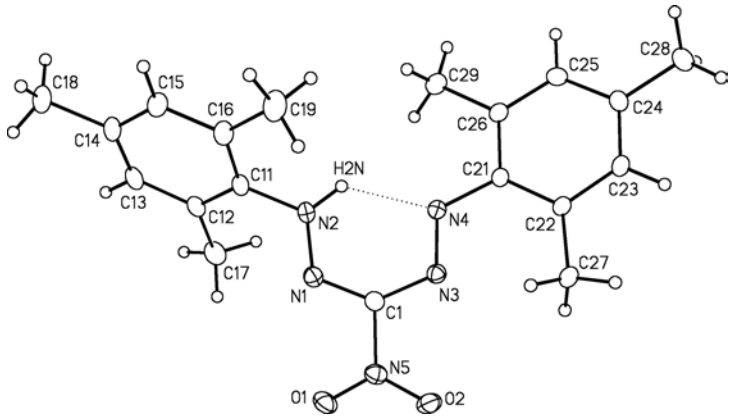

O1	N5	1.225(2)	
O2	N5	1.225(2)	
N1	N2	1.299(2)	
N1	C1	1.322(2)	
N2	N4	2.615(2)†	
N2	C11	1.425(2)	
N3	N4	1.282(2)	
N3	C1	1.357(2)	
N4	C21	1.416(2)	
N4	H2N	1.97†	
N5	C1	1.468(2)	
C11	C12	1.402(3)	
C11	C16	1.392(3)	
C12	C13	1.388(3)	
C12	C17	1.501(3)	
C13	C14	1.377(3)	
C14	C15	1.388(3)	
C14	C18	1.508(3)	
C15	C16	1.391(3)	
C16	C19	1.507(3)	
C21	C22	1.412(2)	
C21	C26	1.405(2)	
C22	C23	1.390(2)	
C22	C27	1.503(2)	
C23	C24	1.385(3)	
C24	C25	1.386(3)	
C24	C28	1.506(2)	
C25	C26	1.382(2)	
C26	C29	1.508(3)	
N2	N1	C1	117.81(15)
N1	N2	C11	118.79(15)
N4	N3	C1	114.44(15)
N3	N4	C21	117.55(14)
O1	N5	O2	123.61(17)
O1	N5	C1	118.77(17)
O2	N5	C1	117.62(15)
N1	C1	N3	134.26(17)
N1	C1	N5	112.75(15)
N3	C1	N5	112.97(16)
N2	C11	C12	120.70(17)
N2	C11	C16	117.45(16)
C12	C11	C16	121.82(17)

C11	C12	C13	117.19(18)
C11	C12	C17	122.61(17)
C13	C12	C17	120.15(17)
C12	C13	C14	122.83(18)
C13	C14	C15	118.29(18)
C13	C14	C18	120.93(19)
C15	C14	C18	120.8(2)
C14	C15	C16	121.69(19)
C11	C16	C15	118.12(18)
C11	C16	C19	122.02(18)
C15	C16	C19	119.84(19)
N4	C21	C22	124.41(15)
N4	C21	C26	114.78(15)
C22	C21	C26	120.69(16)
C21	C22	C23	117.50(16)
C21	C22	C27	124.16(16)
C23	C22	C27	118.22(16)
C22	C23	C24	122.92(16)
C23	C24	C25	117.94(16)
C23	C24	C28	120.99(17)
C25	C24	C28	121.06(18)
C24	C25	C26	122.19(17)
C21	C26	C25	118.74(16)
C21	C26	C29	121.28(16)
C25	C26	C29	119.97(17)
N2	H2N	N4	129.4†

Table D-13. Bond lengths (Å) and angles (deg) for **3.19**.

C1	N1	1.340(5)
C1	N3	1.354(5)
C1	C2	1.451(5)
C2	N5	1.138(5)
C11	C16	1.386(5)
C11	C12	1.407(5)
C11	N2	1.409(5)
C12	C13	1.372(5)
C12	O1	1.382(4)
C13	C14	1.395(5)
C13	H13	0.9500
C14	C15	1.383(5)
C14	H14	0.9500
C15	C16	1.378(5)

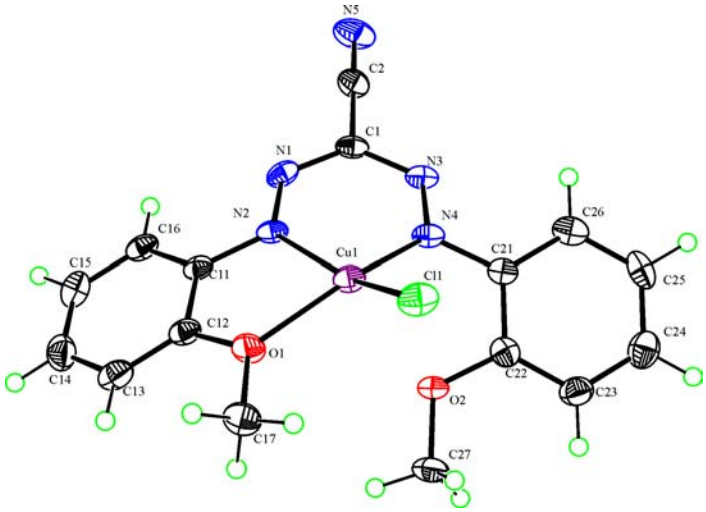

C15	H15	0.9500
C16	H16	0.9500
C17	O1	1.444(4)
C17	H17A	0.9800
C17	H17B	0.9800
C17	H17C	0.9800
C21	C26	1.383(5)
C21	C22	1.396(5)
C21	N4	1.415(5)
C22	O2	1.368(4)
C22	C23	1.383(5)
C23	C24	1.376(6)
C23	H23	0.9500
C24	C25	1.390(6)
C24	H24	0.9500
C25	C26	1.380(5)
C25	H25	0.9500
C26	H26	0.9500
C27	O2	1.425(4)
C27	H27A	0.9800
C27	H27B	0.9800
C27	H27C	0.9800
N1	N2	1.297(4)
N2	Cu1	1.928(3)
N3	N4	1.286(4)
N4	Cu1	1.946(3)
O1	Cu1	2.068(3)
O2	Cu1	2.479(2)
Cu1	Cl1	2.2147(10)

N1	C1	N3	131.4(3)
N1	C1	C2	114.2(3)
N3	C1	C2	113.5(4)
N5	C2	C1	178.7(4)
C16	C11	C12	119.4(4)
C16	C11	N2	125.4(4)
C12	C11	N2	115.2(3)
C13	C12	O1	125.0(4)
C13	C12	C11	120.9(4)
O1	C12	C11	114.1(4)
C12	C13	C14	118.7(4)
C12	C13	H13	120.7
C14	C13	H13	120.7
C15	C14	C13	121.1(4)
C15	C14	H14	119.5
C13	C14	H14	119.5
C16	C15	C14	120.0(4)

C16	C15	H15	120.0
C14	C15	H15	120.0
C15	C16	C11	120.0(4)
C15	C16	H16	120.0
C11	C16	H16	120.0
O1	C17	H17A	109.5
O1	C17	H17B	109.5
H17A	C17	H17B	109.5
O1	C17	H17C	109.5
H17A	C17	H17C	109.5
H17B	C17	H17C	109.5
C26	C21	C22	120.5(4)
C26	C21	N4	123.4(3)
C22	C21	N4	116.2(4)
O2	C22	C23	124.5(4)
O2	C22	C21	115.6(3)
C23	C22	C21	119.8(4)
C24	C23	C22	119.3(4)
C24	C23	H23	120.3
C22	C23	H23	120.3
C23	C24	C25	121.2(4)
C23	C24	H24	119.4
C25	C24	H24	119.4
C26	C25	C24	119.6(4)
C26	C25	H25	120.2
C24	C25	H25	120.2
C25	C26	C21	119.6(4)
C25	C26	H26	120.2
C21	C26	H26	120.2
O2	C27	H27A	109.5
O2	C27	H27B	109.5
H27A	C27	H27B	109.5
O2	C27	H27C	109.5
H27A	C27	H27C	109.5
H27B	C27	H27C	109.5
N2	N1	C1	118.9(3)
N1	N2	C11	115.6(3)
N1	N2	Cu1	127.8(3)
C11	N2	Cu1	116.6(2)
N4	N3	C1	118.5(3)
N3	N4	C21	115.4(3)
N3	N4	Cu1	127.8(3)
C21	N4	Cu1	116.6(2)
C12	O1	C17	118.3(3)
C12	O1	Cu1	113.4(2)
C17	O1	Cu1	127.8(2)

C22	O2	C27	118.3(3)
C22	O2	Cu1	101.6(2)
C27	O2	Cu1	126.9(2)
N2	Cu1	N4	87.62(13)
N2	Cu1	O1	80.10(12)
N4	Cu1	O1	156.12(12)
N2	Cu1	Cl1	155.37(9)
N4	Cu1	Cl1	103.61(10)
O1	Cu1	Cl1	95.79(8)
N2	Cu1	O2	120.54(10)
N4	Cu1	O2	71.26(10)
O1	Cu1	O2	97.47(9)
Cl1	Cu1	O2	84.01(6)

Table D-14. Bond lengths (Å) and angles (deg) for **3.20a**.

Fe	O1	1.9121(17)
Fe	O2	1.9218(18)
Fe	N2	1.846(2)
Fe	N4	1.849(2)
Fe	N30	2.010(2)
Fe	N40	1.997(2)
O1	C12	1.324(3)
O2	C22	1.320(3)
N1	N2	1.310(3)
N1	C1	1.352(4)
N2	C11	1.407(3)
N3	N4	1.310(3)
N3	C1	1.347(4)
N4	C21	1.401(3)
N5	C2	1.137(4)
N30	C31	1.343(4)
N30	C35	1.347(3)
N40	C41	1.350(3)
N40	C45	1.347(3)
C1	C2	1.447(4)
C11	C12	1.415(4)
C11	C16	1.398(4)
C12	C13	1.408(4)
C13	C14	1.383(4)
C14	C15	1.397(5)
C15	C16	1.382(4)

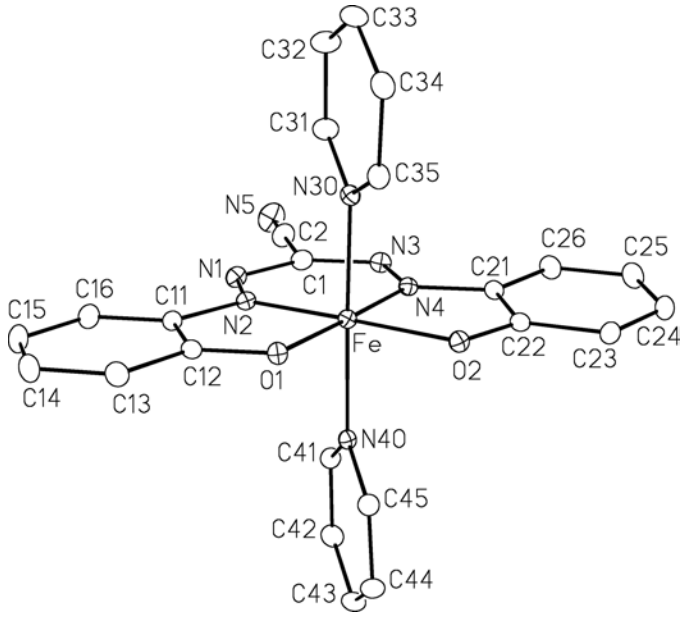

C21	C22	1.420(4)	
C21	C26	1.395(4)	
C22	C23	1.406(4)	
C23	C24	1.381(4)	
C24	C25	1.395(5)	
C25	C26	1.378(4)	
C31	C32	1.381(4)	
C32	C33	1.377(5)	
C33	C34	1.385(5)	
C34	C35	1.382(4)	
C41	C42	1.382(4)	
C42	C43	1.383(4)	
C43	C44	1.388(4)	
C44	C45	1.372(4)	
Cl1S	C1S	1.712(6)	
Cl2S	C1S	1.762(6)	
O1	Fe	O2	94.17(7)
O1	Fe	N2	86.29(8)
O1	Fe	N4	178.82(8)
O1	Fe	N30	88.54(8)
O1	Fe	N40	88.97(8)
O2	Fe	N2	178.64(8)
O2	Fe	N4	86.08(8)
O2	Fe	N30	89.26(8)
O2	Fe	N40	87.76(8)
N2	Fe	N4	93.49(9)
N2	Fe	N30	92.03(9)
N2	Fe	N40	90.98(9)
N4	Fe	N30	90.31(9)
N4	Fe	N40	92.20(9)
N30	Fe	N40	175.96(8)
Fe	O1	C12	110.45(16)
Fe	O2	C22	110.27(15)
N2	N1	C1	117.6(2)
Fe	N2	N1	128.83(17)
Fe	N2	C11	113.02(17)
N1	N2	C11	118.1(2)
N4	N3	C1	118.0(2)
Fe	N4	N3	128.45(18)
Fe	N4	C21	113.28(17)
N3	N4	C21	118.3(2)
Fe	N30	C31	123.25(18)
Fe	N30	C35	118.61(18)

C31	N30	C35	118.1(2)
Fe	N40	C41	123.06(17)
Fe	N40	C45	118.58(17)
C41	N40	C45	118.3(2)
N1	C1	N3	133.6(2)
N1	C1	C2	113.3(2)
N3	C1	C2	113.0(2)
N5	C2	C1	178.4(3)
N2	C11	C12	111.7(2)
N2	C11	C16	126.4(3)
C12	C11	C16	121.9(2)
O1	C12	C11	118.5(2)
O1	C12	C13	123.3(2)
C11	C12	C13	118.2(2)
C12	C13	C14	119.5(3)
C13	C14	C15	121.4(3)
C14	C15	C16	120.6(3)
C11	C16	C15	118.4(3)
N4	C21	C22	111.6(2)
N4	C21	C26	126.7(3)
C22	C21	C26	121.7(2)
O2	C22	C21	118.7(2)
O2	C22	C23	123.5(2)
C21	C22	C23	117.8(2)
C22	C23	C24	119.7(3)
C23	C24	C25	121.5(3)
C24	C25	C26	120.3(3)
C21	C26	C25	118.9(3)
N30	C31	C32	122.4(3)
C31	C32	C33	119.3(3)
C32	C33	C34	118.9(3)
C33	C34	C35	118.9(3)
N30	C35	C34	122.5(3)
N40	C41	C42	122.4(2)
C41	C42	C43	118.8(3)
C42	C43	C44	118.8(3)
C43	C44	C45	119.5(3)
N40	C45	C44	122.1(2)

Table D-15. Bond lengths (Å) and angles (deg) for **3.20b**.

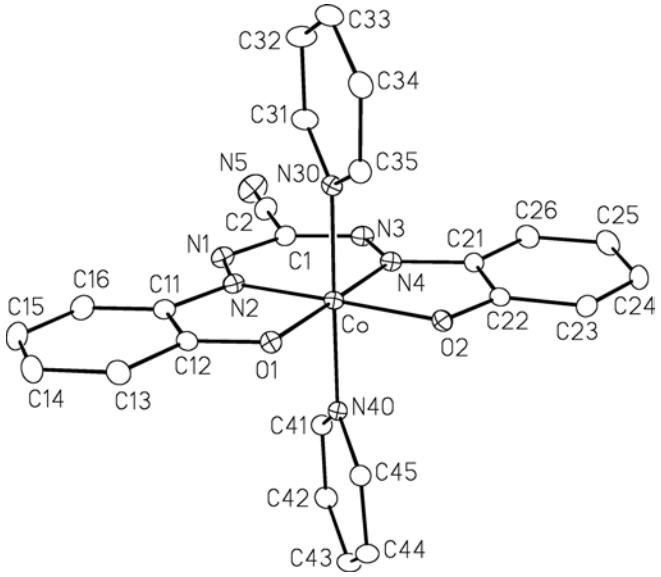

Co	O1	1.8979(18)	
Co	O2	1.9075(18)	
Co	N2	1.856(2)	
Co	N4	1.860(2)	
Co	N30	1.966(2)	
Co	N40	1.954(2)	
O1	C12	1.324(3)	
O2	C22	1.321(3)	
N1	N2	1.288(3)	
N1	C1	1.357(4)	
N2	C11	1.409(3)	
N3	N4	1.286(3)	
N3	C1	1.358(4)	
N4	C21	1.400(3)	
N5	C2	1.143(4)	
N30	C31	1.341(4)	
N30	C35	1.342(3)	
N40	C41	1.346(3)	
N40	C45	1.345(3)	
C1	C2	1.442(4)	
C11	C12	1.412(4)	
C11	C16	1.398(4)	
C12	C13	1.409(4)	
C13	C14	1.380(4)	
C14	C15	1.398(5)	
C15	C16	1.379(5)	
C21	C22	1.417(4)	
C21	C26	1.394(4)	
C22	C23	1.402(4)	
C23	C24	1.379(4)	
C24	C25	1.395(5)	
C25	C26	1.383(4)	
C31	C32	1.380(4)	
C32	C33	1.381(4)	
C33	C34	1.375(4)	
C34	C35	1.384(4)	
C41	C42	1.382(4)	
C42	C43	1.384(4)	
C43	C44	1.387(4)	
C44	C45	1.374(4)	
O1	Co	O2	93.41(8)
O1	Co	N2	86.42(9)

O1	Co	N4	178.75(8)
O1	Co	N30	88.82(8)
O1	Co	N40	89.47(8)
O2	Co	N2	178.91(8)
O2	Co	N4	85.97(9)
O2	Co	N30	89.70(8)
O2	Co	N40	88.26(8)
N2	Co	N4	94.22(10)
N2	Co	N30	91.37(9)
N2	Co	N40	90.66(9)
N4	Co	N30	90.09(9)
N4	Co	N40	91.60(9)
N30	Co	N40	177.26(8)
Co	O1	C12	110.48(16)
Co	O2	C22	110.32(16)
N2	N1	C1	117.5(2)
Co	N2	N1	128.17(19)
Co	N2	C11	112.71(17)
N1	N2	C11	119.1(2)
N4	N3	C1	117.8(2)
Co	N4	N3	127.79(19)
Co	N4	C21	113.41(18)
N3	N4	C21	118.8(2)
Co	N30	C31	124.06(18)
Co	N30	C35	118.04(18)
C31	N30	C35	117.9(2)
Co	N40	C41	123.90(17)
Co	N40	C45	117.89(17)
C41	N40	C45	118.2(2)
N1	C1	N3	134.4(2)
N1	C1	C2	113.1(2)
N3	C1	C2	112.4(2)
N5	C2	C1	178.6(4)
N2	C11	C12	111.2(2)
N2	C11	C16	127.0(3)
C12	C11	C16	121.8(3)
O1	C12	C11	119.1(2)
O1	C12	C13	122.7(2)
C11	C12	C13	118.3(2)
C12	C13	C14	119.5(3)
C13	C14	C15	121.3(3)
C14	C15	C16	120.5(3)
C11	C16	C15	118.6(3)

N4	C21	C22	110.8(2)
N4	C21	C26	127.6(3)
C22	C21	C26	121.6(2)
O2	C22	C21	119.4(2)
O2	C22	C23	122.6(2)
C21	C22	C23	118.0(2)
C22	C23	C24	119.9(3)
C23	C24	C25	121.5(3)
C24	C25	C26	120.0(3)
C21	C26	C25	119.0(3)
N30	C31	C32	122.6(3)
C31	C32	C33	119.2(3)
C32	C33	C34	118.5(3)
C33	C34	C35	119.4(3)
N30	C35	C34	122.4(3)
N40	C41	C42	122.6(2)
C41	C42	C43	118.9(3)
C42	C43	C44	118.5(2)
C43	C44	C45	119.6(3)
N40	C45	C44	122.2(2)

Table D-16. Bond lengths (Å) and angles (deg) for **3.21**.

C1	N1#1	1.3449(19)
C1	N1	1.3449(19)
C1	C2	1.442(4)
C2	N3	1.141(4)
C11	C12	1.395(3)
C11	C16	1.395(3)
C11	N2	1.459(2)
C12	C13	1.397(3)
C12	C17	1.500(3)
C13	C14	1.374(4)
C13	H13	0.9500
C14	C15	1.378(4)
C14	H14	0.9500
C15	C16	1.397(3)
C15	H15	0.9500
C16	C18	1.504(3)
C17	H17A	0.9800
C17	H17B	0.9800
C17	H17C	0.9800
C18	H18A	0.9800

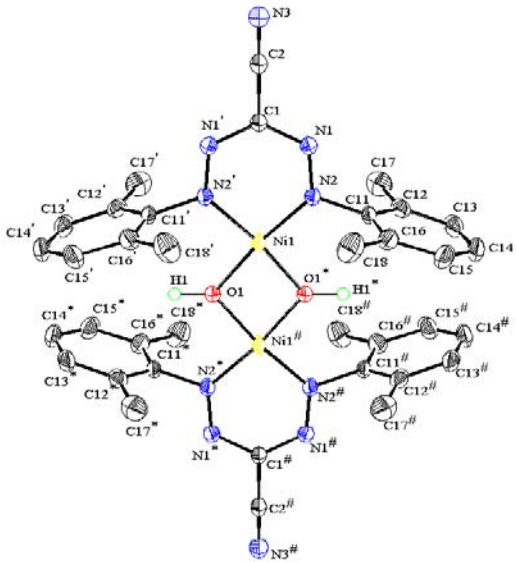

C18	H18B	0.9800
C18	H18C	0.9800
N1	N2	1.288(2)
N2	Ni1	1.8270(15)
Ni1	N2#1	1.8270(15)
Ni1	O1	1.854(2)
Ni1	O1#2	1.854(2)
Ni1	O1B	1.938(5)
Ni1	O1B#1	1.938(5)
Ni1	O1B#3	1.947(5)
Ni1	O1B#2	1.947(5)
Ni1	Ni1#2	2.8984(7)
O1	O1B#3	0.494(5)
O1	Ni1#2	1.854(2)
O1	H1	0.96(5)
O1B	O1B#3	0.985(10)
O1B	Ni1#2	1.947(5)
O1B	H1	1.04(5)
Cl1	C19	1.795(9)
C19	Cl2	1.810(12)
C19	H19A	0.9900
C19	H19B	0.9900
Cl2	C19#4	0.663(19)
Cl3	C20	1.811(13)
Cl3	C20#4	1.811(13)
C20	Cl3#4	1.811(13)
C20	H20A	0.9900
C20	H20B	0.9900
N1#1	C1	N1	129.9(2)
N1#1	C1	C2	114.96(12)
N1	C1	C2	114.96(12)
N3	C2	C1	179.5(4)
C12	C11	C16	123.31(18)
C12	C11	N2	119.05(17)
C16	C11	N2	117.64(17)
C11	C12	C13	116.7(2)
C11	C12	C17	121.96(19)
C13	C12	C17	121.3(2)
C14	C13	C12	121.6(2)
C14	C13	H13	119.2
C12	C13	H13	119.2
C13	C14	C15	120.2(2)
C13	C14	H14	119.9
C15	C14	H14	119.9
C14	C15	C16	121.0(2)

C14	C15	H15	119.5
C16	C15	H15	119.5
C11	C16	C15	117.1(2)
C11	C16	C18	121.50(18)
C15	C16	C18	121.4(2)
C12	C17	H17A	109.5
C12	C17	H17B	109.5
H17A	C17	H17B	109.5
C12	C17	H17C	109.5
H17A	C17	H17C	109.5
H17B	C17	H17C	109.5
C16	C18	H18A	109.5
C16	C18	H18B	109.5
H18A	C18	H18B	109.5
C16	C18	H18C	109.5
H18A	C18	H18C	109.5
H18B	C18	H18C	109.5
N2	N1	C1	119.32(17)
N1	N2	C11	110.89(14)
N1	N2	Ni1	128.60(13)
C11	N2	Ni1	120.50(11)
N2	Ni1	N2#1	92.42(10)
N2	Ni1	O1	172.39(10)
N2#1	Ni1	O1	95.20(10)
N2	Ni1	O1#2	95.20(10)
N2#1	Ni1	O1#2	172.39(10)
O1	Ni1	O1#2	77.19(18)
N2	Ni1	O1B	163.94(15)
N2#1	Ni1	O1B	94.02(15)
O1	Ni1	O1B	14.76(14)
O1#2	Ni1	O1B	78.63(14)
O2	Ni1	O1B#1	94.02(15)
N2#1	Ni1	O1B#1	163.94(15)
O1	Ni1	O1B#1	78.63(14)
O1#2	Ni1	O1B#1	14.76(14)
O1B	Ni1	O1B#1	76.2(3)
N2	Ni1	O1B#3	163.85(15)
N2#1	Ni1	O1B#3	94.23(15)
O1	Ni1	O1B#3	14.67(14)
O1#2	Ni1	O1B#3	78.40(14)
O1B	Ni1	O1B#3	29.4(3)
O1B#1	Ni1	O1B#3	83.5(2)
N2	Ni1	O1B#2	94.23(15)
N2#1	Ni1	O1B#2	163.85(15)
O1	Ni1	O1B#2	78.40(14)
O1#2	Ni1	O1B#2	14.67(14)

O1B	Ni1	O1B#2	83.5(2)
O1B#1	Ni1	O1B#2	29.4(3)
O1B#3	Ni1	O1B#2	75.8(3)
N2	Ni1	Ni1#2	133.79(5)
N2#1	Ni1	Ni1#2	133.79(5)
O1	Ni1	Ni1#2	38.59(9)
O1#2	Ni1	Ni1#2	38.59(9)
O1B	Ni1	Ni1#2	41.86(14)
O1B#1	Ni1	Ni1#2	41.86(14)
O1B#3	Ni1	Ni1#2	41.62(14)
O1B#2	Ni1	Ni1#2	41.62(14)
O1B#3	O1	Ni1	93.4(7)
O1B#3	O1	Ni1#2	92.3(7)
Ni1	O1	Ni1#2	102.81(18)
O1B#3	O1	H1	85.5(8)
Ni1	O1	H1	128.59(9)
Ni1#2	O1	H1	128.59(9)
O1B#3	O1B	Ni1	75.8(4)
O1B#3	O1B	Ni1#2	74.8(4)
Ni1	O1B	Ni1#2	96.5(2)
O1B#3	O1B	H1	61.8(14)
Ni1	O1B	H1	115.3(8)
Ni1#2	O1B	H1	114.7(9)
Cl1	C19	Cl2	112.3(13)
Cl1	C19	H19A	109.1
Cl2	C19	H19A	109.2
Cl1	C19	H19B	109.1
Cl2	C19	H19B	109.2
H19A	C19	H19B	107.8
C19#4	Cl2	C19	103(3)
C20	Cl3	C20#4	68.6(17)
Cl3	C20	Cl3#4	111.4(17)
Cl3	C20	H20A	109.5
Cl3#4	C20	H20A	109.2
Cl3	C20	H20B	109.2
Cl3#4	C20	H20B	109.5
H20A	C20	H20B	107.9

Table D-17. Bond lengths (Å) and angles (deg) for **3.22**.

C1	N3	1.330(3)
C1	N1	1.337(3)
C1	N5	1.457(3)
C11	C12	1.389(4)
C11	C16	1.391(4)

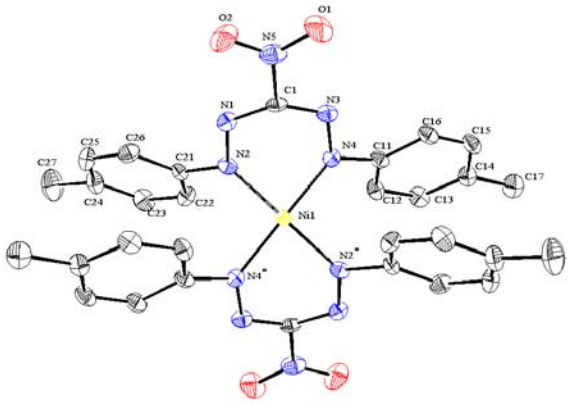

C11	N4	1.427(3)
C12	C13	1.381(4)
C12	H12	0.9500
C13	C14	1.388(4)
C13	H13	0.9500
C14	C15	1.389(4)
C14	C17	1.503(4)
C15	C16	1.376(4)
C15	H15	0.9500
C16	H16	0.9500
C17	H17A	0.9800
C17	H17B	0.9800
C17	H17C	0.9800
C21	C22	1.380(4)
C21	C26	1.386(4)
C21	N2	1.437(3)
C22	C23	1.393(4)
C22	H22	0.9500
C23	C24	1.381(4)
C23	H23	0.9500
C24	C25	1.392(4)
C24	C27	1.512(4)
C25	C26	1.384(4)
C25	H25	0.9500
C26	H26	0.9500
C27	H27A	0.9800
C27	H27B	0.9800
C27	H27C	0.9800
C27	H27D	0.9800
C27	H27E	0.9800
C27	H27F	0.9800
N1	N2	1.293(3)
N2	Ni1	1.867(2)
N3	N4	1.295(3)
N4	Ni1	1.880(2)
N5	O2	1.227(3)
N5	O1	1.235(3)
Ni1	N2#1	1.867(2)
Ni1	N4#1	1.880(2)

N3	C1	N1	128.1(3)
N3	C1	N5	114.8(3)
N1	C1	N5	113.8(3)
C12	C11	C16	119.9(3)
C12	C11	N4	117.2(3)
C16	C11	N4	122.8(3)

C13	C12	C11	119.8(3)
C13	C12	H12	120.1
C11	C12	H12	120.1
C12	C13	C14	121.2(3)
C12	C13	H13	119.4
C14	C13	H13	119.4
C13	C14	C15	117.8(3)
C13	C14	C17	120.5(3)
C15	C14	C17	121.7(3)
C16	C15	C14	122.2(3)
C16	C15	H15	118.9
C14	C15	H15	118.9
C15	C16	C11	119.1(3)
C15	C16	H16	120.5
C11	C16	H16	120.5
C14	C17	H17A	109.5
C14	C17	H17B	109.5
H17A	C17	H17B	109.5
C14	C17	H17C	109.5
H17A	C17	H17C	109.5
H17B	C17	H17C	109.5
C22	C21	C26	121.0(3)
C22	C21	N2	117.2(2)
C26	C21	N2	121.8(2)
C21	C22	C23	118.9(3)
C21	C22	H22	120.6
C23	C22	H22	120.6
C24	C23	C22	121.6(3)
C24	C23	H23	119.2
C22	C23	H23	119.2
C23	C24	C25	117.9(3)
C23	C24	C27	121.0(3)
C25	C24	C27	121.1(3)
C26	C25	C24	121.8(3)
C26	C25	H25	119.1
C24	C25	H25	119.1
C25	C26	C21	118.8(3)
C25	C26	H26	120.6
C21	C26	H26	120.6
C24	C27	H27A	109.5
C24	C27	H27B	109.5
H27A	C27	H27B	109.5
C24	C27	H27C	109.5
H(7A	C27	H27C	109.5
H27B	C27	H27C	109.5
C24	C27	H27D	109.5

H27A	C27	H27D	141.1
H27B	C27	H27D	56.3
H27C	C27	H27D	56.3
C24	C27	H27E	109.5
H27A	C27	H27E	56.3
H27B	C27	H27E	141.1
H27C	C27	H27E	56.3
H27D	C27	H27E	109.5
C24	C27	H27F	109.5
H27A	C27	H27F	56.3
H27B	C27	H27F	56.3
H27C	C27	H27F	141.1
H27D	C27	H27F	109.5
H27E	C27	H27F	109.5
N2	N1	C1	116.8(2)
N1	N2	C21	113.5(2)
N1	N2	Ni1	122.97(18)
C21	N2	Ni1	123.31(17)
N4	N3	C1	116.8(2)
N3	N4	C11	115.5(2)
N3	N4	Ni1	122.79(18)
C11	N4	Ni1	121.34(18)
O2	N5	O1	123.8(3)
O2	N5	C1	118.2(3)
O1	N5	C1	118.0(3)
N2	Ni1	N2#1	180.000(1)
N2	Ni1	N4	85.66(10)
N2#1	Ni1	N4	94.34(10)
N2	Ni1	N4#1	94.34(10)
N2#1	Ni1	N4#1	85.66(10)
N4	Ni1	N4#1	180.000(1)

Table D-18. Bond lengths (Å) and angles (deg) for **3.24**.

Ni	O1A	1.891(5)
Ni	O1A’	1.884(5)
Ni	O1B	1.894(5)
Ni	O1B’	1.893(5)
Ni	N2	1.8304(13)
Ni	N4	1.8305(13)
O2	N5	1.2208(19)
O3	N5	1.225(2)
N1	N2	1.2882(18)
N1	C1	1.332(2)

N2	C11	1.4561(19)
N3	N4	1.2860(18)
N3	C1	1.338(2)
N4	C21	1.4615(19)
N5	C1	1.458(2)
C11	C12	1.397(2)
C11	C16	1.395(2)
C12	C13	1.392(2)
C12	C17	1.509(3)
C13	C14	1.384(3)
C14	C15	1.387(3)
C14	C18	1.513(3)
C15	C16	1.392(2)
C16	C19	1.504(3)
C21	C22	1.400(3)
C21	C26	1.386(3)
C22	C23	1.397(3)
C22	C27	1.502(3)
C23	C24	1.375(3)
C24	C25	1.381(3)
C24	C28	1.519(3)
C25	C26	1.400(2)
C26	C29	1.510(3)

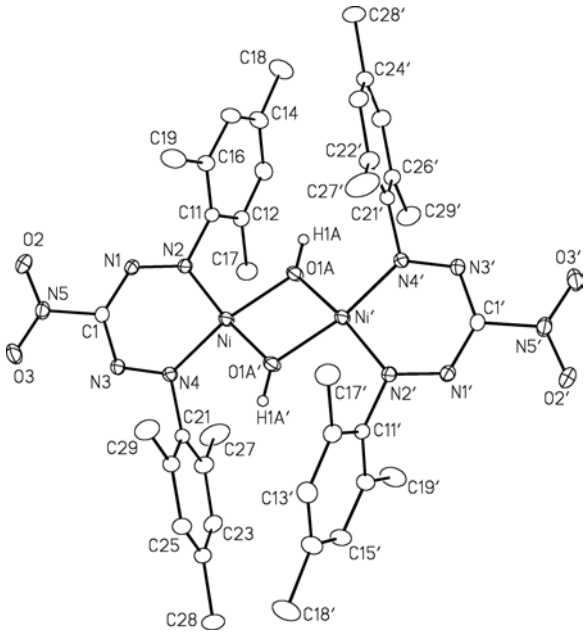

O1A	Ni	O1A’	80.0(2)
O1A	Ni	N2	94.58(15)
O1A	Ni	N4	168.56(13)
O1A’	Ni	N2	168.09(13)
O1A’	Ni	N4	94.55(15)
O1B	Ni	O1B’	80.5(2)
O1B	Ni	N2	94.25(15)
O1B	Ni	N4	167.97(14)
O1B’	Ni	N2	168.27(15)
O1B’	Ni	N4	94.54(15)
N2	Ni	N4	92.54(6)
Ni	O1A	Ni’	100.0(2)
Ni	O1B	Ni’	99.5(2)
N2	N1	C1	118.36(13)
Ni	N2	N1	127.91(11)
Ni	N2	C11	120.44(10)
N1	N2	C11	111.60(12)
N4	N3	C1	118.22(13)
Ni	N4	N3	128.20(11)
Ni	N4	C21	120.78(10)

N3	N4	C21	110.99(12)
O2	N5	O3	123.03(15)
O2	N5	C1	118.43(14)
O3	N5	C1	118.54(14)
N1	C1	N3	132.00(14)
N1	C1	N5	113.71(14)
N3	C1	N5	113.98(14)
N2	C11	C12	118.71(14)
N2	C11	C16	119.04(14)
C12	C11	C16	122.25(15)
C11	C12	C13	117.67(16)
C11	C12	C17	122.05(16)
C13	C12	C17	120.27(16)
C12	C13	C14	121.90(17)
C13	C14	C15	118.57(17)
C13	C14	C18	120.9(2)
C15	C14	C18	120.49(19)
C14	C15	C16	122.10(17)
C11	C16	C15	117.48(17)
C11	C16	C19	121.37(16)
C15	C16	C19	121.15(16)
N4	C21	C22	117.23(15)
N4	C21	C26	119.95(15)
C22	C21	C26	122.82(15)
C21	C22	C23	117.20(18)
C21	C22	C27	121.58(17)
C23	C22	C27	121.21(18)
C22	C23	C24	121.92(18)
C23	C24	C25	118.86(17)
C23	C24	C28	120.2(2)
C25	C24	C28	121.0(2)
C24	C25	C26	122.20(19)
C21	C26	C25	116.97(17)
C21	C26	C29	121.95(16)
C25	C26	C29	121.08(18)

Table D-19. Bond lengths (Å) and angles (deg) for **3.25b** (Molecule A).

Pd	O3	2.0464(13)
Pd	O4	2.0310(13)
Pd	N2	1.9859(15)

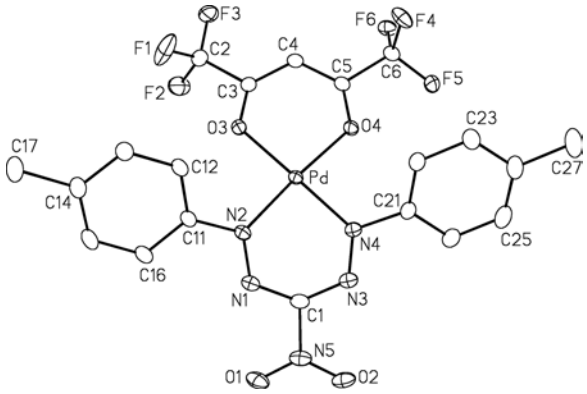

Pd	N4	1.9811(15)	
F1	C2	1.303(3)	
F2	C2	1.313(3)	
F3	C2	1.327(3)	
F4	C6	1.337(2)	
F5	C6	1.328(2)	
F6	C6	1.328(2)	
O1	N5	1.222(3)	
O2	N5	1.225(3)	
O3	C3	1.263(2)	
O4	C5	1.257(2)	
N1	N2	1.279(2)	
N1	C1	1.333(3)	
N2	C11	1.436(2)	
N3	N4	1.277(2)	
N3	C1	1.327(3)	
N4	C21	1.436(2)	
N5	C1	1.465(2)	
C2	C3	1.532(3)	
C3	C4	1.388(3)	
C4	C5	1.387(3)	
C5	C6	1.536(3)	
C11	C12	1.386(3)	
C11	C16	1.393(3)	
C12	C13	1.384(3)	
C13	C14	1.388(3)	
C14	C15	1.383(4)	
C14	C17	1.510(3)	
C15	C16	1.387(3)	
C21	C22	1.375(3)	
C21	C26	1.392(3)	
C22	C23	1.389(3)	
C23	C24	1.384(3)	
C24	C25	1.390(4)	
C24	C27	1.506(3)	
C25	C26	1.381(4)	
O3	Pd	O4	89.42(5)
O3	Pd	N2	93.75(6)
O3	Pd	N4	175.71(6)
O4	Pd	N2	175.34(6)
O4	Pd	N4	89.88(6)
N2	Pd	N4	86.71(6)
Pd	O3	C3	124.26(12)

Pd	O4	C5	125.31(12)
N2	N1	C1	120.48(16)
Pd	N2	N1	122.91(13)
Pd	N2	C11	122.29(12)
N1	N2	C11	114.58(15)
N4	N3	C1	119.52(17)
Pd	N4	N3	123.80(13)
Pd	N4	C21	119.41(12)
N3	N4	C21	115.43(16)
O1	N5	O2	124.41(19)
O1	N5	C1	117.39(19)
O2	N5	C1	118.20(19)
N1	C1	N3	130.92(17)
N1	C1	N5	113.23(17)
N3	C1	N5	113.87(18)
F1	C2	F2	108.5(2)
F1	C2	F3	107.1(2)
F1	C2	C3	111.0(2)
F2	C2	F3	106.3(2)
F2	C2	C3	110.19(19)
F3	C2	C3	113.52(19)
O3	C3	C2	111.84(17)
O3	C3	C4	129.58(18)
C2	C3	C4	118.58(18)
C3	C4	C5	121.78(17)
O4	C5	C4	128.78(17)
O4	C5	C6	112.40(16)
C4	C5	C6	118.77(17)
F4	C6	F5	108.29(17)
F4	C6	F6	106.81(16)
F4	C6	C5	109.54(15)
F5	C6	F6	107.14(16)
F5	C6	C5	112.14(16)
F6	C6	C5	112.68(16)
N2	C11	C12	118.94(16)
N2	C11	C16	121.13(18)
C12	C11	C16	119.93(19)
C11	C12	C13	119.66(19)
C12	C13	C14	121.5(2)
C13	C14	C15	117.9(2)
C13	C14	C17	121.0(2)
C15	C14	C17	121.1(2)
C14	C15	C16	121.8(2)

C11	C16	C15	119.1(2)
N4	C21	C22	118.53(17)
N4	C21	C26	120.87(19)
C22	C21	C26	120.6(2)
C21	C22	C23	119.83(19)
C22	C23	C24	120.7(2)
C23	C24	C25	118.5(2)
C23	C24	C27	120.1(3)
C25	C24	C27	121.5(2)
C24	C25	C26	121.6(2)
C21	C26	C25	118.7(2)

Table D-20. Bond lengths (Å) and angles (deg) for **3.25b** (Molecule B).

Pd	O3	2.0394(12)
Pd	O4	2.0460(12)
Pd	N2	1.9912(14)
Pd	N4	1.9866(15)
F1B	C2	1.291(3)[a]
F2B	C2	1.306(3)[a]
F3B	C2	1.289(3)[a]
F4B	C6	1.308(3)[a]
F5B	C6	1.302(3)[a]
F6B	C6	1.305(3)[a]
F1C	C2	1.295(3)[a]
F2C	C2	1.296(3)[a]
F3C	C2	1.308(3)[a]
F4C	C6	1.298(3)[a]
F5C	C6	1.304(3)[a]
F6C	C6	1.307(3)[a]
O1	N5	1.223(2)
O2	N5	1.227(2)
O3	C3	1.253(2)
O4	C5	1.255(2)
N1	N2	1.284(2)
N1	C1	1.327(2)
N2	C11	1.440(2)
N3	N4	1.276(2)
N3	C1	1.332(2)
N4	C21	1.441(2)
N5	C1	1.472(2)
C2	C3	1.538(3)

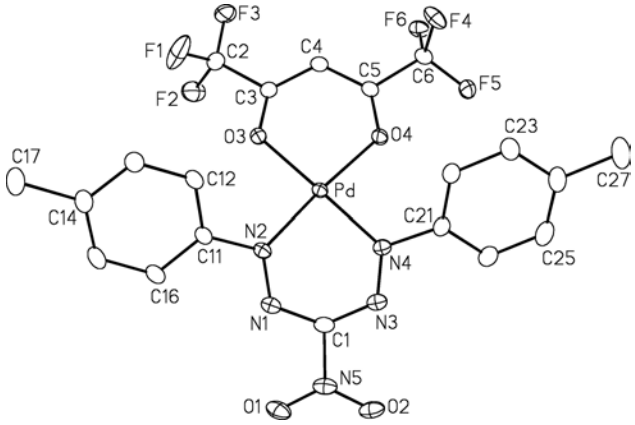

C3	C4	1.386(3)	
C4	C5	1.391(3)	
C5	C6	1.540(3)	
C11	C12	1.380(3)	
C11	C16	1.396(2)	
C12	C13	1.389(3)	
C13	C14	1.391(3)	
C14	C15	1.389(4)	
C14	C17	1.513(3)	
C15	C16	1.380(3)	
C21	C22	1.370(3)	
C21	C26	1.398(2)	
C22	C23	1.388(3)	
C23	C24	1.390(3)	
C24	C25	1.393(3)	
C24	C27	1.509(3)	
C25	C26	1.382(3)	
O3	Pd	O4	89.99(5)
O3	Pd	N2	90.57(6)
O3	Pd	N4	176.60(5)
O4	Pd	N2	176.76(6)
O4	Pd	N4	91.12(5)
N2	Pd	N4	88.15(6)
Pd	O3	C3	123.91(12)
Pd	O4	C5	123.92(12)
N2	N1	C1	120.65(15)
Pd	N2	N1	123.86(12)
Pd	N2	C11	122.16(12)
N1	N2	C11	113.50(14)
N4	N3	C1	120.72(15)
Pd	N4	N3	124.10(12)
Pd	N4	C21	122.27(11)
N3	N4	C21	113.35(14)
O1	N5	O2	124.75(17)
O1	N5	C1	117.86(17)
O2	N5	C1	117.38(16)
N1	C1	N3	131.99(17)
N1	C1	N5	113.91(15)
N3	C1	N5	112.69(16)
F1B	C2	F2B	104.5(6)
F1B	C2	F3B	112.8(6)
F1B	C2	C3	109.1(5)
F2B	C2	F3B	108.1(5)

F2B	C2	C3	110.7(3)
F3B	C2	C3	111.3(4)
F1C	C2	F2C	105.6(6)
F1C	C2	F3C	99.4(6)
F1C	C2	C3	112.5(5)
F2C	C2	F3C	107.9(5)
F2C	C2	C3	116.1(3)
F3C	C2	C3	113.8(4)
O3	C3	C2	113.42(15)
O3	C3	C4	129.62(17)
C2	C3	C4	116.94(16)
C3	C4	C5	122.18(17)
O4	C5	C4	129.23(17)
O4	C5	C6	112.99(16)
C4	C5	C6	117.77(16)
F4B	C6	F5B	103.8(6)
F4B	C6	F6B	106.8(6)
F4B	C6	C5	111.6(4)
F5B	C6	F6B	109.6(8)
F5B	C6	C5	110.2(5)
F6B	C6	C5	114.3(5)
F4C	C6	F5C	110.8(8)
F4C	C6	F6C	108.9(9)
F4C	C6	C5	111.2(5)
F5C	C6	F6C	103.5(8)
F5C	C6	C5	111.2(6)
F6C	C6	C5	111.0(6)
N2	C11	C12	119.47(16)
N2	C11	C16	119.82(18)
C12	C11	C16	120.69(18)
C11	C12	C13	119.29(19)
C12	C13	C14	121.3(2)
C13	C14	C15	118.1(2)
C13	C14	C17	120.8(2)
C15	C14	C17	121.0(2)
C14	C15	C16	121.8(2)
C11	C16	C15	118.8(2)
N4	C21	C22	119.12(16)
N4	C21	C26	119.91(16)
C22	C21	C26	120.90(17)
C21	C22	C23	119.52(18)
C22	C23	C24	121.17(19)
C23	C24	C25	118.12(18)

C23	C24	C27	120.9(2)
C25	C24	C27	120.92(19)
C24	C25	C26	121.56(18)
C21	C26	C25	118.68(18)

Table D-21. Bond lengths (Å) and angles (deg) for **3.25d**.

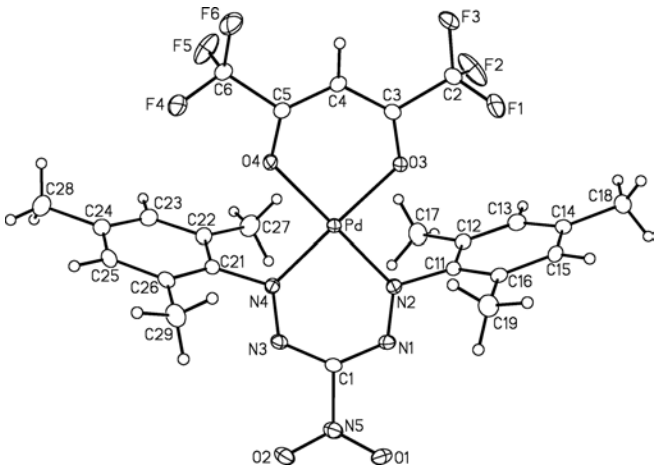

Pd	O3	2.030(2)
Pd	O4	2.042(2)
Pd	N2	1.959(3)
Pd	N4	1.963(3)
F1	C2	1.291(5)
F2	C2	1.309(5)
F3	C2	1.299(5)
F4	C6	1.308(4)
F5	C6	1.309(5)
F6	C6	1.314(4)
O1	N5	1.220(4)
O2	N5	1.220(4)
O3	C3	1.257(4)
O4	C5	1.254(4)
N1	N2	1.280(4)
N1	C1	1.329(4)
N2	C11	1.447(4)
N3	N4	1.277(4)
N3	C1	1.339(4)
N4	C21	1.458(4)
N5	C1	1.460(4)
C2	C3	1.533(5)
C3	C4	1.382(5)
C4	C5	1.372(5)
C5	C6	1.534(5)
C11	C12	1.392(5)
C11	C16	1.394(5)
C12	C13	1.380(5)
C12	C17	1.498(5)
C13	C14	1.387(6)
C14	C15	1.382(6)
C14	C18	1.513(5)
C15	C16	1.385(5)
C16	C19	1.511(5)

C21	C22	1.390(5)	
C21	C26	1.384(5)	
C22	C23	1.394(5)	
C22	C27	1.498(5)	
C23	C24	1.383(6)	
C24	C25	1.373(6)	
C24	C28	1.518(6)	
C25	C26	1.401(5)	
C26	C29	1.503(6)	
O3	Pd	O4	90.48(9)
O3	Pd	N2	89.51(11)
O3	Pd	N4	178.09(11)
O4	Pd	N2	177.48(11)
O4	Pd	N4	90.46(10)
N2	Pd	N4	89.48(11)
Pd	O3	C3	123.7(2)
Pd	O4	C5	122.9(2)
N2	N1	C1	120.6(3)
Pd	N2	N1	125.2(2)
Pd	N2	C11	119.3(2)
N1	N2	C11	114.6(3)
N4	N3	C1	120.4(3)
Pd	N4	N3	125.4(2)
Pd	N4	C21	119.4(2)
N3	N4	C21	114.9(3)
O1	N5	O2	123.6(3)
O1	N5	C1	118.3(3)
O2	N5	C1	118.1(3)
N1	C1	N3	132.0(3)
N1	C1	N5	114.0(3)
N3	C1	N5	113.4(3)
F1	C2	F2	107.4(4)
F1	C2	F3	107.7(4)
F1	C2	C3	111.4(3)
F2	C2	F3	106.8(4)
F2	C2	C3	109.8(4)
F3	C2	C3	113.5(4)
O3	C3	C2	111.5(3)
O3	C3	C4	128.4(3)
C2	C3	C4	120.1(3)
C3	C4	C5	123.5(3)
O4	C5	C4	129.1(3)
O4	C5	C6	112.6(3)

C4	C5	C6	118.3(3)
F4	C6	F5	108.5(3)
F4	C6	F6	106.4(4)
F4	C6	C5	111.5(3)
F5	C6	F6	107.1(3)
F5	C6	C5	110.1(3)
F6	C6	C5	112.9(3)
N2	C11	C12	118.8(3)
N2	C11	C16	119.0(3)
C12	C11	C16	122.1(3)
C11	C12	C13	117.8(4)
C11	C12	C17	122.1(3)
C13	C12	C17	120.0(4)
C12	C13	C14	121.9(4)
C13	C14	C15	118.7(4)
C13	C14	C18	121.7(4)
C15	C14	C18	119.6(4)
C14	C15	C16	121.7(4)
C11	C16	C15	117.8(4)
C11	C16	C19	121.7(3)
C15	C16	C19	120.4(4)
N4	C21	C22	117.9(3)
N4	C21	C26	118.6(4)
C22	C21	C26	123.5(4)
C21	C22	C23	117.0(4)
C21	C22	C27	122.4(3)
C23	C22	C27	120.6(4)
C22	C23	C24	121.7(4)
C23	C24	C25	119.2(4)
C23	C24	C28	120.6(5)
C25	C24	C28	120.1(5)
C24	C25	C26	121.8(4)
C21	C26	C25	116.9(4)
C21	C26	C29	122.9(4)
C25	C26	C29	120.2(4)

Table D-22. Bond lengths (Å) and angles (deg) for **4.7a**.

O1	C12	1.222(3)
N11	N12	1.368(3)

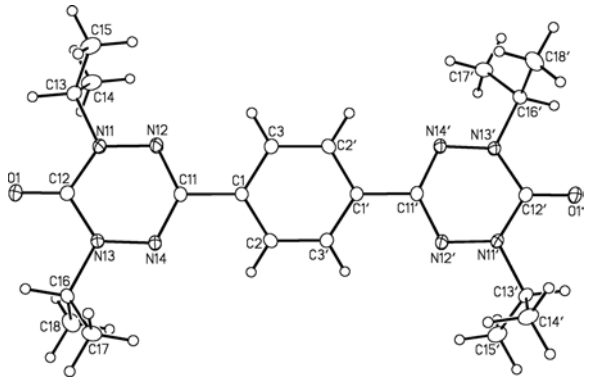

N11	C12	1.371(4)	
N11	C13	1.478(4)	
N12	C11	1.329(4)	
N13	N14	1.365(3)	
N13	C12	1.378(4)	
N13	C16	1.476(3)	
N14	C11	1.330(4)	
C1	C2	1.393(4)	
C1	C3	1.390(4)	
C1	C11	1.475(4)	
C2	C3'	1.381(4)	
C13	C14	1.515(5)	
C13	C15	1.509(5)	
C16	C17	1.512(4)	
C16	C18	1.508(5)	
N12	N11	C12	124.4(2)
N12	N11	C13	114.3(2)
C12	N11	C13	121.2(2)
N11	N12	C11	114.9(2)
N14	N13	C12	124.0(2)
N14	N13	C16	116.1(2)
C12	N13	C16	119.8(2)
N13	N14	C11	115.2(2)
C2	C1	C3	118.9(3)
C2	C1	C11	120.6(3)
C3	C1	C11	120.5(3)
C1	C2	C3'	120.8(3)
C1	C3	C2'	120.3(3)
N12	C11	N14	127.0(2)
N12	C11	C1	115.9(2)
N14	C11	C1	117.1(2)
O1	C12	N11	122.8(3)
O1	C12	N13	122.8(3)
N11	C12	N13	114.4(2)
N11	C13	C14	109.2(3)
N11	C13	C15	110.2(3)
C14	C13	C15	112.1(3)
N13	C16	C17	110.1(2)
N13	C16	C18	109.5(2)
C17	C16	C18	112.7(3)

Table D-23. Bond lengths (Å) and angles (deg) for **4.7b**.

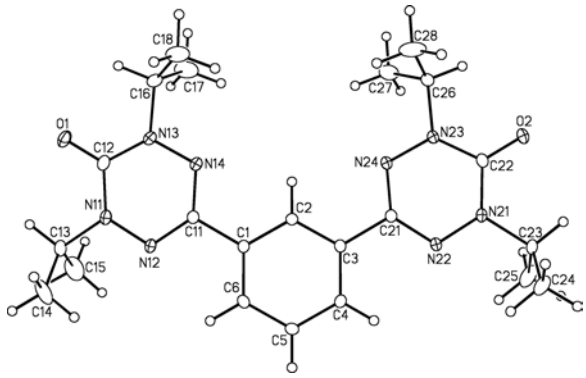

O1	C12	1.2229(17)	
O2	C22	1.2176(16)	
N11	N12	1.3705(16)	
N11	C12	1.376(2)	
N11	C13	1.4831(18)	
N12	C11	1.3313(18)	
N13	N14	1.3659(16)	
N13	C12	1.3770(19)	
N13	C16	1.4730(19)	
N14	C11	1.3276(18)	
N21	N22	1.3662(15)	
N21	C22	1.3793(18)	
N21	C23	1.4853(17)	
N22	C21	1.3276(17)	
N23	N24	1.3626(16)	
N23	C22	1.3777(18)	
N23	C26	1.4794(18)	
N24	C21	1.3288(18)	
C1	C2	1.3907(19)	
C1	C6	1.390(2)	
C1	C11	1.4840(18)	
C2	C3	1.3908(18)	
C3	C4	1.3896(19)	
C3	C21	1.4873(18)	
C4	C5	1.382(2)	
C5	C6	1.383(2)	
C13	C14	1.505(3)	
C13	C15	1.501(3)	
C16	C17	1.500(3)	
C16	C18	1.500(3)	
C23	C24	1.514(2)	
C23	C25	1.508(2)	
C26	C27	1.516(2)	
C26	C28	1.494(3)	
N12	N11	C12	124.35(12)
N12	N11	C13	115.27(12)
C12	N11	C13	120.04(12)
N11	N12	C11	114.91(12)
N14	N13	C12	124.53(12)
N14	N13	C16	114.76(12)
C12	N13	C16	120.38(12)

N13	N14	C11	115.05(12)
N22	N21	C22	124.51(11)
N22	N21	C23	115.17(11)
C22	N21	C23	120.23(11)
N21	N22	C21	114.96(11)
N24	N23	C22	124.76(12)
N24	N23	C26	114.89(11)
C22	N23	C26	120.34(11)
N23	N24	C21	114.93(11)
C2	C1	C6	119.36(13)
C2	C1	C11	119.86(12)
C6	C1	C11	120.77(12)
C1	C2	C3	120.62(12)
C2	C3	C4	119.52(12)
C2	C3	C21	119.77(12)
C4	C3	C21	120.71(12)
C3	C4	C5	119.80(13)
C4	C5	C6	120.78(13)
C1	C6	C5	119.90(13)
N12	C11	N14	127.06(13)
N12	C11	C1	117.18(12)
N14	C11	C1	115.76(12)
O1	C12	N11	123.09(14)
O1	C12	N13	122.93(14)
N11	C12	N13	113.98(12)
N11	C13	C14	110.48(14)
N11	C13	C15	109.75(14)
C14	C13	C15	111.89(18)
N13	C16	C17	109.68(14)
N13	C16	C18	110.92(14)
C17	C16	C18	112.10(16)
N22	C21	N24	127.10(12)
N22	C21	C3	116.87(12)
N24	C21	C3	116.03(12)
O2	C22	N21	123.20(13)
O2	C22	N23	123.14(13)
N21	C22	N23	113.65(11)
N21	C23	C24	110.09(12)
N21	C23	C25	110.03(13)
C24	C23	C25	111.29(14)
N23	C26	C27	109.42(13)
N23	C26	C28	110.34(14)
C27	C26	C28	112.45(17)

Table D-24. Bond lengths (Å) and angles (deg) for **4.13**.

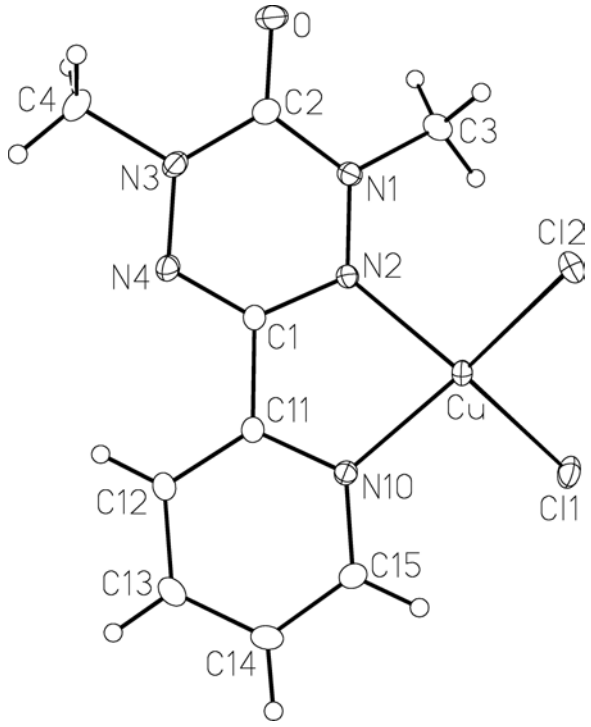

Cu	Cl1	2.2234(5)	
Cu	Cl2	2.1965(5)	
Cu	N2	1.9992(14)	
Cu	N10	1.9921(15)	
O	C2	1.210(2)	
N1	N2	1.349(2)	
N1	C2	1.385(2)	
N1	C3	1.463(2)	
N2	C1	1.358(2)	
N3	N4	1.342(2)	
N3	C2	1.379(3)	
N3	C4	1.463(2)	
N4	C1	1.306(2)	
N10	C11	1.343(2)	
N10	C15	1.339(2)	
C1	C11	1.469(2)	
C11	C12	1.387(3)	
C12	C13	1.380(3)	
C13	C14	1.381(3)	
C14	C15	1.379(3)	
Cl1	Cu	Cl2	102.02(2)
Cl1	Cu	N2	142.31(5)
Cl1	Cu	N10	96.03(5)
Cl2	Cu	N2	99.56(4)
Cl2	Cu	N10	147.44(5)
N2	Cu	N10	81.34(6)
N2	N1	C2	124.09(15)
N2	N1	C3	117.34(15)
C2	N1	C3	117.85(15)
Cu	N2	N1	127.43(11)
Cu	N2	C1	111.77(11)
N1	N2	C1	114.34(14)
N4	N3	C2	124.11(15)
N4	N3	C4	116.64(16)
C2	N3	C4	119.14(16)
N3	N4	C1	115.90(15)
Cu	N10	C11	114.56(12)
Cu	N10	C15	126.69(13)
C11	N10	C15	118.75(16)
N2	C1	N4	126.96(16)
N2	C1	C11	114.64(15)
N4	C1	C11	118.38(16)

O	C2	N1	122.39(18)
O	C2	N3	123.30(18)
N1	C2	N3	114.28(16)
N10	C11	C1	113.74(15)
N10	C11	C12	122.75(17)
C1	C11	C12	123.49(16)
C11	C12	C13	117.79(18)
C12	C13	C14	119.75(19)
C13	C14	C15	119.14(18)
N10	C15	C14	121.80(18)

Table D-25. Bond lengths (Å) and angles (deg) for **4.14**.

Cu	Cl1	2.2136(13)	
Cu	Cl2	2.2140(11)	
Cu	N2	2.058(3)	
Cu	N10	2.009(3)	
O	C2	1.219(6)	
N1	N2	1.355(5)	
N1	C2	1.402(6)	
N1	C3	1.482(6)	
N2	C1	1.351(5)	
N3	N4	1.348(6)	
N3	C2	1.375(8)	
N3	C6A	1.483(2)†	
N3	C6B	1.481(2)†	
N4	C1	1.313(5)	
N10	C11	1.334(5)	
N10	C15	1.337(5)	
C1	C11	1.473(6)	
C3	C4	1.520(7)	
C3	C5	1.523(7)	
C6A	C7A	1.520(2)†	
C6A	C8A	1.519(2)†	
C6B	C7B	1.520(2)†	
C6B	C8B	1.520(2)†	
C11	C12	1.388(6)	
C12	C13	1.383(7)	
C13	C14	1.368(7)	
C14	C15	1.385(6)	
Cl1	Cu	Cl2	96.46(5)

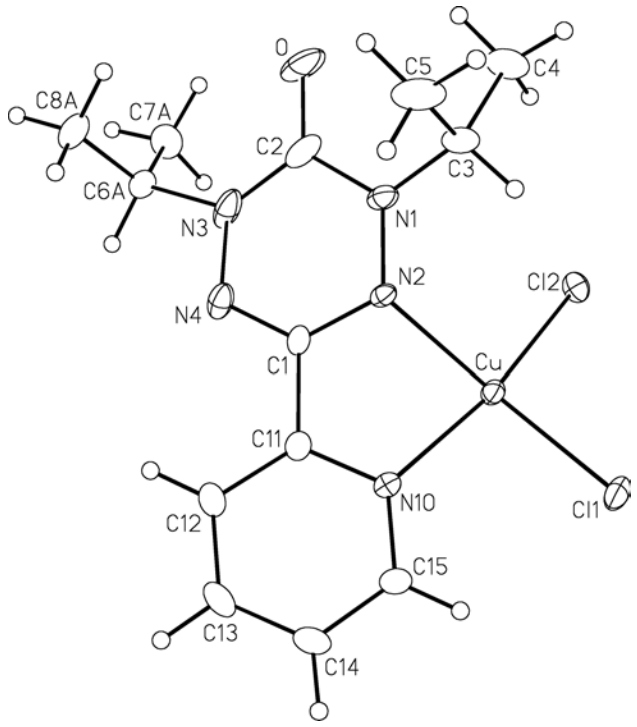

Cl1	Cu	N2	154.36(11)
Cl1	Cu	N10	95.27(10)
Cl2	Cu	N2	94.63(9)
Cl2	Cu	N10	164.26(10)
N2	Cu	N10	78.98(13)
N2	N1	C2	121.9(4)
N2	N1	C3	115.0(4)
C2	N1	C3	120.8(4)
Cu	N2	N1	128.8(3)
Cu	N2	C1	107.6(3)
N1	N2	C1	115.2(3)
N4	N3	C2	123.2(4)
N4	N3	C6A	107.3(6)
N4	N3	C6B	129.1(5)
C2	N3	C6A	129.4(6)
C2	N3	C6B	104.5(6)
N3	N4	C1	115.4(4)
Cu	N10	C11	113.0(3)
Cu	N10	C15	128.1(3)
C11	N10	C15	118.7(4)
N2	C1	N4	127.5(4)
N2	C1	C11	113.4(3)
N4	C1	C11	119.0(4)
O	C2	N1	121.2(6)
O	C2	N3	122.8(5)
N1	C2	N3	115.9(4)
N1	C3	C4	113.3(5)
N1	C3	C5	109.6(4)
C4	C3	C5	112.9(4)
N3	C6A	C7A	112.2(13)
N3	C6A	C8A	106.9(7)
C7A	C6A	C8A	118.5(16)
N3	C6B	C7B	104.9(16)
N3	C6B	C8B	104.9(7)
C7B	C6B	C8B	107.3(16)
N10	C11	C1	114.2(3)
N10	C11	C12	123.0(4)
C1	C11	C12	122.8(4)
C11	C12	C13	117.6(4)
C12	C13	C14	119.5(4)
C13	C14	C15	119.6(4)
N10	C15	C14	121.5(4)

Table D-26. Bond lengths (Å) and angles (deg) for **4.15**.

Cu	O21	1.971(2)
Cu	O22	2.234(2)
Cu	O31	1.985(2)
Cu	O32	1.948(2)
Cu	N2	2.544(3)
Cu	N11	1.961(3)
F21	C21	1.314(4)
F22	C21	1.291(5)
F23	C21	1.308(5)
F24	C25	1.291(4)
F25	C25	1.314(5)
F26	C25	1.299(5)
F31	C31	1.305(4)
F32	C31	1.324(5)
F33	C31	1.334(5)
F34	C35	1.316(5)
F35	C35	1.299(5)
F36	C35	1.329(5)
O1	C2	1.207(4)
O21	C22	1.260(4)
O22	C24	1.231(4)
O31	C32	1.260(4)
O32	C34	1.256(4)
N1	N2	1.361(4)
N1	C2	1.381(4)
N1	C3	1.451(4)
N2	C1	1.327(4)
N3	N4	1.359(4)
N3	C2	1.376(4)
N3	C4	1.465(4)
N4	C1	1.328(4)
N11	C11	1.334(4)
N11	C12	1.372(4)
N12	C11	1.353(4)
N12	C13	1.366(4)
N12	C14	1.468(4)
C1	C11	1.470(4)
C12	C13	1.344(5)
C21	C22	1.535(5)
C22	C23	1.373(5)
C23	C24	1.406(5)
C24	C25	1.539(5)

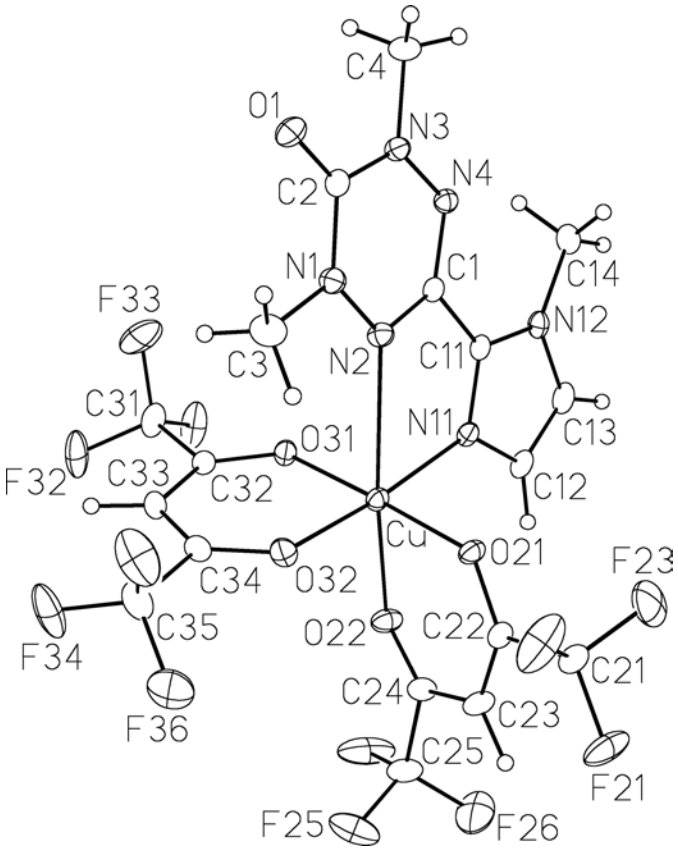

C31	C32	1.531(5)	
C32	C33	1.384(4)	
C33	C34	1.378(5)	
C34	C35	1.526(5)	
O21	Cu	O22	88.65(9)
O21	Cu	O31	177.93(9)
O21	Cu	O32	87.20(10)
O21	Cu	N2	97.73(9)
O21	Cu	N11	91.31(10)
O22	Cu	O31	90.37(9)
O22	Cu	O32	92.91(10)
O22	Cu	N2	165.90(9)
O22	Cu	N11	95.48(10)
O31	Cu	O32	91.04(9)
O31	Cu	N2	83.63(9)
O31	Cu	N11	90.59(10)
O32	Cu	N2	99.92(9)
O32	Cu	N11	171.44(10)
N2	Cu	N11	71.92(10)
Cu	O21	C22	126.0(2)
Cu	O22	C24	120.4(2)
Cu	O31	C32	124.5(2)
Cu	O32	C34	126.2(2)
N2	N1	C2	124.1(3)
N2	N1	C3	116.3(3)
C2	N1	C3	119.6(3)
Cu	N2	N1	136.0(2)
Cu	N2	C1	108.37(19)
N1	N2	C1	115.0(3)
N4	N3	C2	125.3(3)
N4	N3	C4	115.6(3)
C2	N3	C4	119.0(3)
N3	N4	C1	114.0(3)
Cu	N11	C11	124.1(2)
Cu	N11	C12	129.8(2)
C11	N11	C12	105.9(3)
C11	N12	C13	106.9(3)
C11	N12	C14	128.8(3)
C13	N12	C14	124.3(3)
N2	C1	N4	127.8(3)
N2	C1	C11	113.4(3)
N4	C1	C11	118.7(3)
O1	C2	N1	122.8(3)
O1	C2	N3	123.4(3)
N1	C2	N3	113.8(3)
N11	C11	N12	110.4(3)

N11	C11	C1	121.1(3)
N12	C11	C1	128.5(3)
N11	C12	C13	109.4(3)
N12	C13	C12	107.3(3)
F21	C21	F22	107.5(3)
F21	C21	F23	106.3(3)
F21	C21	C22	114.3(3)
F22	C21	F23	104.9(4)
F22	C21	C22	112.2(3)
F23	C21	C22	111.0(3)
O21	C22	C21	111.8(3)
O21	C22	C23	130.7(3)
C21	C22	C23	117.6(3)
C22	C23	C24	123.6(3)
O22	C24	C23	128.5(3)
O22	C24	C25	116.0(3)
C23	C24	C25	115.5(3)
F24	C25	F25	106.2(4)
F24	C25	F26	108.5(4)
F24	C25	C24	113.1(3)
F25	C25	F26	104.9(4)
F25	C25	C24	111.1(3)
F26	C25	C24	112.6(3)
F31	C31	F32	107.6(3)
F31	C31	F33	107.1(3)
F31	C31	C32	112.2(3)
F32	C31	F33	106.6(3)
F32	C31	C32	112.9(3)
F33	C31	C32	110.1(3)
O31	C32	C31	113.4(3)
O31	C32	C33	128.7(3)
C31	C32	C33	117.8(3)
C32	C33	C34	121.3(3)
O32	C34	C33	128.2(3)
O32	C34	C35	112.9(3)
C33	C34	C35	118.9(3)
F34	C35	F35	108.3(4)
F34	C35	F36	106.3(4)
F34	C35	C34	113.4(3)
F35	C35	F36	106.3(4)
F35	C35	C34	111.2(3)
F36	C35	C34	111.1(4)